Doungporn Sirikittikul

Modification of Pigment Surfaces with Polymer Monolayers

Cuvillier Verlag Göttingen

Modification of Pigment Surfaces with Polymer Monolayers

Dissertation

Zur Erlangung des Doktorgrades

Der Fakultät für Angewandte Wissenschaften

Der Albert-Ludwigs-Universität Freiburg

vorgelegt von

Doungporn Sirikittikul

aus Khon-Kaen, Thailand

Freiburg im Breisgau

July 2004

Bibliografische Information Der Deutschen Bibliothek
Die Deutsche Bibliothek verzeichnet diese Publikation in der Deutschen Nationalbibliografie; detaillierte bibliografische Daten sind im Internet über http://dnb.ddb.de abrufbar.
1. Aufl. - Göttingen : Cuvillier, 2004
Zugl.: Freiburg, Univ., Diss., 2004
ISBN 3-86537-195-7

Dekan: Prof. Dr. Thomas Ottmann
Vorsitzender: Prof. Dr. Gerald A. Urban
1. Gutachter: Prof. Dr. Jürgen Rühe
2. Gutachter: Prof. Dr. Wolfgang Knoll
Beisitzender: Prof. Dr. Oliver Paul

Tag der mündliche Prüfung: 27.07.2004

Nonnenstieg 8, 37075 Göttingen
Telefon: 0551-54724-0
Telefax: 0551-54724-21
www.cuvillier.de

1. Auflage, 2004
Gedruckt auf säurefreiem Papier

ISBN 3-86537-195-7

Content

List of the abbreviation

δ	graft density of surface-attached polymer [gram polymer per gram pigment]
δ_{Azo}	graft density of surface-attached initiator [mol g^{-1}]
δ_C	graft density of surface-attached polymer [gram polymer per gram pigment] calculated from carbon content
δ_H	graft density of surface-attached polymer [gram polymer per gram pigment] calculated from hydrogen content
Γ	graft density of surface-attached polymer [mol m^{-2}]
Γ_0	originate graft density of initiator
Γ_{Azo}	graft density of surface-attached initiator
Γ_t	graft density of polymer at time *t*
ρ	graft density surface-attached polymer [group nm^{-2}]
ρ_{PMMA}	density of PMMA
$\bar{\nu}$	kinetic chain length
ν_i	reaction rate of initiation
ν_p	rate of polymerization
ν_t	reaction rate of termination
C_I	chain transfer constant for initiator
C_M	chain transfer constant for monomer
C_P	chain transfer constant for polymer
C_S	chain transfer constant for solvent
d	average distance between anchor groups
D	polydispersity
f	initiator efficiency
H_{dec}	molar enthalpy of decomposition of initiator
$[I]$	initiator concentration
I_C	intensity of carbon in XPS
I_{dec}	exothermic decomposition in DSC trace of immobilized initiator
I_F	intensity of fluorine in XPS

k_d	rate constant of initiator decomposition
k_p	temperature-dependent reaction constant of chain propagation
k_t	temperature-dependent reaction constant of chain termination
L	layer thickness of polymer grafted
$[M]$	monomer concentration
M	molecular weight of the polymer repeating unit
M_0	molecular weight of the monomer
M_n	number-average molecular weight of the polymer
M_w	weight-average molecular weight of the polymer
m_C	atom mass of carbon
m_H	atom mass of hydrogen
N_A	avogadro's constant
N_C	number of carbon atom
N_F	number of fluorine atom
N_H	number of hydrogen atom
$[P]$	polymer concentration
R_g	radius of gyration of corresponding polymer molecules in solvent
$[S]$	solvent concentration
SA_{sp}	specific surface area of the pigment particles
S_C	atomic sensitivity of carbon
S_F	atomic sensitivity of fluorine
t	polymerization time
T	polymerization temperature
$\overline{X}_n$	number-average degree of polymerization
X_0	number-average degree of polymerization obtained in absence of transfer agent

γ-APS	γ-aminopropyltriethoxysilane
ABCA	4,4′-azobis-(4-cyanopentanoic acid)
ABCC	4,4´-azobis-(4-cyanopentanoyl chloride)
ABCC-AE	4-cyano-4-[1-cyano-3-(2,5-dioxo-pyrrolidin-1-yloxy carbonyl)-1-methyl-propylazo]-4-methyl-butyric acid 2,5-dioxo-pyrrolidin-1-yl ester
ADS	4,4´-azobis-(4-cyanopentanoic acid-(3´-chlorodimethyl silyl)propyl-ester
AEP	2-aminoethyldihydrogenphosphate
AIBN	α,α´-azo-isobutyronitrile
AQ	anthraquinone
CCl_3CF_3	1,1,2-trichlor-trifluorethane (freon)
CD_2Cl_2	dichloromethane-d_2
CD_3OD	methanol-d_4
$CDCl_3$	chloroform-d_3
CH_2Cl_2	dichloromethane
$CHCl_3$	chloroform
DCC	dicyclohexylcarbodiimide
DMAA	*N*,*N*´-dimethylacrylamide
DMSO	dimethylsulfoxide
DPP	diketopyrrolo pyrrole
EtOH	ethanol
H_2SO_4	sulfuric acid
HDFDA	1-(3,3,4,4,5,5,6,6,7,7,8,8,9,9,10,10,10-heptadeca fluoro-decyloxy)prop-2-en-1-ol: (perfluoroalkyl acrylate)
KBr	potassium bromide
LPEI	linear polyethyleneimine
LPEI-ABCC	linear polyethyleneimine containing ABCC initiator
MA	methacrylate monolayer
MAA	methacrylic acid
MA-Cl	2-methyl-acryloyl chloride

Mel-ABCC	4-cyano-4-{1-cyano-3-[6-(4,6-diamino-[1,3,5]triazin-2-ylamino)-hexylcarbamoyl]-1-methyl-propylazo}-*N*-[6-(4,6-diamino-[1,3,5]triazin-2-ylamino)-hexyl]-4-methyl-butyramide
Mel-C_6H_{12}-NH_2	*N*-(6-amino-hexyl)-[1,3,5]triazine-2,4,6-triamine
Mel-Cl	2-chloro-4,6-diamino-1,3,5-triazine
Mel-PFB	*N*-[6-(4,6-diamino-[1,3,5]triazin-2-ylamino)-hexyl]-2,3,4,5, 6-pentafluoro-benzamide
Mel-Silane	1-(4,6-diamino-[1,3,5]triazin-2-yl)-3-{3´-[tris-(2-hydroxy-ethyl)-silanyl]-propyl}-urea
MeOH	methanol
MMA	methylmethacrylate
MPS	3-methycryloylpropyl trimethoxysilane
NEt_3	triethylamine
NHS	*N*-hydroxysuccinimide
PCl_5	phosphorpentachloride
PDMAA	poly(*N*,*N*´-dimethylacrylamide)
PFB-Cl	pentafluorobenzoyl chloride
PHDFDA	poly(1-(3,3,4,4,5,5,6,6,7,7,8,8,9,9,10,10,10-heptadeca fluoro-decyloxy)prop-2-en-1-ol)
PMAA	poly(methacrylic acid)
PMMA	poly(methylmethacrylate)
QD	quinacridone
PCG2020	Paliocrom Gold 2020
PCG2020-ABCC	ABCC-attached PCG2020 surfaces
PCG2020-AEP	AEP-attached PCG2020 surfaces
PCG2020-PMMA	PMMA-attached PCG2020 surfaces
PGL1155	Pigment Yellow 185; 2-cyano-*N*-methyl-2-[3-(2,4,6-trioxo-tetrahydro-pyrimidin-5-ylidene)-2,3-dihydro-isoindol-1-ylidene]-acetamide
PGL1155-Azo	ABCC-attached PGL1155 surfaces
PGL1155-MA	MA-attached PGL1155 surfaces

PGL1155-PDMAA	PDMAA-attached PGL1155 surface
PGL1155-PFB	PFB-attached PGL1155 surfaces
PGL1155-PHDFDA	PHDFDA-attached PGL1155 surface
PGL1155-PMAA	PMAA-attached PGL1155 surface
PGL1155-PMMA	PMMA-attached PGL1155 surface
PGL1155-PS	PS-attached PGL1155 surface
PGL1840	Pigment Yellow 139; 5-[3-(2,4,6-trioxo-tetrahydro-pyrimidin-5-ylidene)-2,3-dihydro-isoindol-1-ylidene]-pyrimidine-2,4,6-trione
PGL1840-Azo	ABCC-attached PGL1155 surfaces
PGL1840-MA	MA-attached PGL1840 surfaces
PGL1840-PDMAA	PDMAA-attached PGL1840 surface
PGL1840-PFB	PFB-attached PGL1840 surfaces
PGL1840-PHDFDA	PHDFDA-attached PGL1840 surface
PGL1840-PMAA	PMAA-attached PGL1840 surface
PGL1840-PMMA	PMMA-attached PGL1840 surface
PGL1840-PS	PS-attached PGL1840 surface
SAIMs	self-assembled azo-initiator monolayers
SAMs	self-assembled monolayers
TiO_2	titanium dioxide
TiO_2-ABCC	ABCC-attached TiO_2 surfaces
TiO_2-ADS	ADS-attached TiO_2 surfaces
TiO_2-AEP	AEP-attached TiO_2 surfaces
TiO_2-MPS	MPS-attached TiO_2 surfaces
TiO_2-PMMA	PMMA-attached TiO_2 surfaces

b	broad
d	doublet
s	singlet
m	multiplet
t	triplet
q	quadruplet

1 Introduction

1.1 Historical perspective

Color plays an important role in our lives. For example, in relishing food we eat or in choosing the quality of fruits or vegetables by the richness of their color. It also influences our moods and emotions. Color can be divided into *natural color*, which is around us, in the earth, sky, sea etc. and *synthetic color* which is used in textiles, paints, plastics, in a wide range of multicolored printed materials such as posters, magazines, ceramics and cosmetics. Colorant, on the other hand, can be classified into *dyes* and *pigments*[1,2].

The use of color from natural resources has been known since prehistoric times (> 30 000 years ago), for example, in decorating their bodies, in coloring the furs and skins that they wore and in the painting of cave dwellings[1]. The dyes used to color clothing were commonly extracted either from vegetable sources including plants, trees, seeds, fruit skins etc., or from animal sources such as crushed insects and mollusks. The pigments for the paints were obtained form colored minerals such as ochre, haematite and other mineral-based pigments[3].

One of the most important natural dyes, which has been used over the centuries, is indigo (s. Figure 1-1a) obtained both from dyer's woad, a plant extract in Europe, and from *Indigofera tinctoria*, a native plant of Asia. A related product is Tyrian purple (6,6´-dibromoindigo, s. Figure 1-1b), which was extracted from the glands of *Murex brandaris*, a shellfish found on the Mediterranean and Atlantic coasts[2].

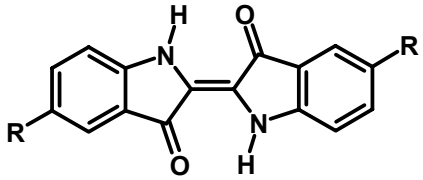

a) R = H → Indigo blue dye

b) R = Br → Tyrian purple dye

Figure 1-1: Chemical structure of a) Indigo blue and b) Tyrian purple dye.

The most important of the natural red dyes was Alizarin (1,2-dihydroxyanthraquinone; s. Figure 1-2) obtained from madder Campeachi wood extract imported from Africa[1].

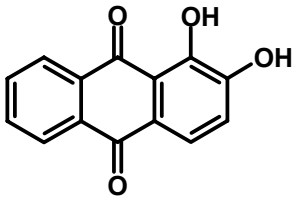

Figure 1-2: Chemical structure of 1,2-dihydroxyanthraquinone (Alizarin).

Synthetic colorants were developed by the ancient Egyptians and used in paints for many thousands of years. The earliest synthetic pigments were Alexandra blue, a ground glass colored with a copper ore, and Egyptian blue, a mixed silicate of copper and calcium, which has been identified in mural painting dating from around 1000 BC[1]. The oldest synthetic colorant still used today is Prussian blue (Berlin Blue), hydrated iron(III) hexacyanoferrate(II) ($Fe_4[Fe(CN)_6]_3 \cdot nH_2O$)[3].

The first synthetic dye was picric acid (s. Figure 1-3) obtained by P. Woulfe in 1771 by treating indigo with nitric acid[1]. A more efficient synthetic procedure to obtain picric acid using phenol as the starting material was developed many years later. This dye was used for dying silk giving a bright greenish-yellow. However, it did not achieve any commercial significance because of the lack of lightfastness[1], i.e. low light stability.

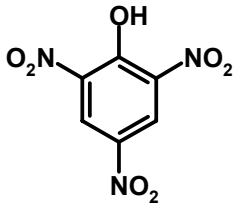

Figure 1-3: Chemical structure of picric acid.

The foundation of the synthetic dye industry is attributed to William Henry Perkin by his discovery in 1856 of a purple dye known as Mauve (s. Figure 1-4)[1,2]. At the beginning, the structure of Mauve was believed to be as compound a in Figure 1-4. An analytical investigation of an original sample recently showed that the dye rather is a mixture of compounds b and c. Perkin found that the crude compound produced an intense bluish purple solution with methanol and that it dyed silk in a rich color which did not wash out nor fade upon exposure to sunlight over a week. He decided to patent his discovery and to manufacture it commercially. The production started in 1857[1].

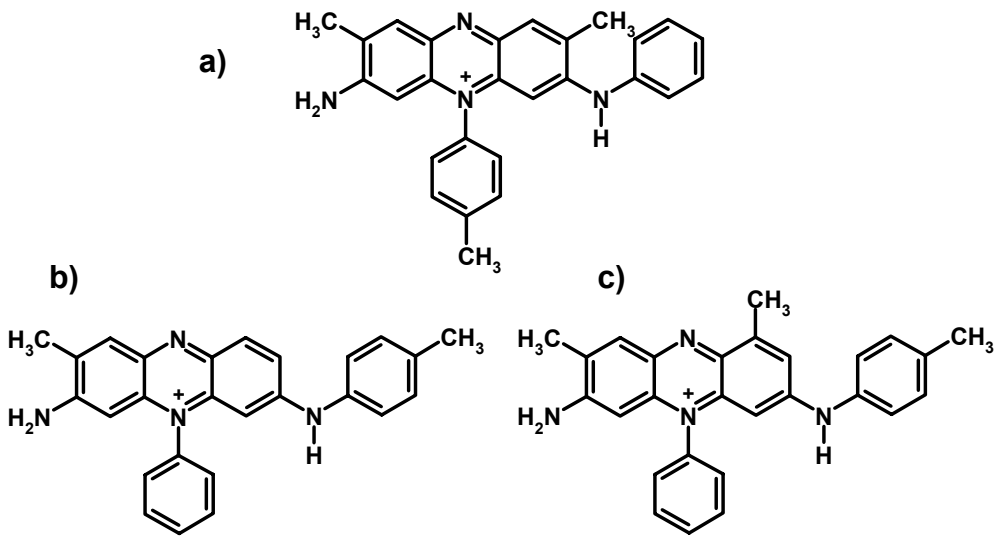

Figure 1-4: Chemical structure of Mauve dye.

In 1858, P. Griess demonstrated that the treatment of an aromatic amine with nitrous acid gave rise to an unstable salt (a diazonium salt)[1]. This salt could be used to prepare a colored compound. The first commercial azo dye was 4-aminoazobenzene (Aniline Yellow; s. Figure 1-5a), although it proved to have quite poor dyeing properties. A much more successful commercial product was Bismarck Brown (original named Manchester Brown; s. Figure 1-5b), which was introduced commercially in 1861[1]. Figure 1-5c shows the first commercial Disazo dye (Biebrich Scarlet), which was developed in 1879[1].

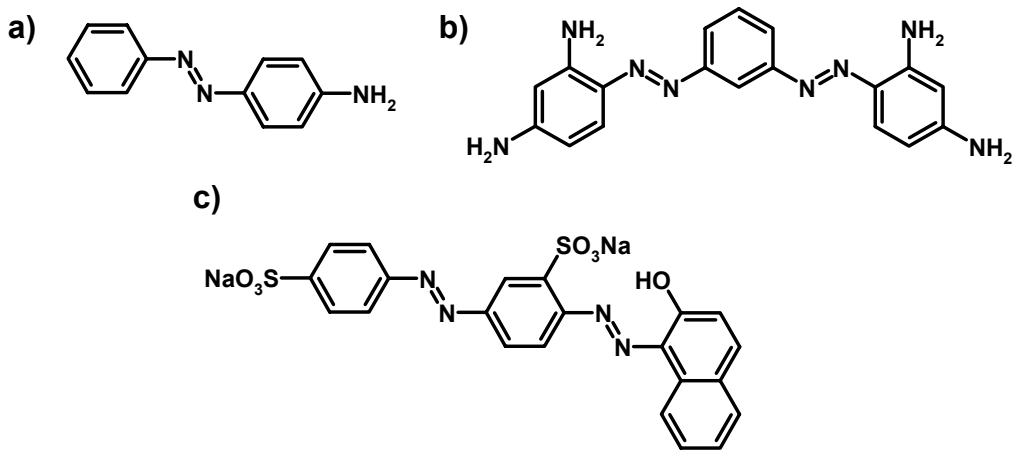

Figure 1-5: Chemical structure of azo dyes: a) Aniline Yellow, b) Bismarck Brown and c) Biebrich Scarlet.

In the late 19th century, a range of organic pigments was developed, especially for paint application. Initially, most of these pigments were obtained from water-soluble textile dyes. For example, anionic dyes were precipitated onto inert colorless inorganic substrates such as alumina and barium sulfate to give insoluble pigments. Such products were commonly referred as *lakes*[1].

The first water insoluble organic pigments were the red β-naphthol pigments (1885), which did not contain substituents (acidic or basic groups) capable of salt formation. In 1909, Hansa Yellow (s. Figure 1-6) was introduced to the market as the first monoazo yellow pigment. The first red Naphthol AS pigment was synthesized in 1912. Figure 1-7 shows a general structure of a numerous azo pigments[4].

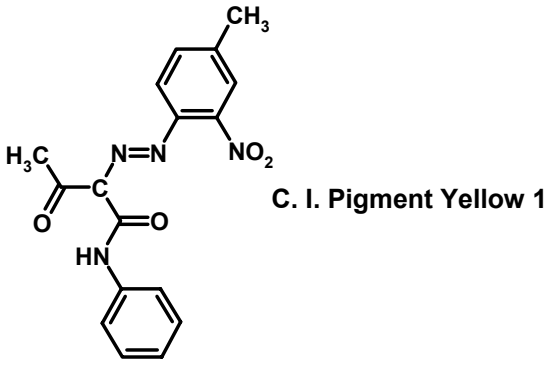

Figure 1-6: Chemical structure of Hansa Yellow.

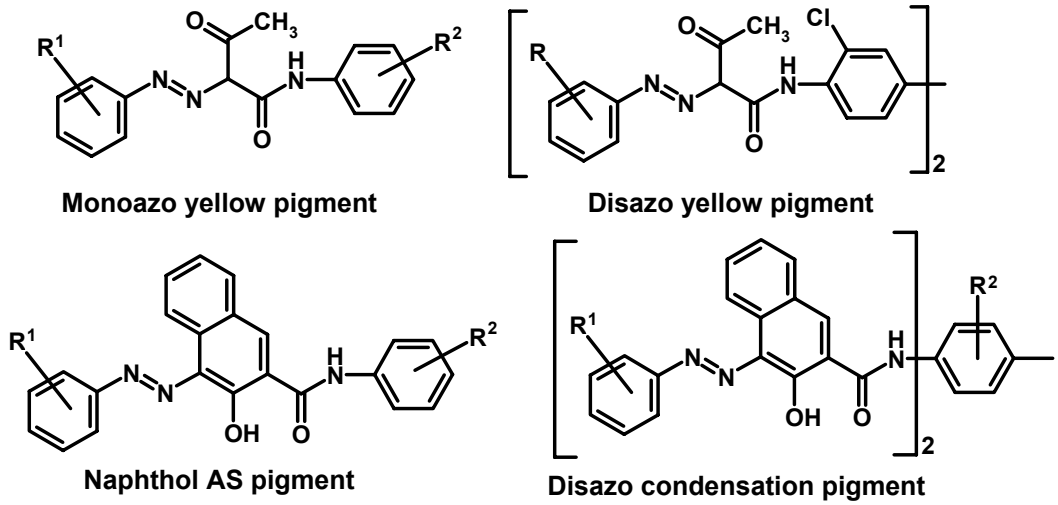

Figure 1-7: General structure of mono- and disazo pigments: R, R^1 and R^2 represent various substituents.

In 1928, the discovery of copper phthalocyanine (s. Figure 1-8a), a blue pigment, which offers excellent intensity and brightness comparable to many inorganic pigments, stimulated the development of a range of high-performance organic pigments[4] such as quinacridones, isoindolines, perylenes, diketopyrrolo pyrroles and antraquinones which are shown in Figure 1-8b-f.

The study on many high-performance pigments surface modifications as well as the application of polymeric dispersants to improve rheological characteristics of modern high-solids solventborne pigment dispersions have been reported[5]. In addition, surface modification of pigments and the use of compatible polymeric dispersants have made an important contribution toward lowering paint viscosities[6]. The surfaces of the pigments such as anthraquinones (AQ), and diketopyrrolo pyrroles (DPP) were treated with an anchor group containing acidic moiety[6]. After surface treatment, they were dispersed in the polymeric dispersants such as tertiary amino functions of aromatic or non-aromatic character on a polyurethane chain. It was shown that the combination of a surface modified pigment with an appropriate polymeric surfactant could inhibit the reagglomeration and subsequent flocculation of individual pigment particles. As a result, the surface treatment of the pigments show a significant lowering effect of the viscosity compared to unmodified pigment.

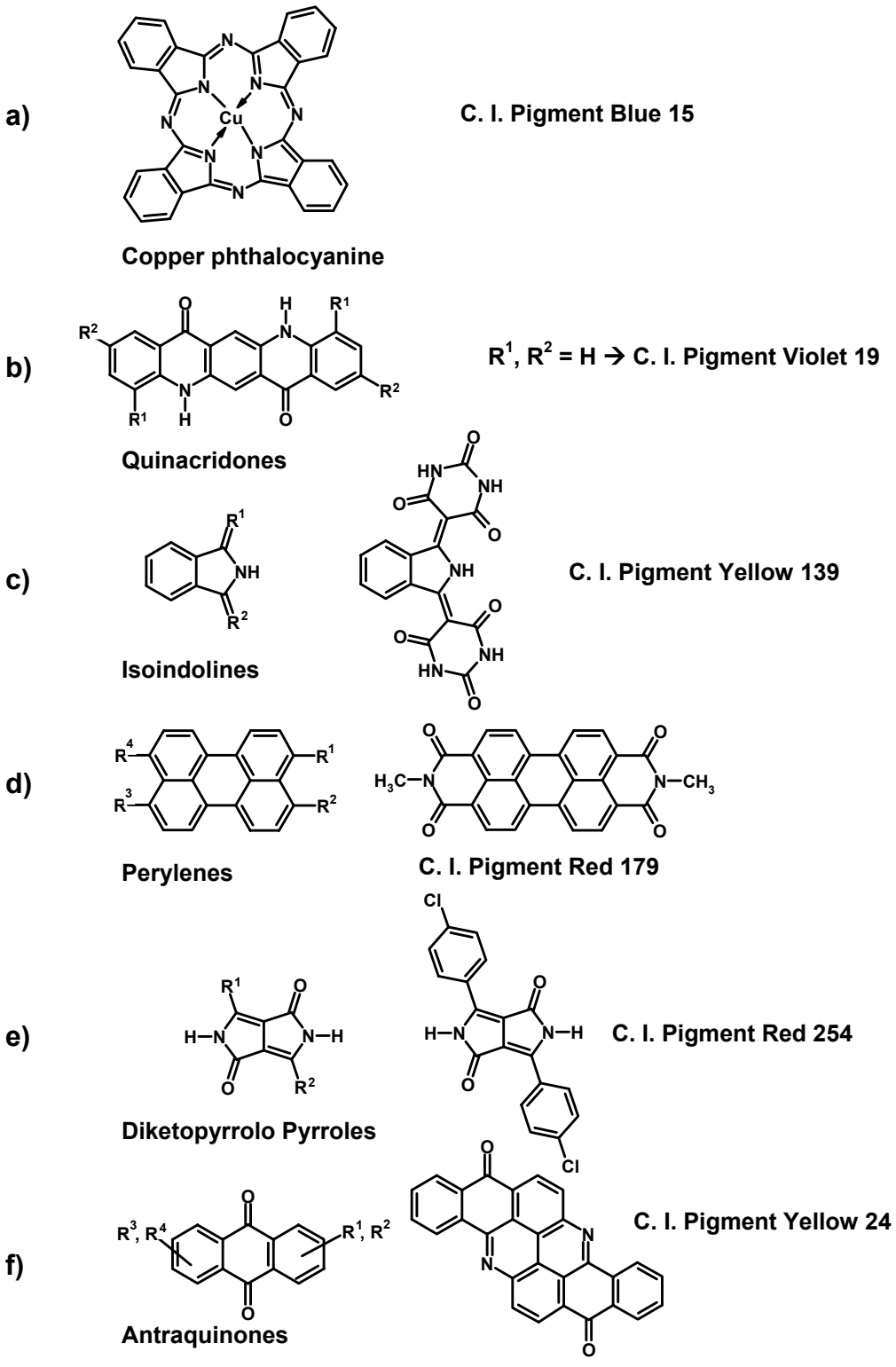

Figure 1-8: Chemical structures of some high-performance organic pigments: a) copper phthalocyanine b) quinacridones, c) isoindolines, d) perylenes, e) diketopyrrolo pyrroles and e) anthraquinones: R^1, R^2, R^3 and R^4 represent various substituents.

The inorganic pigment industry started in the 18th century with products such as Berlin blue (1704), cobalt blue (1777), Scheele's green and chrome yellow (1778)[3]. In the 19th century ultramarine, Guignet's green, cobalt pigments, iron oxide pigments and cadmium pigments were developed. In the past few decades, the synthetic colored pigments such as cadmium red, manganese blue, molybdenum red and mixed oxides with bismuth came onto the market[3].

Titanium dioxide was also introduced in the 19th of the past century as new synthetic white pigment. The natural abundant modifications of titanium dioxide (TiO_2) are rutile, anatase and brookite[3,7]. However, brookite is difficult to produce, therefore, rutile and anatase are more important for industrial production. TiO_2 is the most important white pigment compared to all other white pigments such as zinc white (ZnO) or white lead (basic lead carbonate) because of its high degree of opacity and whiteness (maximum light scattering with minimum light absorption)[3]. It also shows excellent durability and non-toxicity. TiO_2 is chemically very stable and is not attacked by most organic and inorganic reagents. Nevertheless, it dissolves in concentrated sulfuric acid and in hydrofluoric acid. TiO_2 pigment is commonly used in paints, coatings and printing ink as well as in plastic industry and fibers. Due to the high demand and the fact that there is not enough natural rutile, it is steadily being replaced by the synthetic variety. The worldwide production of TiO_2 pigment as well as the synthetic processes is shown in Table 1-1. The largest producers are located in Australia, the Republic of South Africa and Sierra Leone[8].

Table 1-1: World production and synthetic processes of TiO_2 pigment[9-11].

Year	Sulfate process		Chloride process		Total
	[10^3 t/a]	%	[10^3 t/a]	%	[10^3 t/a]
1965	1254	90.3	135	9.7	1389
1970	1499	77.4	437	22.6	1936
1977	1873	72.3	716	27.7	2589
1988	1781	60.2	1178	39.8	2959
1995	1481	46.0	1739	54.0	3220
2000*	1540	40	2310	60.0	3850

* estimated.

The surface modification of TiO_2 is of great interest due to its importance for medical implants, catalysis and photocatalysis, polymer fillers and so forth. Reactions of monofunctional silanes (R_3SiX)[12], tri- and tetrafunctional silane coupling agents[13-16] and

various functionalized $RSi(OEt)_3$[17-21] as well as organosilicon hydrides ($RSiH_3$)[15,22,23] with the surface of oxidized titanium and titanium dioxide have been published.

The surface modification of TiO_2 particles with phosphonic acids $RPO(OH)_2$ is currently an attractive growing interest for numerous applications such as self-assembled monolayers[24-26], ceramic membranes[27], and enzymatic catalyses[28]. The P–C bond is stable against hydrolysis to the same extent as the Si–C bond and the versatile phosphorus chemistry gives access to a wide range of functional organic groups. The stability of P–O–M bonds has been illustrated by the numerous metal phosphate and phosphonate compounds reported in the last 20 years[29,30].

1.2 Dyes and pigments

Dyes and pigments are used commercially for large-scale coloration purposes, i.e. dyeing of textile fibers, for pigment coloration of e.g. plastic, paints and printing ink. Both are commonly supplied by manufacturers as colored powders. They may have a quite similar chemical structure. The difference between these two types of coloring agents is, however, their solubility.

Dyes are substrates, which are soluble in the application medium, mostly in water. Frequently, dyes such as acid dyes and cationic dyes dissolve completely and easily in water and are applied from this dissolved state. However, water solubility is not a requirement for every textile dye application. For example, vat dyes for the cellulosed fibers are in the as obtained state completely insoluble in water. However, a chemical reduction process can convert them into a water-soluble form, which may then be applied to the fibers[2]. There are also non-textile applications of dyes especially in the electronic and reprographic industries. These dyes are preferably dissolved in specific organic solvents[2].

In contrast, pigments are finely divided solid coloring materials, which are essentially insoluble in the application medium. Pigments are applied into a medium by a dispersion process in which clusters or agglomerates of pigment particles are broken down into primary particles and/or small aggregates. However, they do not dissolve in the medium, i.e. they are still solid particles held in place mechanically, usually in a polymer matrix[4].

Pigments are required to show solvent resistance to minimize problems such as bleeding and migration. However, most organic pigments exhibit a least a limited solubility, typically a few mg l^{-1} in polar organic solvents[2].

In contrast to dyes that must possess a specific affinity to the substrates for which they are used, pigments only need to have a weak affinity for the surrounding matrix as only the surface of the pigment particle is in contact with the medium.

In the Color Index (C. I.), each dye or pigment is given two reference numbers on the basic of the colorist and the chemical classification, respectively[31]. One refers to the area of application and method of coloration; it is called the C. I. Generic Name (e.g. C. I. Pigment Yellow 185 for isoindoline[32]). The other is termed the C. I. Constitution Number (e.g. C. I. 56280 for isoindoline[32]). Under the C. I. Generic Name, all commercial dyes or pigments are mentioned which have the same chemical structure. They should not be called identical as they may differ significantly with respect to crystal structure (important for pigments), particle size (pigments, disperse and vat dyes), additives and impurities (all dyes and pigments)[2].

1.3 Pigments for special effects

Pigments for special effects such as metallic, pearlescent and fluorescent pigments are used for their ability to produce unusual optical effect[1]. The most important metallic pigment is aluminium flake (C. I. Pigment Metal 1), which is used in car finishes, in printing ink and plastic applications. This pigment exhibits a high reflection and stability due to the thin, tenacious oxide film on the pigment surfaces. Pearlescent pigments give rise to a white pearl effect often accompanied by a colored iridescence. The most important these pigments consist of thin platelets of mica coated with titanium dioxide, which partly reflect and partly transmit incident light. These pigments are used mainly in automotive finishes, plastics and cosmetics. Fluorescent pigments consist of fluorescent dyes dissolved in a transparent and colorless polymer. These pigments are mostly based on a toluenesulfonamide-melamine-formaldehyde resin matrix. The pigments are mostly applied in advertising and in the field of safety due to their extremely high visibility and their ability to attract attention.

1.4 Properties of pigments

The properties of pigments, such as their shade, color strength, dispersibility, and flowability, depend on their chemical composition and on physical properties such as crystallinity, particle size, size distribution and surface characteristics[3,4].

1.4.1 Chemical properties of organic pigments

Commercial organic pigments display variable fastness properties, which are dependent either on the molecular structure or on the nature of the intermolecular association in the solid state.

The *hue* refers to a system of conjugated double bonds that is responsible for the absorption of visible light. These colors are due to $\pi \rightarrow \pi^*$ electronic transitions associated with extensively conjugated aromatic systems. The chemical constitution of the pigment, especially the substitution pattern of the coupling component, determines the basic color of a pigment. In contrast, the different shades within this color are influenced by physical characteristics (crystal geometry, particle size and shape, and particle size and distribution, etc.).

For example, azo pigments provide a shade ranging from greenish yellow to orange, red, blue, violet and brown depending on the substituents on the azo pigment: electron donors are more bathochromically active than electron acceptors. Figure 1-9 shows the chemical structure of the chlorinated derivatives of Pigment Red 9 (R = H) and Pigment Brown 1 ($R = OCH_3$)[4].

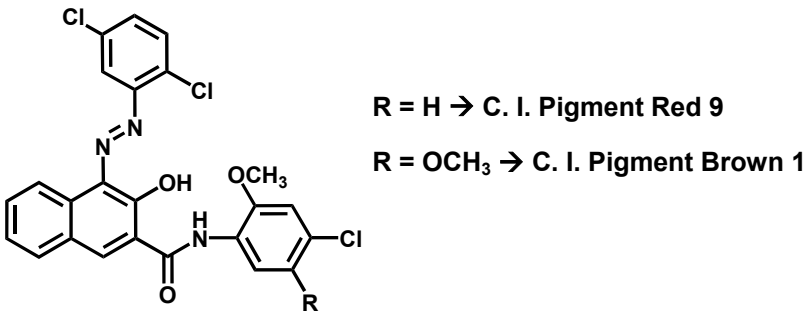

Figure 1-9: Chemical structure of Naphthol AS Pigments: chlorinated derivatives of Pigment Red 9 (R = H) and Pigment Brown 1 ($R = OCH_3$)[4].

The almost completely planar structure of the red pigment is distorted in the brown pigment by an addition of a methoxy group forcing the molecule out of the molecular plane. Therefore, not only the conjugation pattern gets interrupted, but also the entire crystal geometry is changed as shown in Figure 1-10[4].

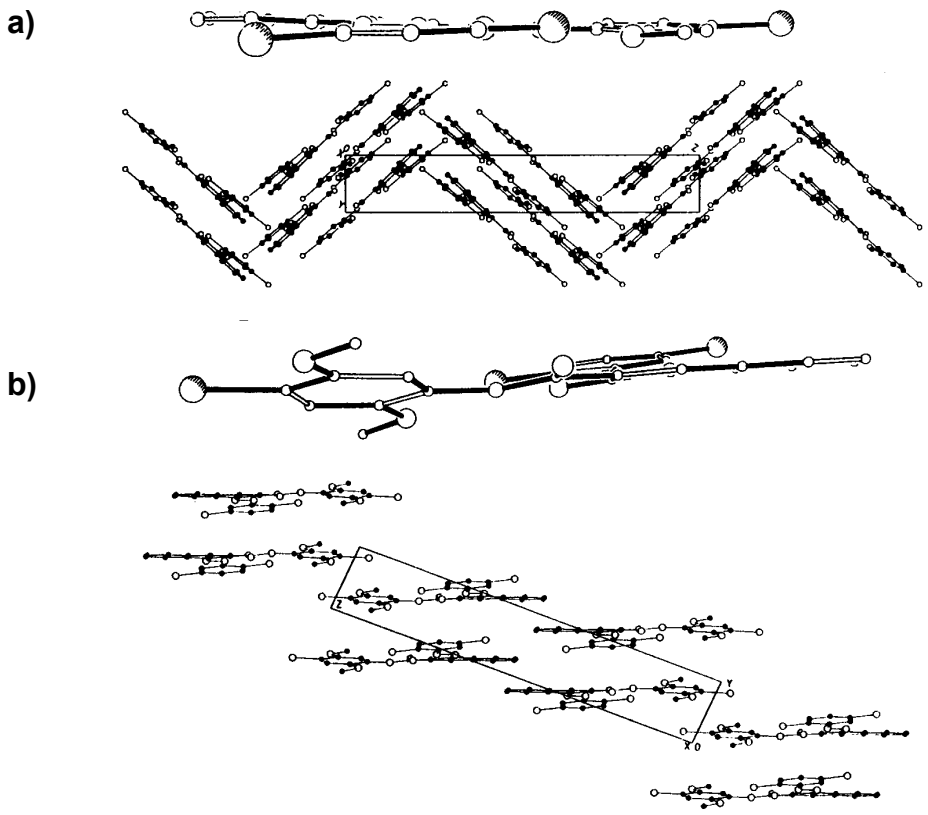

Figure 1-10: Three dimensional X-ray diffraction of a) Red and b) Brown Naphthol AS Pigment: single unit (above) and with in the crystal lattice (below)[4].

Hydrogen bonds are an important feature of some organic pigments: intramolecular hydrogen bonding enforces planarity in a molecule and intermolecular hydrogen bonding may play an important role in determining the basic color of a pigment. For example, Quinacridones depend on hydrogen bonds to define their crystal structure during crystal formation[4]. The synthesis of this pigment yields a crude α-quinacridone, which does not show sufficient fastness. This modification, however, can be converted to a β- or γ-phase by using different organic solvents. Nonpolar solvents generally give the β-modification (violet), while polar solvents can produce the γ-phase (red). Both modifications exhibit much higher fastness against light and weather than the α-phase.

The *tinctorial strength* of a pigment defines its tendency to absorb light and the molar extinction coefficient (ε_{max}) can be used to estimate this property. However, it also depends on physical parameters. A higher degree of conjugation is associated with a bathochromic shift, i.e. color strength improves with the intensity of absorption. An extension of electron delocalization can be achieved by enhancing the aromaticity of a polycyclic pigment, a transition from monoazo to disazo compounds, by promoting planarity in a molecule or introducing π-electron species into the conjugated part of a pigment molecule.

As mentioned above, the ideal pigment is practically insoluble in its matrix. However, many organic pigments do not fulfill this requirement completely for all given applications. Dissolved pigment may then migrate to the surface of the matrix or into neighboring material. These processes are termed bleeding and blooming[4]. The chemical structure can influence the solvent and migration resistance. Increasing the molecular weight of the pigment, avoiding solubilizing substituents (long-chain alkyl, alkoxy, or alkylamino as well as sulfonic acid functions), the formation of insoluble polar salts or metal complexes can help to reduce solubility[4]. Furthermore, amide (-NHCO-) groups enhance fastness not only against solvent, but also against light and heat due to strong dipolar interactions and hydrogen bonding (intramolecular and intermolecular). Incorporation of halogen substituents and of metal ions, especially of the earth alkaline and transition metal ions, can also improve the fastness of a pigment[1].

1.4.2 Chemical properties of inorganic pigments

Most inorganic pigments are oxides, sulfides, oxide hydroxides, silicates, sulfates or carbonates[3]. Normally, they are single-component particles, e.g. red iron oxide (α-Fe_2O_3) with well defined crystal structures. However, mixed and substrate pigments are also commercially used. Inorganic pigments can be classified from various points of view as shown in Table 1-2.

The most important inorganic pigments are white pigments (titanium dioxide), black pigments (carbon black) and colored pigments such as metal oxide (iron and chromium), cadmium sulfides, lead chromates, ultramarine and Prussian blue[3]. Most inorganic pigments are crystallized in the following forms:

- cubic: zinc blende lattice (e.g. precipitated CdS), spinel lattice (e.g. Fe_3O_4, $CoAl_2O_4$)
- tetragonal: rutile lattice (e.g. TiO_2, SnO_2)
- rhombic: goethite lattice (e.g. α–FeOOH)
- hexagonal: corundum lattice (e.g. α–Fe_2O_3, α–Cr_2O_3)
- monoclinic: monazite lattice (e.g. $PbCrO_4$)

The cause of the color of inorganic pigment is mostly due to the charge transfer transitions. The electron can be transferred either from ligand to metal (e.g. in lead chromates; $PbCrO_4$) or between two metals of different oxidation states (e.g. in Berlin blue). The blue color of Berlin Blue ($\overset{+III}{Fe}_4[\overset{+II}{Fe}(CN)_6]_3 \cdot nH_2O$) is due to electron transfer from Fe(II) atom to a neighboring Fe(III) atom[7]. In contrast, the color of ultramarines ($Na_4[Al_3Si_3O_{12}]S_n$) is based on radical anions trapped in the crystal lattice, e.g. the radical anion S_3^- responses for the blue color of the ultramarine pigment[7].

Table 1-2: Classification of inorganic pigments[3].

Term	**Definition**
white pigments	the optical effect is caused by nonselective light scattering (e.g. titanium dioxide, zinc sulfide pigments)
colored pigments	the optical effect is caused by selective light absorption and also to a large extent by selective light scattering (e.g. iron oxide red and yellow, cadmium pigments)
black pigments	the optical effect is caused by nonselective light absorption (e.g. carbon black pigments, iron oxide black)
luster pigments	the optical effect is caused by regular reflection or interference
metal effect pigments	regular reflection takes place on mainly flat and parallel metallic pigment particles (e.g. aluminum flakes)
nacreous pigments	regular reflection takes place on highly refractive parallel pigment platelets (e.g. titanium dioxide on mica)
interference pigments	the optical effect of colored luster pigments is caused fully or mainly by interference phenomena (e.g. iron oxide on mica)
luminescent pigments	the optical effect is caused by the capacity to absorb radiation and emit it as light of a longer wavelength
fluorescent pigments	light of longer wavelength is emitted after excitation without a delay (e.g. silver-doped zinc sulfide)
phosphorescent pigments	light of longer wavelength is emitted within several hours after excitation (e.g. copper-doped zinc sulfide)

1.4.3 Physical properties

Pigments are required to exhibit an appropriate range of fastness characteristics. *Fastness properties* refer to the ability of pigment to resist color changes when exposed to certain conditions such as light, weather, heat, solvent or to chemicals such as acids and bases[1,4].

Pigment properties can be optimized by adjusting physical parameters like the geometry of the unit cell, the crystal lattice pattern and crystal shape. However, little is known about the relation between chemical constitution and lightfastness or weatherfastness of pigments. Various pigments can undergo similar degradation upon exposure to light, regardless of whether they are crystalline or in solution. As a result, the surrounding medium can also interfere with the stability of a pigment to light.

Pigments are morphologically described by a standardized terminology[33]: single or primary particles, aggregates or agglomerates (s. Figure 1-11). The optimum particle size is called the primary pigment particles. The particle size of the pigment can influence the rheological properties and the opacity.

Figure 1-11: Types of pigment particles: primary particles, agglomerates and aggregates according to DIN 53 206[33].

Primary particles are an individual unit that can have any shape or structure. Typical shapes are cubes, platelets, needles, bars but also irregular shapes.

Agglomerates are groups of single crystals and/or aggregates, joined at their corners and edges but not grown together. A dispersion process can separate them. The total surface area of the agglomerate may not differ from the sum of the surfaces of the individual particles.

Aggregates are primary particles that are grown together at their surfaces. The total surface area of an aggregate is smaller than the sum of the surfaces of the individual particles. Dispersion processes do not break aggregates.

Flocculates are referred to an assembly of wetted crystallites and/or aggregates or smaller agglomerates in a suspension (e.g. in pigment-binder system). Flocculates are mechanically more labile than agglomerates and can usually be broken up by weak shear forces, e.g. during stirring.

Polymorphous pigments are pigments, which occur in more than one modification or crystal structure. The identical chemical composition may differ in the arrangement within the crystal lattice. Some example, copper phthalocyanine blue forms at least five morphologies (α, β, γ, δ, ε), quinacridone pigments and various azo pigments display at least three different modifications[4] as well as in some inorganic pigment such as titanium dioxide which can be crystallized in rutile, anatase or bookite modification[7]. The modification occurred depends on the thermodynamic stability. The transformation from an unstable modification into a stable one may need a certain amount of activation energy, e.g. the anatase can be rapidly converted to the more stable form rutile by heating over 700 °C[7]. Also, such a series in different solvent systems has been studied for the three modifications of Pigment Red 1[4]. X-ray diffraction analysis is the most important technique to determine the crystal modification.

Pigment *dispersion* refers to the distribution of a pigment throughout a matrix accompanied by a reduction of the agglomerate size to afford primary particles and aggregates or at least smaller agglomerates. The dispersion process serves four purposes[3]:

- *desagglomeration*: agglomerates are broken down through mechanical shearing forces.
- *wetting*: the surface of the pigment particle is wetted by binder and by other components of the medium.

- *distribution*: the resulting wetted pigment particles are distributed throughout the entire medium.
- *stabilization*: the dispersed solids are stabilized to prevent reagglomaration and/or flocculation.

The chemical interaction between the pigment and the medium strongly influences the wetting of the pigments as they are incorporated into the medium. Favorable interaction between the pigments and the medium are a requirement for a good dispersion. The morphology of the pigment particles also influences the dispersion characteristics of agglomerates[34].

The particle size distribution that can vary from batch to batch can be determined by sedimentation techniques in ultracentrifuges and specialized disk centrifuges as well as by electron microscopy[3]. The measurement depends largely on sample preparation and especially on the quality of the dispersion. The important physical properties and particle size analysis techniques are summarized in Table 1-3.

Table 1-3: Particle size, particle size distribution and characteristic quantities[35].

Term	**Definition**
particle size	geometrical value characterizing the spatial state of a particle
particle diameter D_{eff}	diameter of a spherical particle or characteristic dimension of a regularly shaped particle
equivalent diameter D	diameter of a particle that is considered as a sphere
particle surfaces S_T	surface area of a particle: a distinction is made between the internal and external surface areas
particle volume V_T	volume of a particle: a distinction is made between effective volume (excluding cavities) and apparent volume (including cavities)
particle mass m_T	mass of a particle
particle density Q_T	density of a particle
particle size distribution	statistical representation of the particle size of a particulate material
distribution density	gives the relative amount of a particulate material in relation to a given particle size diameter. Density distribution functions must always be normalized
cumulative distribution	normalized sum of particles that have a diameter less than a given particle size parameter
fraction and class	a fraction is a group of particles that lies between two set values of the chosen particle size parameter that limits the class
mean value and other similar parameters	the mean values of particle size parameters can be expressed in many ways, some values are used frequently in practice
distribution spread	parameter for characterizing the non-uniformity of the particle size

1.5 Surface treatments of pigments

As mentioned above, the properties of pigments, such as the color strength and the dispersibility depend on their chemical structure and on physical properties. Surface treatments are commonly used to improve the quality of pigment formulations. To improve the properties of solid oxides as well as those of pigment particles such as dispersibility, weathering or the stability against chemicals such as acids and alkalis, different synthetic strategies to coat the particle surfaces with polymer monolayers were developed.

1.5.1 Physisorption

The adsorption of synthetic polymers onto the surfaces of particles is one of the important methods of surface modification of pigments. The good dispersibility of pigments treated with synthetic polymers is largely due to the fact that polymer chains, adhering to the pigment surface, prevent pigment particles from agglomerating via steric stabilization[36-40]. The preparation of the polymer adsorbed to the pigment surfaces can be achieved easily by suspension of pigments in the polymer solution and subsequent filtration.

Recently, Schaller et al.[41,42] have investigated the pigment-polymer interaction by using copolymers with different molecular architecture consisting of polar and relatively non-polar residues as well as the adsorption mechanism of these copolymers, e.g. the interaction of inorganic oxide particles (TiO_2, Al_2O_3, SiO_2 and ZrO_2) with poly(styrene-*b*-acrylic acid), poly((meth)acrylic acid-*g*-styrene) and acrylic acid/isobutene copolymer.

The stabilization of carbon black dispersions with siloxane surfactants, consisting of a poly(dimethylsiloxane) backbone with grafted polyether chain, used as pigment in black ink, was studied by Lin and coworker[43]. Surfactants are expected to adsorb onto the carbon black particles with their hydrophobic parts and extend their hydrophilic parts into the aqueous medium to yield steric stabilization.

The surface treatment of copper phthalocyanine blue (C. I. Pigment Blue 15:3) by adsorption with poly(ethylene glycol)s (PEG) of various molecular weights was reported[44]. PEG can improve the wettability of pigments in aqueous media. The effect of surface treatment depends largely on the molecular weights and on the amount of adsorbed PEG.

1.5.2 Chemisorption

However, physisorption processes are equilibrium processes and adsorption and desorption to and from the surfaces occur[45]. In addition, the displacement of the macromolecules by low molecular weight substrates was also observed[46].

Due to these disadvantages, the modification of the solid surfaces with polymers which are covalently attached to the surfaces has been investigated by various research groups[47-58]. Polymer monolayers can be formed on the surface of solid oxides, such as silica and various inorganic pigments, either by polymerization reactions carried out on the solid surfaces via surface-attached initiator, surface-attached monomers incorporated into polymer chains growing in solution or by reaction of reactive hydroxyl groups on the substrate with chemically active functional groups of the polymers[47,49,51-53,57,59-61] as shown in Figure 1-12.

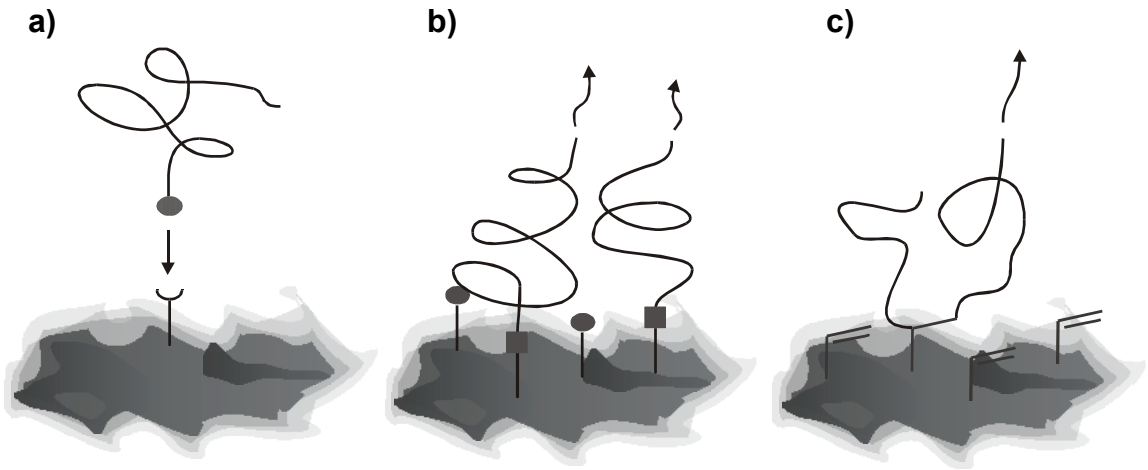

Figure 1-12: Grafting of polymers onto surfaces: a) "grafting-to" via reaction of end-functional groups of a polymer chain with reactive site on the substrate, b) "grafting-from" via surface-bound initiating groups which can trigger growth of a polymer chain and c) grafting of polymers via surface-bound monomer.

1.5.2.1 Attachment of the polymer chains containing terminal functional groups

In "grafting-to" processes (s. Figure 1-12a), the polymer chain carrying end-functional groups are reacted to suitable functional groups on the substrate surfaces[47,62-69]. Typical systems are polymer chains containing chloro- or alkoxysilane groups which are coupled to hydroxyl groups on the solid surfaces[47,48,50,62,66,68]. Termination reaction of living polymer chains onto active groups on the surfaces were also reported[47,63-65,70].

For organic pigments, the grafting of polymers to amino groups (quinacridone: QD, diketopyrrolo pyrrole: DPP, anthraquinone: AQ; s. Figure 1-13) has been reported[70]. The amino groups of QD, DPP, and AQ can react with living poly(isobutyl vinyl ether) (poly(IBVE)) and poly(2-methyl-2-oxazoline) cations. By grafting poly(IBVE) onto QD surface, the nature of the surface changes from hydrophilic to hydrophobic. However, the number of the grafted polymer chains on the organic pigment surface decreased with increasing molecular weight of the living polymer, due to steric hindrance. As a result, only rather thin films (3 – 5 nm)[71,72] can be formed by this technique.

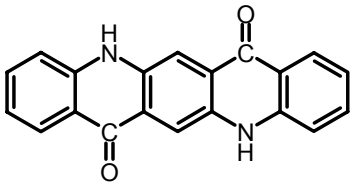

Quinacridone (QD)

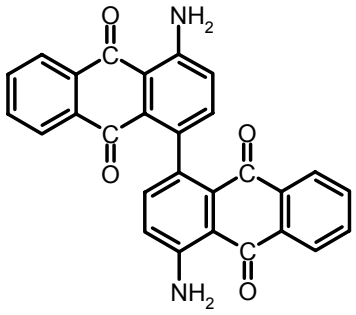

Anthraquinone (AQ)

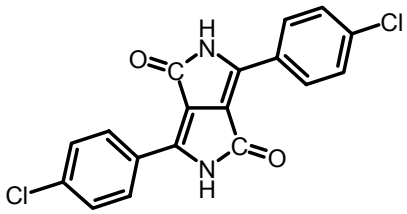

Diketo–pyrrolopyrrole (DPP)

Figure 1-13: Chemical structure of Quinacridone (QD), Anthraquinone (AQ), and Diketopyrrolo pyrrole (DPP).

1.5.2.2 Grafting polymerization using surface-attached initiating groups

Due to the low graft density and low thickness of the polymer films obtained by grafting-to techniques, surface-initiated polymerization reactions have attracted considerable attention in recent years. By this technique, the initiating groups can be ionic species (anionic or cationic) to generate the living polymerization[73-79], or azo groups to start a free radical polymerization process[47,52-55]. In contrast to a "grafting-to", only monomer molecules have to diffuse to the surfaces and, therefore, high graft densities of the attached polymers and controllable layer thicknesses are available.

Tsubokawa and co-workers have reported that the anionic, cationic and radical polymerization of various monomers can successfully be initiated by potassium carboxylate[80], acylium[81], benzylium perchlorate[82,83], peroxyester[84], and azo groups[83,85] introduced to inorganic particle surfaces of silica, titanium dioxide and carbon black. They also attempted to graft polymer onto organic pigments containing suitable functional groups for free radical[55,56] and anionic ring-opening[56] polymerization.

The introduction of azo groups and trichloroacetyl groups onto inorganic particle surfaces was achieved by the reaction of the surface hydroxyl groups with 4,4'-azobis(4-cyanopentanoic acid) and trichloroacetyl isocyanate respectively (s. Figure 1-14). The trichloroacetyl groups can be immobilized to the surfaces in one step (s. Figure 1-14b) and to silica surfaces in two steps (s. Figure 1-14c). The radical polymerization of vinyl monomers initiated by azo groups onto Ti/Si-R-OH (polymethylsiloxane-coated titanium dioxide modified with alcoholic hydroxyl groups)[60] (s. Figure 1-14a) and by the system consisting of trichloroacetyl groups on inorganic particle surfaces and $Mo(Co)_6$[60,61] (s. Figure 1-14d) have been reported. Investigations of the wettability of polymer modified surfaces and of the stability of dispersions are also reported.

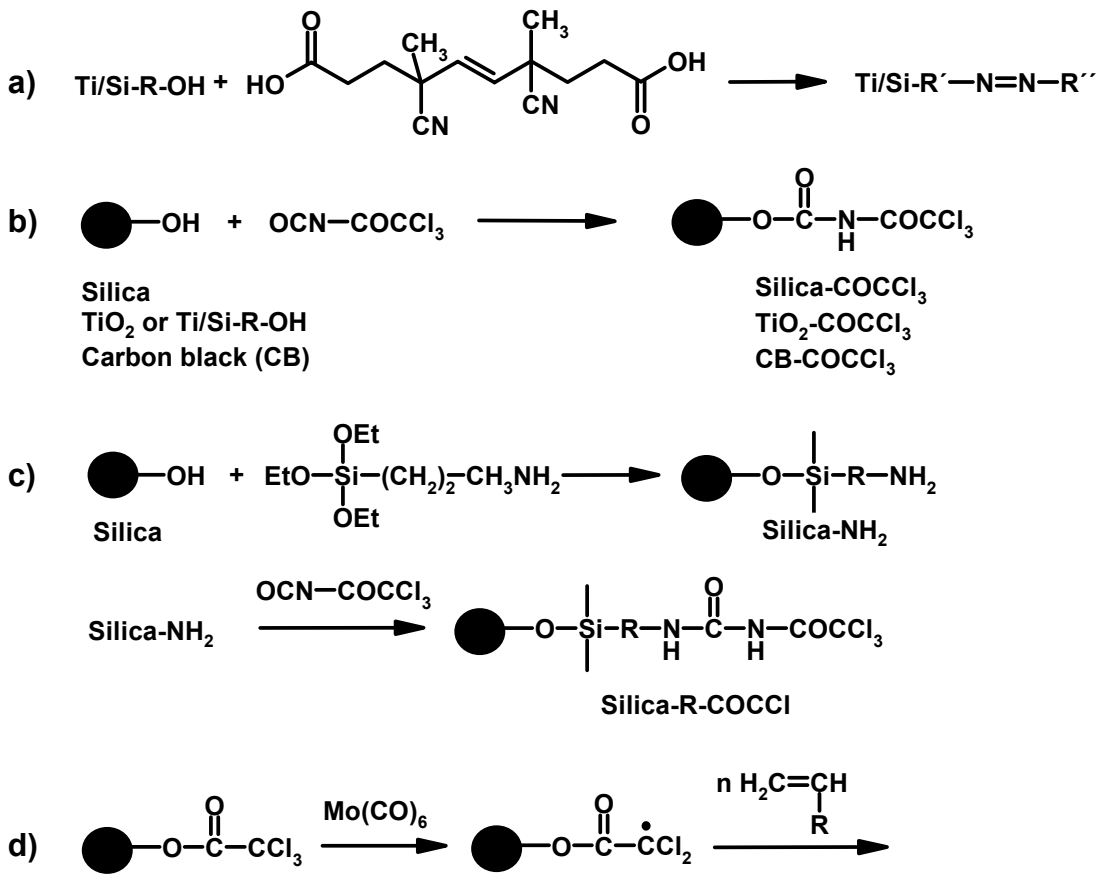

Figure 1-14: Graft polymerizations of vinyl monomers onto silica, titanium dioxide and carbon black surfaces initiated by systems containing azo groups or trichloroacetyl groups.

The surfaces grafting of polyesters onto organic pigments, such as quinacridone (QA) and anthraquinone (AQ), by anionic ring-opening alternating copolymerization of epoxides and cyclic acid anhydrides initiated by potassium carboxylate ($-COO^-K^+$) groups introduced onto these pigment surfaces has also been reported[56]. The $-COO^-K^+$ groups attached on the pigment surfaces were formed by two different methods:

1) The reaction of potassium carboxylate with surface-attached acid chloride groups introduced by the reaction of surface amino groups with adipoyl dichloride (s. Figure 1-15a and b).
2) The graft polymerization of potassium acrylate initiated by azo groups introduced onto the surfaces (s. Figure 1-15c).

The dispersibility of organic pigments in organic solvents was improved by grafting polyesters onto these surfaces.

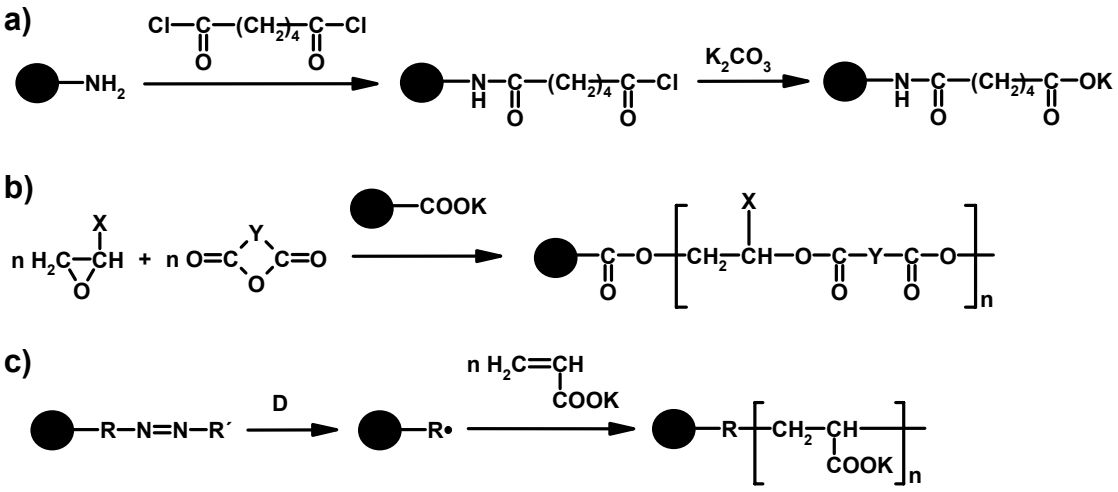

Figure 1-15: Anionic ring-opening alternating copolymerization of epoxides with cyclic acid anhydrides initiated by $-COO^{-}K^{+}$ groups introduced onto organic pigment surfaces (QD and AQ).

The immobilization of azo groups on the surfaces of organic pigments (QD, AQ, DPP) was achieved by the following two methods:

1) Introduction of isocyanate groups on pigment surfaces by the reaction of surface amino groups with tolylene 2,4-diisocyanate (TDI). The surface isocyanate groups can either react with 4,4′-azobis(4-cyanopentanoic acid) (ACPA) or with 2,2′-azobis(2-cyano-*n*-propanol) (ACP) (s. Figure 1-16) to yield surface-attached azo layers.

2) Introduction of acid chloride groups by the modification of surface amino groups with terephthaloyl dichloride (TPDC). The surface acid chloride groups can either react with ACP or with 2,2′-azobis[2-(imidazolin-2-yl)-propane] (AIP) (s. Figure 1-17).

Using the azo groups attached onto these organic pigment surfaces, the radical graft polymerization of vinyl monomers, such as styrene, methyl methacrylate, and 2-isocyanatoethyl methacrylate were successfully initiated[55]. Polymer-grafted organic pigments formed stable dispersions in good solvents for the grafted polymers.

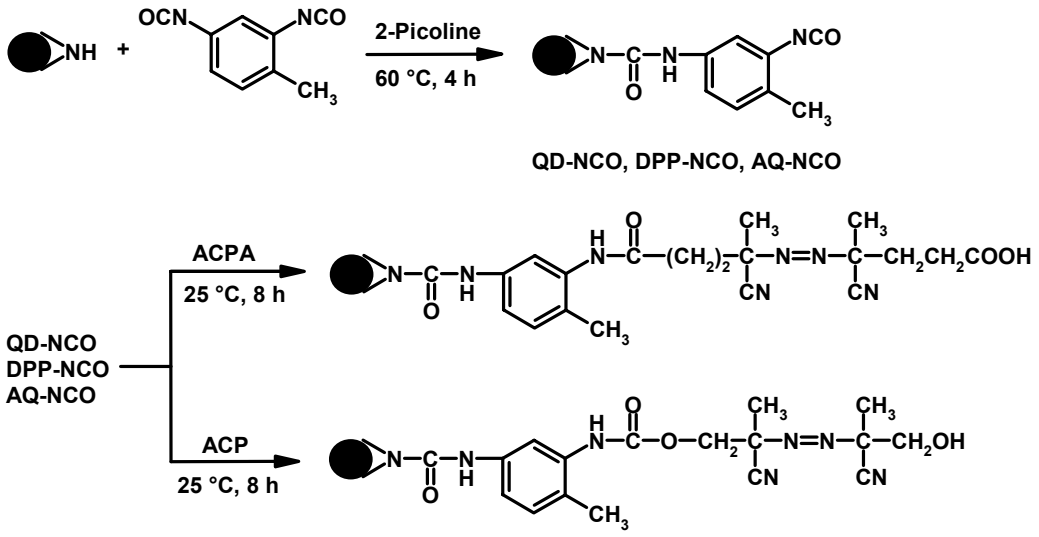

Figure 1-16: Introduction of azo groups onto the surfaces of QD, DPP and AQ in two steps: reaction of amino groups on the surface with tolylene 2,4-diisocyanate (TDI) and subsequent reaction of isocyanate groups on the surface with 4,4′-azobis(4-cyanopentanoic acid) (ACPA) or 2,2′-azobis(4-cyanopropanol) (ACP).

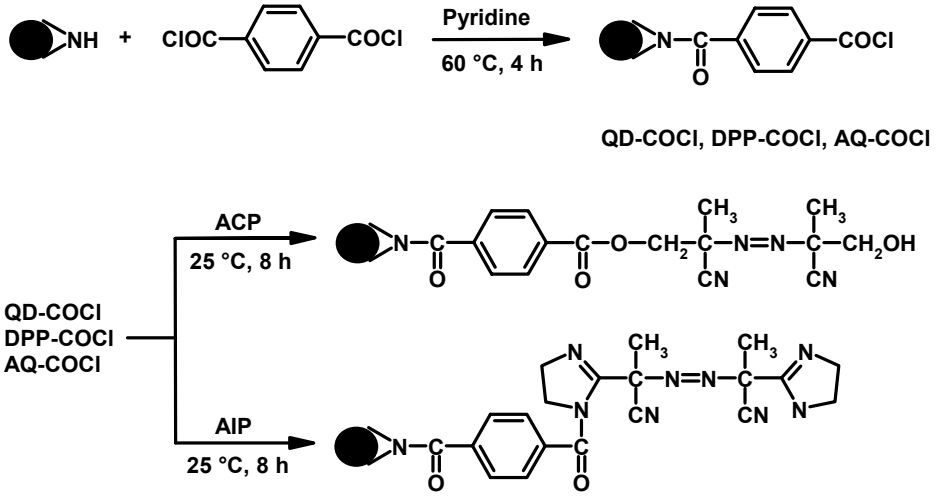

Figure 1-17: Attachment of acid chloride groups onto the surfaces of organic pigment by the reaction of amino groups of the surface with terephthaloyl dichloride (TPDC) and subsequent reaction of acid chloride on the surface with 2,2′-azobis(4-cyanopropanol) (ACP) or 2,2′-azobis[2-(imidazolin-2-yl)-propane] (AIP) to yield azo groups on the surface.

The immobilization of the initiator groups on the pigment particles, as described above, was achieved in several surface reaction steps. As a result, the graft densities of surfaced-attached initiator were rather low and cannot be easily reproduced. Consequently the obtained polymer film is also rather thin under the given reaction conditions. Furthermore, the side reaction can also occur which is difficult to characterize due to the small amount of the grafted material. The kinetic and mechanism of radical chain polymerization have also not been described.

In recent years Rühe et al.[53,54,86] have reported that it is possible to decorate surfaces of inorganic particles with dense monolayers of terminally grafted polymer chains by using a different "grafting-from" approach (s. Figure 1-18). In this technique, self-assembled azo-initiator monolayers (SAIMs) could be attached to the surfaces of solid substrates in a one-step reaction and were subsequently used for an *in situ* free radical polymerization, yielding polymer overcoats with controllable thickness and graft densities. The graft density of various azo chlorosilanes on silica gels or silicon substrates can be varied from 0.8 – 1.6 initiator molecules per nm^2, i.e. the average distance between two anchoring groups is 0.8 – 1.0 nm. The film thickness of the subsequently formed polymer monolayer can be driven to several hundred nanometers.

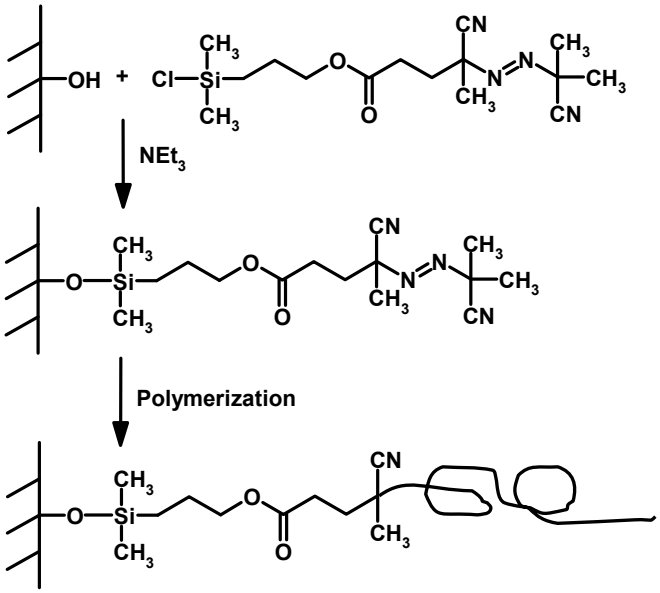

Figure 1-18: Polymer monolayers terminally attached to SiO_x surfaces by using self-assembled azo-initiator monolayers (SAIMs).

1.5.2.3 Grafting polymerization using surface-attached monomer units

For the grafting of polymer via copolymerizable groups[47,67,69,87,88] (s. Figure 1-12c) the reaction is initiated in solution and a macroradical is formed which eventually captures a surface-attached monomer. Then the polymer chains can grow from the surfaces through further addition of monomer to the active chain.

Recently, Bialk et al.[57] have studied such a system to understand the kinetics of the reaction and the limitation of such a system with regards to the layer thickness and graft density of the polymer. In their studies, 3-methycryloyl trimethoxysilane (MPS) was immobilized to the SiO_x surface to provide polymerizable methacrylate monolayers and copolymerized with styrene using AIBN as initiator. The polymerization parameters (initiator concentration and polymerization time) were varied to study the grafting process.

1.5.3 Encapsulation of particles

In the last ten years, a variety of encapsulation techniques have been developed for the synthesis of nanocomposite particles for applications in catalysis, optics and also for coatings[89-91]. One of the most common methods is emulsion polymerization[91-93]. Successful encapsulations have been reported for, e.g. titanium dioxide pigments[92-95] and colloidal silica[96-99] using various polymeric materials. For example, MPS adsorbed onto nanosized silica was dispersed in 2-propanol and polymerized *in situ* with *tert*-butyl acrylate in the presence of an initiator[99].

Recently, Lelu et al[58]. have reported the encapsulation of copper phthalocyanine blue pigments in polystyrene latex particles using a mini-emulsion polymerization process to improve the dispersibility in aqueous solution for painting applications.

For successful encapsulation, however, the particles must be correctly dispersed in the continuous phase to avoid the enclosure of large aggregates. For this reason, and also because of the complexity of the particle nucleation mechanism in emulsion polymerization, it often appears difficult to achieve high encapsulation efficiencies by this technique.

2 Strategy of the described work

As described above, pigments are widely used in a variety of fields such as cosmetics, paints, textile printing, printing inks, coloration of rubber and plastics, etc[2]. However, weathering and long-time exposure to light triggers the photo-induced degradation of pigments by generating radicals from the ambient matrix. This deteriorates significantly important the matrix properties. In order to avoid these phenomena, it is important to modify the pigments with groups, which can improve the photo and/or oxidation stability. Another important property of pigments, which can be controlled by surface modification, is their dispersibility in the matrix medium.

2.1 Concept of the surface modification

The surface modification of the pigments can be achieved by covering the surface with a polymer monolayer as shown in Figure 2-1. This monolayer should be able to prevent chemical reactions, e.g. photoreactions or reactions with alkaline ions, between the pigment surfaces and the polymer matrix or the medium with which they are in contact. In addition, they should also allow for compatibility between the pigment particles and the polymer matrix.

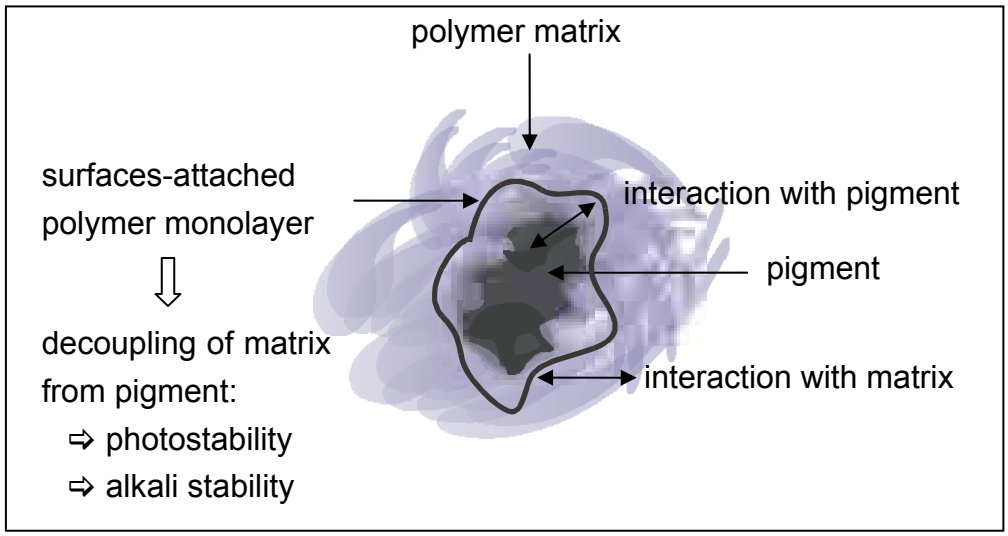

Figure 2-1: Concept of the surface modification of the pigment particles covered with a polymer monolayer.

Based on the structure of the pigments, two synthetic strategies can be used to modify the pigment surfaces. One approach is the non-covalent attachment of a polymer monolayer to the pigment surface. The other approach comprises a covalent attachment.

The organic pigments used in this study consist of imide functional groups (–NHCONH–) similar to the structure of cyanuric acid or barbituric acid, which enable intermolecular interactions such as H-bonding to complementary molecular components, e.g. melamine derivatives (s. Figure 2-2a). The hydrogen bonding motif can be used for the attachment of polymers as described in the following chapter. As an alternative, the imine groups present in these pigments can also be used for the attachment of polymer molecules. Here the active moiety is introduced through an acylation reaction as described further below (s. Figure 2-2b). In the case of inorganic pigments, the pendant hydroxyl functional groups on the surface can be used for subsequent covalent attachment of the polymer chains.

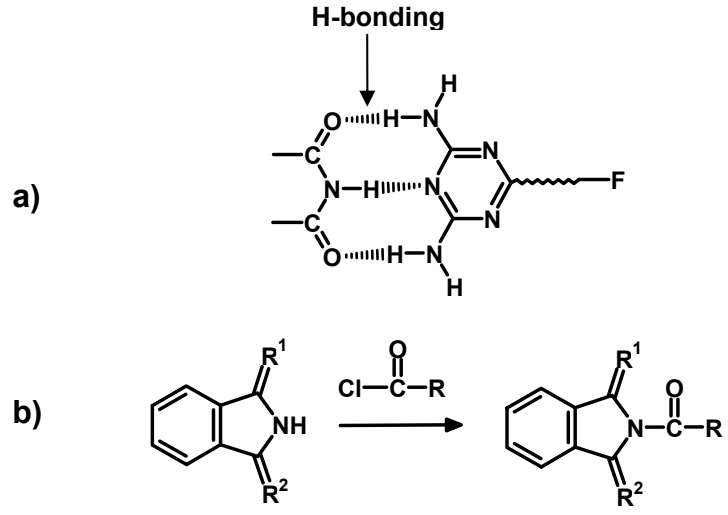

Figure 2-2: Available functional groups on the organic pigments, which can be used to modify the pigment surfaces: a) imide functional group which can form H-bonding with the complementary molecules such as melamine derivatives and b) imine functional group which can react with the acid chloride.

2.2 Pigments used in this work

To demonstrate the possibilities of the different chemical strategies developed in the work, two organic and two inorganic model pigments were employed. As organic pigments, isoindoline pigments namely C. I. Pigment Yellow 185 (Paliotol Gelb D/L 1155; PGL1155) and C. I. Pigment Yellow 139 (Paliotol Gelb L 1840; PGL1840) were chosen. As inorganic pigments, a white pigment (C. I. Pigment White 6; TiO_2) and a pigment for special effects (Paliocrom Gold L2020; PCG2020) were selected. All isoindoline based pigments and PCG2020 were supplied by BASF. TiO_2 pigments were recieved by Degussa AG.

2.2.1 Isoindoline pigments

Isoindoline pigments[4,32] are high quality products having high hiding power and good dispersibility. The properties of these pigments depend strongly on their chemical structure as well as particle size and shape. These pigments give a shade from yellow to orange to red and brown. They show a good lightfastness and weatherfastness. Isoindoline pigments are used in general and in high-grade industrial paints, in automobile and automotive refinishes, in plastics, in high-grade printing inks, especially for metal deco, laminated plastic sheets and in printing inks for bank notes and securities. Figure 2-3 shows the UV absorption as well as the chemical structure of PGL1155 and PGL1840 used in this work.

- PGL1840 is a reddish yellow pigment, used in plastics, paints and printing inks. The pigment performs very poorly in contact with alkali, i.e. it changes its color. Therefore, it is not suitable for use in amine hardening systems or in emulsion paints, which are to be applied on basic substrates.

- PGL1155 provides clean greenish shades of yellow. It is mainly used in plastic and printing inks. PGL1155 shows a good tinctorial strength and high gloss on prints made from NC-based inks. However, it is not stable against bases. In addition, its weatherfastness is rather poor and therefore it is preferably used for indoor applications.

PGL1840 is a commercially most important product[32]. In the beginning of 2000, PGL1840 was produced in a volum of around 1200 tons per year by BASF. BASF is to date the only supplier of PGL1155.

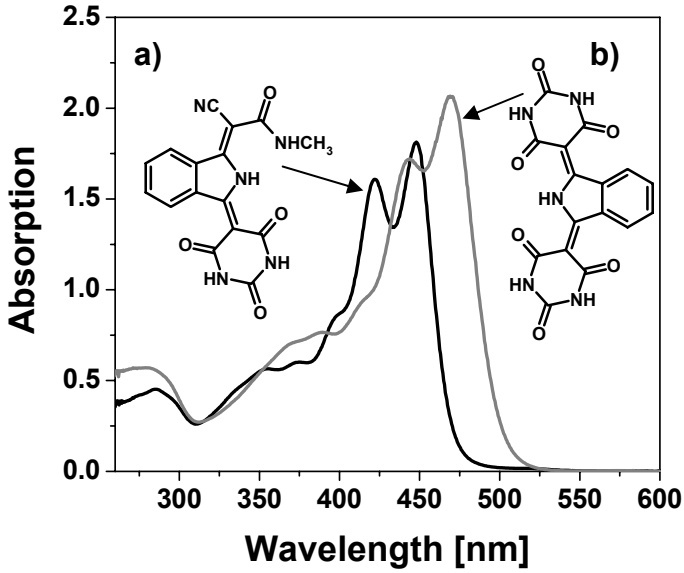

Figure 2-3: UV absorption of a) Pigment Yellow 185 (47 µmol l^{-1}) and b) Pigment Yellow 139 (56 µmol l^{-1}): DMSO as solvent.

2.2.2 Titanium dioxide

TiO_2 was chosen as a model for an inorganic pigment because of its great commercial importance and as it is known that TiO_2 as a strong Lewis acid can induce a photochemical degradation of the surrounding polymer matrix. Thus, it would be very interesting to develop a method or methods, which allow to decouple the polymer matrix from the TiO_2.

However, despite these interesting aspects, the surface-attachment of polymer on these particles has not been investigated to a great extent. Tsubokawa et al.[60] have reported the radical polymerization of vinyl monomer initiated by azo groups onto Ti/Si-R-OH and by the system consisting of trichloroacetyl groups on TiO_2 and $Mo(Co)_6$ to improve the wettability of the TiO_2 surface.

2.2.3 Pigment for special effects

Such pigment used for our study is PCG2020. It is aluminum covered with iron(III)oxide (paste: 65% pigment and 35% mineral spirits). It is used for effected paints for vehicles, industry and construction. It exhibits a very high chroma, very good hiding power and high cost-effectiveness.

2.3 Modification of pigment surfaces with polymer monolayers through hydrogen bonding

Because hydrogen bonds are directional and of moderate strength, they are widely used in host-guest chemistry, e.g. for the recognition of urea[100], barbiturates[101] and other polar guests as well as in self-assembly for making capsules[102] and tubules[103]. The strong interaction in those systems mainly originates from a large number of hydrogen bonding sites, e.g. in DNA base pairs.

It has been known that melamine derivatives and cyanurates can self-assemble through intermolecular interaction[104-107]. The surface of pigments used contains a hydrogen bonding motif that can bind with a complementary molecule. The latter can be along functional groups, such as an initiator unit, which can allow for the modification of the pigment surfaces. As a result, the initiator molecules can be fixed on the pigment surfaces using modified melamine (s. Figure 2-4a). Alternatively, instead of small molecules also polymers can be adsorbed and linked to the surface via H-bonding. Here, modified polythylene imine is to be used (s. Figure 2-4b). The graft polymerization can be generated *in situ* by using this surface-attached initiator.

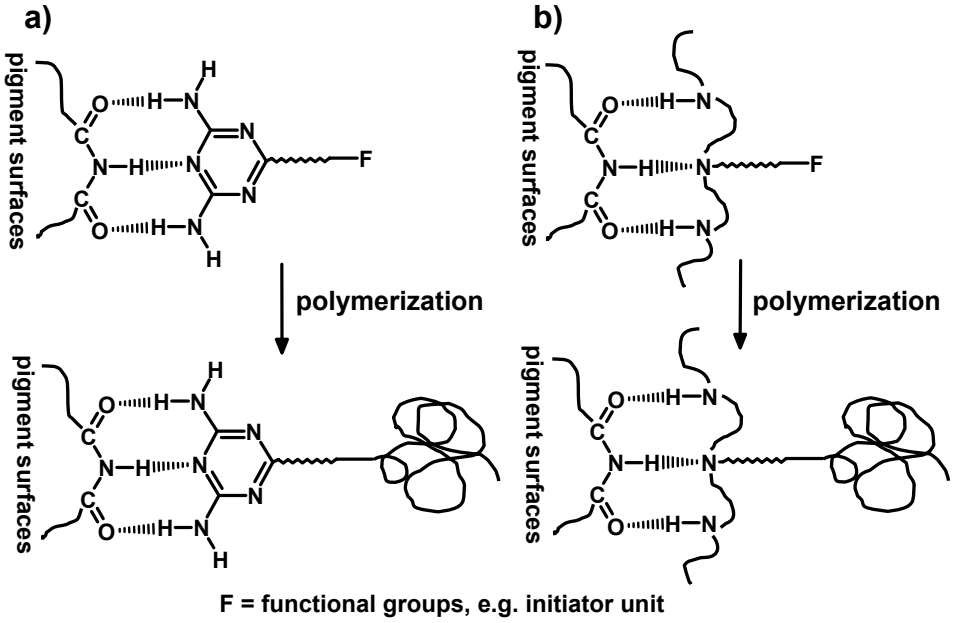

Figure 2-4: Surface modification of pigment particles via hydrogen bonding: a) using a melamine derivative as anchor group and b) adsorption of a polymer such as a modified polythylene imine.

2.4 Modification of pigment surfaces through covalent bonds

The modification of pigment particles through surface-attachment can be achieved by the reaction of functional groups on the pigment surfaces, i.e. imine groups on the organic pigment surfaces and hydroxyl groups on the inorganic pigment surfaces, with suitable anchor groups. Functionalized initiator or monomer moieties will be covalently attached on the pigment surfaces. Subsequently, the preparation of polymer monolayers on the pigment particles using surface-initiated polymerization (s. Figure 2-5) and via surface-attached monomers incorporated into polymer chains growing in solution (s. Figure 2-6) are investigated.

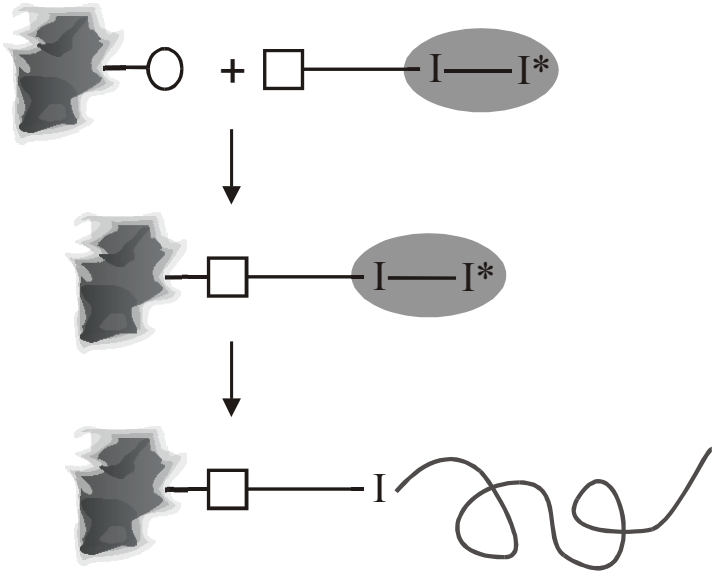

Figure 2-5: Graft polymerization onto pigment particles using self-assembled azo-initiator monolayers (SAIMs): reactive groups on the surface react with suitable anchor groups of an initiator. Subsequent in situ free radical polymerization leads to the formation of surface-attached polymers with controllable thicknesess and graft densities.

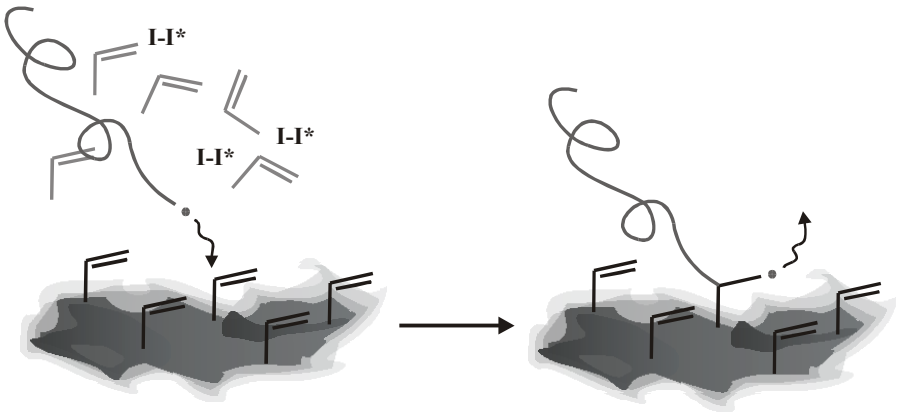

Figure 2-6: Graft polymerization onto pigment particles using surface-attached monomers: after immobilization of the polymerizable group on the pigment surfaces, the copolymerization of vinyl monomers in the presence of α,α′-azo-isobutyronitrile (AIBN) as initiator can proceed.

2.4.1 Modification of organic pigment particles

The organic pigments used in this study carry imino groups to which suitably functionalized acid chlorides can be readily coupled to generate self-assembled azo-initiator monolayers (SAIMs) or metharylate monolayers generated by an acylation reaction using acid choride as anchor group. Subsequently, polymer can be generated at the surfaces by free radical polymerization using SAIMs or using metharylate monolayers respectively. Compared to the immobilization of the initiator onto organic pigments particles reported by Tsubokawa and co-workers[55,56,70], in this study, the immobilization of initiator can be realized in only one-step reaction. The graft density of the initiator is characterized by the following thermal decomposition of the azo groups introduced onto the pigment particle.

To gain control and an understanding of the subsequent polymerizations, the influence of several polymerization parameters, i.e. monomer concentration or polymerization time, on the properties of the formed polymer layers is studied. Additionally, a variety of different monomers is tested for their polymerization behavior in order to explore the versatility of these techniques.

2.4.2 Modification of inorganic pigment particles

In this study, the modification of TiO_2 and PCG2020 surfaces using chlorosilane or alkoxysilane as well as phosphonic acid as a coupling agent is investigated. Azo initiators or monomers molecules that carry such anchor groups are synthesized. The surface immobilization behavior of these molecules is studied.

As mentioned above for the organic pigments, the polymerization behavior of the different systems will be studied and compared to each other. Different surface analytical techniques such as IR, XPS and elemental analysis are used to investigate the chemical composition of the polymer films on the inorganic particles and to quantitatively determine the graft densities of the polymer.

2.5 Investigation of the fastness property of unmodified and modified pigments

One of the important objectives in this study is to investigate the fastness properties of the modified pigments. Since aging tests are very time consuming and require special techniques, only the stability of the polymer-modified organic pigment against strong bases is investigated and compared to the properties of the unmodified pigment.

3 Self-Organization of Melamine-Cyanuric Acid Analogues

The generation of supramolecular structures via multiple hydrogen bonds is interesting for chemists and biochemists as well as material scientists due to the strength and directionality of H-bond formation[108-110]. It has been know that the H-bonds play an important role in many biological processes, e.g. the organization of DNA base pairs as well as for enzyme catalysis. Most of the biological molecular recognition processes occur in aqueous media or at the interface of cell membranes, therefore, studies of the H-bonding between complementary molecules at the air-water interface have been reported by several research groups[104,111-113].

Cyanuric acid and melamine are among the best-known system and are widely studied as examples for triple hydrogen bonding. The cyanuric acid-melamine complex exists in three forms[114]: linear tape, crinkled tape and cyclic hexamer (s. Figure 3-1). The intermolecular steric interactions that arise between the substituents on the melamine and cyanuric acid define the progression from one motif to another motif, for example from a linear to a crinkled structure as reported by Whitesides and coworker[106,115].

The same group also studied self-assembling structures of melamine-cyanuric acid forming a rosette motif [116,117]. Two different synthesis strategies to facilitate the selective formation of this assembly, namely peripheral crowding and covalent preorganization, were developed. The former can be achieved by increasing the size of substituents on either melamine or cyanuric acid. The latter involves the assembly of trismelamine hub$(M)_3$, in which three melamine units are covalently preorganized through semirigid spacers ("spoke") onto a C_3-symmetrical central hub, with three equivalents of a single cyanurate or barbiturate molecule (s. Figure 3-2)[118].

Lehn et al. introduced the concept of using well-defined secondary interactions based on hydrogen bonding in the synthesis of liquid crystalline polymer. In this system, the repeating units are linked by the triple hydrogen bonding instead of by covalent bonding[119,120].

Lang and Meijer[114] studied the supramolecular interaction based on the triple hydrogen bonding between the alternating copolymer of styrene and meleimide with melamine and with the copolymer of styrene and 2,4-diamino-6-vinyl-1,3,5-triazine.

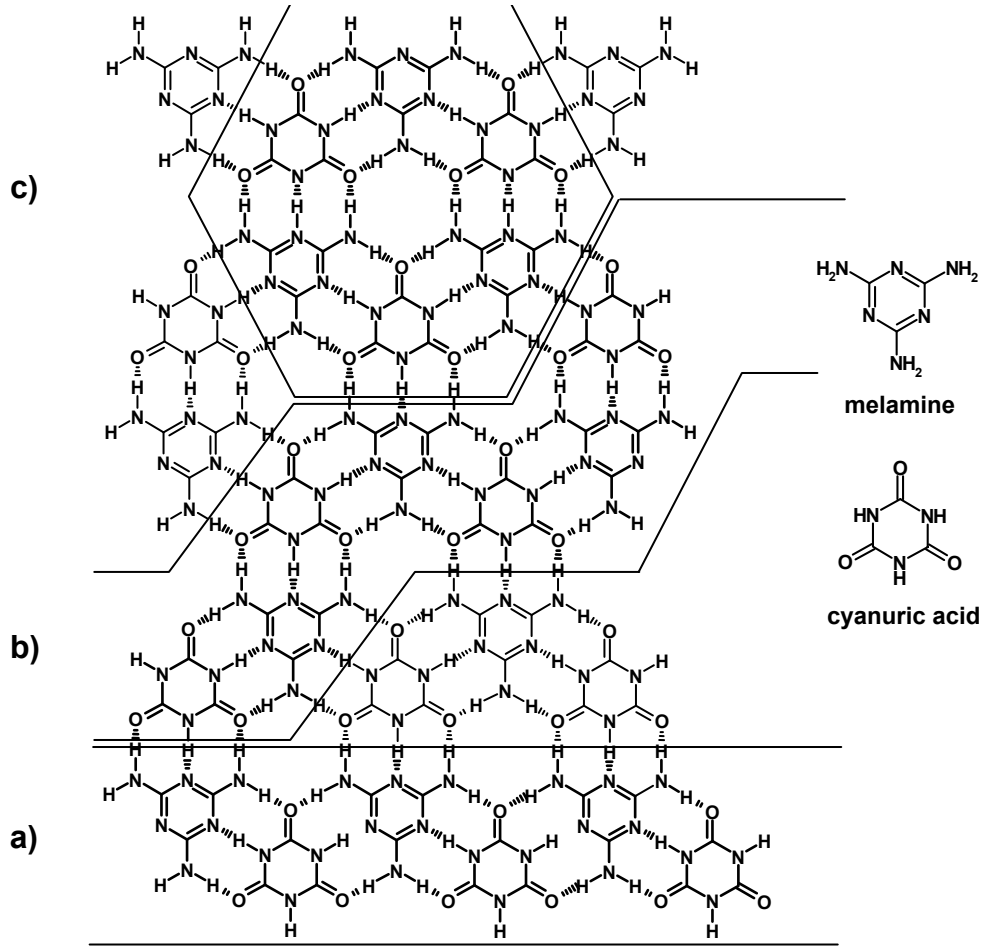

Figure 3-1: Sheet structures of the supramolecular cyanuric acid-melamine complex: a) linear tape, b) crinkled tape and c) cyclic hexamer[114].

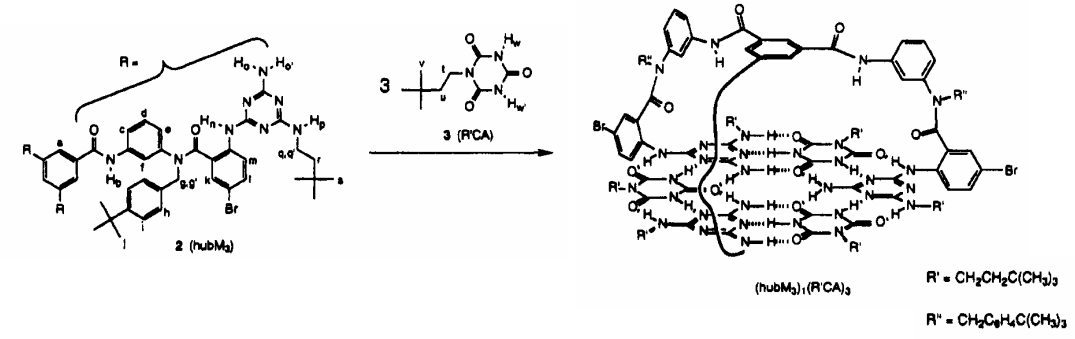

Figure 3-2: Formation of self-assembly of hubM_3 with cyanurate molecule (R´CA) to give a supramolecule 1:3 complex [(hubM_3)$_1$(R´CA)$_3$][118].

In a following chapter, the decoration of pigment surfaces with functional groups, such as initiators through the formation of complexes based on multiple hydrogen bonds between complementary molecular components is described. The approach used in this study is derived from the melamine/cyanuric acid or melamine/barbituric acid system.

The organic pigment used in this study is PGL1840 (s. Figure 2-3). This pigment has the basic structural feature –NHCONH– which is similar to that of cyanuric acid or barbituric acid. Hence these pigments are also expected to form triple hydrogen bonds with melamine derivatives resulting in the formation of pigment-melamine complex derivatives[121]. In order to study the molecular self-assembly directed by hydrogen bonding between melamine derivatives and pigment particles, model supramolecular assemblies on planar surfaces such as silicon substrate are studied (s. Figure 3-3).

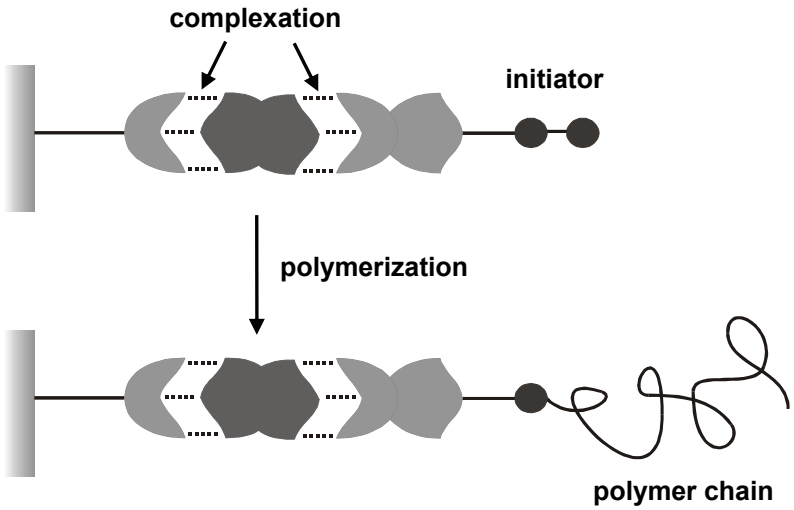

Figure 3-3: Concept of "grafting-from" polymerization using azo initiator on the surface though the complexation: immobilization melamine unit to the SiO_x surfaces and subsequently deposited with the complementary molecule solution for the self-assembly via H-bonding.

It is proposed to synthesize various melamine derivatives bearing different functionalities, such as ethoxysilane and azo groups. Melamine derivatives containing ethoxysilane are used to covalently bind to the silanol groups on the SiO_x surfaces. Melamine derivatives containing free radical initiators can be used to trigger free radical polymerization of various monomers.

3.1 Synthesis of an active ester of the initiator

An active ester of an azo initiator was synthesized in order to modify the melamine molecules. This has been accomplished by reacting the active ester group with the amino group of Mel-C_6H_{12}-NH_2 (s. Chapter 3.2.3). The initiator modified melamine can form H-bonds with the pigment surfaces through the melamine unit. The azo functionality attached to the melamine can now be used to initiate free radical polymerization of monomers. 4,4´-Azobis(4-cyanopentanoic acid) was used as educt because its structure is similar to α,α´-azo-isobutyronitrile (AIBN) which has been known as an initiator for a traditional free radical polymerization.

The synthesis of active esters from the reaction of carboxylic acids with *N*-hydroxysuccinimide (NHS) in the presence of dicyclohexylcarbodiimide (DCC) is well know from peptide synthesis[122]. The addition of the acid to the carbon of the carbodiimide group on DCC generates an intermediate "*acylisourea"* which is particularly reactive against nucleophiles such as the hydroxyl group of NHS (s. Figure 3-4). DCC acts as a condensing agent as mentioned above and is usually recovered as dicyclohexylurea[123,124].

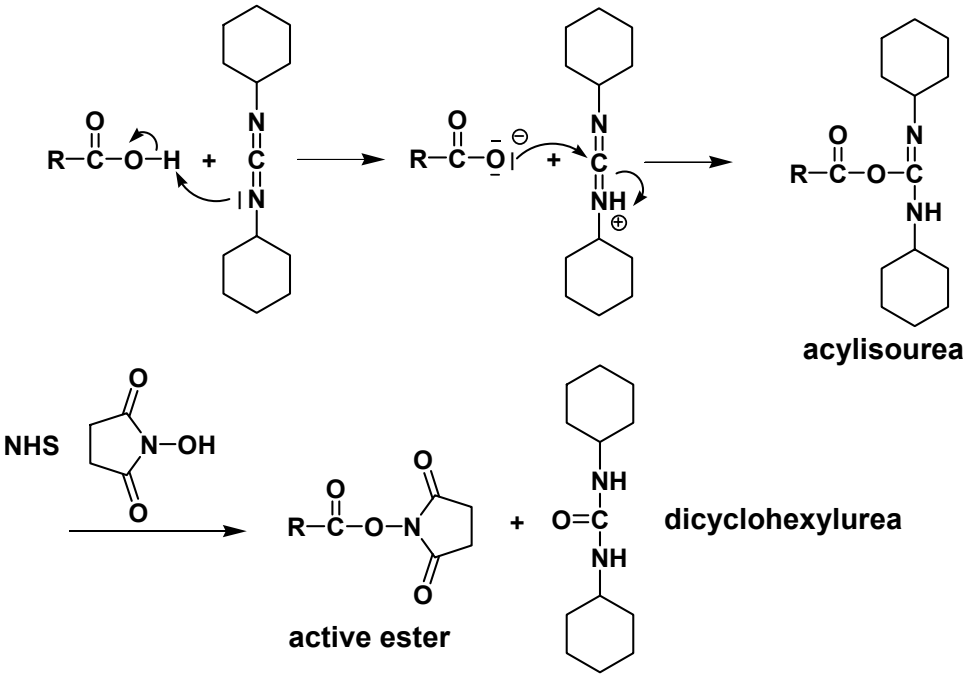

Figure 3-4: Mechanism of the reaction of carboxylic acid and N-hydroxysuccinimide (NHS) in the presence of dicylcohexylcarbodiimide (DCC) as a coupling agent generating an acylisourea as intermediate product.

The synthesis of the initiator active ester, 4-cyano-4-[1-cyano-3-(2,5-dioxo-pyrrolidin-1-yloxycarbonyl)-1-methyl-propylazo]-4-methyl-butyric acid 2,5-dioxo-pyrrolidin-1-yl (ABCC-AE), was performed by the reaction of 4,4′-azobis(4-cyanopentanoic acid) and NHS in the presence of DCC as shown in Figure 3-5.

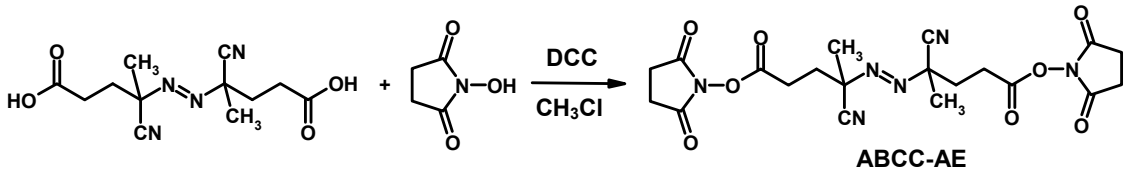

Figure 3-5: Synthesis of 4-cyano-4-[1-cyano-3-(2,5-dioxo-pyrrolidin-1-yloxycarbonyl)-1-methyl-propylazo]-4-methyl-butyric acid 2,5-dioxo-pyrrolidin-1-yl ester.

Figure 3-6 shows the ^{1}H-NMR spectrum of ABCC-AE. The doublet signal which appears at 1.70 and 1.76 ppm is assigned to the two methyl groups and the multiple signals at 2.48 – 2.57 ppm to –COCH$_2$C**H**$_2$C–. The signal of the –C**H**$_2$– group of active ester unit (s. Figure 3-6a) is found around 2.80 ppm and overlaps with that of –COC**H**$_2$CH$_2$– (2.75 – 2.96 ppm). The broad signal at 3.33 ppm results from water residues in DMSO-d_6. The ^{13}C-NMR spectrum is discussed in the experiment part.

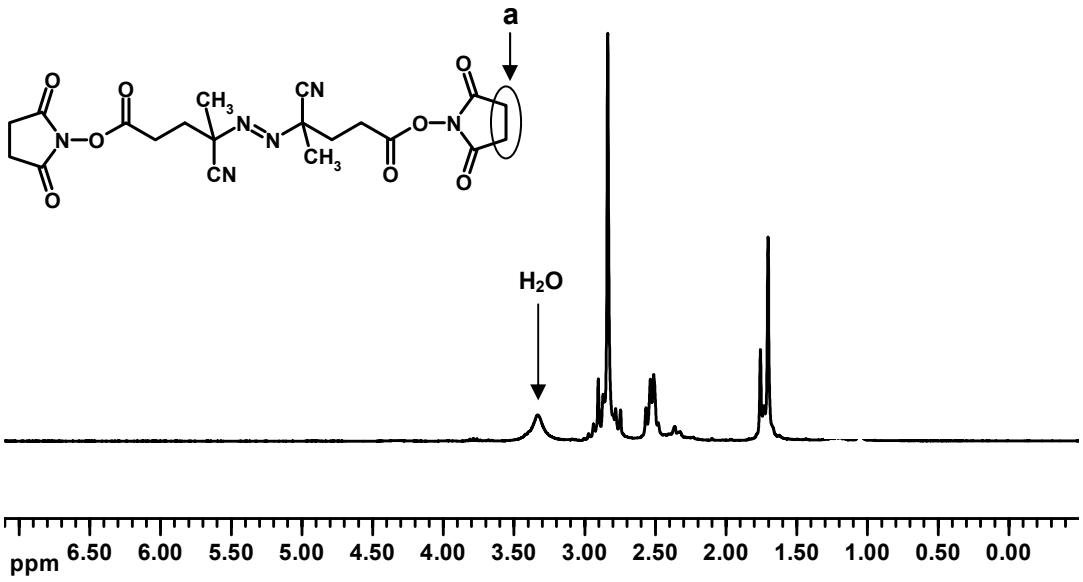

Figure 3-6: ^{1}H-NMR spectrum of ABCC-AE in DMSO-d_6.

The FTIR spectrum of ABCC-AE shows the typical absorption bands of the NHS carbonyl groups at 1825, 1790 and 1740 cm^{-1}, a very weak absorption due to the nitrile group (–C≡N) at 2246 cm^{-1} (2260 – 2200 cm^{-1})[125] and the CH stretching vibrations at 2874 – 3046 cm^{-1} (s. Figure 3-7).

The thermal decomposition of the azo molecules is a strongly exothermic process and can be followed by differential scanning calorimeter (DSC). The decomposition of the azo groups was found at $T_{max.}$ ~ 123 °C and the molar enthalpy of decomposition ΔH_{dec} can be calculated from the integral of the DSC signal. A value of 226 ± 18 kJ mol^{-1} was found. This result is close to that reported for the structural relative AIBN (180 – 200 kJ mol^{-1})[126].

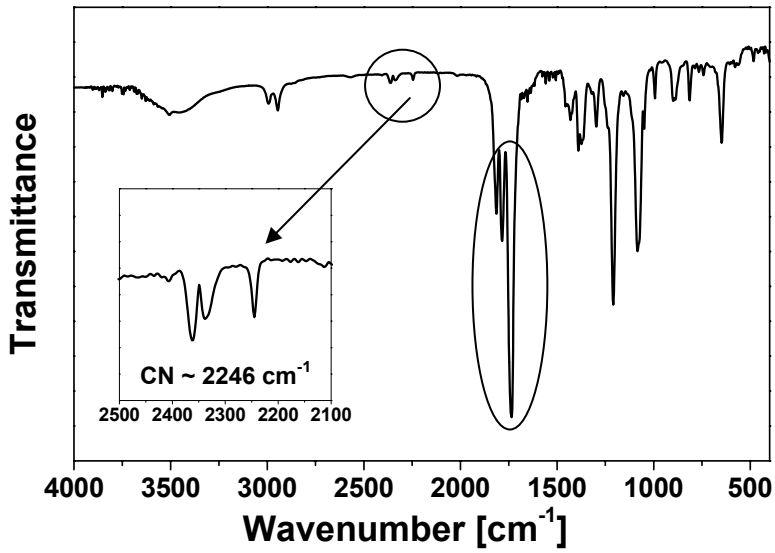

Figure 3-7: Transmission FTIR spectrum of ABCC-AE (KBr pellet).

3.2 Synthesis of a melamine coupling agent

3.2.1 Synthesis of melamine containing trialkoxy silane group

To generate a melamine monolayer on SiO_x surfaces, a melamine derivate 1-(4,6-diamino-[1,3,5]triazin-2-yl)-3-{3´-[tris-(2-hydroxy-ethyl)-silanyl]-propyl}-urea (Mel-Silane) was synthesized through the reaction of 3-isocyanatopropyl-triethoxysilane with melamine (s. Figure 3-8).

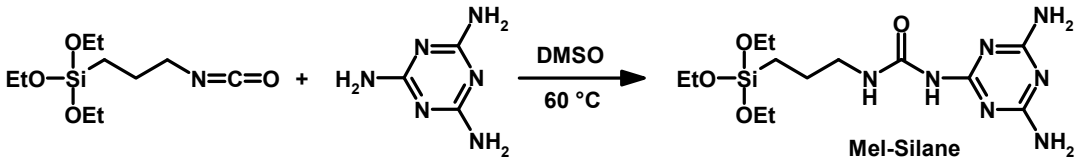

Figure 3-8: Synthesis of 1-(4,6-diamino-[1,3,5]triazin-2-yl)-3-{3´-[tris-(2-hydroxy-ethyl)-silanyl]-propyl}-urea (Mel-Silane).

In this synthesis, only one of the amino groups of the triazine ring adds to carbonyl of the isocyanate group because the reactivity of the other amino groups dramatically reduced by the electron withdrawing urea group. The Mel-Silane compound has two functional groups, namely the ethoxysilane which can be attached to the silanol group of SiO_x surfaces and thus act as "anchor group" and the melamine moiety, which can form H-bonds with other H-bonding such as those present at the surface of pigment particles.

Figure 3-9 shows the ^{1}H-NMR spectrum of the Mel-Silane. The broad doublet signal at 6.60 ppm and 7.30 ppm belongs to the 4 protons of the amino groups on the triazine ring (s. Figure 3-9h). The urea group causes a triplet signal at 9.60 – 9.70 ppm (J = 5.53 Hz) and the singlet signal at 9.20 ppm (s. Figure 3-9f and g). The signals of the alkyl group between the urea group and the silicon atom can be assigned according to Figure 3-9c, d, and e (s. also Experiment part). The ^{13}C-NMR spectrum is discussed in the experiment part.

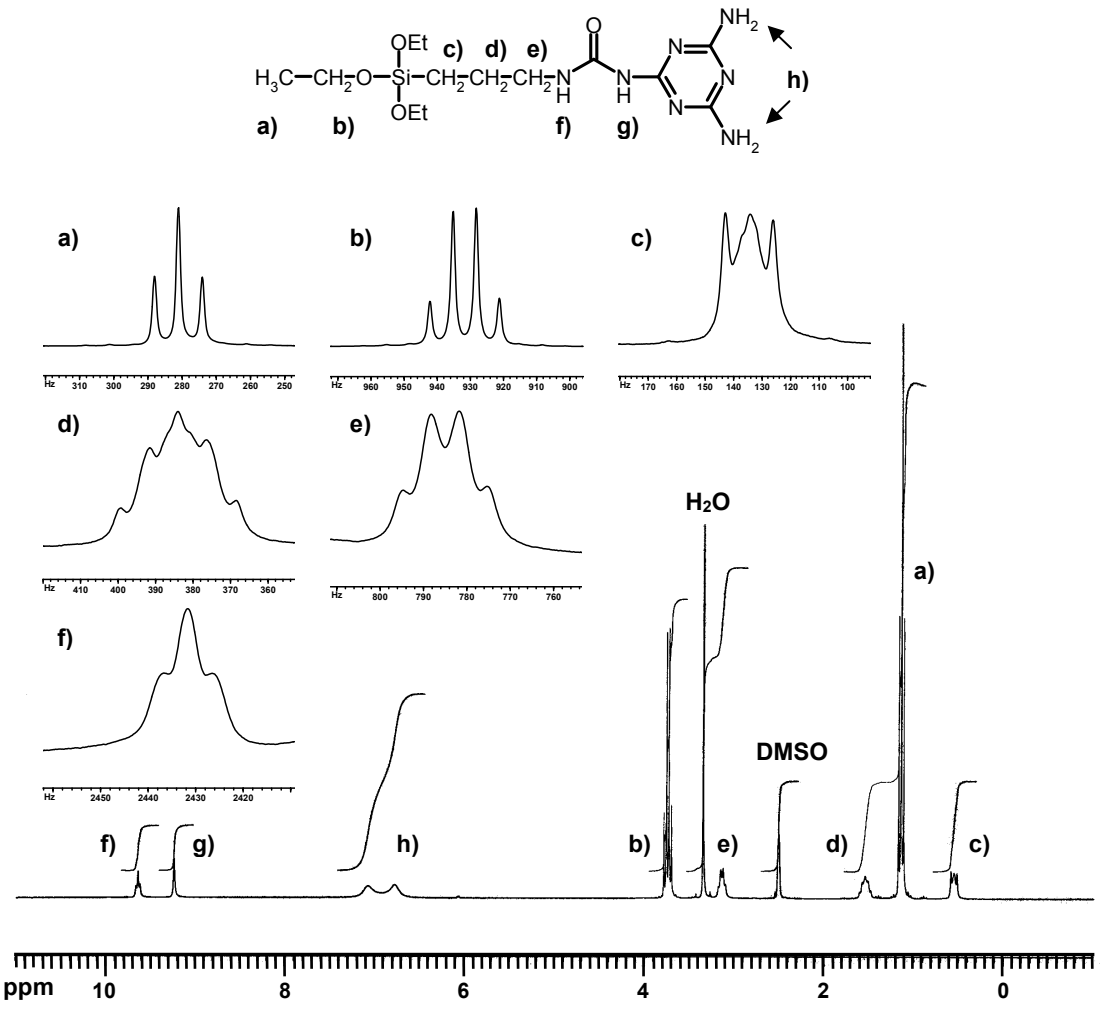

Figure 3-9: ^{1}*H-NMR spectrum of Mel-Silane in DMSO-d*$_6$.

As shown in the FTIR spectra in Figure 3-10, the absorption bands due to NH_2 stretching of melamine at 3418 and 3469 cm^{-1} disappeared after the reaction with the isocyanate compound and the absorption band at 3411 cm^{-1} is obtained. The absorption bands at 2976, 2929 and 2884 cm^{-1} correspond to the CH stretching vibrations of the alkyl groups. Due to the loss of the isocyanate group during the reaction, the strong –N=C=O absorption band at 2274 cm^{-1} (2275 – 2250 cm^{-1})[125] is not present in the spectrum and replaced by an absorption band of the urea group at 1686 cm^{-1} (~1660 cm^{-1})[125]. In addition, the vibration band of triazine ring at 814 cm^{-1} (810 – 815 cm^{-1})[104] is also observed.

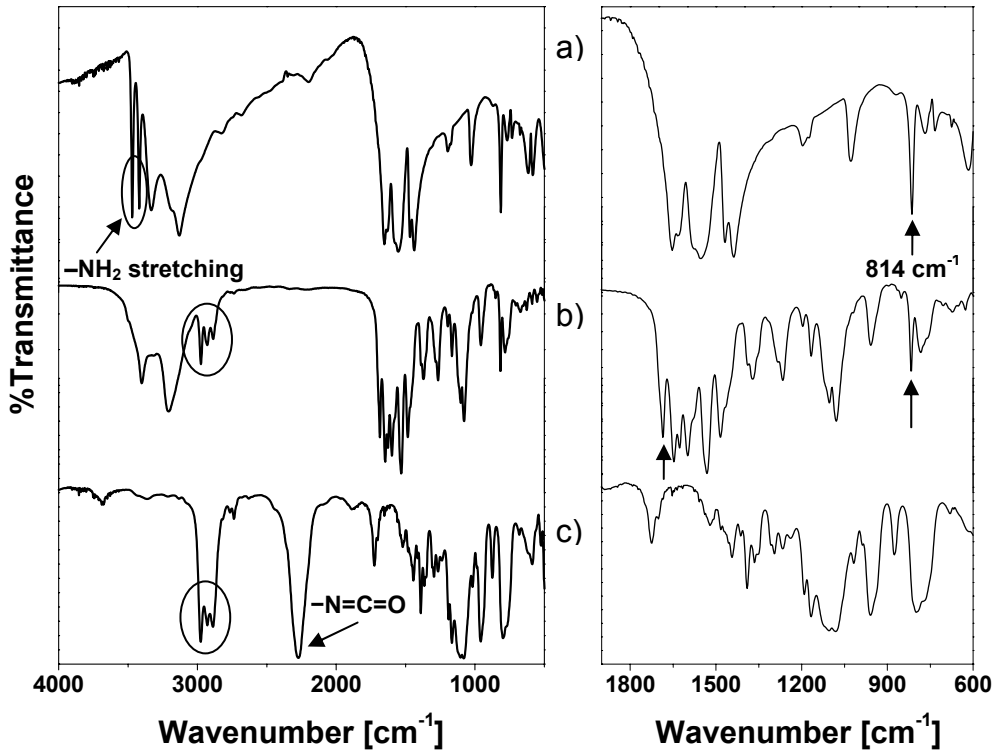

Figure 3-10: Transmission FTIR spectra of a) melamine, b) Mel-Silane and c) 3-isocyanatopropyl-triethoxysilane (KBr pellets).

3.2.2 Synthesis of *N*-(6-amino-hexyl)-[1,3,5]triazine-2,4,6-triamine

The nucleophilicity of the amino group of melamine is lower than that of alkylamines because the nitrogen lone pair electrons are delocalized with in the π-system of the triazine ring. Furthermore, the solubility of melamine in common organic solvent is rather low. Therefore, the attachment of a functional group to melamine is rather difficult. Consequently, 2-chloro-4,6-diamino-1,3,5-triazine (Mel-Cl) is used for the synthesis of functional melamine because of the higher reactivity of the chlorine on the triazine ring and the higher solubility of this compound in organic solvents.

Firstly, *N*-(6-amino-hexyl)-[1,3,5]triazine-2,4,6-triamine (Mel-C_6H_{12}-NH_2) was synthesized because the hexylamine end-group of Mel-C_6H_{12}-NH_2 can be reacted with various other functional groups such as active esters or acid chlorides. As a result, a

melamine derivative, which contains groups which can initiated a polymerization reaction or which act as a label in spectroscopic experiments.

Figure 3-11 shows the reaction of Mel-Cl and 1,6-diaminohexane in the presence of K_2CO_3 acting as a base. This synthesis was carried out using an excess of the diaminohexane. The product purification can be readily achieved by precipitating the reaction mixture in water in order to separate the formed salt and the nonreacted of the diaminohexane.

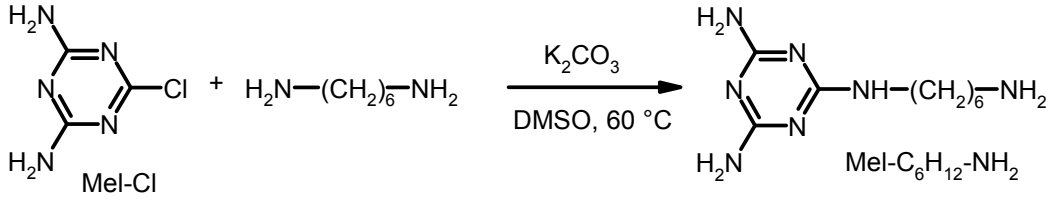

Figure 3-11: Reaction of 2-chloro-4,6-diamino-1,3,5-triazine and 1,6-diaminohexane in the presence of K_2CO_3.

Figure 3-12 shows the ^{1}H-NMR spectra of Mel-C_6H_{12}-NH_2 in comparison to Mel-Cl. The broad doublet signal at 7.11 and 7.19 ppm of NH_2 groups of the triazine ring of Mel-Cl is shifted to higher field at 6.17 and 6.02 ppm (s. Figure 3-12b2) after reaction with 1,6-diaminohexane because the strong electron withdrawing effect of the chlorine on aromatic ring changed to the electron donor effect of the new amino group. In addition, the triplet signal of –N**H**CH_2– at 6.28 – 6.33 ppm (J = 5.66 Hz) and the quadruplet signal of –CH_2N**H**$_2$ at 2.96 – 3.04 ppm (J = 6.63 Hz) are also observed (s. Figure 3-12b1 and 3).

The multiplet signals of –NHC**H**$_2$– and –C**H**$_2$$NH_2$ are found at 2.40 – 2.55 ppm (overlapped with signals from residual H_2O; s. Figure 3-12b4) as well as those of the –CH_2C_4**H**$_8CH_2$– due to alkyl spacer at 1.09 – 1.30 ppm (s. Figure 3-12b5). The ^{13}C-NMR spectrum is discussed in the experiment part.

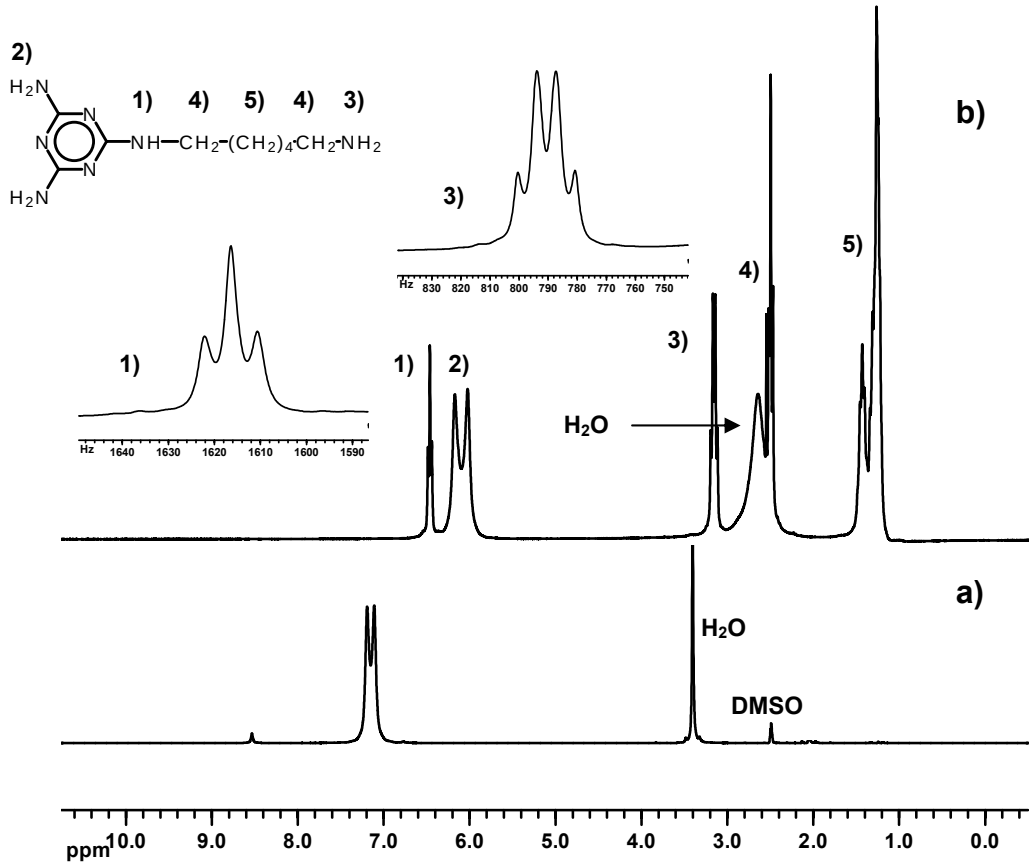

Figure 3-12: ^{1}H-NMR spectra (DMSO-d_6) of a) Mel-Cl and b) Mel-C_6H_{12}-NH_2.

The FTIR spectrum of Mel-C_6H_{12}-NH_2 is shown in Figure 3-13b. The CH stretching vibrations of the alkyl chain are observed at 2933 and 2854 cm^{-1} as well as the NH_2 deformation vibrations at around 1550 cm^{-1} (1650 – 1560 cm^{-1})[125]. The triazine ring vibration of Mel-Cl at 798 cm^{-1} (s. Figure 3-13a) was shifted to the higher frequency at 815 cm^{-1}which is typical for melamine derivatives[104].

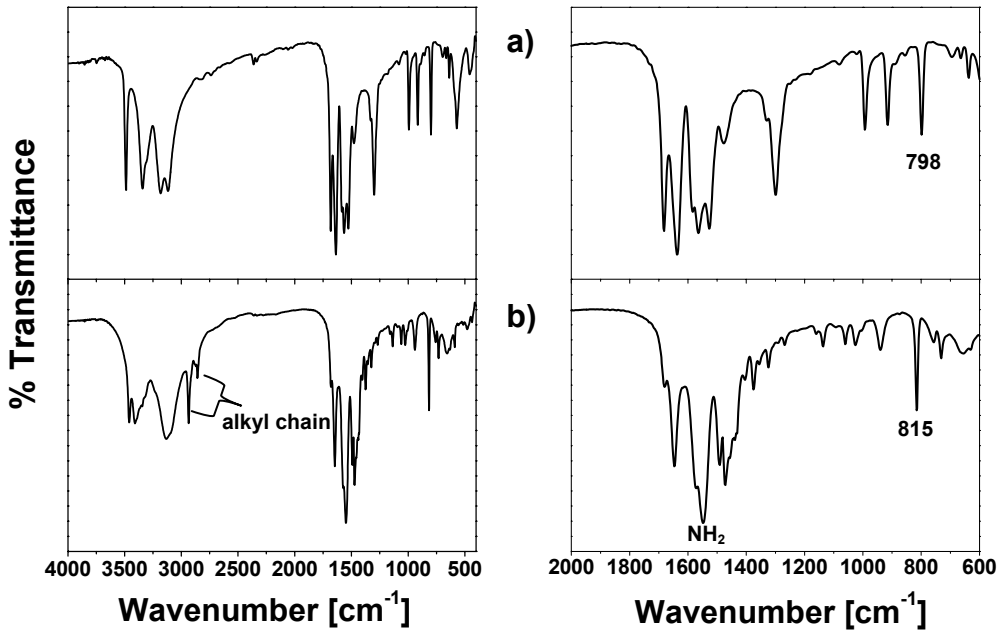

Figure 3-13: Transmission FTIR spectra of a) Mel-Cl and b) Mel-C_6H_{12}-NH_2 (KBr pellet).

3.2.3 Reaction of *N*-(6-amino-hexyl)-[1,3,5]triazine-2,4,6-triamine with an active ester or acid chloride

As mentioned above, the reactivity of the hexylamine end-group of Mel-C_6H_{12}-NH_2 is higher than that of the amine group of the triazine ring. As a result, acylation reactions can be carried out selectively at the hexylamine end-group.

The base catalyzed reaction of the active esters and amines is well studied[127,128]. Due to the basic nature of Mel-C_6H_{12}-NH_2, the reaction of Mel-C_6H_{12}-NH_2 with active ester can be accelerated by its own basicity no additional base for the reaction is needed. If, however, acid chlorides are used, the addition of triethylamine (NEt_3) is advantageous.

Figure 3-14 shows the synthetic strategies for melamine derivatives through the reaction of Mel-C_6H_{12}-NH_2 with active esters and acid chlorides.

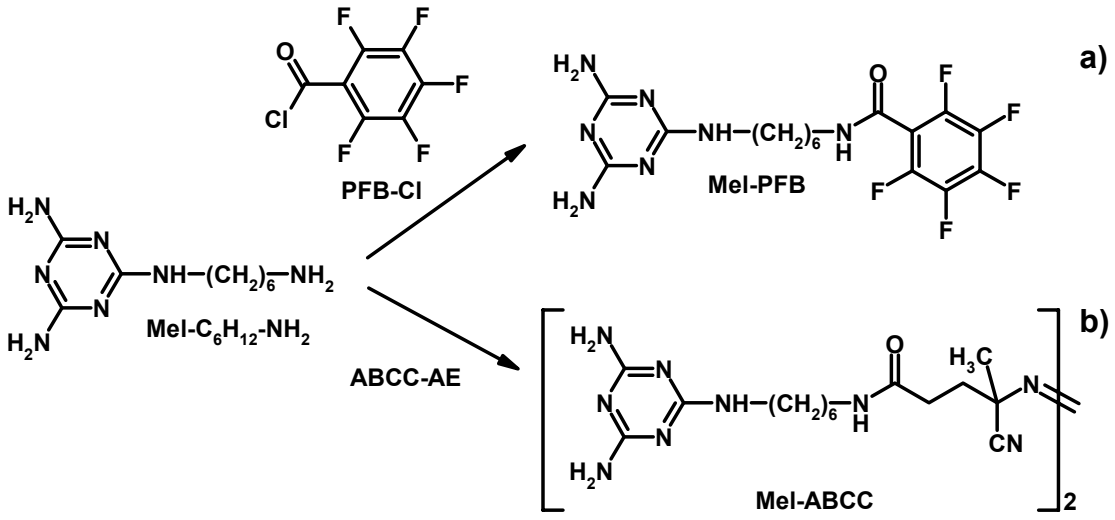

Figure 3-14: Synthesis of melamine derivatives through the reaction of Mel-C_6H_{12}-NH_2 with acid chlorides or active esters: a) N-[6-(4,6-diamino-[1,3,5]triazin-2-ylamino)-hexyl]-2,3,4,5,6-pentafluoro-benzamide (Mel-PFB) and b) 4-cyano-4-{1-cyano-3-[6-(4,6-diamino-[1,3,5]triazin-2-ylamino)-hexylcarbamoyl]-1-methyl-propylazo}-N-[6-(4,6-diamino-[1,3,5]triazin-2-ylamino)-hexyl]-4-methyl-butyramide (Mel-ABCC).

^{1}H-NMR spectra of Mel-C_6H_{12}-NH_2 and its derivatives are shown in Figure 3-15. The broad doublet signal at 6.17 and 6.02 ppm of NH_2 group of the triazine ring of Mel-C_6H_{12}-NH_2 is slightly shifted to higher field at 6.10 and 5.91 ppm after the acylation reaction for all products due to the high electronegativity of the amide groups. The triplet signal of –N**H**CH_2– at 6.39 – 6.59 ppm (J = 5.66 Hz) from Mel-C_6H_{12}-NH_2 was also slightly shifted to higher field (~ 6.33 to 6.50 ppm, J = 5.67 Hz). The new triplet signal of –CON**H**– can be observed at 7.85 – 8.05 ppm (J = 5.53 Hz) and 8.55 – 8.65 ppm (J = 5.61 Hz) for Mel-ABCC and Mel-PFB, respectively, due to the formation of an amide group by acylation. In addition, the multiplet signals of –NHC**H**$_2$$CH_2$– at 2.40 – 2.55 ppm are shifted to lower field (Mel-ABCC: 3.21 – 3.08 ppm and Mel-PFB: 3.29 – 3.08 ppm) close to that of –C**H**$_2$CONH– at 3.07 – 2.95 ppm for Mel-ABCC and 3.24 – 3.26 ppm for Mel-PFB. The signals of the remaining –C**H**$_2$– groups are not significant changed (1.15 – 1.50 ppm). ^{13}C-NMR and FTIR spectra are discussed in the experiment part.

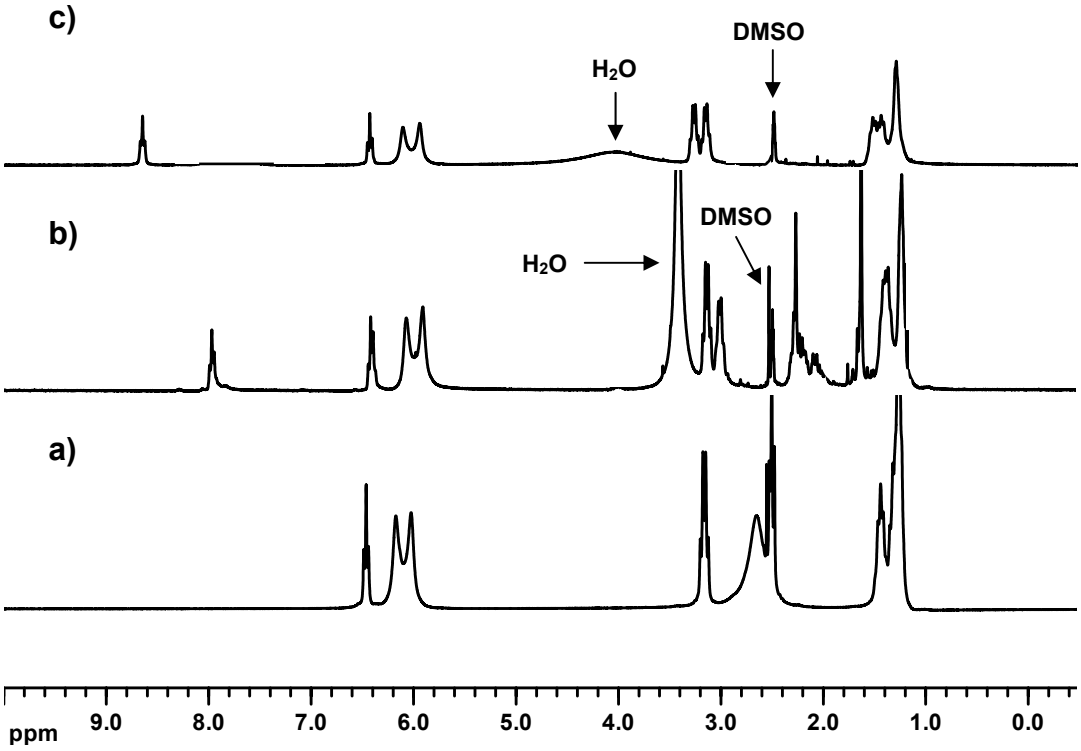

Figure 3-15: ^{1}H-NMR spectra (DMSO-d_6) of a) Mel-C_6H_{12}-NH_2, b) Mel-ABCC, and c) Mel-PFB.

3.3 Model reactions on planar substrate: polymer monolayers through surface initiated polymerization

In this experiment, model experiments on planar surfaces such as silicon substrates was performed. Firstly, a melamine monolayer was deposited onto SiO_x surfaces though the reaction of Mel-Silane and the silanol group on SiO_x surfaces (s. Figure 3-16a). Next, the pigment (PGL1840) was exposed to the melamine monolayer (s. Figure 3-16b) and finally the melamine containing azo group (Mel-ABCC) on that layer (s. Figure 3-16c). The polymer chains were then grown *in situ* from the surface by using a surface-initiated polymerization, i.e. "grafting-from" technique (s. Figure 3-16d). For the characterization of each layer, x-ray reflectivity measurements were performed for the determination of the layer thickness of monolayers and XP spectroscopy for the chemical analysis of the surfaces.

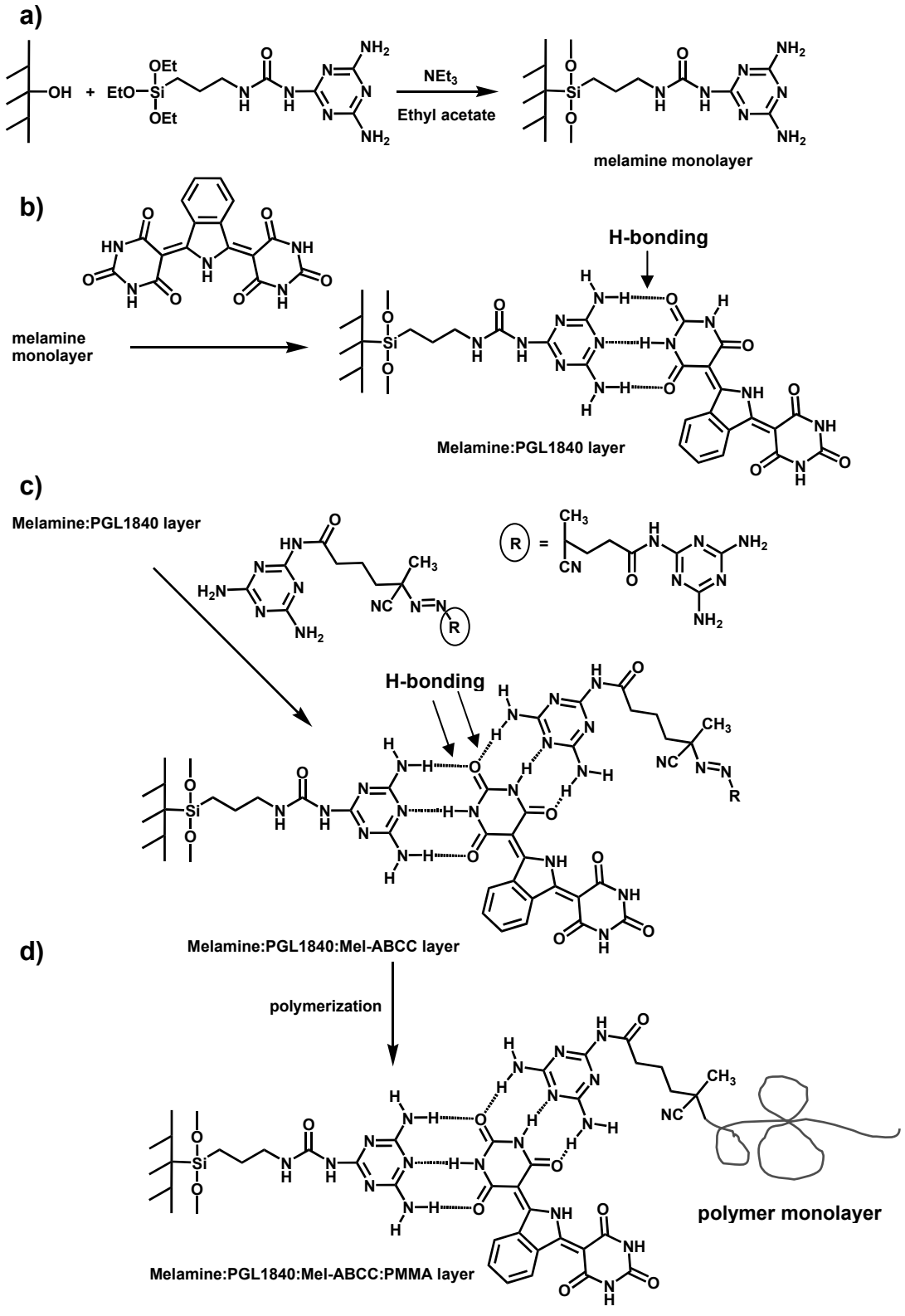

Figure 3-16: Concept for the preparation of polymer monolayers via a combination of supramolecular assembly for the generation of an initiator monolayer and subsequent surface-initiated polymerization.

3.3.1 Immobilization of a melamine moiety onto a planar substrate

As described above, Mel-Silane (s. Chapter 3.2.1) was used as self-assembling agent to build up a melamine monolayer on the planar SiO_x surfaces. The immobilization of Mel-Silane to the SiO_x surfaces was carried out in dry ethyl acetate in the presence of NEt_3 as an acid scavenger at 60 °C for 4 hours (s. Figure 3-17).

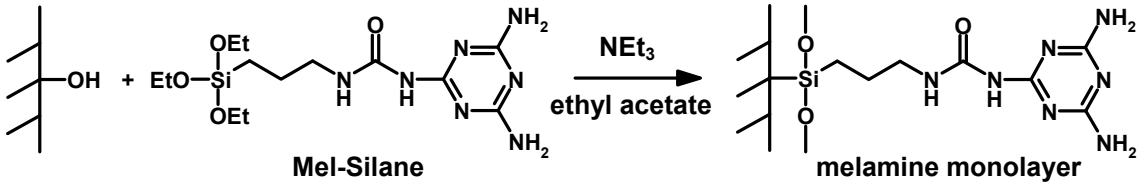

Figure 3-17: Immobilization of Mel-Silane in absolute ethyl acetate to the SiO_x substrate in the presence of NEt_3 at 60 °C for 4 hours: [Mel-Silane] ~ 5 mM.

The layer thickness of the Mel-Silane on the SiO_x substrate was determined by x-ray reflectivity measurements and a thickness of ca. 9.6 ± 0.8 Å (average of 3 measurements) was found as shown in Figure 3-18b. Due to the rather thin layer (~ 1 nm) and the absence of water during the immobilization process, it can be concluded that no multilayer built up on the SiO_x surfaces occurred. The root mean roughness σ of sample after immobilization was calculated approximately σ = 0.3 nm, which is slightly lower than of the silicon substrate before the immobilization (0.5 nm).

Figure 3-19 shows XP survey and C(1s) detail spectra obtained from an unmodified silicon substrate and one containing a self-assembled melamine monolayer. After immobilization of the Mel-Silane to the SiO_x surfaces and extraction with DMSO for 24 hours, the new signal of N(1s) at 401 eV due to nitrogen atoms originating from the Mel-Silane is observed besides the signals of C(1s) at 288 eV, Si(2s) at 153 eV, and Si(2p) at 102 eV (s. Figure 3-19a2). From a comparison of the C(1s) detail spectra, it is obvious that the intensity of the C(1s) signal obtained from the melamine monolayer is higher than that obtained from the unmodified silicon substrate (s. Figure 3-19b).

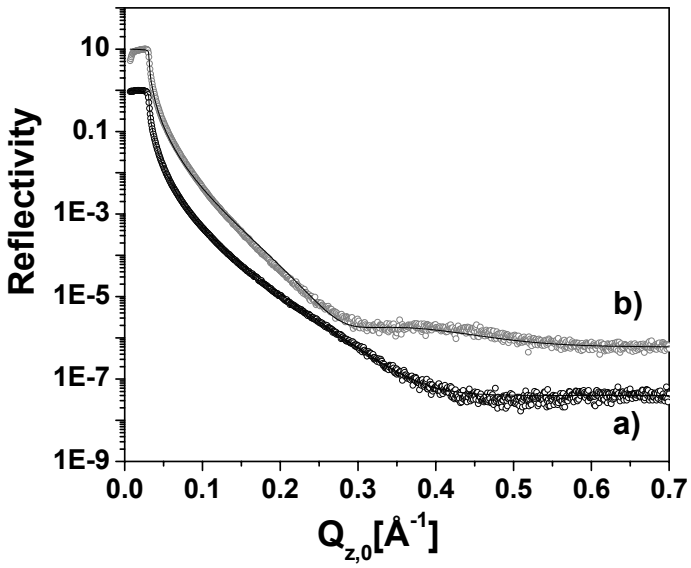

Figure 3-18: X-ray reflectivity of a) before and b) after immobilization of Mel-Silane to the SiO_x surfaces.

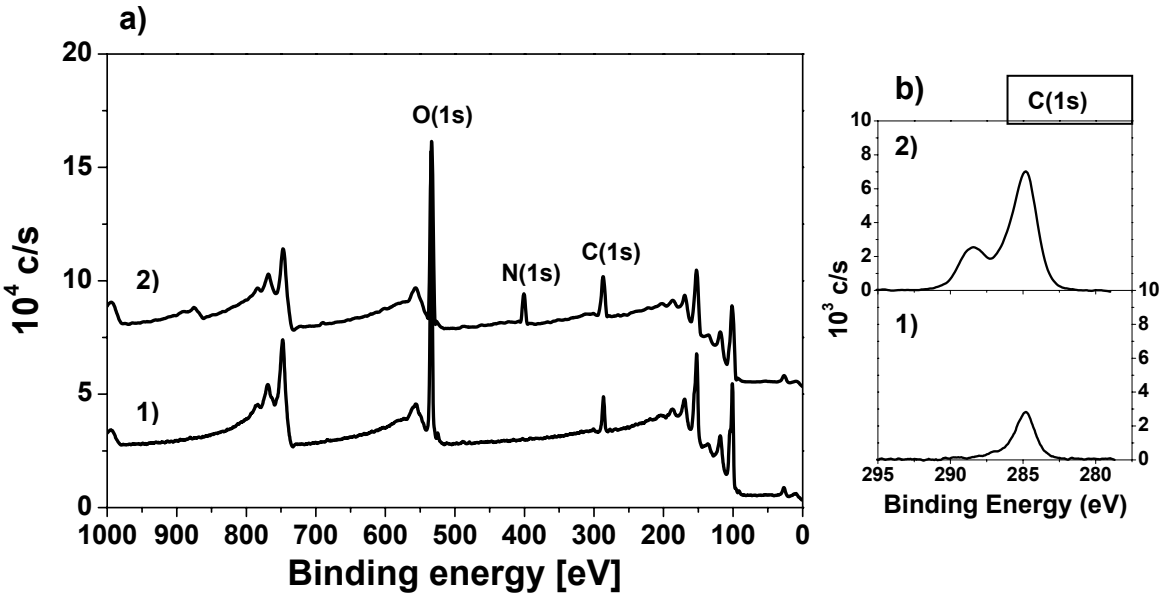

Figure 3-19: a) XP survey spectra and b) C(1s) detail spectra of 1) before and 2) after immobilization of Mel-Silane to the silicon substrate.

3.3.2 Preparation of a Melamine:PGL1840-PFB layer

In order to allow the formation of the second layer, PGL1840-PFB (s. Chapter 4.1 for the synthesis) was used to form hydrogen bonds with the melamine monolayer because the fluorine atoms of PGL1840-PFB layer can be readily detected by XPS.

The melamine monolayer was exposed to a PFL1840-PFB solution in CH_2Cl_2 for a given time, then rinsed with CH_2Cl_2 and dried with N_2. As shown in Figure 3-20, PGL1840-PFB is expected to bind to the melamine monolayer via three hydrogen bonds.

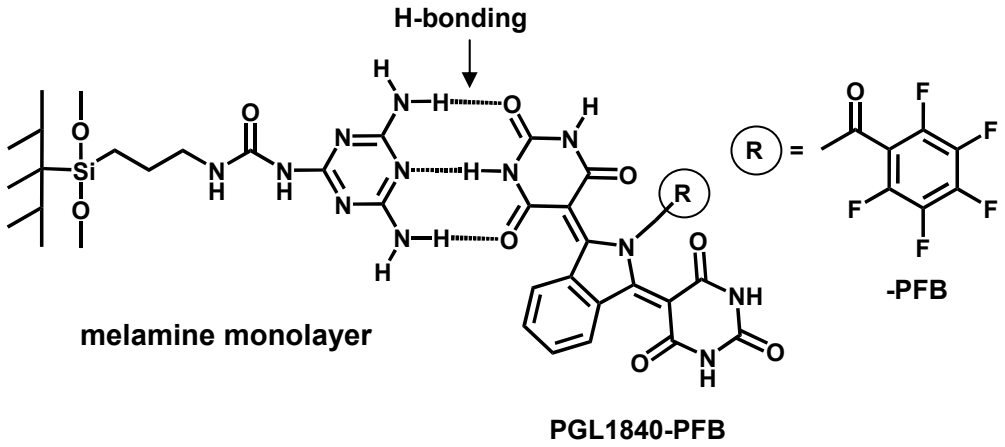

Figure 3-20: Complexation of PGL1840-PFB on the melamine monolayer.

Figure 3-21 shows XP spectra of the melamine monolayers and the subsequently attached PGL1840-PFB for different reaction times (30 and 150 minutes). For both cases (s. Figure 3-21b), only very weak F(1s) signals at 688 eV (688.2 eV reported for fluorine in $–CF_3$ groups)[129,130] are observed, indicating that no multilayer of PGL1840-PFB is formed on the surface even after longer reaction times.

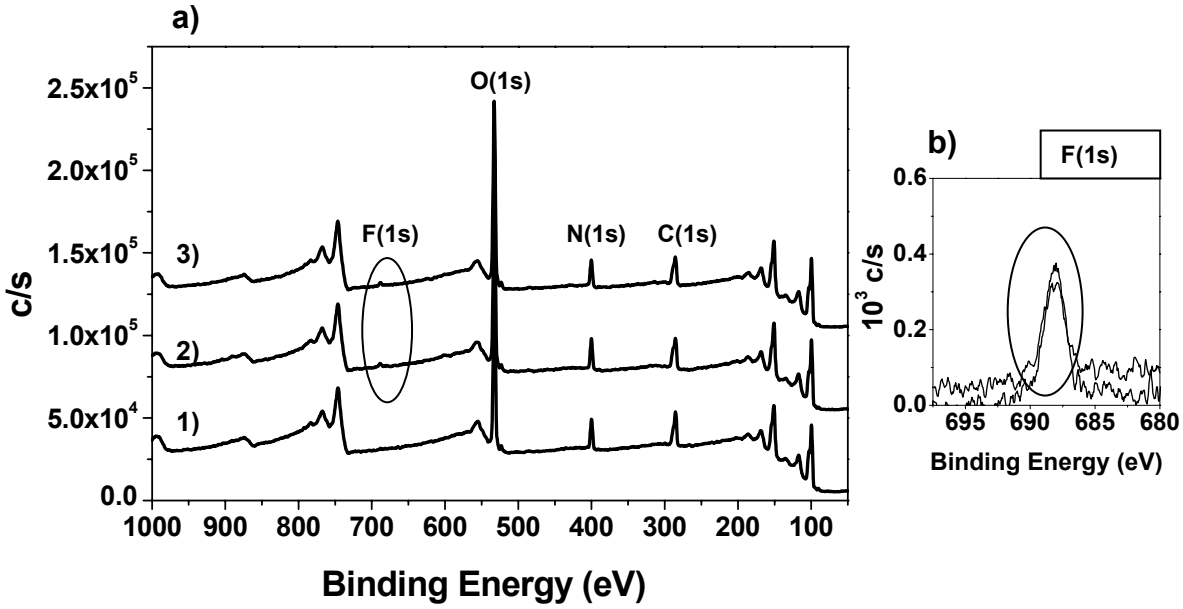

Figure 3-21: a) XP survey spectra and b) F(1s) detail spectra: 1) melamine monolayers, 2) after 30 minutes and 3) 150 minutes exposure of the melamine monolayer to PGL1840-PFB solutions.

3.3.3 Preparation of a Melamine:PGL1840:Mel-PFB layer

As described above, the complex of melamine and PGL1840-PFB was achieved though the molecular self-assembly directed by H-bonding. Therefore, it can be assumed that PGL1840 itself will also form hydrogen bonds to the melamine monolayer in the same fashion. In this experiment, the melamine monolayer was exposed to a PGL1840 solution for 30 minutes and then to a Mel-PFB solution (CH_2Cl_2 as solvent) for varying reaction times (s. Figure 3-22). Similarly to using PGL1840-PFB, the Mel-PFB can also be readily detected by XPS due to the fluorine atoms of Mel-PFB.

Figure 3-23 shows the XP spectra of melamine monolayer exposed to the PGL1840 solution and subsequently to the Mel-PFB solution depending on the reaction times (5 – 240 min.). The signal of F(1s) is observed at 688 eV after exposed the melamine:PGL1840 layer to the Mel-PFB solution (s. Figure 3-23c-h).

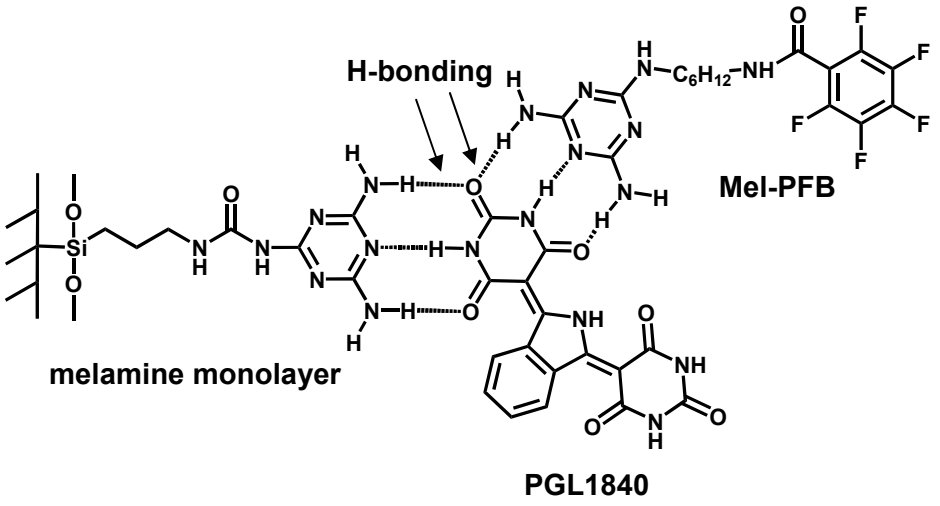

Figure 3-22: Complexation of PGL1840 to a melamine monolayer and subsequent self-assembly of Mel-PFB to that layer.

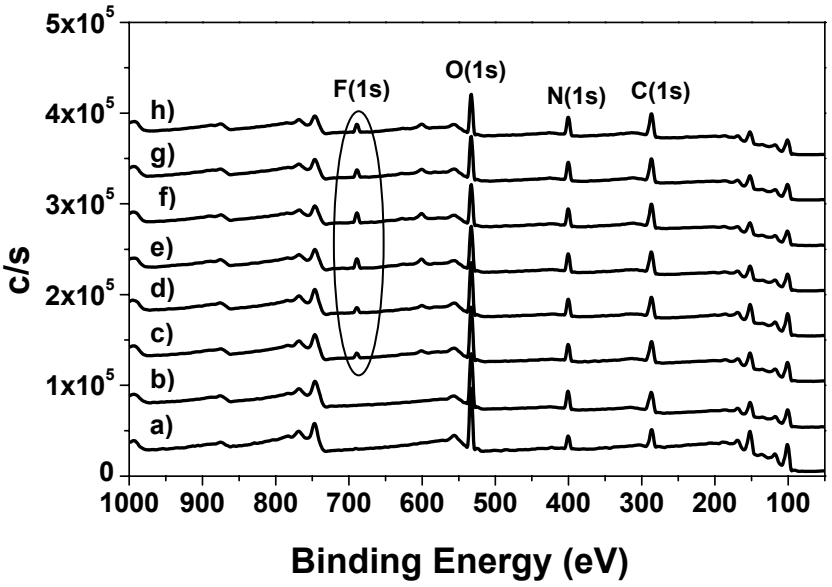

Figure 3-23: XP survey spectra of a) melamine monolayer, b) Melamine:PGL1840 bilayers and Melamine:PGL1840:Mel-PFB trilayers prepared at various reaction times: after c) 5 min., d) 15 min., e) 30 min., f) 60 min., g) 120 min. and h) 240 min.

The integral intensity of the F(1s) signals as derived from the detail spectra (s. Figure 3-24a-f) is plotted as a function of the exposure time in Figure 3-24g. It can be seen that the F(1s) signal increases initially until about 30 minutes exposure and then levels off at a roughly constant value. This result suggests that alternating layers of melamine and PGL1840 compounds can be built up in the suggested way.

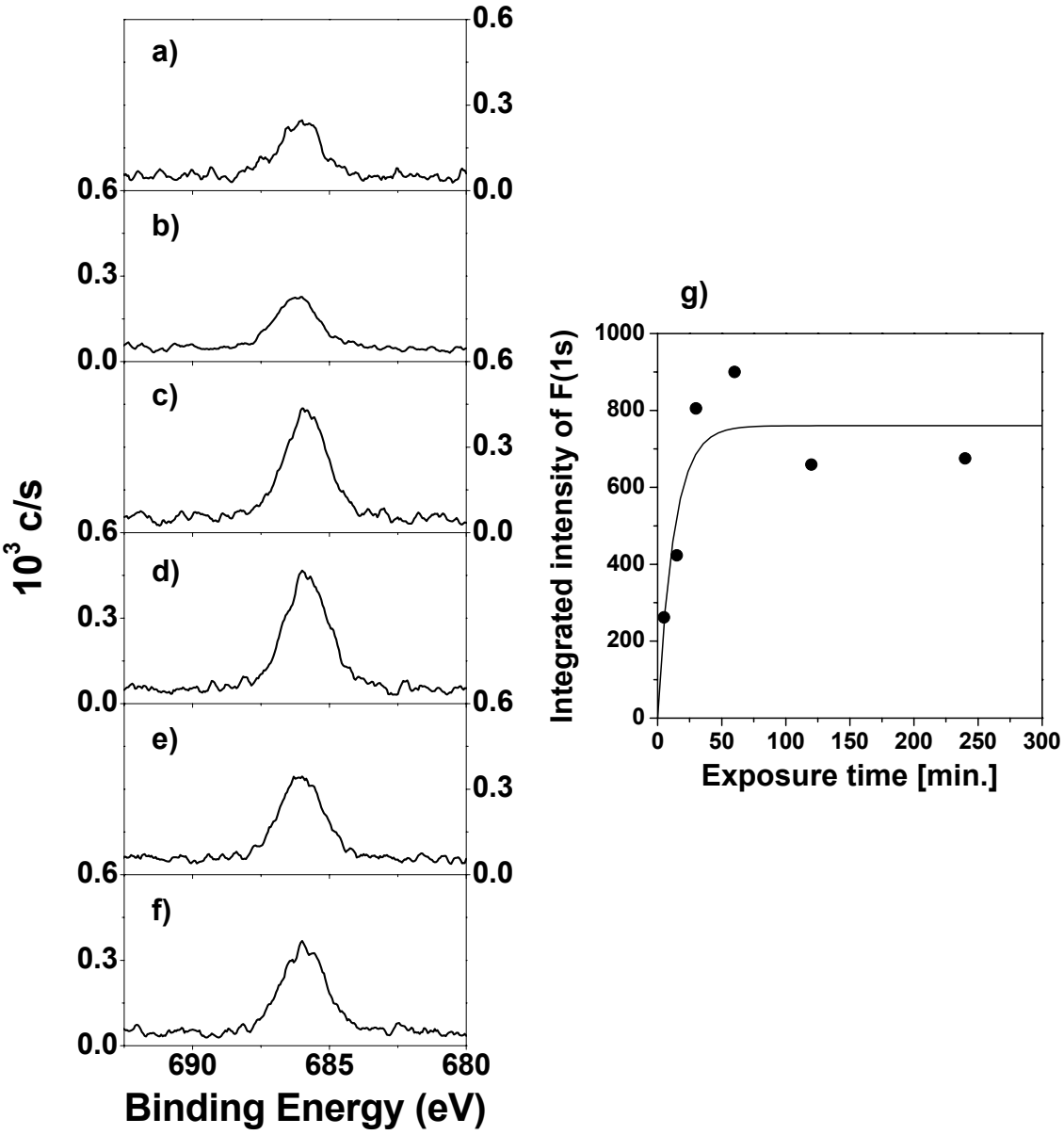

Figure 3-24: F(1s) detail spectra of Melamine:PGL1840:Mel-PFB trilayers prepared at various reaction times: after a) 5 min., b) 15 min., c) 30 min., d) 60 min., e) 120 min., f) 240 min. and g) integrated intensity of the F(1s) signal as a function of the exposure time.

3.3.4 Preparation of a Melamine:PGL1840:Mel-ABCC:PMMA layer

In further investigations the concept of supramolecular complex formation via H-bonding was combined with the concept of surface-initiated polymerization for the generation of a surface-attached polymer monolayer. To this, again PGL1840 was adsorbed to a melamine monolayer and the resulting surface-bound complex was used for the attachment of a melamine containing initiator (Mel-ABCC). This layer was used for the surface-initiated polymerization of MMA as show in Figure 3-16d.

To prepare the self-assembled initiator layer, the conditions as described above were applied. MMA was polymerized in the bulk at 60 °C for 4.5 hours. Each layer was characterized by x-ray reflectometry to measure the layer thickness and by XPS to investigate the chemical composition.

Figure 3-25 shows the x-ray reflectivity curves of each layer. The layer thickness of the initial melamine monolayer was estimated to ~ 1 nm, followed by a second layer of PGL1840 (~ 6 Å), and a third layer of Mel-ABCC (~ 7 Å). After the surface-initiated polymerization of MMA a 7 Å thick polymer layer was obtained.

XP survey spectra and detail spectra of the C(1s) and N(1s) region are shown in Figure 3-26. The C(1s) detail spectra show that the integrated intensity of each complex layer (silicon substrate, Mel-Silane, PGL1840, Mel-ABCC and PMMA layer, respectively) increases due to the increasing number of carbon atoms within each layer. In contrast to that, the integrated intensity of the nitrogen originating from the melamine monolayer slightly decreases after exposure to the PGL1840 solution and increases after exposure to the Mel-ABCC solution. Due to the polymer which does not contain any nitrogen, the integrated intensity of nitrogen signal decreases again.

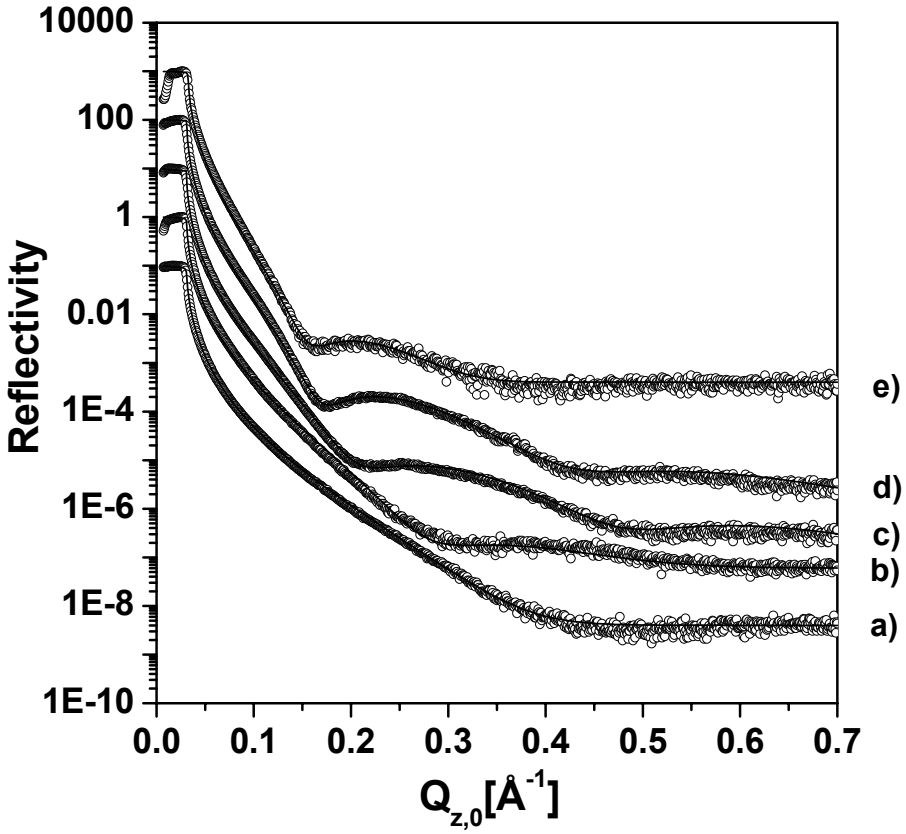

Figure 3-25: X-ray reflectivity curves obtained a) before and b) after immobilization of Mel-Silane to SiO_x surfaces as well as c) Mel-Silane:PGL1840 bilayers, d) Mel-Silane:PGL1840:Mel-ABCC trilayers, and e) Mel-Silane:PGL1840: Mel-ABCC:PMMA multilayer obtained by in situ polymerization of MMA (bulk polymerization) at 60 °C for 4.5 hours.

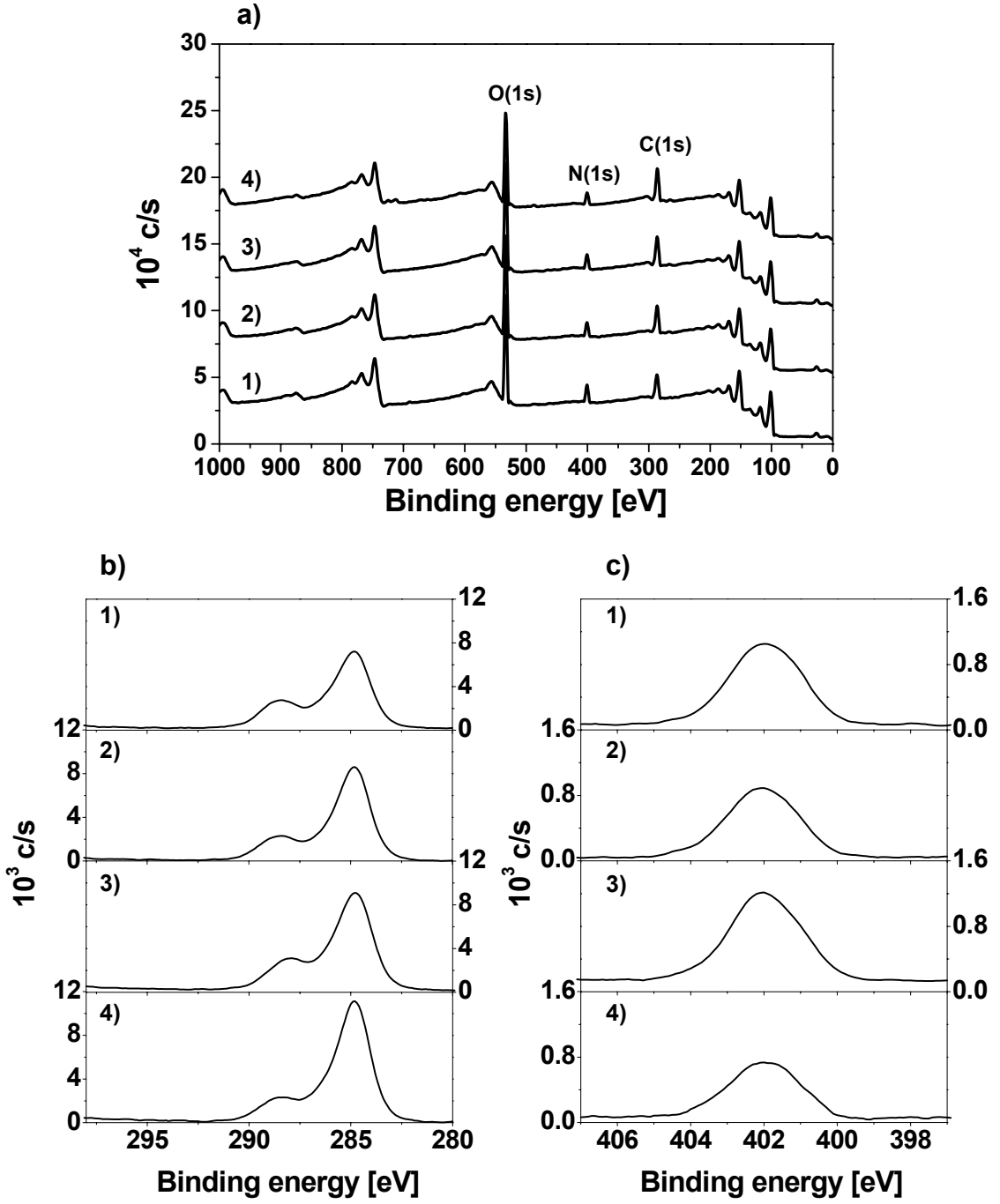

Figure 3-26: a) XP survey spectra, b) C(1s) detail spectra and c) N(1s) detail spectra: 1) after immobilization of Mel-Silane to SiO_x surfaces, 2) Mel-Silane:PGL1840 bilayers, 3) Mel-Silane:PGL1840:Mel-ABCC trilayers and 4) Mel-Silane: PGL1840:Mel-ABCC:PMMA multilayer obtained by in situ polymerization of MMA (bulk polymerization) at 60 °C for 4.5 hours.

3.3.5 Preparation of a Melamine:PGL1840:LPEI-ABCC:PMMA layer

Stöhr and coworkers[131] introduced a system that uses blockcopolymer macroinitiators physisorbed to the surface of planar SiO_x substrates for a subsequent surface-initiated free radical polymerization of *n*-butyl methacrylate. The thickness of the polymer monolayers obtained by that approach could be controlled over a thickness range from 10 to 100 nm. In this system, a poly(*ε*-caprolactone) macroinitiator was used which strongly physisorbes to hydrophilic surfaces[132,133].

As an alternative concept, linear polythylene imine (LPEI) containing 5.5 mol% of azo initiator (LPEI-ABCC) was synthesized (s. Figure 3-27) and made to adsorb onto the Melamine:PGL1840 bilayers. The imine groups (−NH−) on the polymer chains can form hydrogen bond with the imide groups on the pigment surfaces. The azo groups attached to the polymer chain can now be used for initiation of free radical polymerization. The complexation and polymerization was carried out under the same conditions as described above.

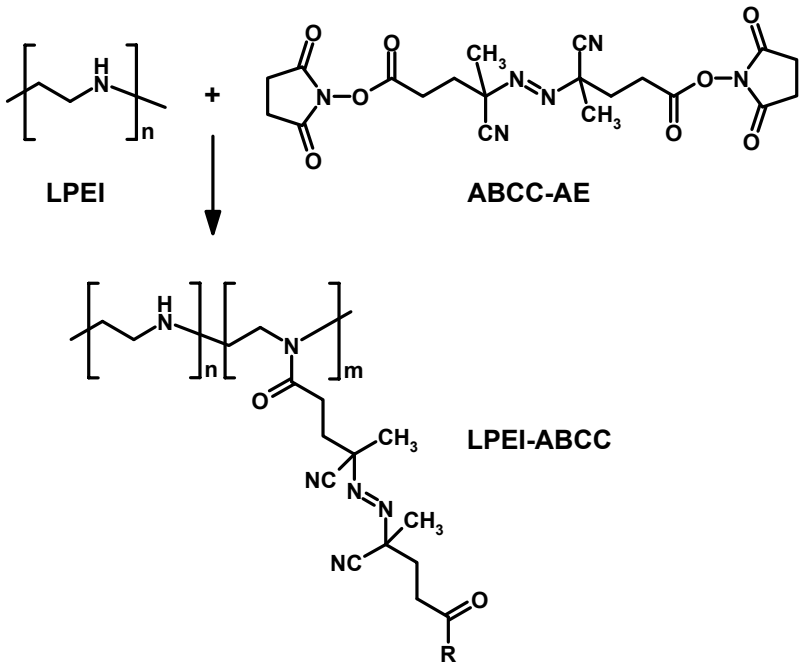

Figure 3-27: Synthesis of LPEI-ABCC used for surface-initiated polymerization reactions.

Figure 3-28 shows XP survey spectra as well as C(1s) and N(1s) detail spectra of each layer. The XP survey spectra of the melamine monlayers and the Melamine:PGL1840 bilayers show the same behavior as described above, i.e. an increasing intensity of the C(1s) signal and a decreasing intensity of the N(1s) signal (s. Figure 3-28b2-3 and c2-3). After exposing LPEI-ABCC to that layer, the intensities of C(1s) and N(1s) increase due to the carbon and nitrogen atoms of the polythylene imine chains. The intensity of C(1s) of LPEI-ABCC layer is higher than that of the Mel-ABCC layer which suggests that more polythylene imine than Mel-ABCC is absorbed to the PGL1840 layer.

The deconvolution of the C(1s) signal of Melamine:PGL1840:LPEI-ABCC trilayers and Melamine:PGL1840:LPEI-ABCC:PMMA multilayers are shown in Figure 3-29. The C(1s) signals of trilayers shows three signals at 284.4 eV (C−C and C−H; 52.7 %), 285.5 eV (C−N; 27.9 %) and 287.3 (CONH overlap with CN; 19.4 %) (s. Figure 3-29a). After *in situ* polymerization with MMA (s. Figure 3-29b), the signal of C−C and C−H was observed at 284.7 eV (62.9 %) and that of C−N at 285.8 (12.5 %). Those signals were shifted ~ 0.3 eV in comparison with before the polymerization. In addition, the new two signals at 286.6 eV (12.7 %) and 288.5 eV (11.9 %) corresponding to C−O and $COOCH_3$ due to PMMA overcoat to the surfaces were observed overlap to the signal of CONH and CN. However, the whole intensity of the C(1s) peak from the trilayer decreases after the polymerization.

In a reference experiment, a polymerization was performed without any initiator, i.e. only in the present of a Mel-Silane:PGL1840 bilayers. It was found by XPS that some of the PGL1840 was removed under these conditions, which might be due to the competition adsorption of monomer, which desorbs the PGL1840 from the surface.

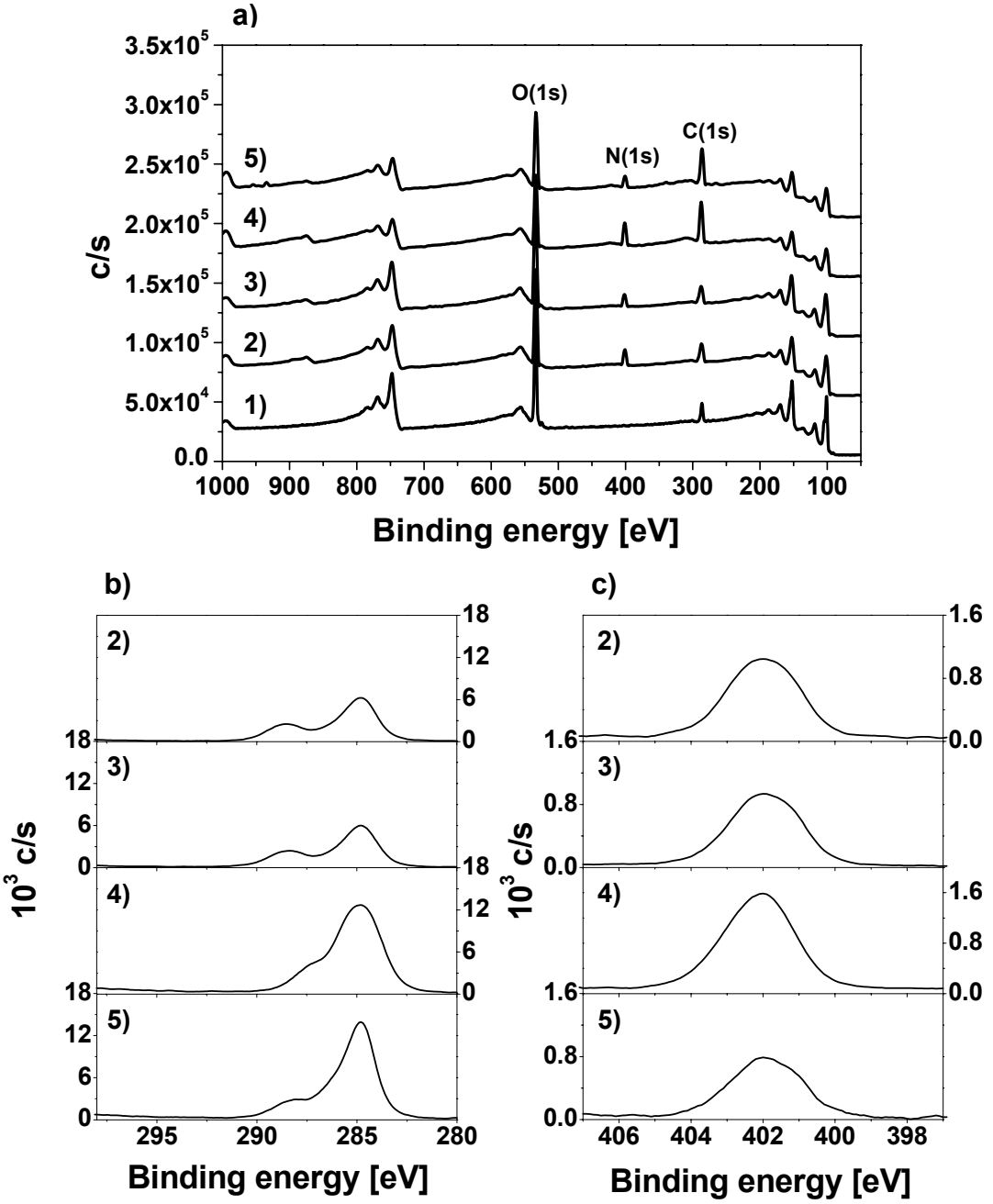

Figure 3-28: a) XP survey spectra, b) C(1s) detail spectra and c) N(1s) detail spectra: 1) unmodified SiO_x surfaces, 2) after immobilization of Mel-Silane to SiO_x surfaces. The melamine monolayer was prepared by immobilization Mel-Silane in absolute ethyl acetate (~ 5 mM) to SiO_x surfaces in presence of NEt_3 at 60 °C for 4 hours, 3) exposure of melamine monolayer with PGL1840 in CH_2Cl_2 for 30 minutes and then of that complex layer with 4) LPEI-ABCC in MeOH (3 mM) for 30 minutes and 5) in situ polymerization of MMA (bulk polymerization) at 60 °C for 4.5 hours.

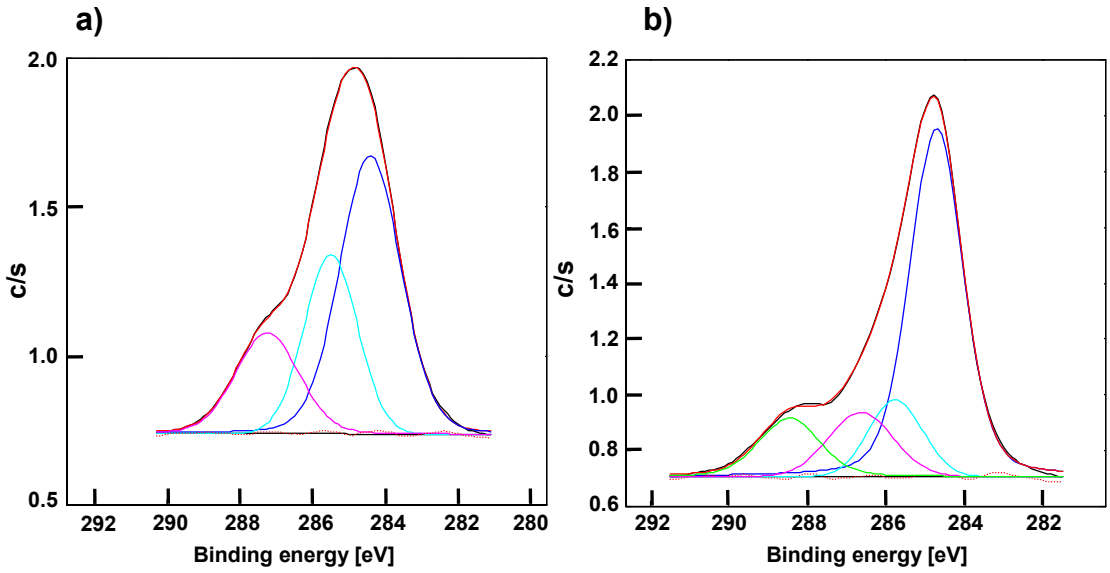

Figure 3-29: Deconvolution of the C(1s) signal of a) Melamine:PGL1840:LPEI-ABCC trilayer and b) Melamine:PGL1840:LPEI-ABCC:PMMA multilayer using Gauss-Lorentz functions for the signals and a Shirley type function to account for the baseline. Details are giving in the text.

3.3.6 Discussion

The stability of H-bonded complexes in solution is very dependent on the solvent. The stability is usually highest in apolar solvents without H-bonding properties, such as alkanes. The stability is lower for solvents that can act as either a H-bond donor or an acceptor, due to the competitive H-bonding with the solvent. In addition, the dissociation rates of H-bonded assemblies rapidly decrease with the number of H-bonds that are broken in the dissociation of a particular component.

It can be expected that during the free radical polymerization of MMA, MMA can replace or form new H-bonding with the complementary molecules on the surfaces. As a result, the loss of initiator moiety on the melamine or polythylene imine from the surfaces could be observed. Another reason could be that the stretching of chains caused by the strong crowding of the polymer chains exert a very strong pull on the H-bonds and causes them to break. Therefore, the “grafting-from” polymerization using self-assembled initiator monolayer introduced via the hydrogen bonds leads to rather thin polymer films in contrast with system of covalently attached initiator monolayers on pigment surfaces as described in Chapter 4.

4 Surface Modification of Organic Pigments

As mentioned above, the polymer layer generated by surface-initiated polymerization from hydrogen bonded monolayers is rather thin due to the instability of the bonds to the surface. In order to achieve covalent binding, the pigment surfaces are modified either with initiators or with monomers. In the former case, surface-attached initiators could be used to initiate free radical polymerization of various monomers resulting in the formation of a polymer overcoat. Alternatively, surface-attached monomers could be copolymerized using sacrificial free radical initiators in the presence of comonomer in solution, also yielding similar polymer overcoats. The various parameters influencing the formation of polymer layers using both approaches has been investigated.

The organic pigments used in this study carry imino group (s. Figure 2-2), which can be used to generate self-assembled azo-initiator monolayers (SAIMs) or monolayers with copolymerizable groups on the pigment surfaces by acylation as shown in Figure 4-1.

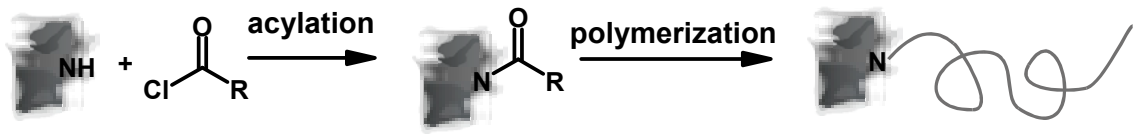

R contains azo group or copolymerizable group

Figure 4-1: Immobilization of azo or copolymerizable groups to the pigment surfaces and subsequent the formation of polymer monolayers using surface-initiated polymerization ("grafting-from" polymerization) or via surface-attached monomers incorporated into polymer cahin growing in the solution ("grafting in between" polymerization).

4.1 XPS studies on the modification of various pigments with fluorinated probe molecules

XPS was used as a very surface sensitive technique to study the extent of surface grafting. As a probe molecule pentafluorobenzoyl chloride (PFB-Cl) was chosen because the XPS signals originating from fluorine atoms of this probe are characteristic for the layer deposited on the pigment. In addition, the sensitivity of the XPS experiment against fluorine is high.

Through this model reaction, it can be expected that PFB group which are covalently attached to the organic pigment surfaces (s. Figure 4-2) can be easily detected.

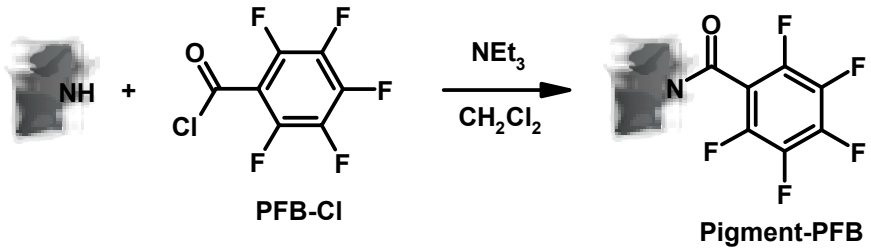

Figure 4-2: Immobilization of pentafluorobenzoyl chloride (PFB-Cl) on organic pigment surfaces through binding to surface imino groups.

Figure 4-3 shows the XP survey spectra of the unmodified and the PFB-modified pigment. Both XP spectra show the characteristic peaks due to C(1s) at 285 eV, N(1s) at 400 eV, and O(1s) at 531 eV coming from the surface of the pigment. However, the spectrum after immobilization of PFB group on the pigment surfaces (s. Figure 4-3b) shows a small peak of F(1s) at 689 eV originating from the surface-attached PFB group. The C(1s) and F(1s) detail spectra of PGL1155-PFB are shown in Figure 4-4.

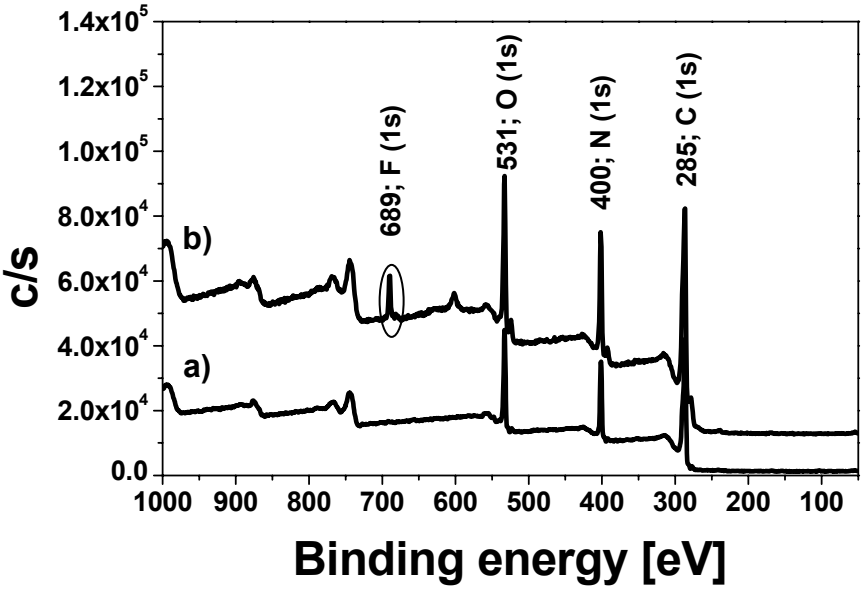

Figure 4-3: XP survey spectra of a) unmodified PGL1155 and b) PFB-modified PGL1155.

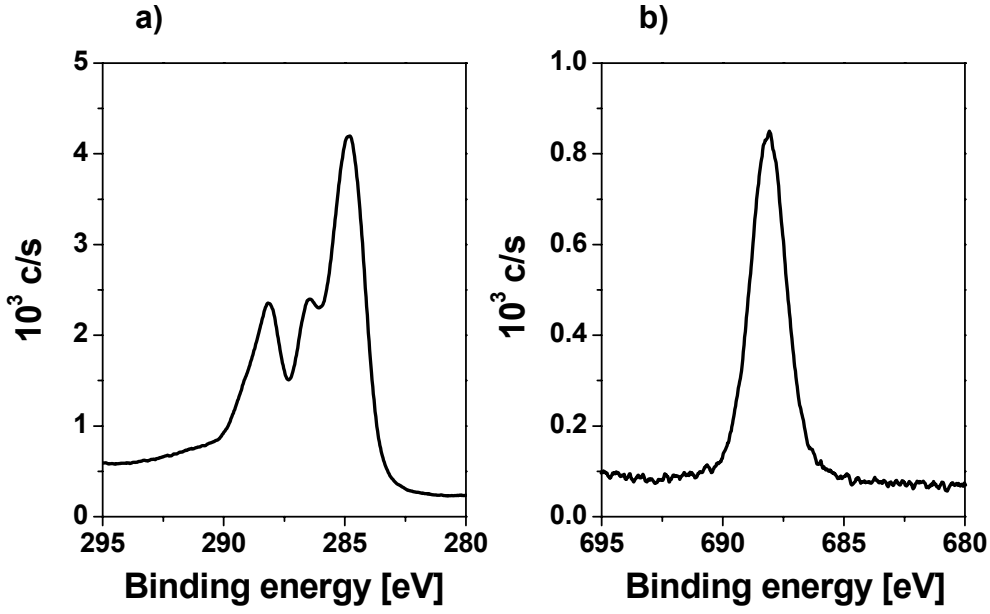

Figure 4-4: Detail spectra of a) C(1s) and b) F(1s) from PGL1155-PFB.

The relationship between the number and the intensity of carbon and fluorine is given by the Equation 4-1.

$$\frac{N_C}{N_F} = \frac{I_C}{I_F} \cdot \frac{S_F}{S_C} \qquad \textit{Equation 4-1}$$

N_C and N_F are the number of the carbon and fluorine atom from PFB group. I_C and I_F are the intensity of carbon and fluorine originated from PFB group, while S_C and S_F are atomic sensitivity of carbon and fluorine, respectively.

As shown in Figure 4-5, λ is the inelastic mean free path of the electron. X is path length of the electron in a giving material (x ~ 3λ assumed to be ca. 10 nm). Θ is the take-off angle relative to the sample surface (in the described experiment is Θ = 45°). Based on this relationship, the depth up to which atoms can be detected *D* is calculated to be ca. 70 Å. As a result, the layer thickness *d* of the PFB group on the surfaces can be estimated by using the Equation 4-1 and Equation 4-2.

$$\frac{d}{D} = \frac{I_C}{I} \qquad \textit{Equation 4-2}$$

I is here the whole intensity of all carbon signals originating from the pigment itself and from the PFB group.

The results of the integral intensity of each atom are set off in Table 4-1. As each atom has a different sensitivity in the XP experiment, the integrated intensity of each atom must be divided with the corresponding atom sensitivity factor. The layer thickness of the PFB group on PGL1155 and PGL1840 (results s. Chapter 10.1) is estimated to be around 4 Å. The theoretical calculation of the structure length of the PFB group is around 7 Å, showing that the PFB does not have an ideal packing on the pigment surface. However, the relative good agreement of measured and expected valves shows on the other hand, that the reaction proceeds as expected.

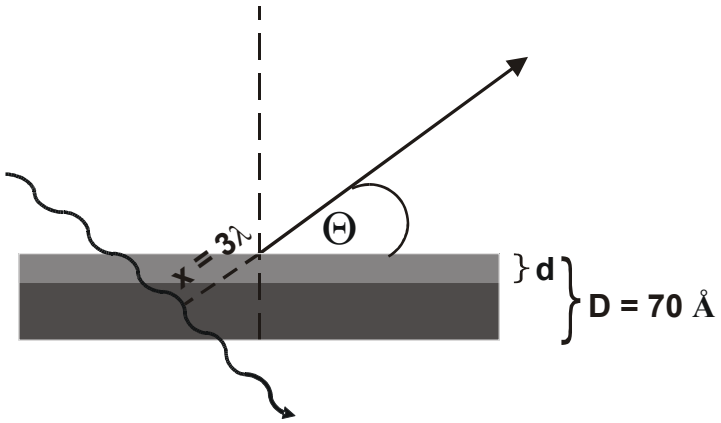

Figure 4-5: Description of the path way of the x-ray and the ion ejection to the detector.

Table 4-1: Atomic sensitivities and intensities of C(1s), N(1s), O(1s) and F(1s) from PFB-modified PGL1155.

atom	sensitivity	integral intensity	integral intensity / sensitivity
C	0.314	12637	40245
N	0.499	5512	11046
O	0.733	6925	9447
F	1.000	1529	1529

Thus, the model reaction shows that the PFB group can be covalently attached to the pigment surfaces via reaction between acid chloride and imino groups on the pigment surfaces. The result suggests that the acid chloride can be used as an anchor group for immobilization of initiator or monomer groups to the pigment surfaces.

4.2 Synthesis and immobilization of the initiator

This chapter describes investigations that one aimed at the modification of pigment surfaces with initiators in order to decorate the surfaces with a "polymer brush" following the so-called "grafting-from" approach[52-54]. This technique uses self-assembled azo-initiator monolayers (SAIMs) for the surface-initiated polymerization of vinyl monomers.

As shown in Chapter 4.1, the acid chloride acts as an anchor group that can be immobilized to the pigment surfaces through reaction with imino group on the surfaces. In order to build up SAIMs on the pigment surfaces, 4,4´-azobis-(4-cyanopentanoyl chloride) (ABCC) was synthesized. ABCC has an initiator moiety, which is similar in structure to AIBN which can initiate free radical polymerization, and an acid chloride group to anchor it to the pigment surfaces in the same fashion as mentioned in Chapter 4.1.

The synthesis of the initiator ABCC was carried out as shown in Figure 4-6[49,86]. PCl_5 in CH_2Cl_2 was added to a suspension of 4,4′-azobis-(4-cyanopentanoic acid) (ABCA) in CH_2Cl_2 and stirred at room temperature for 16 hours. After removing the excess of PCl_5, ABCC was precipitated in hexane at 0 °C, washed with cold hexane, dried in vacuum and kept under inert gas. The chemical structure of ABCC was verified by NMR and FTIR spectroscopy (s. Experimental).

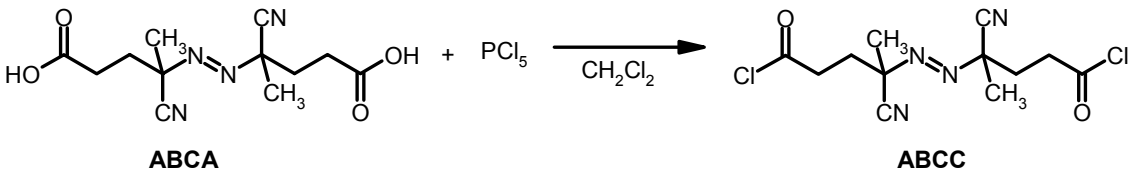

Figure 4-6: Synthesis of 4,4´-azobis-(4-cyanopentanoyl chloride) (ABCC).

The decomposition of the azo groups was followed by DSC measurement (data not shown). The molar enthalpy of decomposition can be calculated from the integration of the DSC signal giving a value of 190 ± 8 kJ mol^{-1} ($T_{max.}$ ~ 121 °C)

Analogous to the immobilization of PFB-Cl described in Chapter 4.1, ABCC was immobilized onto the pigment surfaces (s. Figure 4-7) in dry CH_2Cl_2 in the presence of NEt_3 under N_2-atmosphere.

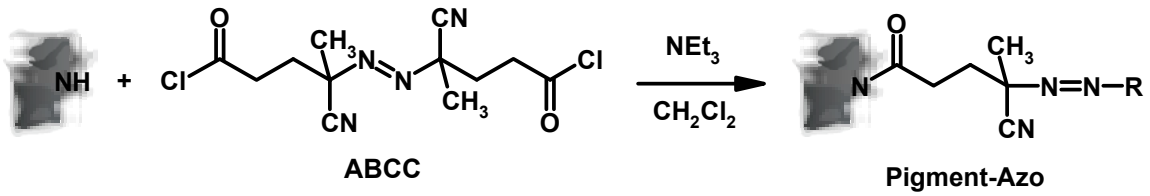

Figure 4-7: Immobilization of azo initiator ABCC to organic pigment surfaces.

The amount of azo initiator deposited onto the pigment surfaces was determined through DSC measurements by monitoring the exothermal decomposition of the azo group. In order to remove the last traces of the used solvent, the measurement was carried out in three steps. In the first step, the sample was heated from 20 °C to 100 °C and held at this temperature for 30 seconds. In the second step, the sample was cooled from 100 °C to 20 °C and held at this temperature for 5 minutes. In the last step, the sample was heated from 20 °C to 200 °C. The heating rate for the every step was 10 °C min^{-1}. Figure 4-8 shows typical DSC traces obtained from the pigments prior to and after deposition of ABCC (last step only).

The DSC measurements of the unmodified pigments, which were carried out as control experiments, show no endo- or exothermal feature between 30 °C to 180°C (s. dashed line in Figure 4-8). After immobilization of ABCC, the DSC-traces of both pigments show an exothermal peak at around 120 °C (121 °C for PGL1155-Azo and 117 °C for PGL1840-Azo) due to the decomposition of the azo group on the pigment surfaces. The not surface-attached ABCC shows the exothermal peak at 120 °C[86].

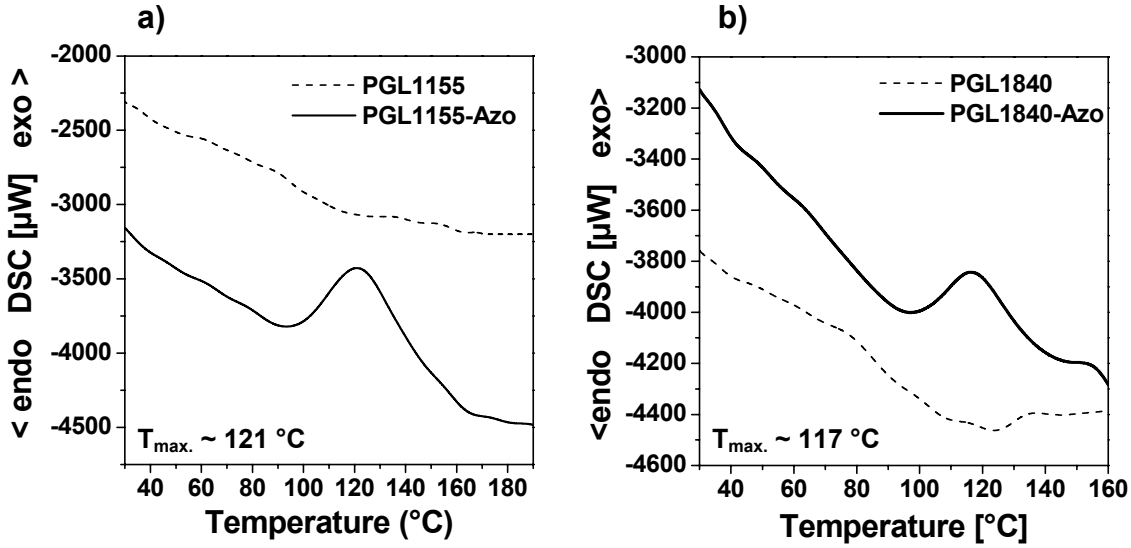

Figure 4-8: DSC traces of azo-modified pigments (solid line) in comparison to unmodified pigments (dashed line): a) PGL1155 and PGL1155-Azo as well as b) PGL1840 and PGL1840-Azo; heating rate 10 °C min^{-1}.

The grafted amount of the initiator δ_{Azo} [µmol g^{-1}] can be calculated from the enthalpy of the decomposition process by using Equation 4-3[53]:

$$\delta_{Azo} = \frac{I_{dec}}{\Delta H_{dec}} \qquad \textit{Equation 4-3}$$

where I_{dec} is the area under the signal from the exothermic decomposition in the DSC trace of the immobilized initiator and ΔH_{dec} is the molar enthalpy of decomposition of the ABCC (190 ± 8 kJmol^{-1}).

The graft density of the azo initiator Γ_{Azo} [µmol m^{-2}] and average distance d [nm] between two anchor groups on the pigment surfaces can then be calculated from Equation 4-4 and Equation 4-5, respectively.

$$\Gamma_{Azo} = \frac{\delta}{SA_{sp}} \qquad \textit{Equation 4-4}$$

$$d = \sqrt{\frac{1}{\Gamma_{Azo} N_A}} \qquad \textit{Equation 4-5}$$

SA_{sp} is the specific surface area of the pigment particles which was determined by the supplier (N_2-BET method: $SA_{PGL1155}$ ~ 44 ± 0.1 $m^2\ g^{-1}$ and $SA_{PGL1840}$ ~ 66 ± 0.1 $m^2\ g^{-1}$) and N_A is Avogadro's number.

The graft densities of the initiator-modified pigments were calculated from the results of DSC-measurement and are summarized in Table 4-2.

Table 4-2: Graft densities of the azo initiator on the pigment particles as determined by DSC as well as the average distance between two azo groups.

Pigment-Azo	I_{dec}* [J g^{-1}]	δ_{Azo} [µmol g^{-1}]	Γ_{Azo} [µmol m^{-2}]	average distance between azo groups d [nm]
PGL1155-Azo	9.29 ± 0.47	51	1.2	1.2
PGL1840-Azo	2.72 ± 0.26	11	0.2	2.9

* average of 3 measurements.

From a value of the graft density of 1.2 µmol m^{-2}, it can be derived that about 0.7 initiator molecules per nm^2 are immobilized, giving an average distance between two anchor sites of 1.2 nm. Prucker et al.[52] have studied the immobilization of various azo chlorosilanes to silica gels or silicon substrates and obtained about 0.8 – 1.6 initiator molecules per nm^2 giving average distance between two anchoring groups 0.8 – 1.0 nm. It can be seen that the graft density of initiator molecules on the organic pigment in this study is comparable to that found on SiO_x surfaces.

As can be seen form Table 4-2, the graft density of the initiator on PGL1840 surfaces is 6 times lower than that on PGL1155 surfaces. As described for the azo pigments (s. Introduction; Figure 1-10), the almost completely planar structure of the red pigment is distorted by an addition of the methoxy group forcing the molecule out of the molecular plane. Therefore, not only the conjugation pattern gets interrupted, but also the entire crystal geometry is changed. The geometrical structure of both pigments studied

here is also different as shown in Figure 4-9. PGL1840 can be packed well due to the π, π interaction and the intermolecular H-bonding. In contrast, the packing of pigment PGL1155 is less than that of PGL1840 due to steric hindrance of methyl group (–CH_3) in the structure and its asymmetric structure which may interfere with packing themselves. The packing coefficient of PGL1840 (0.80) is also reported higher than that of PGL1155 (0.78)[32]. As a result, it can be assumed that the anchor groups can reach the imino groups on the PGL1155 surfaces more easily than those on PGL1840 surfaces because PGL1155 molecules on the surfaces have more space available for the reaction with ABCC (s. Figure 4-10). The average distance between anchor groups also confirms this prediction (s. Table 4-2). The distance between anchor groups of the PGL1155 surfaces is 1.2 nm and that of PGL1840 is 2.9 nm.

The self-assembled azo-initiator monolayers on both pigments were used to initiate the radical polymerization as will be described in the following chapter. The results of polymerization using PGL1840-Azo are summarized in Chapter 10.

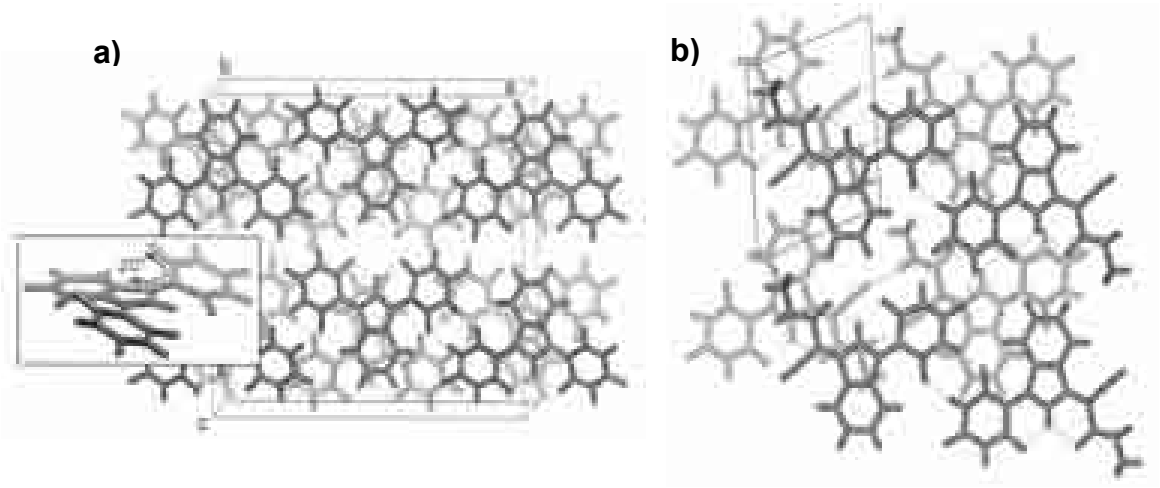

Figure 4-9: a) Molecular structure and packing diagram of PGL1840 and b) projection of PGL1155 along the b-axis showing two adjacent layer of moleculs: dashed lines represent intra- and intermolecular hydrogen bonds[32].

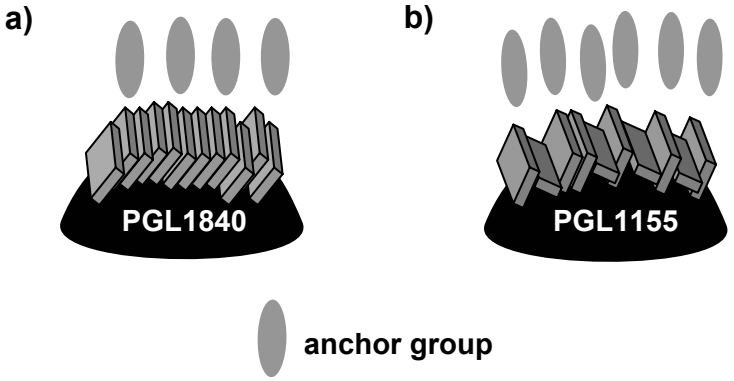

Figure 4-10: Artists impression of the reaction of anchor groups with imino groups on the pigment surfaces: a) PGL1155 and b) PGL1840.

4.3 "Grafting-from" polymerization via self-assembled azo-initiator monolayers

In this chapter, initiator-modified pigments, which were prepared as described in Chapter 4.2, were used to generate the polymer monolayers covalently attached to the pigment surfaces. The polymerization parameters (monomer concentration, polymerization time) are varied in order to study the influence on the amount of polymer grafted on the surfaces. In addition, the various vinyl monomer were also polymerized using these initiator-modified pigments to explore the versatility of these technique.

4.3.1 Layer thickness as a function of monomer concentration

To study the relationship between the layer thickness and monomer concentration, a series of polymerizations using initiator-modified pigment (PGL1155-Azo) was carried out at various concentrations of methylmethacrylate (MMA) in toluene at 60 °C for 16 hours. Non-attached polymer was removed through extensive washing with toluene. The free PMMA was precipitated in MeOH and characterized by GPC. UV-VIS spectroscopy and elemental analysis were used to characterize the polymer-grafted pigment.

The UV absorption spectra of polymer-grafted pigments and the integrated intensity between 385 nm and 470 nm as a function of the monomer concentration are shown in Figure 4-11a and b, respectively.

In Figure 4-11a, it can be seen that the absorption bands of the pigments become less intense as higher monomer concentrations were used for the preparation of the hybrid materials. This observation can be explained by a higher grafted amount for the materials which then consists of more UV-inactive PMMA. This fact becomes more obvious, if the integral intensity of the absorption band is normalized to the amount of the pigment used for recording the spectra and plotted against the MMA concentration used for preparation. The result is a linear relationship as shown in Figure 4-11b.

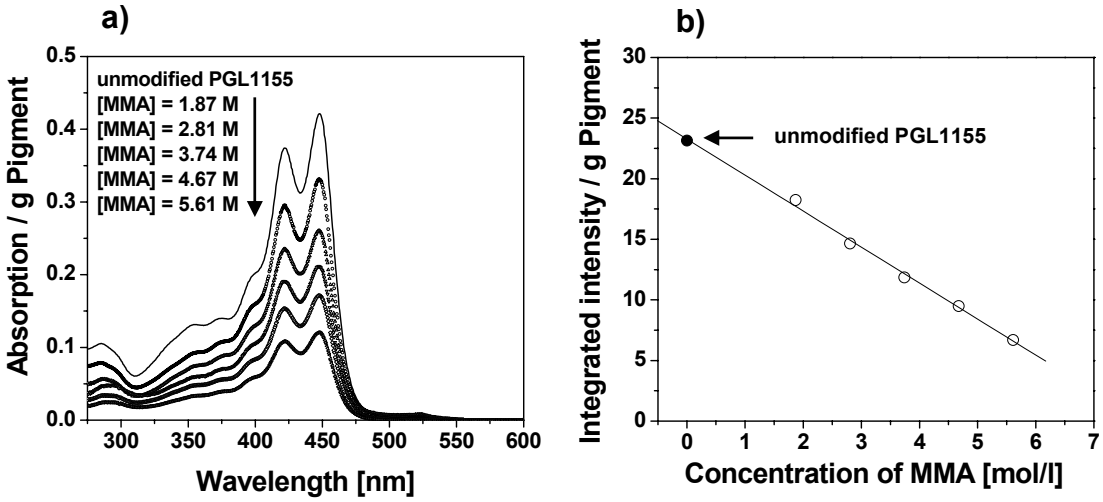

Figure 4-11: a) UV absorption of the polymer-grafted pigment in comparison to unmodified PGL1155; b) integrated intensity of the absorption band between 385 nm and 470 nm (per gram pigment) as a function of MMA concentration.

To obtain the grafted amount of polymer in terms of gram polymer per gram pigment, first a calibration curve was recorded by measuring UV spectra of unmodified pigment at different concentrations (s. Figure 4-12). The integrated intensities from the polymer-modified pigments can then be compared to the calibration curve. The results of these calculations are shown in Figure 4-13b (open circles).

Due to the fact that the nitrogen content originates only from the pigment, it can be expected that the grafted amount of polymer can be also determined from nitrogen content of material measured by elemental analysis. The increase of the amount of polymer attached on the pigment surfaces results in an increase of carbon and hydrogen content in the modified pigment. As a result, it leads to a reduction of the nitrogen content in the polymer grafted pigment. As shown in Figure 4-13a, it can be clearly seen that the nitrogen content of pigments obtained after polymerization decreases with increasing MMA concentration.

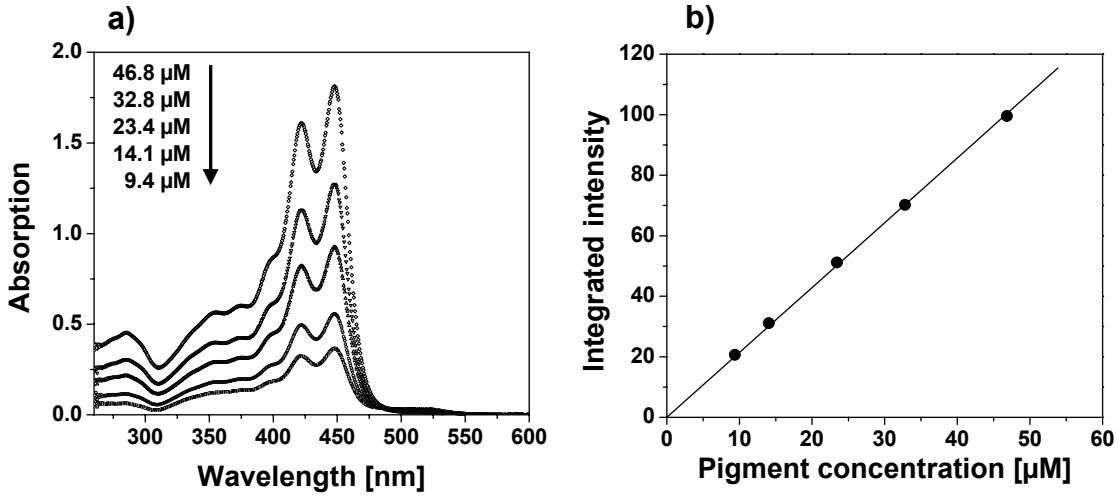

Figure 4-12: a) UV spectra of unmodified PGL1155 with various pigment concentration and b) calibration curve via integration of the UV absorption between 385 nm and 470 nm as a function of the pigment concentration.

The amount of polymer grafted can be also determined from the nitrogen content of the material using Equation 4-6.

$$N_{pigment-polymer} = aN_{pigment} + (1-a)N_{polymer}$$
$$a = \frac{N_{pigment-polymer}}{N_{pigment}} \qquad \textit{Equation 4-6}$$

The results of polymer grafted obtained from nitrogen content are summarized in Figure 4-13 together with the results obtained from UV absorption. Clearly, the calculation from both methods shows comparable results and the amount of attached polymer can be calculated by either UV absorption or elemental analysis.

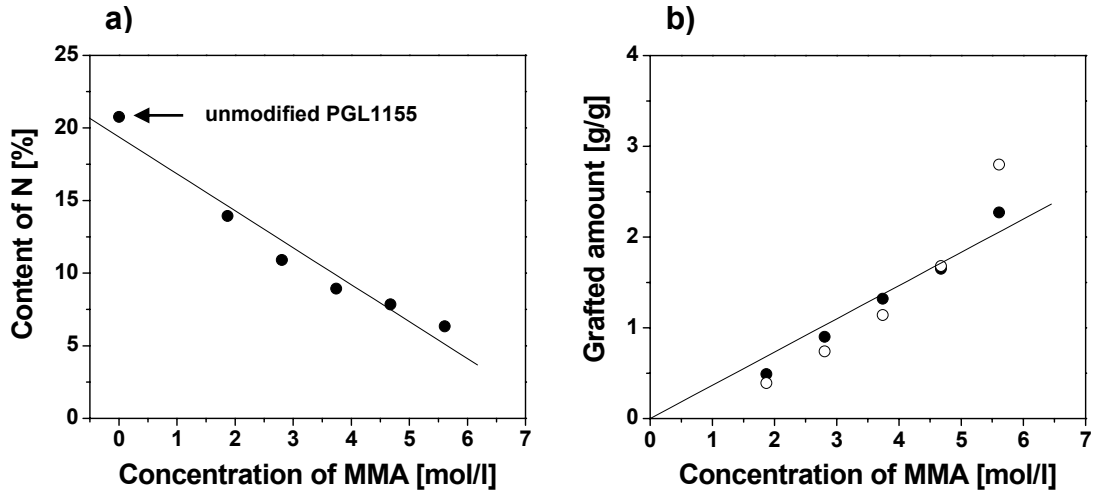

Figure 4-13: a) Nitrogen content of polymer modified PGL1155 pigments as a function of MMA concentration during polymerization determined by elemental analysis; b) grafted amount of polymer as a function of the MMA concentration calculated from a) [●] for compared the results obtained from UV absorption [○] are shown.

From the grafted amount δ (gram polymer pro gram pigment), the layer thickness of the polymer L [nm] on the pigments can be calculated by using Equation 4-7

$$L = \frac{\delta}{SA_{sp} \cdot \rho_{PMMA}} \qquad \textit{Equation 4-7}$$

where ρ is material density of the polymer (ρ_{PMMA} ~1.2 g ml^{-1})[134] and SA_{sp} is the specific surface area of pigment.

As shown in Figure 4-14, the layer thickness increases with increasing monomer concentration and was in the experiments described here from 9 nm to 43 nm.

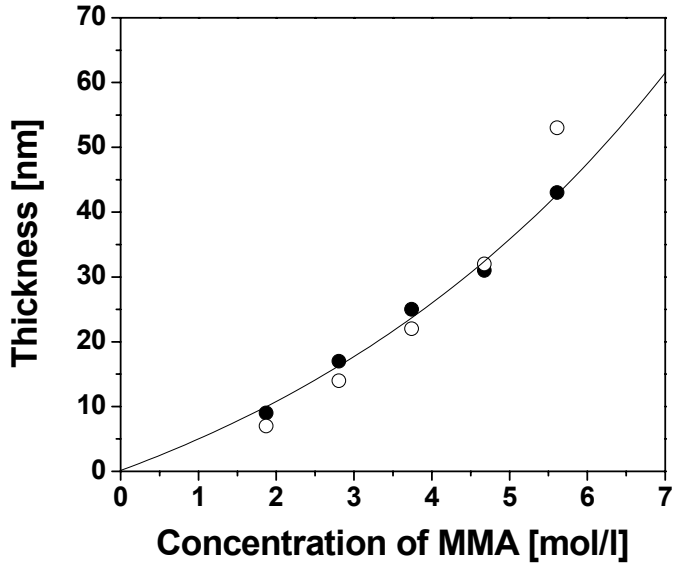

Figure 4-14: Layer thickness of the polymer monolayers as a function of the MMA concentration as calculated from nitrogen contents measured by elemental analysis [●] and from UV spectra [○].

In general, the molecular weight of a polymer generated by radical chain polymerization is directly proportional to the monomer concentration[135]. Therefore, the increase of the layer thickness with the monomer concentration is largely caused by an increase in the molecular weight of the surface-attached polymers. The deviation from the linear slope is due to transfer to solvent (toluene) and monomer as it has been shown for the formation of PMMA brushes on silicon substrate[136].

The molecular weight of polymer prepared by free radical polymerization depends on parameters like initiator concentration, monomer concentration, temperature, solvent or chain transfer[135,137]. It is known that the rate of polymerization v_p is linearly proportional to the monomer concentration and to the square root of the initiator concentration as described in Equation 4-8[135,137]

$$v_p = k_p \cdot \sqrt{\frac{fk_d}{k_t}} \cdot [I]^{0.5} \cdot [M] \qquad \textit{Equation 4-8}$$

where k_p, k_t and k_d are temperature-dependent reaction constants for chain propagation, chain termination and initiator decomposition. f is the initiator efficiency, while [I] and [M] are the initiator and monomer concentration.

However, chain transfer reactions to monomer, polymer, initiator or solvent are observed during the polymerization reaction. Therefore, the number-average degree of polymerization $\overline{X}_n$ can be written as[138]

$$\frac{1}{\overline{X}_n} = \frac{1}{X_0} + C_M + C_I\frac{[I]}{[M]} + C_S\frac{[S]}{[M]} + C_p\frac{[P]}{[M]} + \cdots \qquad \textit{Equation 4-9}$$

$$X_0 = \frac{k_p[M]}{\sqrt{2fk_dk_t[I]}}$$

where X_0 is the number-average degree of polymerization obtained in the absence of transfer reactions. C_M, C_I, C_S and C_P are chain transfer constant for monomer, initiator, solvent and polymer. [*I*], [*M*], [*S*], and [*P*] are the initiator, monomer, solvent and polymer concentration, respectively.

The chain transfer constants for initiator and polymer are small and [*S*] is much larger compared than all other concentration so that Equation 4-9 can be reduced to[138]

$$\frac{1}{\overline{X}_n} = \frac{1}{X_0} + C_M + C_S\frac{[S]}{[M]} \qquad \textit{Equation 4-10}$$

From this equation, the molecular weight of polymers attached to the surfaces can be calculated as shown in Figure 4-15 (solid line) and compared to the molecular weight of the non-attached polymers as determined by GPC (solid circle). It can be seen that the number-average molecular weight calculated from Equation 4-10 is comparable to that obtained by GPC measurements. This result agrees with the conventional free radical polymerization in the solution as described by Mayo.

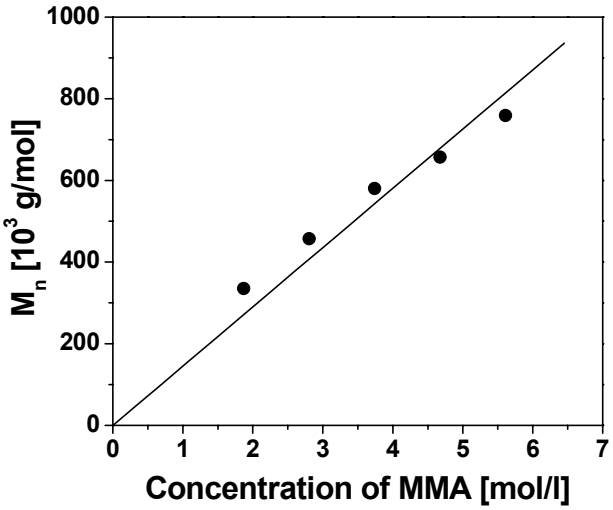

Figure 4-15: Number-average molecular weight of free polymer as determined by GPC [●] in comparison to those calculated from Equation 4-10 (solid line) as a function of the MMA concentration.

The same effect was found by Schimmel[136]. He used the azo initiator layer attached to planar SiO_x substrates to polymerize MMA. The initiator concentration in his system was very low and the polymerization was dominated by the chain transfer to monomer or solvent for the termination reaction. Therefore, the average molecular weight of the polymer attached to the surfaces was same as the non-attached polymer in the solution. In contrast to those results, Prucker[86] has used an azo initiator attached to silica particles ($\delta_{(Azo)}$ = 525 µmol g^{-1}; $[I_0]$ = 3.2 mmol l^{-1}). He found that under some reaction condition the recombination between radicals on the polymer chain in solution is dominating and that the molecular weight of surface-attached and free polymer differs.

In this study, the initiator concentration (0.64 mmol l^{-1}) is rather dilute (8 times lower than that of the azo initiator attached silica particles). It can be assumed that the polymerization of MMA with PGL1155-Azo has a behavior similar to the system from Schimmel and that the number-average molecular weight of surface-attached polymer and that of the polymers formed in solution are similar. In addition, methylacrylates are only weakly prone to recombination reactions which take place in solution polymerizations also only at a relatively low yield. Therefore, the molecular weight of the polymer formed in solution will be used for the calculation of the graft density of polymer chains attached to the surface in the following experiments.

4.3.2 Graft density as a function of polymerization time

To study the influence of the initiator conversion on this grafting-from process several experiments were carried out using identical conditions ([MMA] = 4.67 mol l^{-1} and T = 60 °C) but varying the polymerization time. Again, non-attached polymer was removed through extraction und the resulting PMMA-modified pigments were analyzed by elemental analysis and UV-VIS spectroscopy.

As shown in Figure 4-16 and Figure 4-17a, the UV absorption and the nitrogen content obtained from elemental analysis decreases with increasing polymerization time. With higher conversion of initiator, an increase of the number of attached polymer chains on the pigment surfaces is observed. Again, the amounts of grafted polymer determined from the integrated intensity of the UV absorptions and from the nitrogen contents measured by elemental analysis are comparable (s. Figure 4-17b). In addition, it should be noted that the reaction was carried out with separately prepared pigment initiators termed azo 1 (○) and azo 2 (△) in Figure 4-16b. The good agreement of the results shows, that the initiator monolayer can be reproduced in a reproducible fashion.

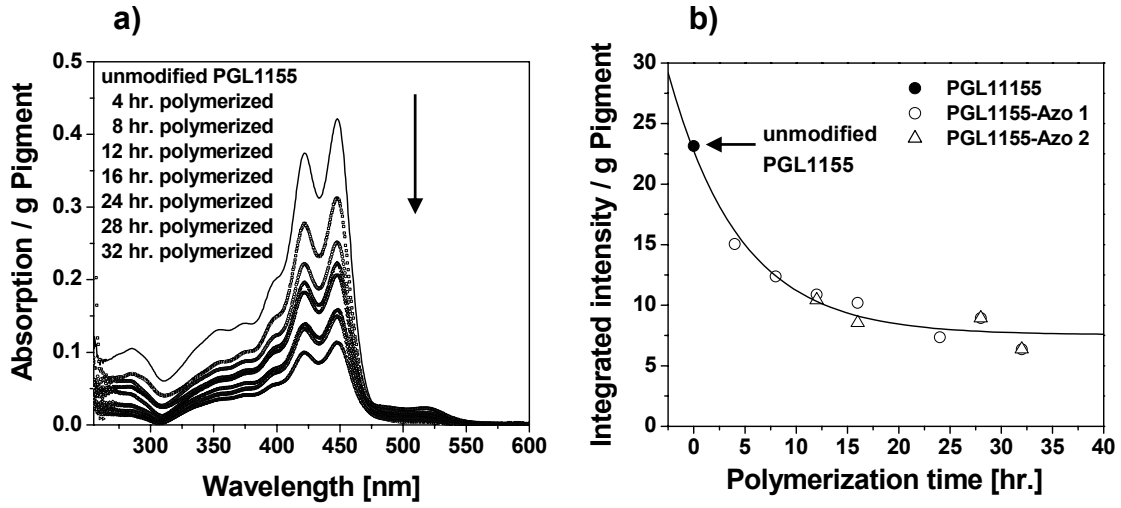

Figure 4-16: a) UV absorption spectra obtained from polymer-grafted PGL1155 in comparison to unmodified PGL1155; b) integral intensity of the UV bands as a function of polymerization time: PGL1155-Azo 1 [○] and PGL1155-Azo 2 [△] indicate independent series of experiments.

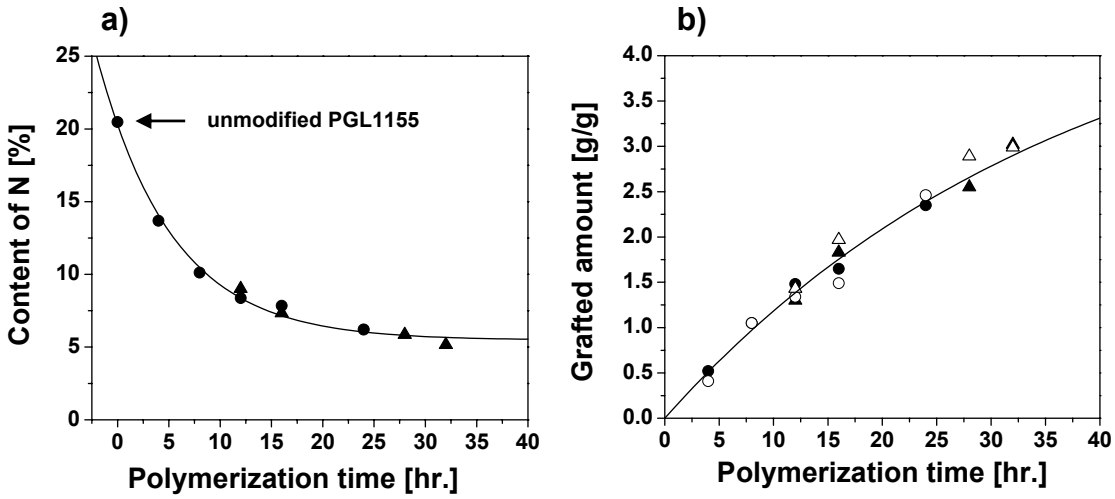

Figure 4-17: a) nitrogen content measured by elemental analysis and b) grafted amount calculated from nitrogen content (solid symbol: ● and ▲) in comparison to that calculated from UV spectra (open symbol: ○ and △) as a function of polymerization time: circle and triangle symbols indicate independent series of experiments.

As shown in Equation 4-8, the rate of polymerization and the molecular weight of the polymer are dependent on [*M*] and [*I*] but independent of the polymerization time. In this system, the number-average molecular weight of the non-attached polymer (PMMA) determined by GPC is comparable for all experiments except at polymerized until 32 hours (s. Figure 4-18). In the case of polymerization MMA to 32 hours, the molecular weight of the polymer attached to surfaces probably increases due to the gel effect[135,137], because of the high viscosity of the system at high monomer conversion.

As shown in Figure 4-18, the number-average molecular weight M_n at short polymerization time is ~ 662 000 g mol^{-1} and the weight-average molecular weight M_w ~ 1 410 000 g mol^{-1}. The polydispersity ($D = M_w/M_n$) of the polymers is around 2.1, which is typical value observed in free radical polymerization of methylmethacrylate.

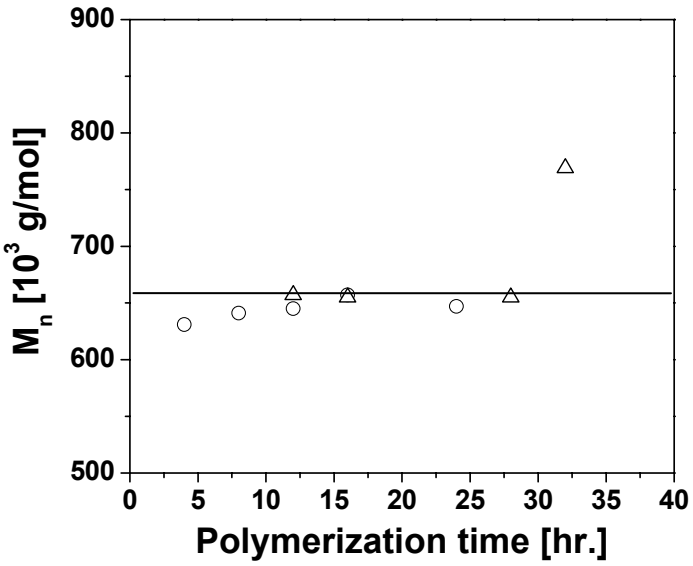

Figure 4-18: Number-average molecular weight of free polymer as determined by GPC.

In order to calculate the graft density Γ_{PMMA} [mol m^{-2}] of PMMA on the pigment surfaces, Equation 4-11 was used

$$\Gamma_{PMMA} = \frac{\delta}{M_n SA_{sp}} \qquad \textit{Equation 4-11}$$

Here M_n is the number-average molecular weight of the non-attached polymer as determined by GPC.

The layer thickness as determined by Equation 4-7 and graft density of the PMMA on the pigments are shown in Figure 4-19.

The initiator decomposition follows a first order kinetics[135] which can be used to calculate the graft density as

$$\Gamma_t = \Gamma_0 \cdot f(1 - e^{k_d t}) \qquad \textit{Equation 4-12}$$

where Γ_t is the graft density of the polymer at time t, Γ_0 is the originate graft density of the initiator, f is the radical efficiency and k_d is the rate constant of the initiator decomposition.

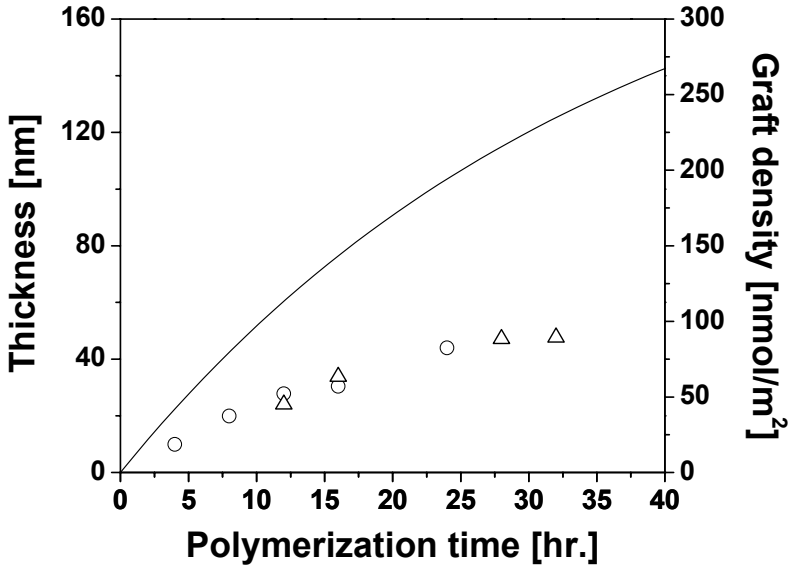

Figure 4-19: Layer thickness (left) and graft density (right) of PMMA as a function of the polymerization time: the solid line describes the kinetics of free radical polymerization using Equation 4-12 (Γ_0 ~ 1.2 µmol m^{-2}, f = 0.33 and k_d ~ 7.8 x 10^{-6} s^{-1} for AIBN[126]).

As expected, the layer thickness, i.e. the graft density of the polymer, initially increases and levels off at 57 nm (89 nmol m^{-2}) after 16 hours polymerization time. Increasing the polymerization time further has no influence on the polymer film thickness, i.e. the graft density of the polymer. However, the graft densities of the polymer calculated using Equation 4-11 are lower than those calculated using Equation 4-12. This might be due to a loss of the initiator from the pigment surfaces through partial solubility of the pigment in the polymerization solution. To study the solubility issue, PGL1155-Azo was treated under the same conditions, however, the polymerization solution was kept at room temperature for 16 hours. The pigment was then directly filtered off and dried in vacuum. The initiator graft density was found to be only 0.9 µmol m^{-2} as determined by DSC (s. Table 10-2 in Chapter 10). This experiment confirms the assumption that a part of

initiator attached pigment surfaces goes into solution during the polymerization. Therefore, the graft density of the initiator and accordingly the graft density of the polymer are not so high as expected from the simple reaction analysis. Another explanation would be that the molecular weights obtained by GPC are not quite correct.

The average distance *d* [nm] between two grafted polymer chains is given by

$$d = \sqrt{\frac{1}{\Gamma_{PMMA} N_A}} \qquad \textit{Equation 4-13}$$

where Γ_{PMMA} is the graft density of polymer and N_A is Avogadro's constant.

As shown in Figure 4-20, the average distance of the grafted polymer decreases from 9 nm after 4 hours of polymerization time to 4 nm after 24 hours, and then reaches a constant value.

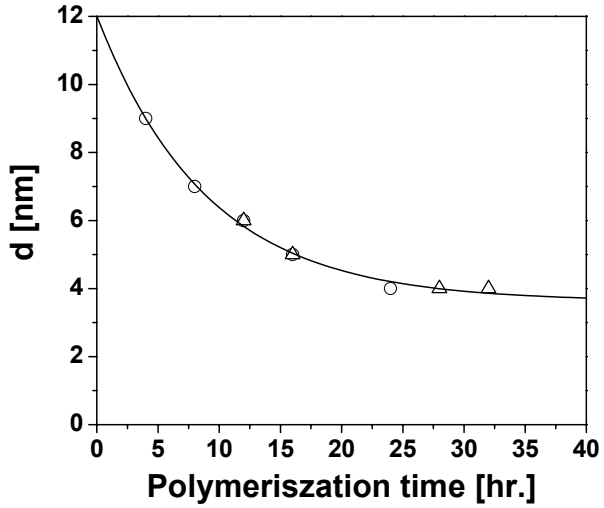

Figure 4-20: Average distance between two grafted polymer chains on the pigment as a function of polymerization time.

The radius of gyration R_g of a polymer molecule in a solvent can be calculated according to[139]

$$R_g = K\overline{M}_w^{\nu} \qquad \textit{Equation 4-14}$$

with K being a constant (K = 1.1 x 10^{-2} for PMMA), ν = 0.596 and $\overline{M}_w$ is around 1 410 000 g mol^{-1} determined by GPC.

According to this, the radius of gyration of the polymers formed in this experiment would be 51 nm in a good solvent. The distance between two chains on the surface is much smaller than that value which indicates the polymer obtain a brush-like conformation at the surfaces.

4.3.3 Polymerization with different monomers

In order to explore the versatility of this technique for the modification of pigment surfaces a variety of different monomers were tested for their performance during surface-initiated free radical polymerization.

As shown in Figure 4-21, hydrophilic monomers (methacrylic acid (MAA) and *N*,*N*′-Dimethylacrylamide (DMAA)) as well as hydrophobic monomers such as styrene and 1-(3,3,4,4,5,5,6,6,7,7,8,8,9,9,10,10,10-heptadecafluoro-decyloxy)prop-2-en-1-ol (HDFDA) were polymerized using the initiator-modified pigments. The polymerization conditions of each monomer are summarized in Table 4-3.

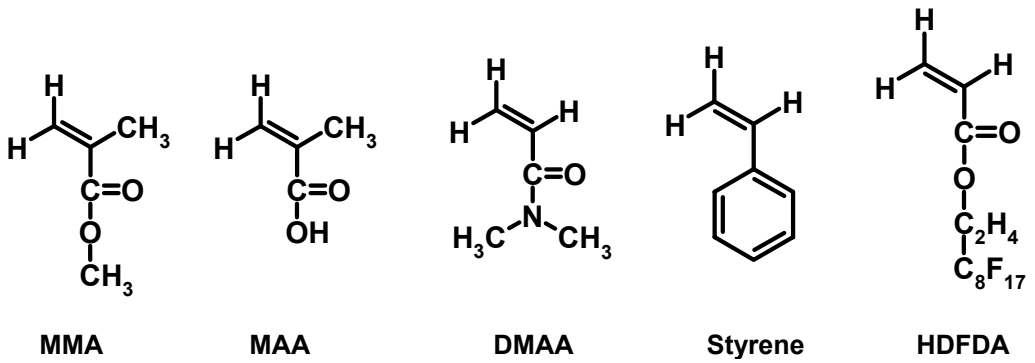

Figure 4-21: Monomers initiated by SAIMs attached onto pigment surfaces.

Table 4-3: Conditions of polymerisation of various monomers by SAIMs attached on PGL1155.

monomer	concentration [mol l^{-1}]	solvent	time [hours]
MMA	1.87 – 5.61	toluene	16
MAA	3.54 – 4.72	water	16
DMAA	3.88	$CHCl_3$	16
styrene	4.36 – 8.73	toluene	16
HDFDA	0.90	CCl_3CF_3	24

all polymerisation reactions were carried out at 60 °C.

In order to gain structural qualitative about these materials, the polymer-modified pigments as well as unmodified pigment PGL1155 were characterized by XP spectroscopy. The spectra are shown in Figure 4-22.

Besides the signal of C(1s) at 285 eV, N(1s) at 400 eV, and O(1s) at 531 eV originating from the pigment material itself (s. Figure 4-22a), the survey spectrum of PGL1155-PHDFDA (s. Figure 4-22f) shows a strong of F(1s) signal at 689 eV due to the existing fluorine atom from the surface-attached polymer molecules. Because of the high layer thickness (L_{PMAA} ~ 40 nm and L_{PMMA} ~ 31 nm determined as described above) on the surface, the N(1s) signal of PMAA- and PMMA-modified pigment is strongly attenuated (s. Figure 4-22b and c, respectively) since those surface-attached polymers do not contain any nitrogen atom in their chemical structures. In contrast, the O(1s) signals of both polymer-modified pigments increase in comparison to the pigment without polymer (s. Figure 4-22a, b and c) caused by oxygen atom from the polymer chains.

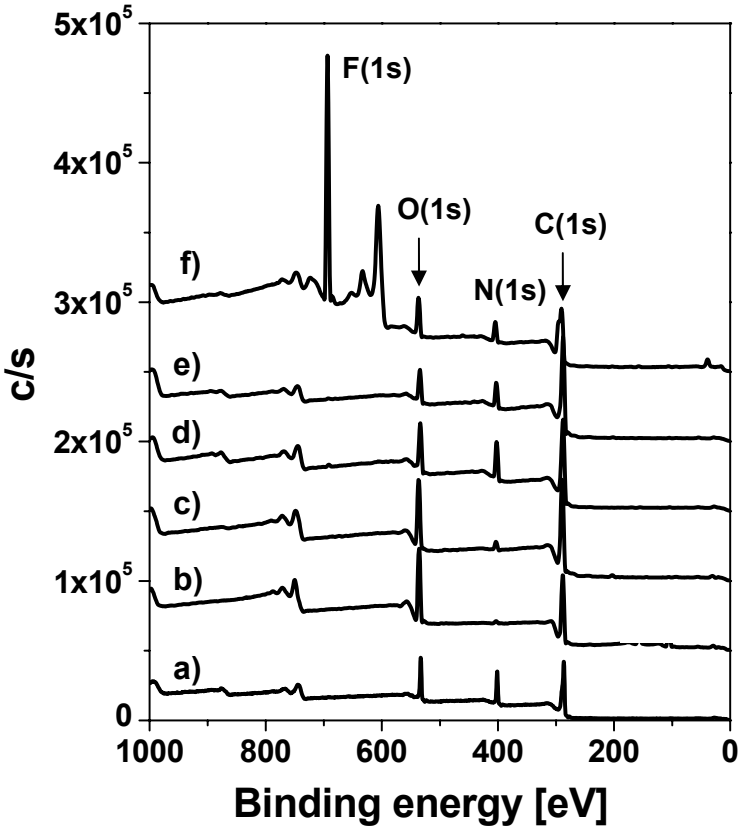

Figure 4-22: XP survey spectra of a) unmodified PGL1155, b) PGL1155-PMAA [L ~ 40 nm], c) -PMMA [L ~ 31 nm], d) -PDMAA [L ~ 5 nm], e) -PS [L ~ 5 nm] and f) -PHDFDA [L ~ 7 nm].

Figure 4-23 shows the C(1s) detail spectra of the unmodified PGL1155 and polymer-modified pigments. The binding energies (BE) and peak assignments are shown in Table 4-4 (fitted curves of the C(1s) signals are shown in Chapter 10; Figure 10-10). Besides the typical signals from the pigment substrate [C-C, C-H at 284.6 eV , C-O and C-N at 286.5 eV (286.3 eV)[21], CN at 288.0 eV (287.6 eV)[86,140], CONH at 288.9 eV (289.0 eV)[21] and $\pi \rightarrow \pi^*$ at 290.3 eV (290 eV)[141]], additional features at 284.6 eV due to C-C and C-H and the typical signals based on the surface-attached polymers are observed after polymerization of the respective monomers, e.g. COOH at 289.2 eV (PMAA), $COOCH_3$ at 288.6 eV (PMMA), $CONH(CH_3)_2$ at 288.9 eV (PDMAA) and $\pi \rightarrow \pi^*$ at 291.3 eV (PS). In addition, the C(1s) signals from CF_2 (291.4 eV) and CF_3 (293.5 eV) were found after polymerizing HDFDA with the PGL1155-Azo initiator (s. Figure 4-23f). The obtained values for the CF-signals are similar to those reported for typical fluorinated compounds in the literatures (291.9 – 294.0 eV)[129,130,142]. Due to the high layer thickness

of PMAA and PMMA, the peak of C≡N and $\pi \rightarrow \pi^*$ coming from the pigment surfaces are almost invisible.

Table 4-4: Binding energies (BE; eV) of C(1s) and contributions from structural features of the polymer-modified PGL1155 to the overall C(1s) intensity.

Assignment	**PGL1155 eV; (%)**	**PMAA eV; (%)**	**PMMA eV; (%)**	**PDMAA eV; (%)**	**PS eV; (%)**	**PHDFDA eV; (%)**
C-C, C-H	284.6; (53)	284.6; (78)	284.6; (66)	284.6; (58)	284.6; (69)	284.7; (35)
C-O, C-N	286.3; (18)	285.8; (17)	286.2; (19)	285.4; (17)	286.5; (16)	286.3; (22)
C≡N	288.0; (16)	–	–	287.9; (14)	288.4; (7)	287.8; (5)
CONH or COO	288.9; (7)	289.2; (5)	288.6; (8)	288.9; (8)	289.3; (5)	288.8; (10)
$\pi \rightarrow \pi^*$	290.3; (6)	–	–	290.8; (3)	291.3; (3)	290.3; (3)
CF_2	–	–	–	–	–	291.4; (21)
CF_3	–	–	–	–	–	293.5; (4)

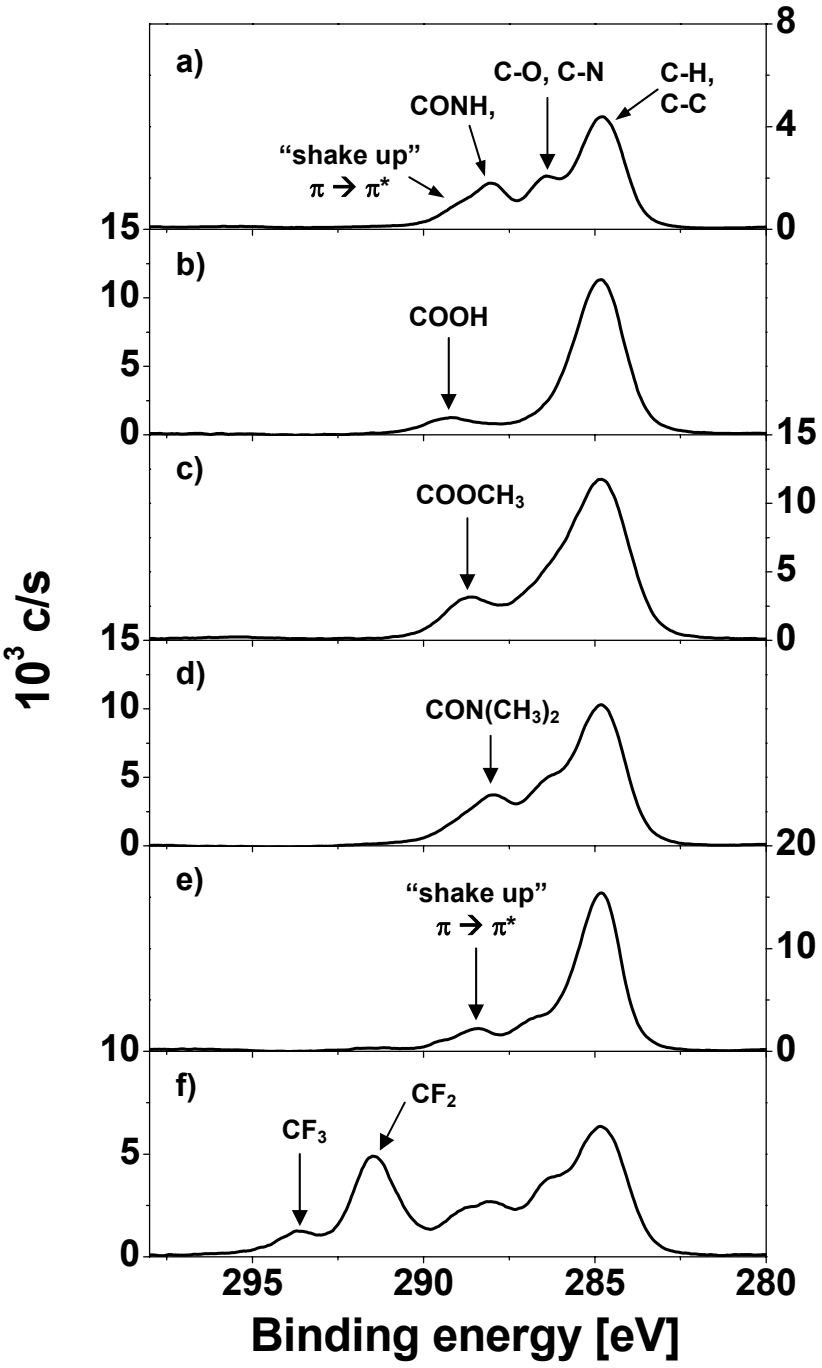

Figure 4-23: Detail scan of the C(1s) signals of polymer-modified pigments compared to the unmodified pigment: a) unmodified PGL1155, b) PGL1155-PMAA, c) -PMMA, d) -PDMAA, e) -PS and f) -PHDFDA.

Table 4-5 shows the layer thickness of the different polymer layers attached to pigment surfaces. The behavior of layers build up from MMA and MAA monomer seem to be similar. The layer thickness of both polymers can be adjusted by variation of the monomer concentration. Styrene and HDFDA monomer give only relatively thin layers which might be due to agglomeration of the particles in the unpolar solvent/monomer mixture. This could lead to a very low radical efficiency. PDMAA layers are also rather thin because the pigment dissolves in the polymerization solution to a significant extent, which can then initiate radical polymerization in solution (s. Figure 4-24).

Table 4-5: Layer thickness L of the different polymer attached pigment surfaces.

monomer	concentration [mol l^{-1}]	L* [nm]
MMA	1.87	9.3
	2.81	17.1
	3.74	25.1
	4.67	31.2
	5.61	43.1
MAA	3.54	18.2
	4.72	39.8
DMAA	3.88	4.9**
styrene	4.36	3.3
	8.73	4.9
HDFDA	0.90	6.6

* calculated from nitrogen content measured by elemental analysis using Equation 4-6 and Equation 4-7, respectively.

** determined from the integral intensity of UV absorption and subsequently using Equation 4-7.

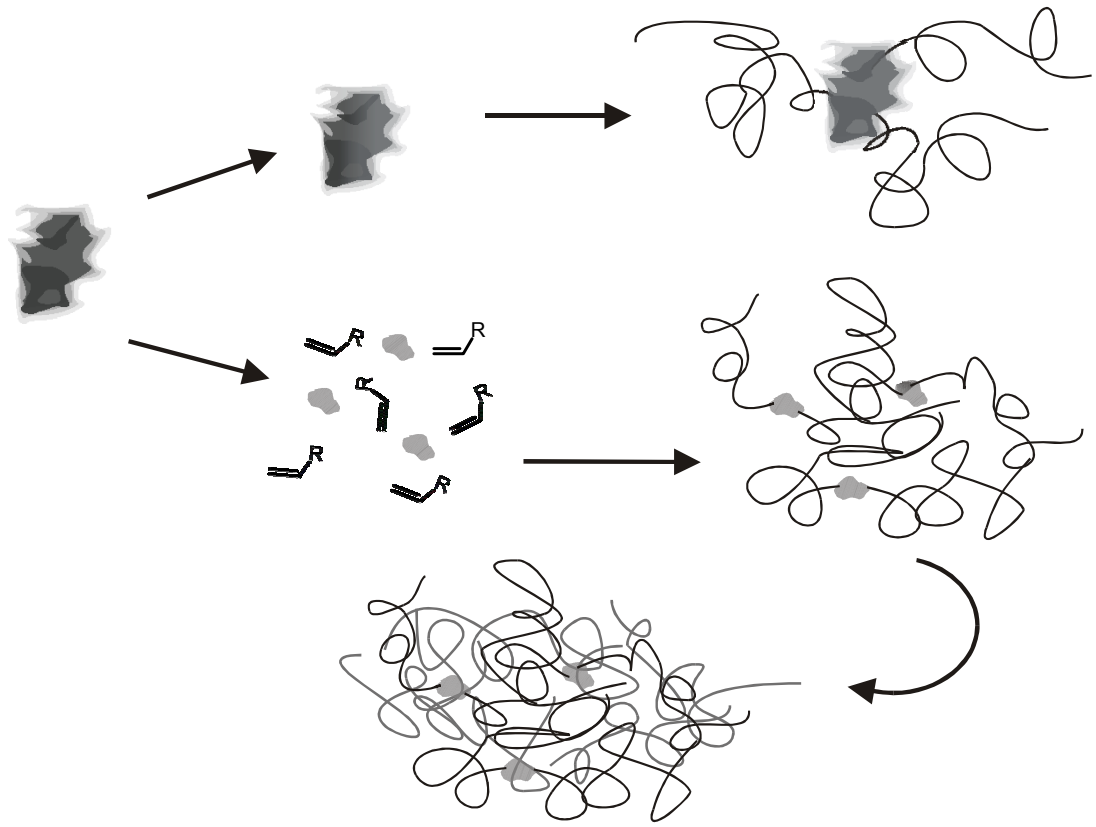

Figure 4-24: Demonstration of a release of groups from the pigment surfaces during the polymerization: the black lines represent polymer-attached surfaces and the chains drawn in gray are free polymer chains.

To prove this assumption, a set of the reference experiments in which the unmodified pigment PGL1155 (no surface-attached initiator) was treated under the same reaction conditions as the PGL1155-Azo (initiator-attached pigment), i.e. a complete polymerization reaction was carried out, but without initiator on the surface of the pigment. Table 4-6 shows the nitrogen content according to elemental analysis as well as the yield of non-attached polymer which was obtained using unmodified PGL1155 and PGL1155-Azo to polymerize the various monomers. The yield of non-attached polymer y [%] was determined by using Equation 4-15

$$y = \frac{free\ polymer\ formed\,[g]}{monomer\ charge\,[g]} \times 100 \qquad \textit{Equation 4-15}$$

Table 4-6: Yield of non-attached polymer obtained from polymerization of vinyl monomers using unmodified PGL1155 and PGL1155-Azo as well as nitrogen contents of the composite material according to elemental analysis.

	PGL1155		PGL1155-Azo	
	N [%]	*y*** [%]	N [%]	*y* ** [%]
untreated pigment	20.47	–	20.36 ± 0.13***	–
[MMA]* = 4.67 mol l^{-1}	18.94	1.4	7.84	49.2
[MAA]* = 3.54 mol l^{-1}	19.34	7.6	10.93	88.1
[DMAA]* = 3.88 mol l^{-1}	19.81	26.9	19.55	73.2
[styrene]* = 8.73 mol l^{-1}	20.05	0.9	16.98	5.4
[HDFDA]* = 0.90 mol l^{-1}	19.62	0.0	14.99	6.5

* pigments were polymerized with the corresponding monomer solution: MMA and styrene in toluene, MAA in water, DMAA in $CHCl_3$ and HDFDA in freon.
** yield of non-attached polymer obtained (calculated using Equation 4-15).
*** average of 6 measurements.

The nitrogen content of PGL1155 after polymerization shows no significant difference from the original value. In contrast to those, the nitrogen content of PGL1155-Azo after polymerization is less than the original value due to the increase of carbon and hydrogen from the polymer attached on the surfaces, except in the case of polymerization with DMAA. Because not only content of carbon or hydrogen increases, also the increase of the nitrogen content due to the monomer plays an important role for the nitrogen content.

The amount of non-attached polymer obtained from unmodified PGL1155 and initiator attached PGL1155 was also shown in Table 4-6. The results demonstrate that some of vinyl monomer was polymerized in the presence of unmodified PGL1155. In the case of the polymerization of HDFDA with PGL1155, no free polymer could be found after polymerization. In contrast to this, in the case of styrene, MMA, MAA and DMAA free polymer was obtained with a yield of ca. 1 %, 1 %, 8 % and 27 %, respectively. In contrast to those, the polymerization of vinyl monomer with PGL1155-Azo can form 49 % PMMA, 88 % PMAA, 73 % PDMAA, 5 % PS and 7 % PHDFDA, so that in all cases much more polymer was deposited of the azo was attached to the surface.

In order to determine the amount of pigment in the free polymer, the non-attached polymer (except PS and PHDFDA because both polymers are essentially insoluble in DMSO) was dissolved in DMSO and the light absorption of the solution was measured by UV spectroscopy. The concentration of non-attached polymer was ~ 2 – 5 mg polymer in 5 ml DMSO. The amount of pigment in the non-attached polymer was determined from the integrated intensity of UV band as mentioned above (s. Chapter 4.3.1). The results are summarized in Table 4-7.

Table 4-7: Determination of pigment content in free polymer using UV absorption.

polymer	concentration of monomer [mol l^{-1}]	pigment in free polymer [%]	
		PGL1155*	PGL1155-Azo*
PMMA	1.87	–	0.0
	2.81	–	0.1
	3.74	–	0.2
	4.67	0.1	0.6
	5.61	–	2.7
PMAA	3.54	0.8	22.0
	4.72	–	28.4
PDMAA	3.88	16.0	24.6

* corresponding monomer was polymerized with PGL1155 (non-attached initiator) or PGL1155-Azo (initiator-attached pigment): T = 60 °C and t = 16 hours.

As shown in Table 4-7, polymerization of the vinyl monomer using unmodified PGL1155 shows less than 1 % pigment in the free polymer, except for the PDMAA case, where ~ 16 % pigment were observed in the free polymer. Under this condition, the pigment could be somehow dissolved easier in the free PDMAA than in the free PMMA or PMAA.

The polymerization carried out using azo-modified PGL1155 shows that 1 – 3 % pigments were found in free PMMA showing that the pigment is very stable under these conditions. However, in the case of polymerization of MAA and DMAA from azo-modified PGL1155, 22 – 28 % of pigments were found in non-attached PMAA and 25 % of pigments were found in non-attached PDMAA.

The high amount of pigments found in the free PMMA polymerized using the azo-modified PGL1155 might be due to the strong H-bonding between the acid groups

from the polymer chain (PMAA) and H_2O (solvent used for polymerization). Thus, it is difficult to separate the modified pigment from the polymerization mixture after the polymerization reaction.

As shown by polymerization of DMAA using unmodified PGL1155 (non-attached initiator), 16 % pigments were already lost to the polymer solution. Consequently, it can be expected that during polymerization of DMAA using azo-modified PGL1155, the pigment can be also released in the reaction solution, i.e. the loss of surfaces-attached initiator. As a result, the layer thickness of the PDMAA attached pigment was found rather thin (~ 5 nm) as mentioned above.

4.3.4 Discussion and comparison with the pigment PGL1840

The self-assembled azo-initiator monolayers on the pigment surface can be obtained in a two step reaction: the preparation of an initiator with an appropriate anchor group and the immobilization of the initiator to the pigment surface via an acylation reaction. PGL1155-Azo and PGL1840-Azo can be used as analog to AIBN for initiation of the free radical polymerization. The free radical process used for the formation of the surface-attached monolayers tolerates the use of a wide variety of different monomers. The graft density and layer thickness of the surface-attached polymer can be adjusted via variation of important polymerization parameters such as polymerization time as initiator conversion or monomer concentration, which influence either the graft density or the molecular weight of the chains independently from each other. Generally, PGL1155-Azo shows higher polymer graft density than PGL1840-Azo due to the higher initiator graft density on the surfaces (1.2 and 0.2 µmol m^{-2} for PGL1155-Azo and PGL1840-Azo, respectively). PGL1155-Azo can be used to grow controlled layers with layer thickness up to 50 nm. In contrast, the layer thickness of PMMA can reached up to 30 nm by polymerization with PGL1840-Azo.

The average distance d of the two polymer grafted is found 4 nm and 9 nm for the polymerization using PGL1155-Azo and PGL1840-Azo, respectively. The distance between two chain anchors on the surface is much smaller than the dimension of the corresponding free polymer chain in good solvent (R_g = 51 nm and 46 nm of free polymer initiated by PGL1155-Azo and PGL1840-Azo respectively). This result suggests that the polymer chains attached on the pigment surfaces were stretching out themselves, i.e. formed so-called “polymer brushes” with high density.

4.4 Grafting of polymers via copolymerization of surface-attached monomer

In order to investigate an alternative synthetic approach for the modification of the surfaces of organic pigments, a strategy was followed that makes use of immobilized polymerizable groups, which are incorporated into growing polymer chains during free radical polymerization reaction proceeding in the contacting solution. Such approaches have already been investigated over the past decades for the modification of inorganic materials[47,48,50,57,88,143,144]. In this chapter, the monomer unit was immobilized to the organic pigment surfaces through the acylation reaction of acid chloride of a monomer molecule and an imino group on the pigment surface.

4.4.1 Immobilization of 2-methyl-acryloyl chloride (MA-Cl) on pigment surfaces

A methacryloyl group was immobilized on the pigment surfaces through the reaction of 2-methyacryloylchloride (MA-Cl) with the imino groups on the pigment surfaces (s. Figure 4-25) in a similar way as the PFB molecules and the azo initiators.

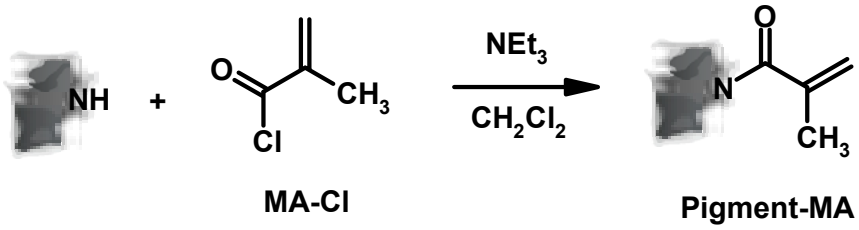

Figure 4-25: Immobilization of 2-methyacryloylchloride (MA-Cl) to the pigment surfaces.

When a polymerization reaction is started in solution with AIBN, every once in a while the growing chain incorporates a monomer immobilized on the surface. In the following, it will be focused on the reactions using the pigment PGL1155 as a model. The polymerization reaction using PGL1840-MA are summarized in Chapter 10.

4.4.2 Layer thickness as a function of monomer concentration

The MA-modified pigment (PGL1155-MA) was suspended in toluene at various MMA concentrations ([MMA] = 1.87 – 5.61 mol l^{-1}) in the presence of AIBN as initiator ([AIBN] = 10 mmol l^{-1} ≈ 0.05 – 0.02 mol%). Then the mixture was polymerized at 60 °C for 16 hours. The layer thickness of the attached polymer was determined by elemental analysis using Equation 4-6 and Equation 4-7 as described in Chapter 4.3.1.

As shown in Figure 4-26a, the layer thickness increases slightly from 4 nm to 11 nm with increasing monomer concentration. The obtained polymer film is rather thin due to the fact that the growing polymer chain is formed in solution and has to diffuse to the surface to react with the methacrylate monolayer. After that the polymer chain grows away from the surface. In many ways, the first step is similar to a "grafting-to" reaction. Due to a kinetic barrier built-up by the previously attached polymers on the surfaces only very thin films can be obtained[47,57,62-69] so that the "grafting-to" reaction becomes rate limiting and film thickness typical for "grafting-to" procedures can be obtained.

To determine the graft density of the chains, it has to be assumed that the growing chains on the surface and in the solution grow to the same chain length. The molecular weight of the free polymer could be determined by GPC (s. Figure 4-26b; ○) and was found to be similar to the theoretical value (s. Figure 4-26b; solid line) calculated by using Mayo's equation (s. Equation 4-10). This equation includes terms that account for chain transfer to monomer and solvent[138]. Using the molecular weight of the free polymer and the layer thickness of the polymer on the pigment surfaces, one can calculate the graft density of the attached polymer molecules, which varies from 0.04 μmol m^{-2} to about 0.1 μmol m^{-2} depending on the monomer concentration (s. Figure 4-26c).

Figure 4-26c shows that the graft density decreases with increasing monomer concentration of the polymerization reaction. As shown in Figure 4-26b, at low monomer concentration the obtained polymer chain is shorter than that at high monomer concentration. This can be explained by the fact that it is the adsorbed amount that determines the point during the polymerization at which the kinetic barrier efficiently blocks further attachment of growing chains. If smaller macromolecules are attached, a higher graft density can be achieved whereas this value will remain low if conditions that lead to long polymer chains are employed. This situation is shown schematically in Figure 4-27.

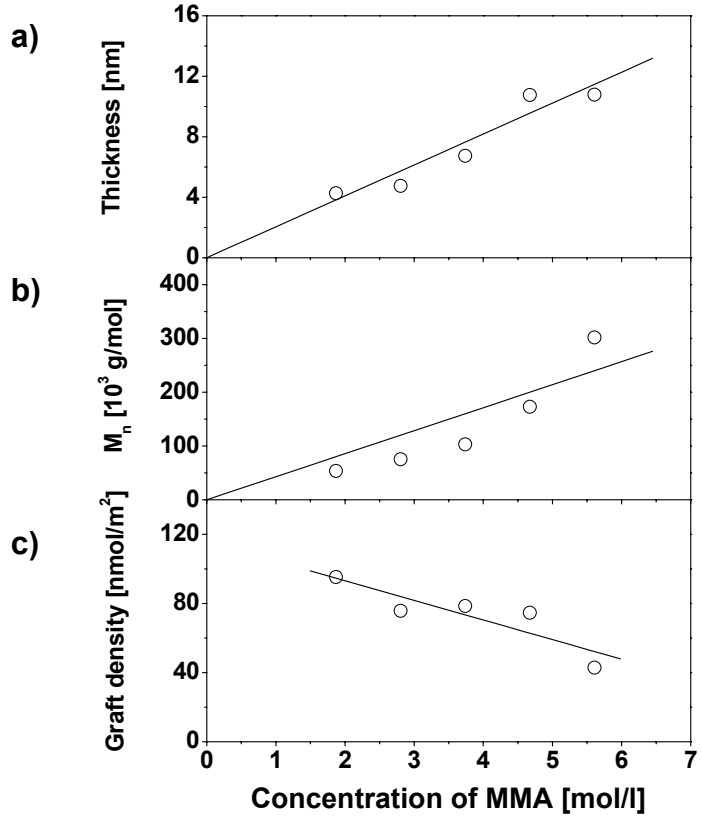

Figure 4-26: a) Layer thickness, b) number-average molecular weight as determined by GPC and c) graft density of polymer as a function of monomer concentration.

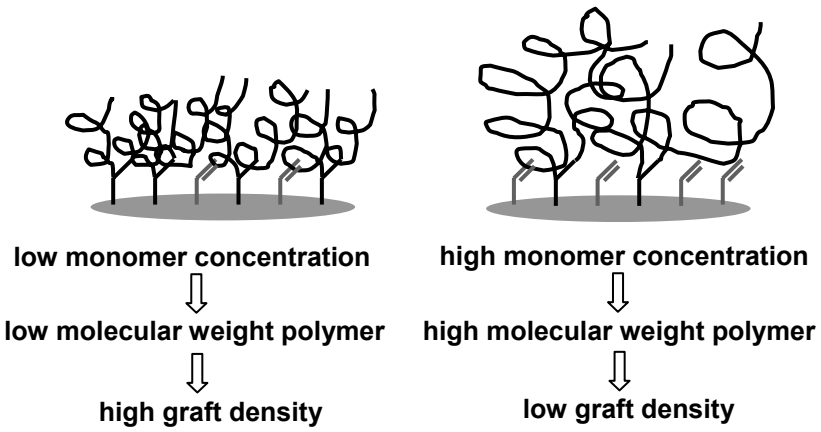

Figure 4-27: Influence of the monomer concentration on the graft density of polymers obtained by copolymerizing surface-attached monomers with monomers in solution.

4.4.3 Influence of the polymerization time

In order to study the influence of the polymerization time on the layer thickness and graft density of the polymer monolayers, a series of polymerizations using PGL1155-MA and MMA (3.74 mol l^{-1}) were carried out in the presence of AIBN (10 mmol l^{-1}) at 60 °C with the polymerization time varying from 4 to 32 hours. The thickness of polymer layers was calculated from elemental analysis data and the results are shown in Figure 4-28a.

The layer thickness is initially a function of the polymerization time but levels off at 7 nm after 8 hours of polymerization. Further polymerization did not lead to higher layer thickness, although during this time further initiator and monomer were consumed. As mentioned above, due to the thermodynamic and kinetic hindrance that arises as soon as the grafted polymer coils on the surfaces begin to overlap, the addition of further polymer chain to the active group on the surfaces becomes rather difficult. However, the free polymer in the solution is still formed during the polymerization process.

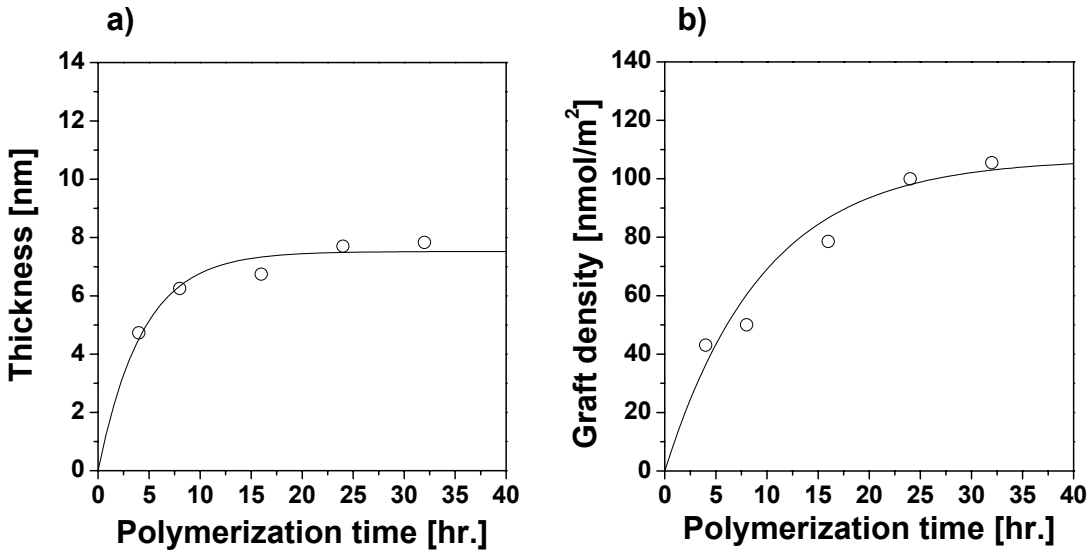

Figure 4-28: a) Layer thickness and b) graft density of the polymer monolayers as a function of polymerization time.

The molecular weight of free polymer shows a number-average molecular weight of 100 000 g mol^{-1} and a weight-average molecular weight of 200 000 g mol^{-1} as determined by GPC. The polydispersity (*D*) is accordingly ca. 2.0 which is a typical value for a free radical polymerization. Based on the assumption that the formation of polymers on the

surface and in the solution is similar, the molecular weight of the free and the attached polymer should be identical. The graft density can then be calculated from the obtained layer thickness and the molecular weight of the free polymer. The graft density increases during a short initial period of polymerization and then reaches a value of 0.1 μmol m^{-2} as shown in Figure 4-28b.

4.4.4 Influence of the initiator concentration

In this series of experiments, the initiator concentration was varied from 2.0 to 20 mmol l^{-1} keeping all other polymerization parameters constant ([MMA] = 3.74 mol l^{-1}, t = 16 hours and T = 60 °C). The layer thickness and the graft density were determined as mentioned above.

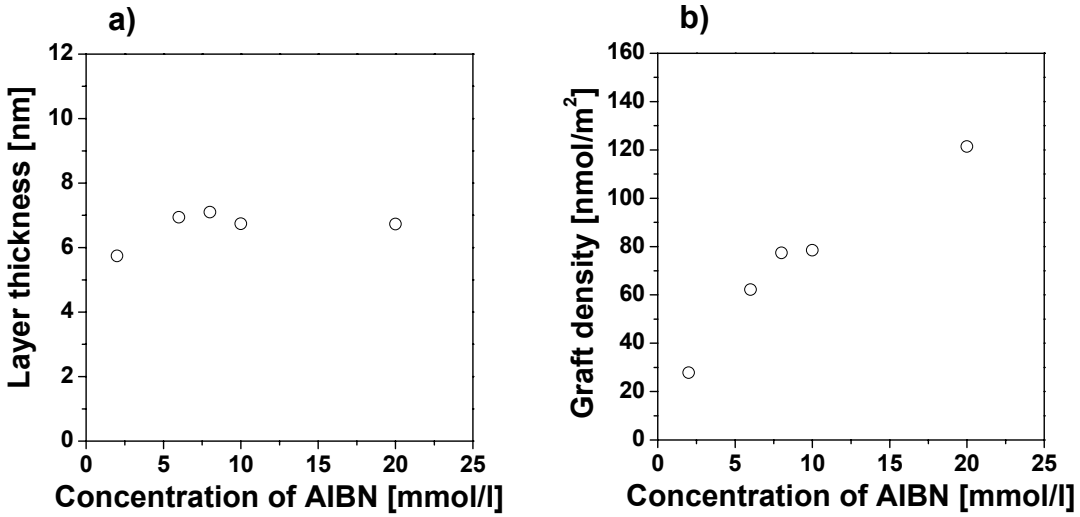

Figure 4-29: a) Layer thickness and b) graft density as a function of the initiator concentration.

As shown in Figure 4-29a, the initiator concentration has no influence on the layer thickness, although the molecular weight decreases with the increasing of the initiator concentration (M_n ~ 250 000 – 67000 g mol^{-1}; [AIBN] = 2 – 20 mmol l^{-1}). From these values the graft density was calculated and it was found that the graft density increases with increasing initiator concentration, i.e. decreasing molecular weight of polymer. This behavior is similar to the results obtained from the polymerizations at different monomer concentrations. Higher initiator concentrations lead to lower molecular weights of the

polymers and, therefore, the diffusion of the macroradical to the surface is possible for longer periods of time as compared to the reversed situation (s. Figure 4-27).

4.4.5 Polymerization with perfluorinated monomer (HDFDA)

The copolymerization of methacrylate groups on the surfaces of pigments (PGL1155-MA) with the perfluorinated monomer HDFDA (0.90 mol l^{-1}) as a hydrophobic monomer was carried out in the presence of AIBN (10 mmol l^{-1}) as the initiator at 60 °C for one hour. Freon was used as the solvent in this reaction.

As described in Chapter 4.3.3, the fluorine signal in the XP spectrum is very characteristic for the polymer shell. Figure 4-30a and b show survey spectra and C(1s) detail spectra of unmodified PGL1155 as well as PGL1155 and PGL1155-MA copolymerized with HDFDA in the presence of AIBN, respectively.

The XP spectrum of the unmodified PGL1155 shows C(1s), N(1s), and O(1s) signals at 285 eV, 400 eV and 531 eV, respectively (s. Figure 4-30a1). After polymerization of HDFDA in the presence of PGL1155-MA and subsequent extraction with freon (CCl_3CF_3) for 24 hours, a F(1s) signals due to the perfluoroalkyl groups of the PHDFDA layer appears at 689 eV (s. Figure 4-30a3). The detail spectra of the C(1s) region show, besides the typical signals of the pigment [C-C, C-H at 284.6 eV , C-O and C-N at 286.5 eV, CN at 288.0 eV, CONH at 288.9 eV and $\pi \rightarrow \pi^*$ at 290.3 eV] (s. Figure 4-30b3 and d), additional feature due to CF_2 and CF_3 groups at 291.4 eV and 293.5 eV. The binding energies (BE) and peak assignments of the surface functionalities are summarized in Table 4-8.

Table 4-8: Components of the C(1s) signals of surface-modified pigments and their assignments to functionalities within the materials.

PGL1155 **BE (eV); (%) ; assignments**	**PGL1155*** **BE (eV); (%) ; assignments**	**PGL1155-PHDFDA*** **BE (eV); (%) ; assignments**
284.6; (53); C-C, C-H	284.6; (54); C-C, C-H	284.5; (33); C-C, C-H
286.3; (18); C-O, C-N	286.2; (18); C-O, C-N	286.1; (24); C-O, C-N
288.0; (16); C≡N	288.0; (14); C≡N	288.1; (7); C≡N
288.9; (7); CONH	288.9; (8); CONH	288.7; (9); CONH, COO
290.3; (6); $\pi \rightarrow \pi^*$	290.3; (3); $\pi \rightarrow \pi^*$	290.0; (3); $\pi \rightarrow \pi^*$
	291.9; (3); CF_2	291.4; (20); CF_2
		293.5; (4); CF_3

* PGL1155 (non-attached monomer) or PGL1155-PHDFDA (MA-attached PGL1155) was copolymerized with HDFDA (0.90 mol l^{-1}) in presence of AIBN (10 mmol l^{-1}) at 60 °C for one hour.

In a reference experiment, unmodified PGL1155 (without surface-attached monomer) was added to a polymerization reaction of HDFDA using the same conditions as described above. The XP survey spectrum and a detail scan of the C(1s) region obtained from the recovered pigment are shown as spectra 2 in Figure 4-30a and b. Only a very small F(1s) peak is observed in the survey spectrum (s. Figure 4-30a2) and also only weak CF_2 and CF_3 components add to the overall C(1s) intensity (s. Figure 4-30b2 and c) indicating a clear difference to the material obtained from the MA-modified pigment. The reason for the presence of some fluoropolymer on the surfaces of the unmodified pigment is unclear. It might be due to either an incomplete extraction or of the attachment of chains growing in solution onto molecules on the pigment surface in form of a chain transfer reaction.

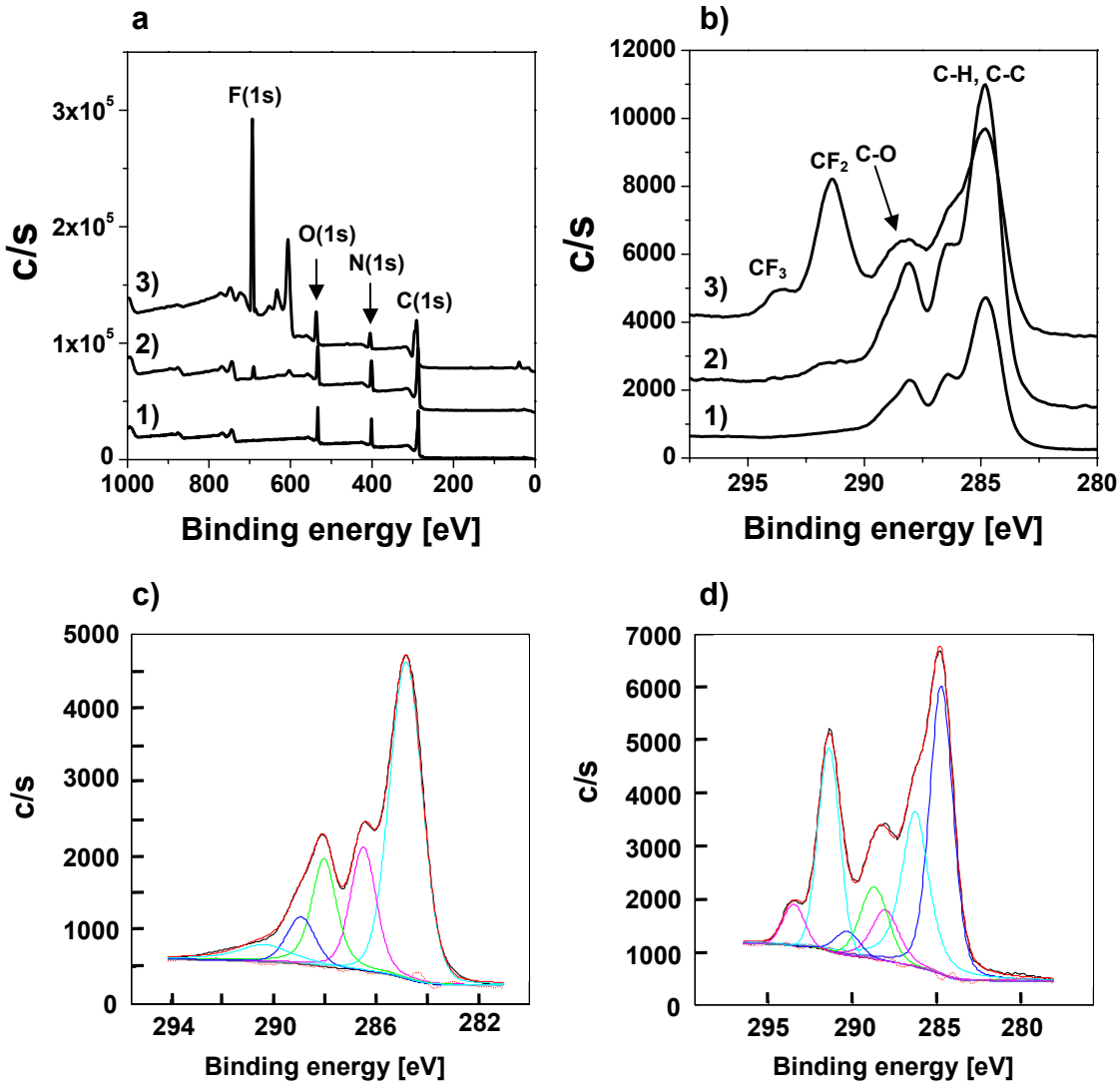

Figure 4-30: a) XP survey spectra and b) C(1s) detail spectra of unmodified PGL1155 (1), PGL1155 without surface-attached monomer (2) and PGL1155-MA copolymerized with HDFDA in the presence of AIBN (3); c) evaluation of C(1s) signals of PGL1155 (b2) and d) that of PGL1155-HDFDA (b3) using Gauss-Lorentz functions for the signals and a Shirley type function for the baseline.

4.4.6 Discussion and comparison with the pigment PGL1840

Copolymerizable groups can be immobilized in a one-step reaction onto the pigment surfaces using MA-Cl. Although, the monomer graft density could not be determined directly, it can be assumed that the reactivity of the acid chloride of 2-methyacryloylchloride towards the imino groups on the pigment surfaces is similar to that of the other acid chlorides immobilized on these materials (initiator, fluorinated substance).

In general, the approach of using these MA-modified pigments during polymerization initiated in solution lead to controlled attachment of thin polymer monolayers on the surfaces. The fact that variations of the exact polymerization conditions do not significantly influence the outcome of the modification reactions shows that this approach is very robust in terms of the amount of polymer that is deposited on the surfaces of the pigments.

5 Surface Modification of Inorganic Pigments

In this chapter, the modification of inorganic pigments with covalently attached polymer layers is described. The immobilization of initiating units and monomer groups onto the surfaces of inorganic pigments was performed using suitable molecules. The influence of selected polymerization parameters (monomer concentration, initiator conversion) on the film properties was investigated.

The inorganic pigments used in this study were rutile (titanium dioxide, TiO_2) and Paliocrom Gold L2020 (PCG2020) which is an aluminum dioxide covered with iron(III)oxide.

5.1 Immobilization of initiators on pigment surfaces

5.1.1 Initiator monolayers from silanes

Self-assembled azo-initiator monolayers (SAIMs) on various surfaces could be obtained by immobilizing molecules in which each of them contains both an anchoring group and an azo group. Self-assembled monolayers of mono- and/or bifunctional azochlorosilane on silicon substrates, glass slides and silica gel are documented in the literature[53,86,136,145]. The azochlorosilane monolayers can be used for the free radical polymerization of various vinyl monomers yielding polymer monolayers on the surfaces with high graft density and controllable thickness.

In this study, 4,4´-azobis-(4-cyanopentanoic acid-(3´-chlorodimethylsilyl)propyl-ester (ADS) as shown in Figure 5-1 was used to form SAIMs on TiO_2 surfaces. The TiO_2 pigment was first dried at 120 °C in vacuum for 6 hours. The concentration of ADS in the solution used for the surface modification was set to 0.2 µmol per m^2 of TiO_2, which corresponds to a 24-fold excess which respect to the available OH groups on the pigment surfaces[26]. The initiator monolayer was characterized by XPS measurement (s. Chapter 5.1.3) and the graft density of the initiator on the surfaces was determined by DSC measurement (s. Chapter 5.1.4).

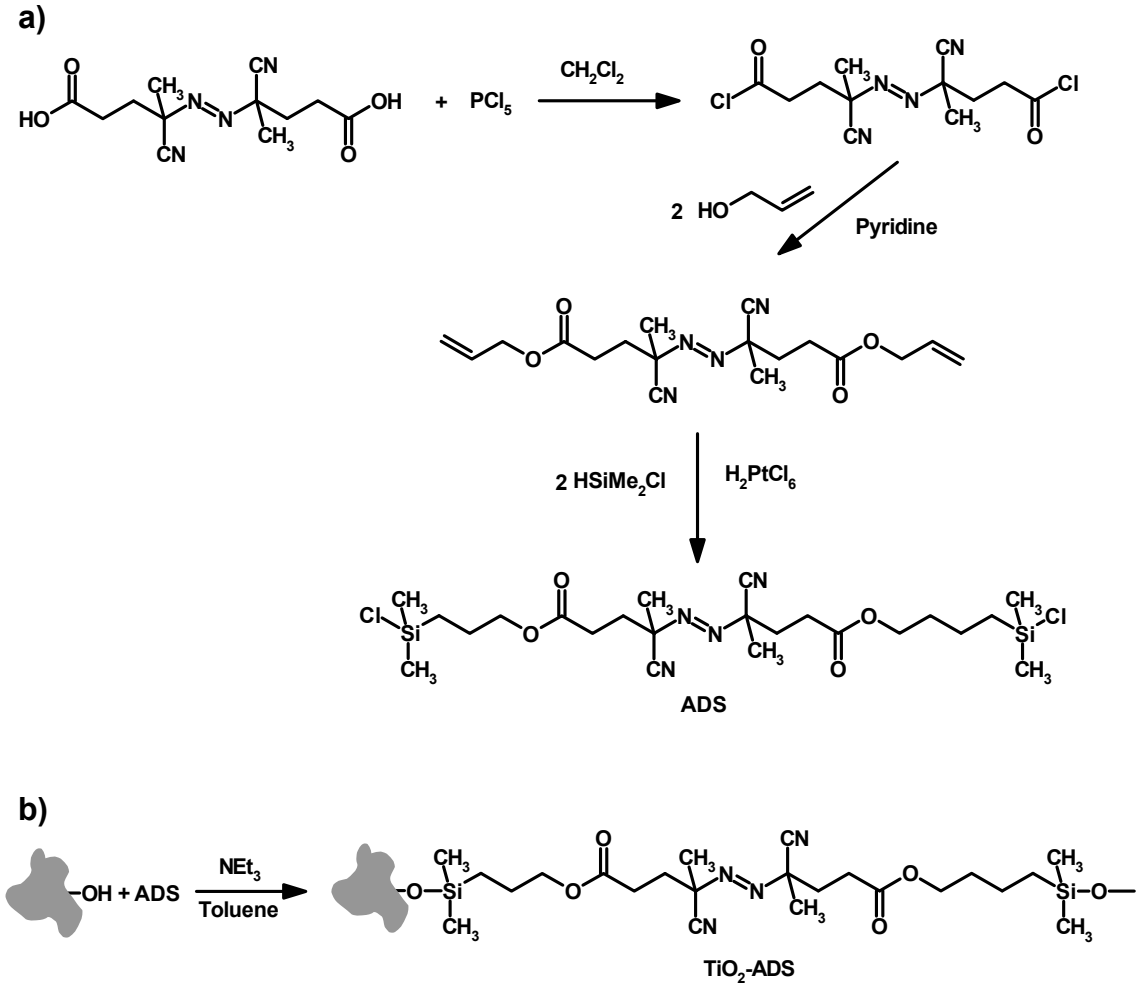

Figure 5-1: a) Synthesis of 4,4′-azobis-(4-cyanopentanoic acid-(3′-chlorodimethylsilyl) propyl-ester (ADS)[86] and b) immobilization of ADS on TiO_2 surfaces.

5.1.2 Initiator monolayers from phosphates

As mentioned in Chapter 1, the formation of self-assembled monolayers on TiO_2 surfaces using phosphonic acids $RPO(OH)_2$ has been reported[24-26]. Surface modification of iron oxide with long chain thiols[146], silane coupling agents[147-151] and alkylphosphonic acids[152] have been also investigated. However, the formation of the SAIMs on those surfaces using phosphate groups as anchor group has not been described so far.

Therefore, in our study, 2-aminoethyldihydrogenphosphate (AEP) was used to immobilize onto the TiO_2 as well as onto PCG2020 surfaces, because the phosphate

group on AEP could act as an anchor group which can attach to the hydroxyl groups on those surfaces (s. Figure 5-2). To this, the amino end-groups can react with the azo initiator ABCC (synthesis s. Figure 4-6) though an acylation reaction and subsequently build up the SAIMs on the pigment surfaces.

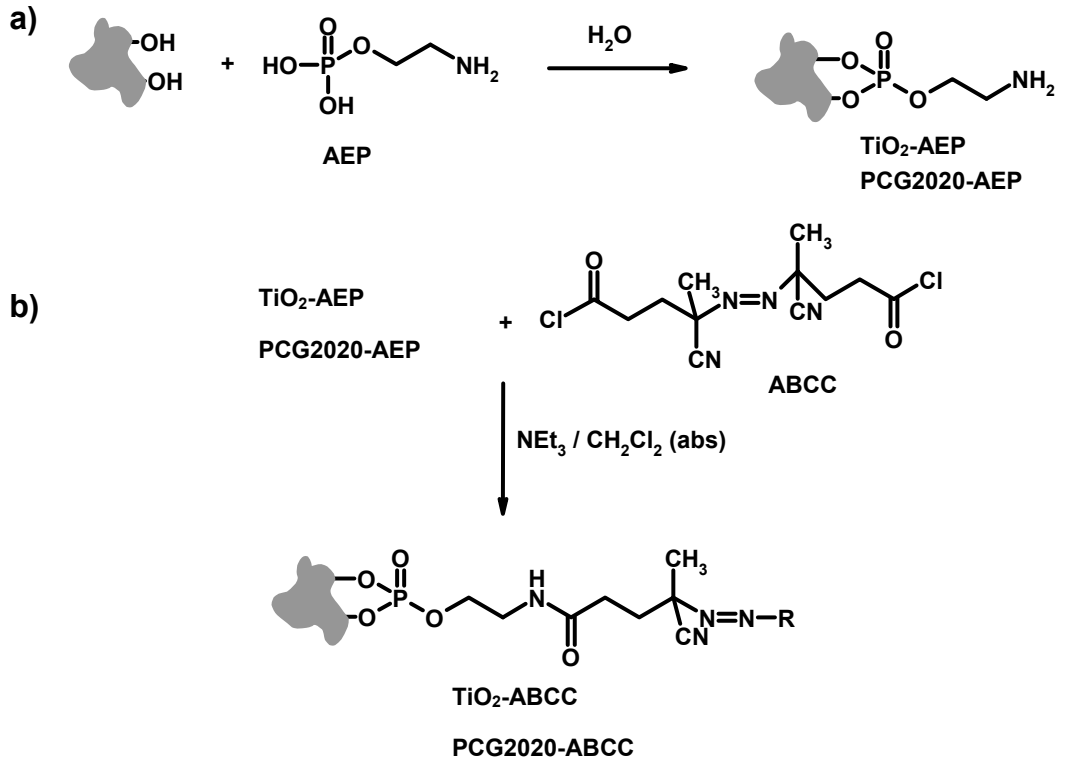

Figure 5-2: a) Immobilization of 2-aminoethyldihydrogenphosphate (AEP) to inorganic pigment surfaces and b) subsequent attachment of the azo initiator ABCC to amino monolayers.

5.1.2.1 Immobilization of 2-aminoethyldihydrogenphosphate (AEP) on TiO_2

The immobilization of AEP was carried out using a constant concentration of AEP (0.2 mmol m^{-2}) in water at various temperatures (room temperature or 100 °C) or at pH 3 for 20 hours. The non-reacted AEP was removed by extraction with water. The graft density of the AEP monolayers was determined by elemental analysis using Equation 5-1:

$$\delta_C = \frac{\%C}{100 \times N_C \times m_C} \qquad \textit{Equation 5-1}$$

In this equation, δ_C is the grafted density [µmol g^{-1}], which was calculated from the carbon content (%C) of the sample. N_C is the number of carbon atoms of the AEP molecule and m_C is the atomic mass of carbon. The results for several samples are summarized in Table 5-1.

Table 5-1: Graft densities of AEP on TiO_2 particles as calculated form Equation 5-1 using data from elemental analysis.

Nr.	reaction condition	C* [%]	graft density δ [µmol g^{-1}]	graft density Γ** [µmol m^{-2}]	graft density ρ [groups nm^{-2}]
1	100 °C***	0.27 ± 0.01	112	2.3	1.4
2	100 °C	0.29 ± 0.03	121	2.4	1.4
3	20 °C	0.35 ± 0.01	146	2.9	1.7
4	20 °C, pH 3	0.21 ± 0.00	87	1.8	1.1
		titration****	106	2.1	1.3

* average of 2 measurements
** SA_{TiO2} is 50 m^2 g^{-1}.
*** TiO_2 was dried at 120 °C under vacuum before the immobilization of AEP.
**** average of 5 measurements.

Both the untreated TiO_2 and the TiO_2 dried at 120 °C show similar values of the graft density of AEP (s. Table 5-1; Nr. 1-2). The graft density of AEP obtained by the reaction at room temperature is a little higher than that at 100 °C (s. Table 5-1; Nr. 2-3). In comparison to this, the graft density of AEP, which was immobilized from an acidic condition, is a little lower than those mentioned above. This might be due to the fact that the amino groups of AEP were protonated in the acidic condition. As a result, the interaction between hydroxyl-groups on the surfaces and amino groups of AEP can be prevented in such a system (s. Figure 5-3b), as observed in the adsorption of γ-aminopropyltriethoxysilane (γ-APS) onto iron and steel oxide surfaces[148,151,153]. So that, after the immobilization reaction the non-reacted molecules can be easily removed by extraction with water.

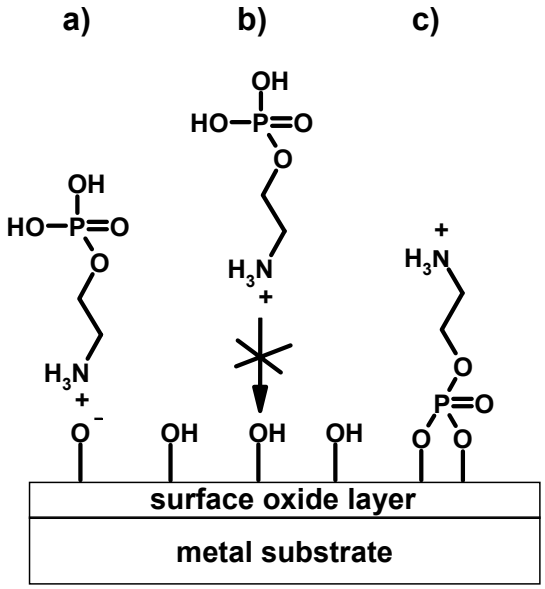

Figure 5-3: Possible adsorbate conformation: a) surface bonding via protonated amine group; b) the amine group of AEP can be protonated under acidic conditions (pH ~3) which inhibits the reaction with hydroxyl groups on the surface; c) surface bonding via condensation of phosphonic acid with hydroxyl surface groups.

5.1.2.2 Immobilization of 2-aminoethyldihydrogenphosphate (AEP) on PCG2020

To study the immobilization of AEP on PCG2020, a series of adsorption experiments of AEP was carried out at different concentrations. The immobilization reactions were performed in water at 100 °C for 16 hours. After reaction, the non-reacted AEP was removed by extraction with H_2O. Figure 5-4 shows the result of elemental analysis and calculated graft density of AEP on PCG2020 using Equation 5-1.

Due to the fact that the specific surface area of the PCG2020 particles is rather low (~ 2.5 m^2 g^{-1}), the determination of the carbon contents of AEP monolayer on the particles is very low at all AEP concentrations (~ 0.1 – 0.5 %C). Therefore, it is difficult to state which concentration is giving the maximum graft density of AEP. However, in our study, the AEP concentration of 2.5 mmol g^{-1} (1 mmol m^{-2}) was used to immobilize onto the PCG2020 particles.

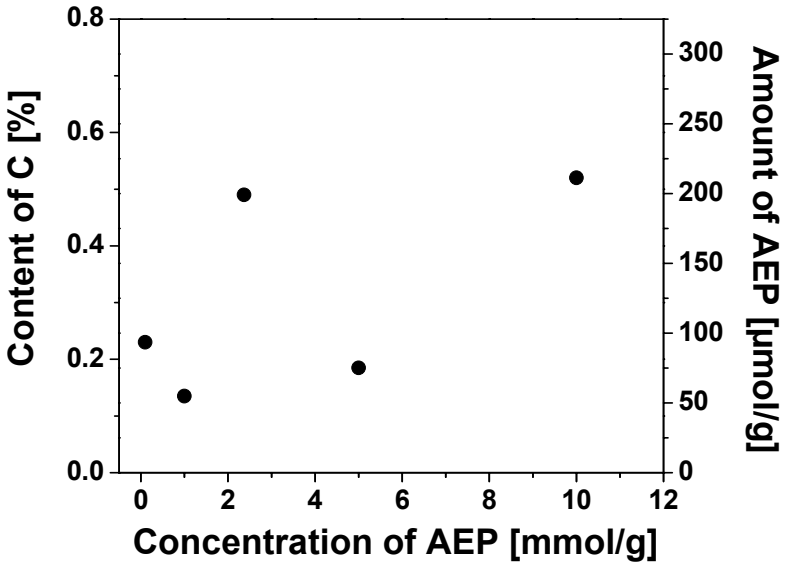

Figure 5-4: a) Carbon content as determined by elmental analysis and b) graft density of AEP on the PCG2020 particles as a function of AEP concentration.

5.1.2.3 Immobilization of ABCC to the surface-attached amino monolayers

The immobilization of ABCC initiator onto the amino monolayers (s. Figure 5-2b) was performed by the drop-wise addition of initiator solution to the AEP-modified pigment suspended in dried dichloromethane. After the reaction, the pigment particles were filtrated off and washed with CH_2Cl_2, EtOH:H_2O (1:1, pH 3, adjusted by hydrochloric acid), EtOH:H_2O and MeOH.

The initiator monolayers on both pigment surfaces were characterized by XPS (s. Chapter 5.1.3). Additionally, the amount of azo groups on the particles was determined by DSC (s. Chapter 5.1.4).

The self-assembled azo-initiator monolayers on both pigments (TiO_2-ABCC and PCG2020-ABCC) were used to initiate the polymerization of vinyl monomers. The results of graft density and the layer thickness of polymer grafted were compared with those prepared using TiO_2-ADS (s. Chapter 5.2).

5.1.3 Qualitative characterization of initiator monolayers on inorganic pigments

5.1.3.1 TiO_2-ADS

When the spectrum of the unmodified TiO_2 is viewed, besides the signals of Ti(2p) at 458 eV, O(1s) at 531 eV and C(1s) at 285 eV, a trace of Molybdenum was observed at 230 eV for Mo(3d) and 402 eV for Mo(3p3) which overlaps with the signal of N(1s) at ~ 402 eV (s. Figure 5-5a1). The survey spectrum of TiO_2-ADS shows the signals of Si(2p) and Si(2s) at 101.7 eV and 152.7 eV due to the anchor groups of the initiator ADS (s. Figure 5-5b).

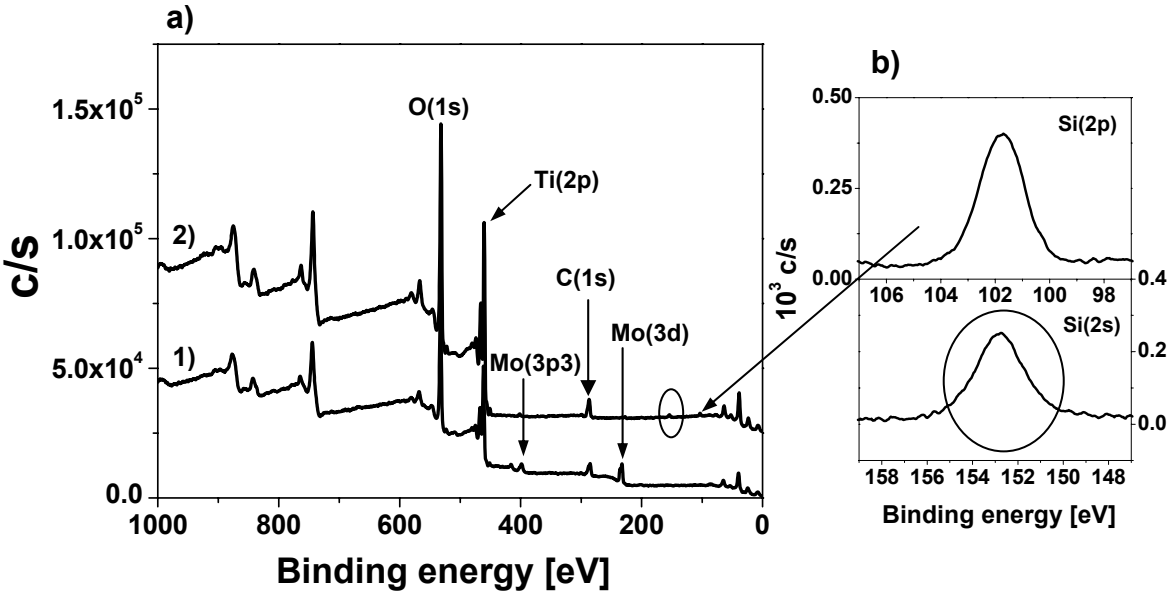

Figure 5-5: a) XP survey spectra of 1) unmodified TiO_2 and 2) TiO_2-ADS; b) detail spectra of Si(2p) and Si(2s) of TiO_2-ADS.

The C(1s) detail spectra of ADS attached TiO_2 is shown in Figure 5-6b. The new peak at 289 eV is visible due to the C≡N and COO group coming from the initiator component. As shown in Figure 5-6c, the evaluation of the C(1s) signal shows that there are four curve corresponded to C-C and C-H at 284.6 eV, C-O and C-N at 286.1 eV, C≡N at 287.5 eV and COO at 288.8 eV.

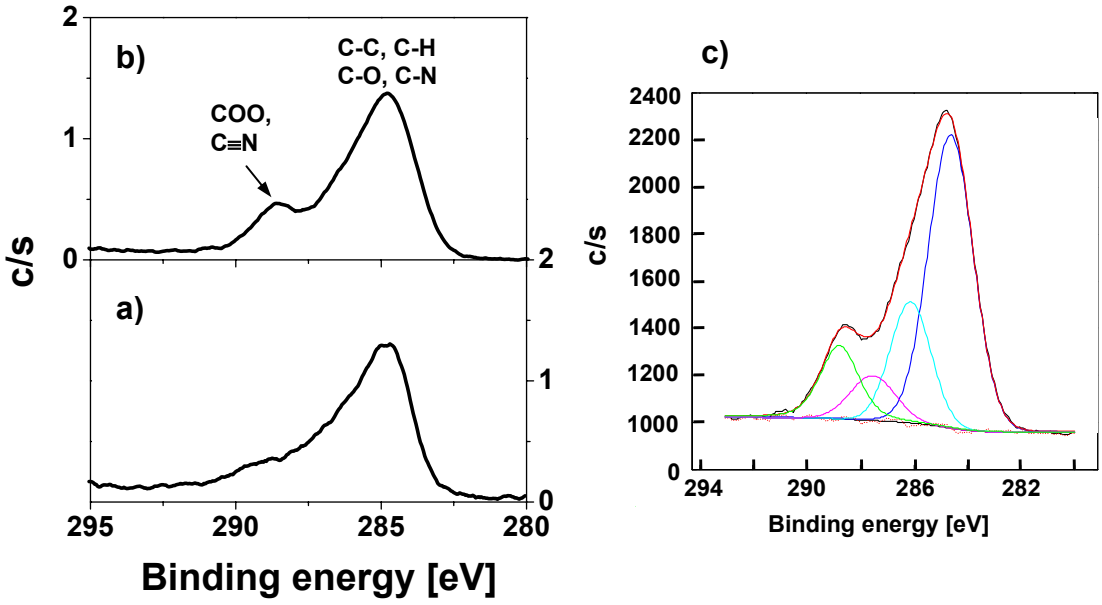

Figure 5-6: C(1s) detail spectra of a) unmodified TiO_2 and b) TiO_2-ADS; c) evaluation of C(1s) signal from TiO_2-ADS using Gauss-Lorentz function for the signals and a Shirley type function for the baseline.

5.1.3.2 TiO_2-ABCC

After immobilization of AEP onto TiO_2 surfaces, the signal of P(2p) appeared at 133 eV (s. Figure 5-7a2) due to the anchor group. The signal intensity of this group reduced after immobilization of ABCC to the AEP monolayer (s. Figure 5-7b).

As described above, the signal of N(1s) overlaps with the signal of Mo(3p) at 402 eV. Therefore, this signal cannot be used for the verification of the structure. However, the integrated intensity of C(1s) increases after immobilization AEP onto the surfaces as shown in Figure 5-8a and b.

Figure 5-8d shows the evaluation C(1s) curve of TiO_2-ABCC. The signal of CONH at 289.4 eV and of C≡N at 288.4 eV was observed besides the signal of C−C and C−H at 284.7 eV, C−O and C−N at 286.3 eV coming from ABCC component.

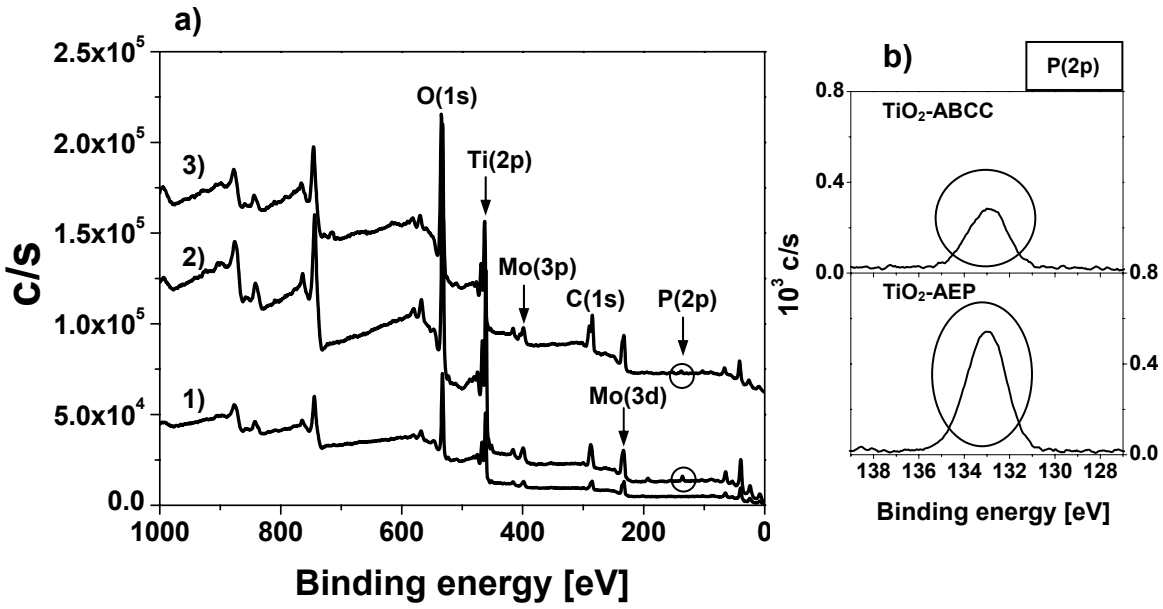

Figure 5-7: a) XP survey spectra of 1) unmodified TiO_2, 2) TiO_2-AEP and 3) TiO_2-ABCC; b) P(2p) detail spectra of TiO_2-AEP in comparison to TiO_2-ABCC.

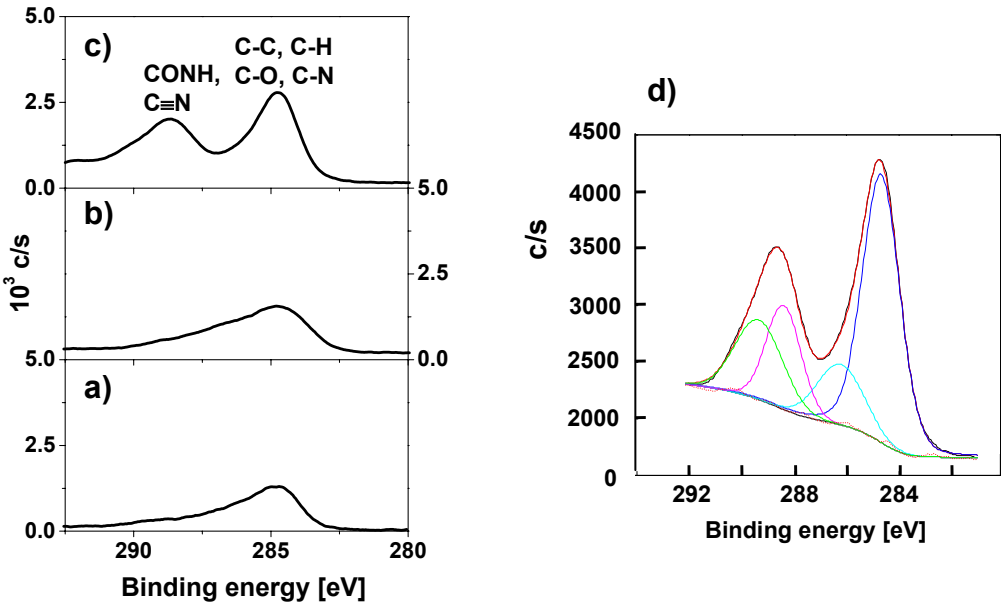

Figure 5-8: C(1s) detail spectra of a) unmodified TiO_2, b) TiO_2-AEP and c) TiO_2-ABCC; d) evaluation of the C(1s) signal from TiO_2-ABCC using Gauss-Lorentz functions for the signals and a Shirley type function for the baseline.

5.1.3.3 PCG2020-ABCC

Figure 5-9 shows the survey spectra of PCG2020-AEP and PCG2020-ABCC as well as of the unmodified PCG2020. C(1s) signals at 285 eV, O(1s) at 531 eV and very small signals due to Al(2s), Al(2p) and Fe(3p) at 119 eV, 74 eV and 55 eV are observed in the XP spectrum of the unmodified PCG2020 (s. Figure 5-9a). It can be seen that after immobilization of AEP to the PCG2020 surfaces (s. Figure 5-9b) and subsequently immobilizing ABCC (s. Figure 5-9c) to the AEP monolayer, new signals of N(1s) at 402 eV, P(2s) at 191 eV and P(2p) at 133 eV were detected.

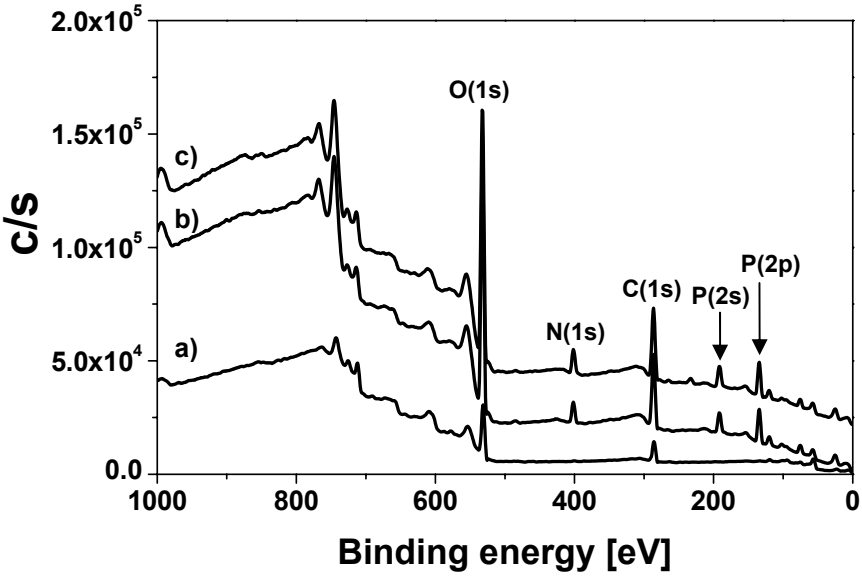

Figure 5-9: XP survey spectra of a) unmodified PCG2020, b) PCG2020-AEP and c) PCG2020-ABCC.

The intensity of C(1s) of AEP monolayer is higher than that of the unmodified PCG2020 (s. Figure 5-10a2 and a1, respectively). However, the intensity of C(1s) after immobilization of the ABCC to the AEP monolayer (s. Figure 5-10a3) did not increase as expected.

The detail spectra of N(1s) also confirmed that AEP and ABCC were covalently attached to the surfaces (s. Figure 5-10b). The intensity of N(1s) is visibly increased after deposition of AEP molecules onto the PCG2020 surfaces as shown in Figure 5-10b2. In contrast to the C(1s) intensity, the intensity of N(1s) increased after attachment of ABCC

to the AEP monolayer due to the increasing of the nitrogen atom coming from ABCC molecules (s. Figure 5-10b2 and b3). The signal of N(1s) from C≡N and N=N was reported at 400.1 eV and 401.2 eV[86,140]. The two signals of C≡N at 399.6 eV and N=N at 401.3 eV can also be observed after immobilization of ABCC to the AEP monolayers (s. Figure 5-10c).

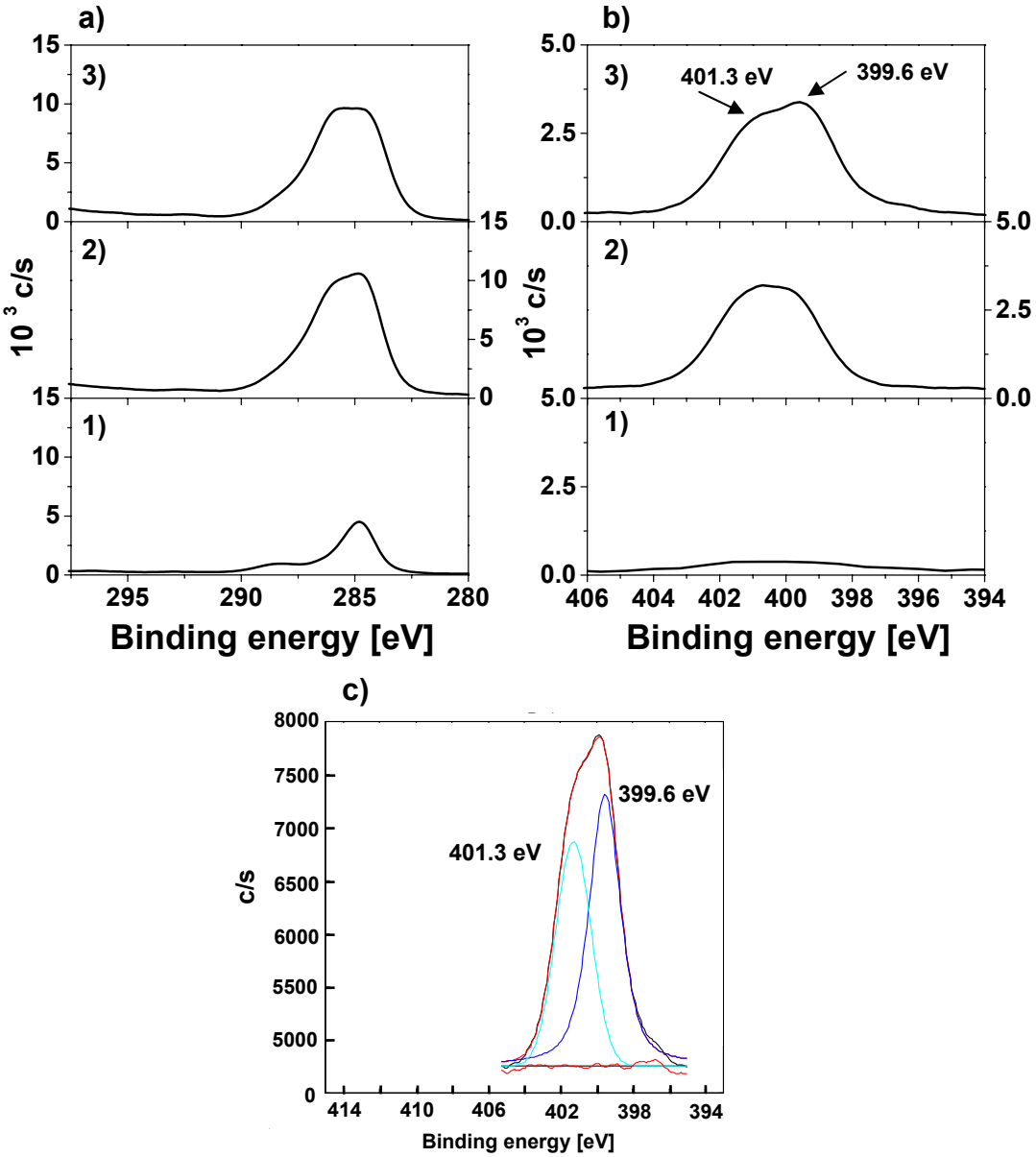

Figure 5-10: Detail spectra of a) C(1s) and b) N(1s) signals of 1) unmodified PCG2020, 2) PCG2020-AEP and 3) PCG2020-ABCC; c) evaluation of the N(1s) signal from PCG2020-ABCC using Gauss-Lorentz functions for the signals and a Shirley type function for the baseline.

5.1.4 Determination of the initiator graft density on the inorganic pigments

The thermal decomposition of the azo molecules attached to the pigment particles is a strongly exothermic process and can be followed by DSC (s. Figure 5-11). The graft density of the azo groups can be calculated from the integral of the DSC signal according to Equation 4-3 (H_{dec} of ABCC = 190 ± 8 kJ mol^{-1} and of ADS[86] = 284 ± 10 kJ mol^{-1}). The DSC measurement is the same procedure as described in Chapter 4.2. The results are summarized in Table 5-2.

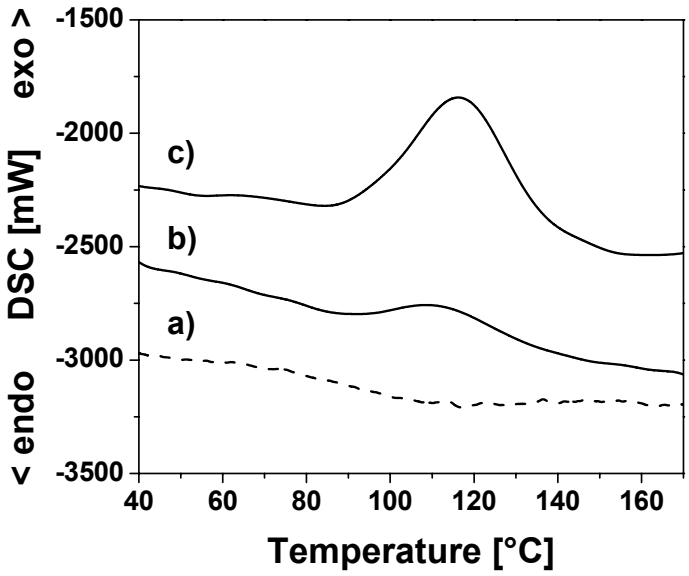

Figure 5-11: DSC traces of a) unmodified TiO_2, b) TiO_2-ADS and c) TiO_2-ABCC; heating rate 10 °C min^{-1}.

From the DSC measurement of TiO_2-ADS, it can be derived that ca. 0.06 initiator molecules per nm^2 were attached to TiO_2 surfaces, which gives an average distance between two surface-attached azo groups ~ 4.1 nm. Although these valves are considerably lower than those of ADS on SiO_2 surfaces[53,86]. It still should be noted that a significant amount of azo compound can be reproducibly become attached.

Table 5-2: Graft densities of the azo initiator on TiO_2 particles as well as average distance between two azo groups.

TiO_2-Azo	I_{dec}* [J g^{-1}]	graft density δ [µmol g^{-1}]	graft density Γ [µmol m^{-2}]	average distance between azo groups d [nm]
TiO_2-ADS	1.42 ± 0.30	5	0.1	4.1
TiO_2-ABCC	8.97 ± 0.31	47	0.9	1.4

* average of 3 measurements.

Helmy and Fadeev[26] have investigated the immobilization of octadecyl chains with different headgroups. They found that the reactivity of $C_{18}H_{37}PO(OH)_2$ was higher than that of $C_{18}H_{37}Si(CH_3)_2Cl$ and the maximum of graft density was also dependent on the immobilization time. Additionally, the graft density of $C_{18}H_{37}PO(OH)_2$ (4.26 groups per nm^2) was also higher than of $C_{18}H_{37}Si(CH_3)_2Cl$ (1.48 groups nm^{-2}). Similarly, in the present investigation, the anchoring of AEP on the TiO_2 surfaces gave a higher graft density (~ 2.3 µmol m^{-2}; s. Table 5-1) of monolayer compared to that of ADS on these surfaces (0.1 µmol m^{-2}; s. Table 5-2).

The graft density of the ABCC initiator is found around 0.9 µmol m^{-2}. It is higher than that of ADS (0.1 µmol m^{-2}). The higher graft density of ABCC initiator might be due to the higher reactivity of the acid chloride with amino groups compared to that of the chlorosilane with hydroxyl groups on the TiO_2. This might also lead to a higher graft density of ABCC after the immobilization of ABCC to the AEP monolayers.

As described above, due to the very low surface area of PCG2020 particles it is rather difficult to determine the graft density of AEP and to detect the decomposition of the azo groups on the particles by DSC. However, the azo molecules attached to the surface could be detected by XPS measurements (s. Figure 5-9 and Figure 5-10).

5.2 "Grafting-from" polymerization via self-assembled azo-initiator monolayers

As a next step, free radical polymerization reactions with the surface-attached initiator were performed, in which some of the polymerization parameters are varied (monomer concentration and polymerization time). The polymerizations were carried out at 60 °C for 16 hours. After removing the non-attached polymer, the polymer-attached pigment surfaces were characterized by FTIR and XP spectroscopy. The graft densities of the polymer were determined from the carbon and hydrogen content determined by the elemental analysis.

5.2.1 Qualitative characterization of the polymer monolayer attached to pigment surfaces

5.2.1.1 FTIR spectroscopy

Figure 5-12 shows the transmission FTIR spectra of the PMMA-modified TiO_2 surfaces grown from TiO_2-ADS and TiO_2-ABCC. Also shown are the unmodified TiO_2 and free PMMA. The absorption band at 1730 cm^{-1} corresponding to the carbonyl group of the methacrylate groups (–$COOCH_3$–) originating from the PMMA is observable after the polymerization MMA using the surface-initiated monolayers ([MMA] = 4.67 mol l^{-1}, T = 60 °C, t = 16 hours). The absorption band at 2915 cm^{-1} and 3000 cm^{-1} due to the CH stretching vibrations of the backbone chains of the polymer is also visible.

The PMMA-modified TiO_2 initiated by TiO_2-ABCC shows a stronger absorption band of the carbonyl group and the CH stretching vibrations than that initiated by TiO_2-ADS in agreement with the higher graft density of initiator (s. Figure 5-12b and c).

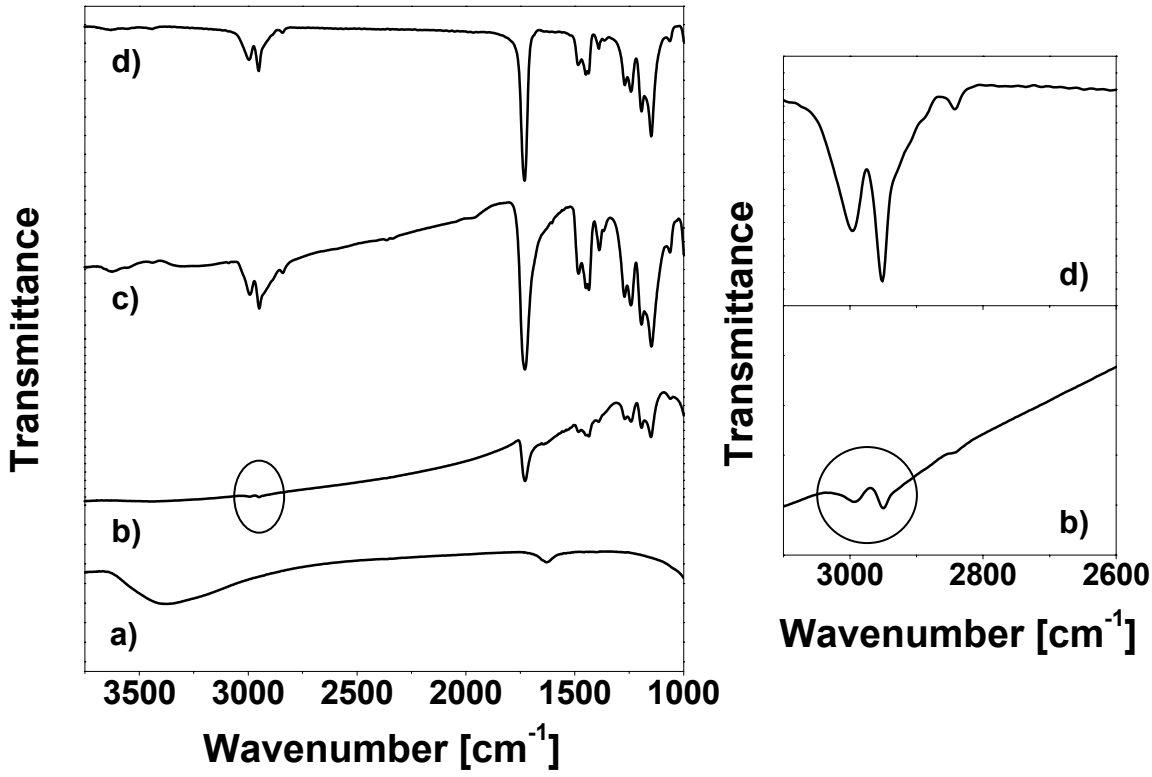

Figure 5-12: Transmission FTIR spectra of a) unmodified TiO_2, b) TiO_2-PMMA initiated by TiO_2-ADS (L ~ 2.4 nm), c) TiO_2-PMMA initiated by TiO_2-ABCC (L ~ 10 nm) and d) free PMMA as reference.

5.2.1.2 X-ray photoelectron spectroscopy (XPS)

The chemical composition of the surface-attached polymer layers can be also characterized by XPS measurements. Figure 5-13 to Figure 5-15 show the survey spectra of the PMMA-modified pigment initiated by TiO_2-ADS, TiO_2-ABCC and PCG2020-ABCC, respectively. In all cases, the signal intensity of C(1s) at 285 eV increases after the polymerization of MMA in comparison to the monolayer with just the surface-attached initiator. The Ti(2p) signal is even a little difficult to observe from TiO_2-PMMA initiated by TiO_2-ABCC due to the high layer thickness of the PMMA (s. Figure 5-13b and Figure 5-14b). In addition, the signal of Mo(3p) and Mo(3d) also disappeared.

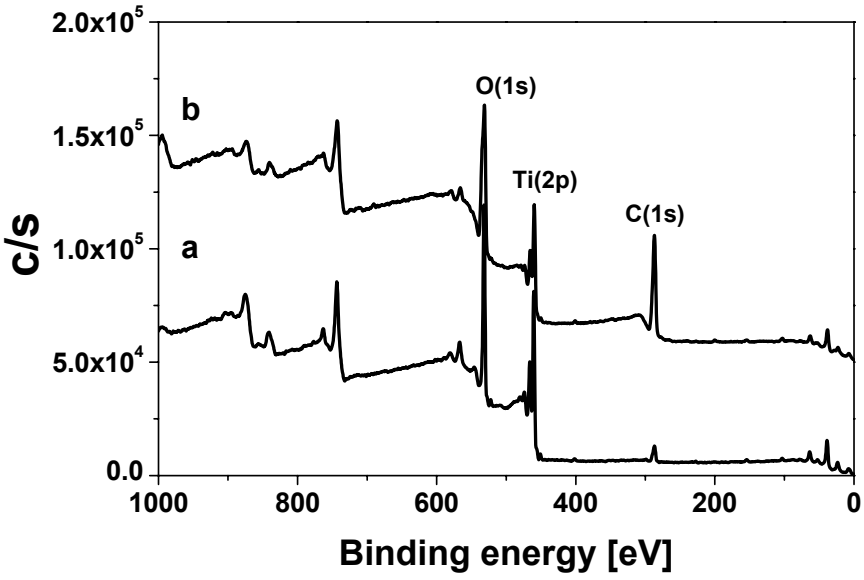

Figure 5-13: XP survey spectra of a) TiO_2-ADS and b) TiO_2-PMMA initiated by TiO_2-ADS (L ~ 2.4 nm).

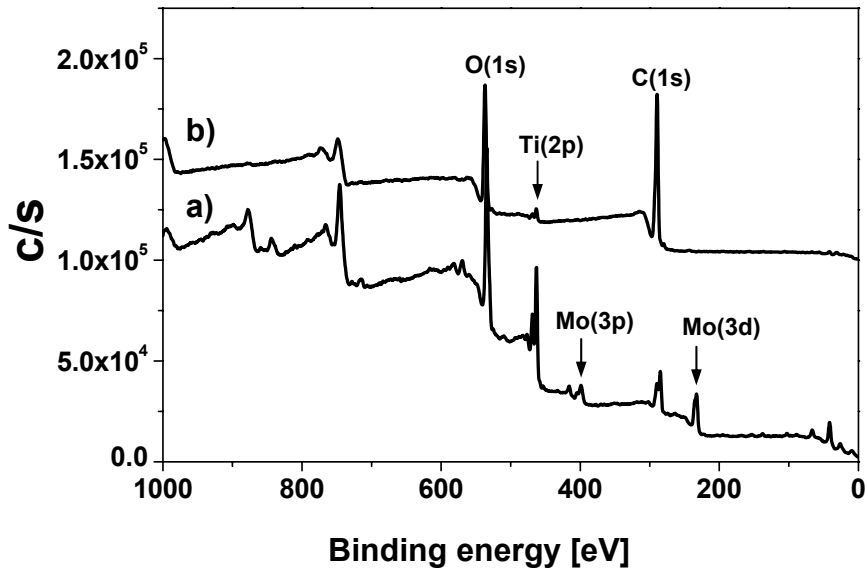

Figure 5-14: XP survey spectra of a) TiO_2-ABCC and b) TiO_2-PMMA initiated by TiO_2-ABCC (L ~ 10 nm).

A very similar result is obtained from PCG2020 substrates where the signals of N(1s) as well as the signals of P(2s) and P(2p) are difficult to observed as the layer thickness of the PMMA layer is around 21 nm (s. Figure 5-15b).

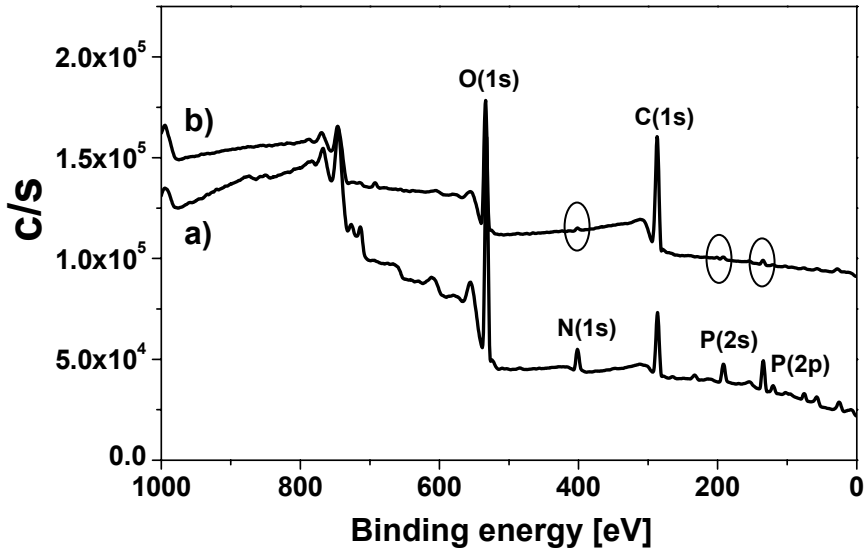

Figure 5-15: XP survey spectra of a) PCG2020-ABCC and b) PCG2020-PMMA initiated by PCG2020-ABCC (L ~ 21 nm).

In reference experiments, unmodified TiO_2 and PCG2020 as well as TiO_2-AEP and PCG2020-AEP were treated under the same polymerization conditions as those, which used surface-attached initiator (PCG2020-ABCC and TiO_2-ABCC). However, these experiments did not result in any polymer attached to the particle surfaces as evidenced by FTIR measurements (data not shown). From this observation, it can be concluded that the polymer chain can be generated only if an initiator is presented at the substrate surface.

5.2.2 Quantitative characterization of polymer-attached surfaces with various polymerization parameters

5.2.2.1 Graft density as a function of monomer concentration

To study the influence of monomer concentration on the layer thickness on the pigment surfaces, the initiator-attached inorganic particles were used for polymerization with different monomer concentrations at 60 °C for 16 hours. The free polymers and the polymer-modified particles were separated by centrifugation. The molecular weight of the non-attached polymers was determined by GPC. The contents of carbon and hydrogen on the modified pigment particles were measured by elemental analysis after extraction of the free polymers from the surface-attached polymers. The results are shown in Figure 5-16. The unmodified TiO_2 and PCG2020 pigments show carbon and hydrogen contents < 0.1 %.

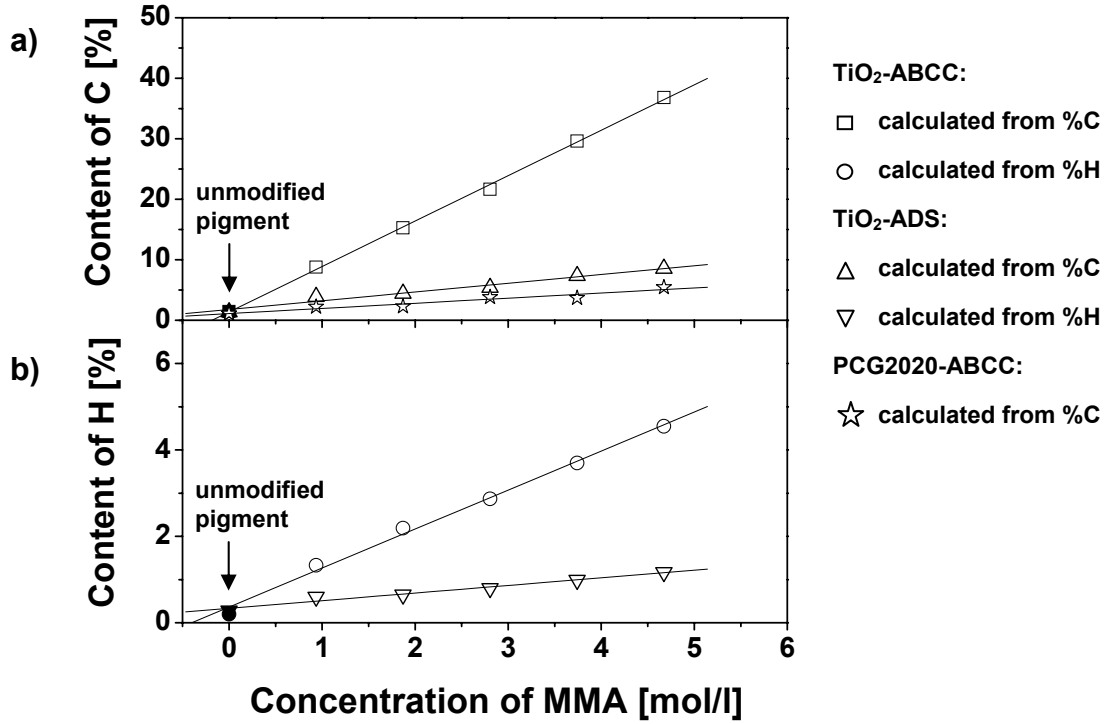

Figure 5-16: Results from elemental analysis obtained after surfaces-initiated polymerization of MMA from TiO_2-ABCC, TiO_2-ADS and PCG2020-ABCC (polymerization condition: T = 60 °C, t =16 hours, toluene as solvent) as a function of MMA concentration: a) carbon and b) hydrogen content.

As shown in Figure 5-16, the increase of carbon and hydrogen content are linear proportional to the monomer concentration.

The amount of grafted polymers was determined by elemental analysis using Equation 5-2.

$$\delta_C = \frac{\%C \times M}{100 \times N_C \times M_C}; \qquad \delta_H = \frac{\%H \times M}{100 \times N_H \times M_H} \qquad \textit{Equation 5-2}$$

δ_C and δ_H are the grafted amount [gram polymer pro gram pigment]. M is the molecular weight of the polymer repeating unit. N_C and N_H are the number of carbon and hydrogen atoms in the polymer repeating unit, while M_C and M_H are the atom masses of carbon and hydrogen, respectively.

As shown in Figure 5-16a, the carbon and nitrogen content is linear proportional to the monomer concentration. Accordingly, the amount of the grafted polymer calculated from %C and %H is also proportional to the monomer concentration (s. Figure 5-17a). The values obtained from both calculations (δ_C and δ_H) are more or less identical.

From the amounts of grafted polymer, the layer thickness can be calculated using Equation 4-7. The layer thickness of the polymer grafted (s. Figure 5-17b) is linear proportional to the monomer concentration as the molecular weight of the surface-attached polymers increases with the increasing of the monomer concentration (s. Figure 5-17c).

Since TiO_2-ABCC has the higher initiator graft density (s. Table 5-2), the polymerization using TiO_2-ABCC also shows higher layer thicknesses than those using TiO_2-ADS (s. Figure 5-17b). In case of using PCG2020-ABCC, the amount of polymer attached to the PCG2020 is lower than that on TiO_2 (s. Figure 5-17a). However, the former has a much smaller specific surface area (SA_{sp} = 2.5 $m^2\ g^{-1}$ for PCG2020 and SA_{sp} = 50 $m^2\ g^{-1}$ for TiO_2) so that the graft density and accordingly the film thickness of the former are actually higher than of the latter.

As can be expected, the molecular weight of the obtained free polymers increases with increasing monomer concentration. Although, the particles have different amounts of initiators attached to the surfaces and different initiator graft densities, the molecular weights of the obtained free polymers are similar for all system.

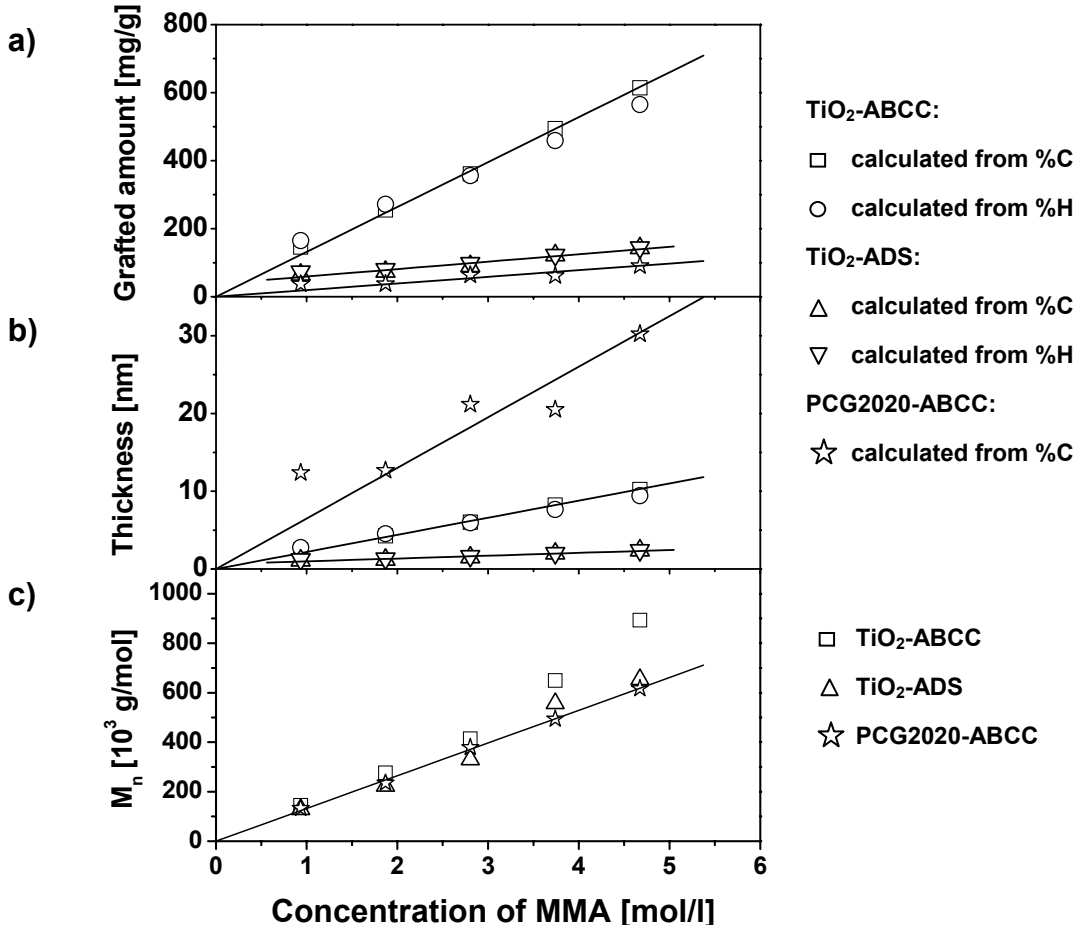

Figure 5-17: a) Amount of grafted polymer and b) layer thickness calculated from %C in comparison to those calculated from %H as a function of monomer concentration; c) number-average molecular weights of the free polymers determined by GPC as a function of monomer concentration.

5.2.2.2 Graft density as a function of polymerization time

To study the initiator conversion, the polymerization reaction with the initiator-attached substrate was carried out with 2.81 mol l^{-1} MMA for TiO_2-ABCC and 3.74 mol l^{-1} MMA for TiO_2-ADS at 60 °C and stopped at a desired polymerization time between 4 – 32 hours. The graft density and the layer thickness of the polymer-attached surfaces were determined by the same method as described above using data from elemental analysis. The results are shown in Figure 5-18.

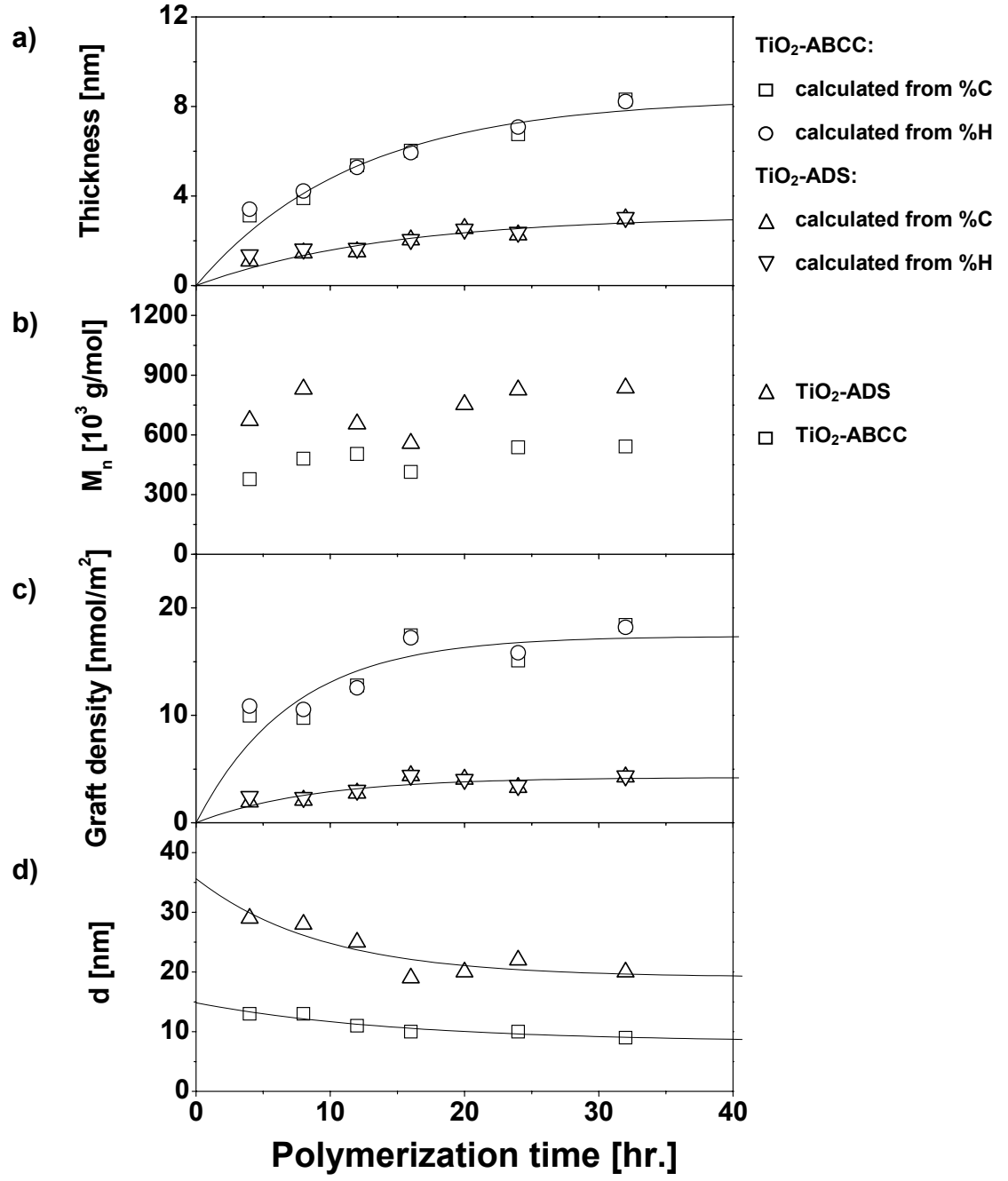

Figure 5-18: a) Layer thickness, b) number-average molecular weight, c) graft density and d) average distance between two polymer chains as a function of polymerization time: solid lines are a fit of the data.

The polymer layer thickness initially increases and then levels off at 2 nm and 8 nm for TiO_2-ADS and TiO_2-ABCC, respectively (s. Figure 5-18a). An increase of the polymerization time has no significant influence to the polymer film thickness.

Due to the nature of radical polymerization, the molecular weight of the polymer is independent of the polymerization time. The molecular weights of the obtained free polymer, which were initiated by TiO_2-ADS or TiO_2-ABCC show comparable values within the corresponding data sets (s. Figure 5-18b). The number-average molecular weight of the free polymer which initiated by TiO_2-ADS or TiO_2-ABCC was found to be around 732 000 g mol^{-1} (M_w ~ 1 620 000 g mol^{-1} and D ~ 2.2) and ca. 476 000 g mol^{-1} (M_w ~ 1 170 000 g mol^{-1} and D ~ 2.5), respectively.

As the molecular weight of the free polymer is constant, if only the reaction time is varied, the graft density of the polymer exhibits a similar behavior as the layer thickness of the polymer (s. Figure 5-18c). The graft density initially increases and then levels off at ca. 4 nmol m^{-2} (d ~ 20 nm) and ca. 17 nmol m^{-2} (d ~ 9 nm) initiated by TiO_2-ADS and TiO_2-ABCC, respectively.

5.2.3 Discussion

Two approaches were successfully used to generate initiator monolayers on TiO_2 and PCG2020 surfaces:

- an initiator silane (ADS) was directly coupled to the surfaces
- and a phosphate based layer was generated by firstly deposition an aminoalkyl phosphate (AEP) to which the initiator was then coupled via attachment of the amino function of the AEP monolayer

It was found that the two-step process yields a higher initiator density on the surfaces than the direct modification as the reactivity of phosphates to TiO_2 is much higher than that of a monochlorosilane. The difference appears to be strong enough so that a higher initiator graft density is obtained although two surface reaction steps are required.

The initiator monolayers were then used for the surface-initiated polymerization of MMA onto TiO_2 and PCG2020. Layer thicknesses of PMMA up to 30 nm for PCG2020-ABCC, 10 nm for TiO_2-ABCC and 5 nm for TiO_2-ADS could be achieved and the process was found to be similar to comparable “grafting-from” polymerizations performed on SiO_2 surfaces.

5.3 Immobilization of 3-methycryloylpropyl trimethoxysilane on TiO_2 particles

In this study, 3-methycryloylpropyl trimethoxysilane (MPS) was immobilized to TiO_2 surfaces to investigate the grafting of polymer onto TiO_2 particles via copolymerization of free monomer with surface-attached monomers. MPS has two functional groups: one is the methoxysilane unit which can be immobilized to the oxide layers of many metals and the other is the polymerizable methacrylate group (s. Figure 5-19).

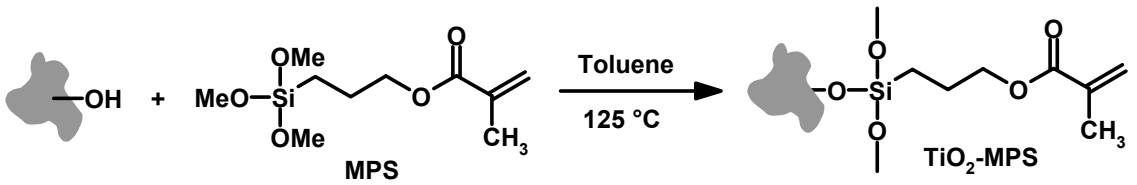

Figure 5-19: Immobilization of 3-methycryloylpropyl trimethoxysilane (MPS) onto TiO_2 surfaces.

5.3.1 Qualitative characterization of the methacrylate monolayer on TiO_2 surfaces

Figure 5-20 show the FTIR spectra of MPS monolayers attached to TiO_2 surfaces as well as unmodified TiO_2 and 3-methycryloylpropyl trimethoxysilane (MPS) bulk substance. Several absorption bands caused by the MPS molecules appear after immobilization of this silane on the TiO_2 surface (s. Figure 5-20b). For example, the absorption band at 1720 cm^{-1} (1725 – 1750 cm^{-1})[125] corresponds to the carbonyl group of ester (–COOR) and the CH vibration is found ~ 2911 –2994 cm^{-1}.

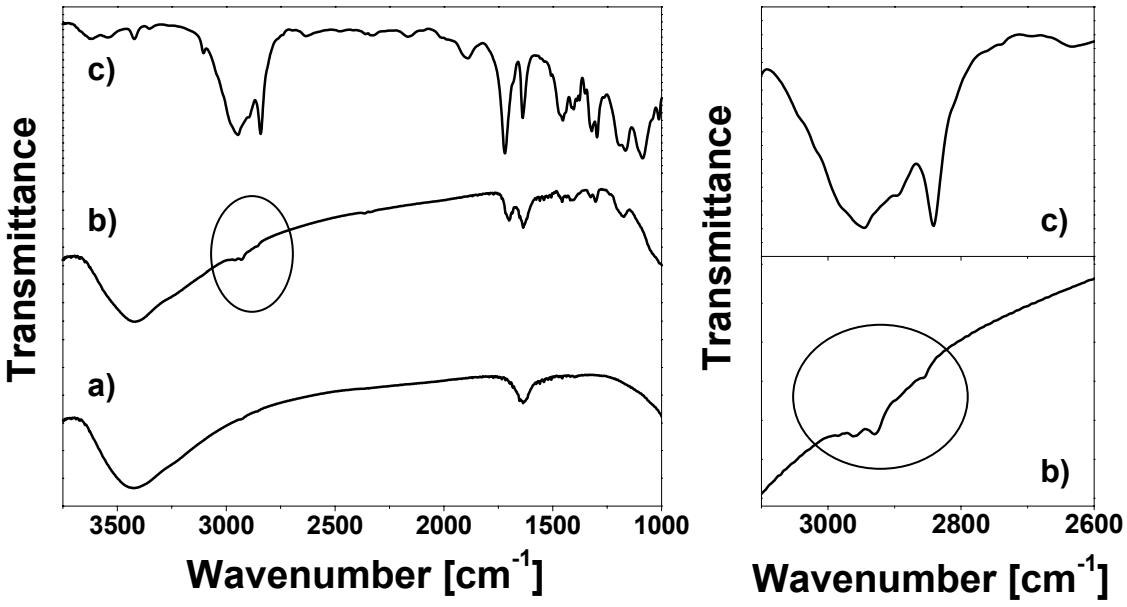

Figure 5-20: Transmission FTIR spectra of a) unmodified TiO_2, b) MPS-modified TiO_2 and c) 3-methycryloylpropyl trimethoxysilane (MPS) as reference.

Figure 5-21 shows the XP survey spectra of unmodified and MPS-modified TiO_2. Besides the signals inherent to the substrate, namely the Ti(2p) and O(1s) signals, new signals appear at 101.7 eV and 152.7 eV which can be assigned to Si(2p) and Si(2s) anchor groups of the MPS molecules (s. Figure 5-21a and b). The intensity of the C(1s) signal significantly increases in comparison to unmodified TiO_2 as shown in Figure 5-22.

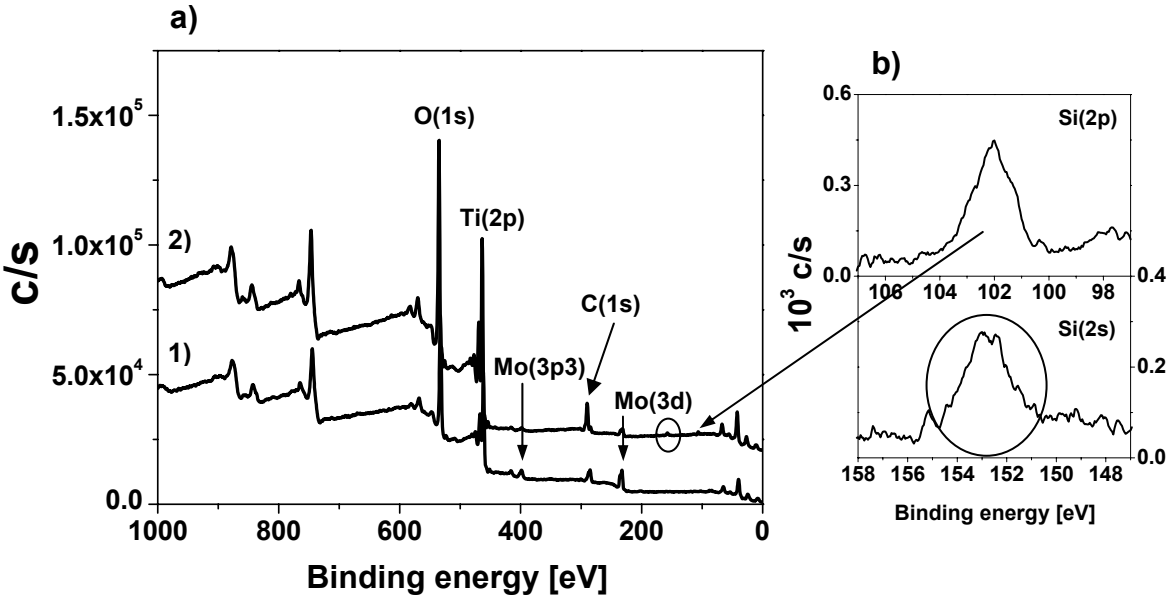

Figure 5-21: a) XP survey spectra of 1) unmodified TiO_2 and 2) TiO_2-MPS; b) high resolution spectra of the Si(2p) and Si(2s) peak areas of TiO_2-MPS.

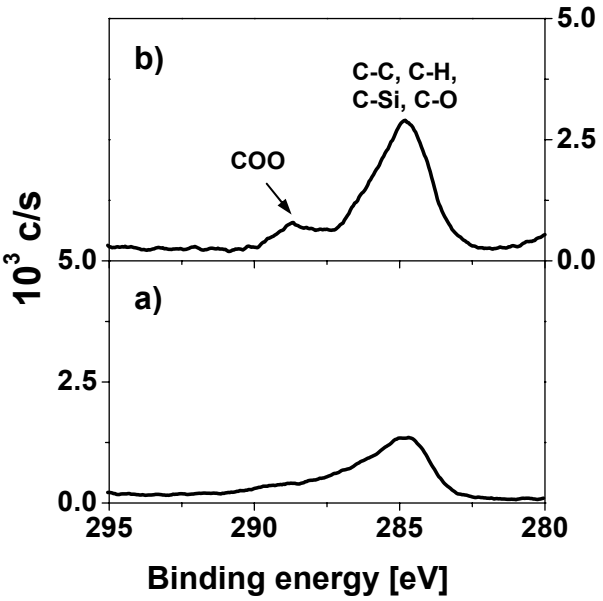

Figure 5-22: C(1s) signals of a) unmodified TiO_2 and b)TiO_2-MPS.

5.3.2 Determination of the graft density of the methacrylate monolayer on TiO_2 surfaces

The immobilization of MPS onto TiO_2 surfaces was performed at various MPS concentrations to find a suitable concentration yielding the maximum graft density. The graft densities of MPS were determined by elemental analysis according to Equation 5-1. The results are presented in Figure 5-23.

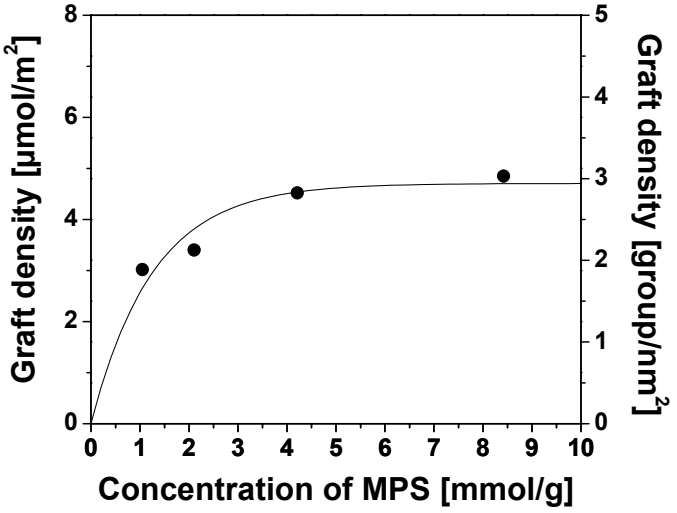

Figure 5-23: Graft density of MPS as a function of the concentration of 3-methycryloylpropyl trimethoxysilane (MPS).

The graft densities of the MPS on the surfaces increases slightly from 1.8 groups nm^{-2} (3.0 µmol m^{-2}) to 3.0 groups nm^{-2} (4.9 µmol m^{-2}) with increasing MPS concentration. These values are lower than those reported for SAMs on the metal oxide surfaces (~ 5 groups nm^{-2})[26,154,155]. However, the graft densities of MPS are in general higher than the graft density of AEP (~ 1.4 groups nm^{-2}) and ADS (~ 0.6 groups nm^{-2}) on the TiO_2 particle.

These results are in contradiction to the results of investigations by Helmy and Fadeev[26]. They found that the reactivity towards TiO_2 decreases in the order $C_{18}H_{37}SiCl_3$ >> $C_{18}H_{37}$-$PO(OH)_2$ > $C_{18}H_{37}Si(CH_3)_2Cl$ > $C_{18}H_{37}Si(OCH_3)_3$ > $C_{18}H_{37}SiH_3$ (immobilization was carried out between 24 hours to 240 hours). A direct comparison of the data obtained

from this study to the results of Helmy and Fadeev, however, is not possible for two reasons:

- In this study, the molecules used have very different chain lengths that can not pack as easily as long chain alkane residues.
- The functionalities of these molecules, especially the amino groups of AEP, may interfere with the immobilization reaction due to acid / base reactions between the NH_2 group and the acidic surface hydroxyl groups[156-158].

5.4 Grafting of polymers via copolymerization of surface-attached monomers

5.4.1 Qualitative characterizations of the polymer-attached pigment surfaces

Figure 5-24 shows the transmission FTIR spectra of the TiO_2 with surface-attached polymer monolayer as well as that of unmodified TiO_2. The new absorption band at 1730 cm^{-1} corresponding to the carbonyl group of the methacrylate groups (–$COOCH_3$) originating from PMMA are observed after the polymerization of TiO_2-MPS with MMA in toluene in the presence of AIBN. The CH stretching vibrations of the backbone chains of PMMA is visible between 2915 and 3000 cm^{-1}.

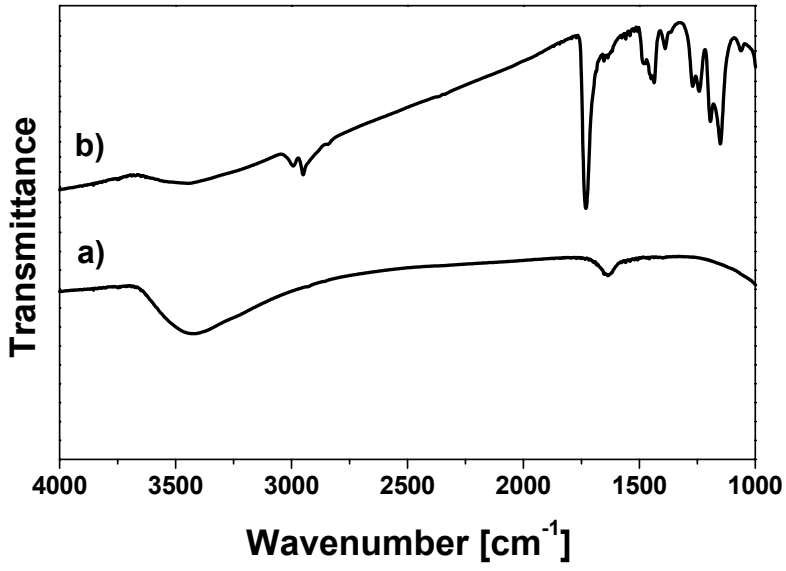

Figure 5-24: Transmission FTIR spectra of a) unmodified TiO_2 and b) TiO_2-PMMA (L ~ 3.3 nm) using TiO_2-MPS copolymerized with MMA in the presence of AIBN.

As shown in Figure 5-25b, due to the PMMA layer on the TiO_2 surfaces, the signal intensity of C(1s) at 285 eV increases after the copolymerization of TiO_2-MPS and MMA compared to the MPS-modified TiO_2. In contrast, the signals of Ti(2p) at 458 eV and Si(2p) at 101.7 eV are significantly attenuated. The copolymerization of TiO_2-MPS and

MMA without AIBN under the same condition did not result in any polymer attached to the particle surfaces.

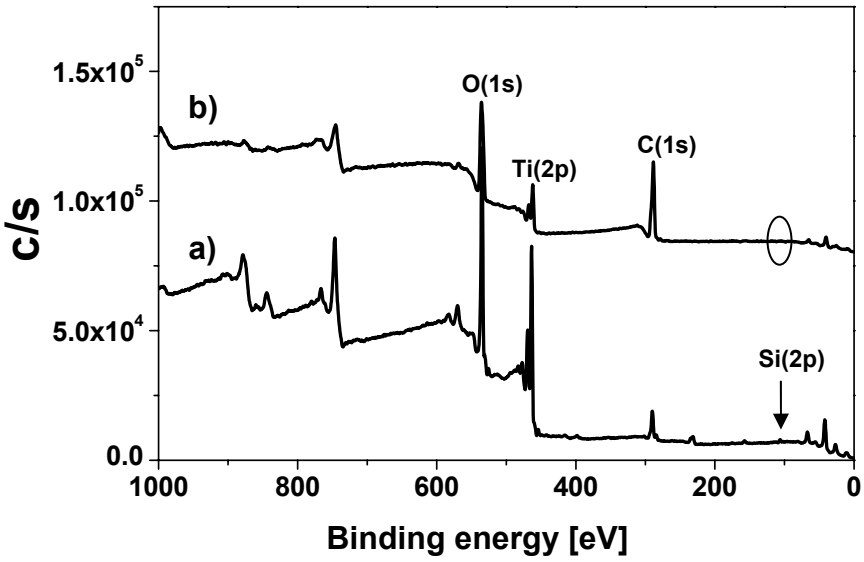

Figure 5-25: XP survey spectra of a) TiO_2-MPS and b) TiO_2-PMMA (L ~ 3.3 nm) using TiO_2-MPS copolymerized with MMA in the presence of AIBN.

5.4.2 Quantitative characterization of polymer-attached surfaces with various polymerization parameters

5.4.2.1 Graft density as a function of monomer concentration

The grafting of MMA using MPS-modified TiO_2 particles was carried out at various MMA concentrations at 60 °C for 16 hours using AIBN (20 mmol l^{-1}) as the initiator and toluene as solvent. The free polymer and surface-attached polymer were separated as mentioned above. The polymer graft densities were calculated from elemental analysis. The molecular weight of the free polymer was determined by GPC measurements.

As shown in Figure 5-26a and b, the amount of grafted polymer (2 to 5 mg m^{-2}) and the layer thickness (1.7 to 4.4 nm) of the PMMA increase with increasing monomer concentration due to an increase of the molecular weight of polymer attached to the surfaces. The molecular weight of the PMMA is directly proportional to the monomer concentration as shown in Figure 5-26c. Therefore, the graft density of the polymer (ca. 79 – 52 nmol m^{-2}) on the surface decreases proportionally to the monomer concentration (s. Figure 5-26d). The reduction of the graft density of the grafted polymer is comparable

to the grafting polymerization of PGL1155-MA as described in Chapter 4.4.2. As already described above, the graft density which can be achieved through this process depends strongly on molecular weight of the growing chains and accordingly on the monomer concentration (s. Figure 4-27). If high molecular weight polymer is attached to the surface, a complete coverage of the surface is reached. Chains growing in later stage of the reaction can no longer easily penetrate this layer and the attachment reaction levels off. As a result, the graft density of the polymer is rather low at high monomer concentration.

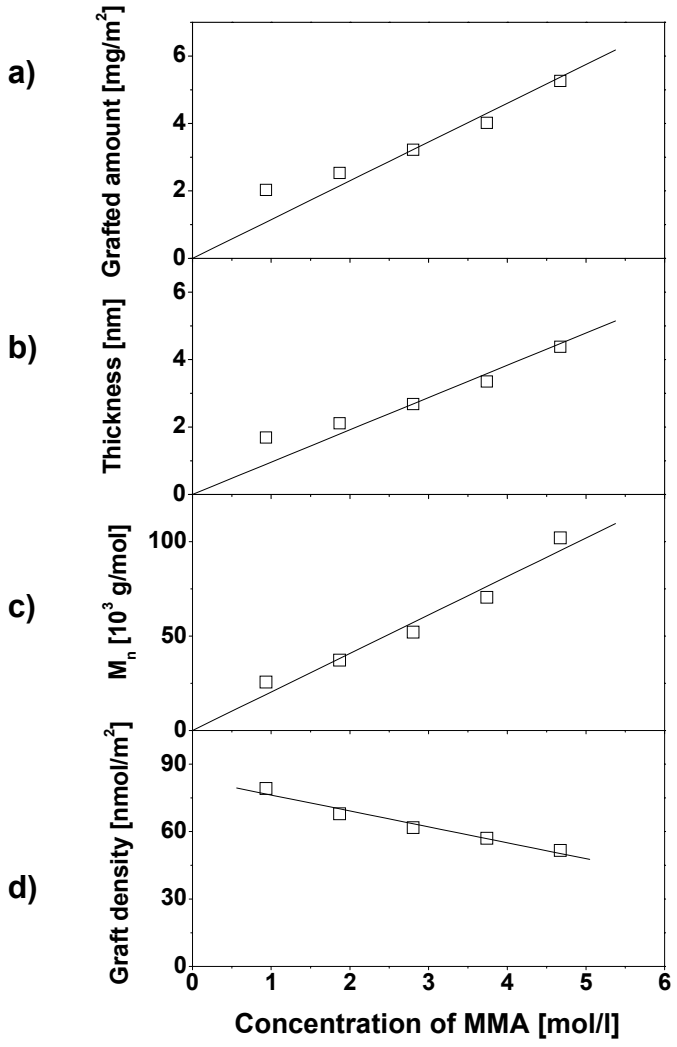

Figure 5-26: a) Amount of grafted polymer and b) layer thickness calculated from %C as a function of monomer concentration; c) number-average molecular weights of the free polymers determined by GPC and d) polymer graft density as a function of the monomer concentration: all solid lines are fitted the data.

5.4.2.2 Graft density as a function of polymerization time

To study the influence of the polymerization time on this process, a series of polymerization were performed at a fixed initiator (20 mmol l^{-1}) and monomer concentration (2.81 mmol l^{-1}) but for different periods of time (4 – 32 hours). The molecular weight of the free PMMA was determined by GPC as shown in Figure 5-27a. It is expected for free radical polymerizations at constant monomer and initiator concentrations that the molecular weight of the polymer should be constant during the reaction, i.e. the molecular weight is independent of the polymerization time. In general, this is also the case for the experiments described here (M_w ~ 833 000 g mol^{-1}, M_n ~ 485 000 g mol^{-1} and D ~ 1.7), except for short polymerization times. The molecular weights of the polymers obtained after 4 and 8 hours are somewhat higher than those of all other polymers. The graft densities of the polymers initially increase and reach a constant value of 64 nmol m^{-2} after 12 hours polymerization reaction (s. Figure 5-27b).

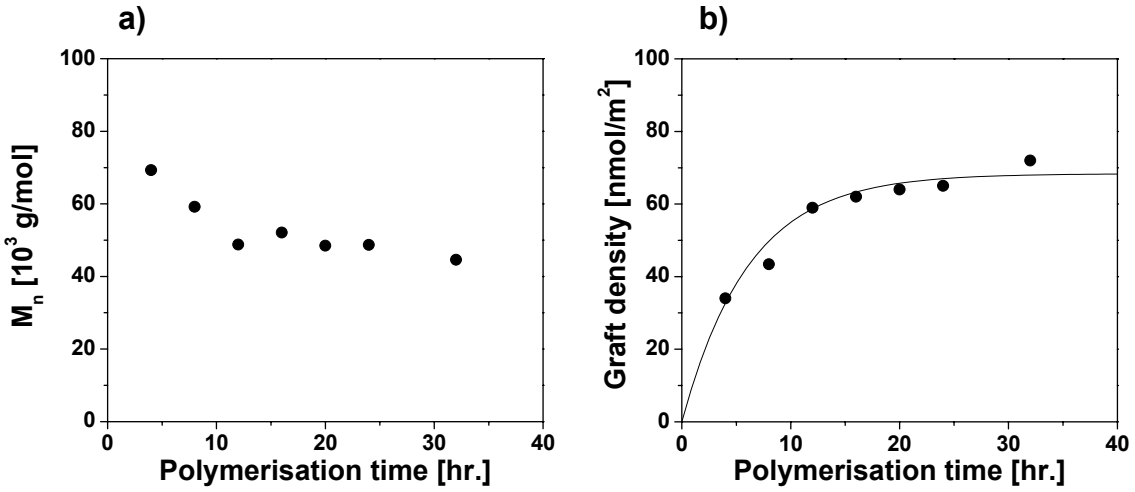

Figure 5-27: a) Number-average molecular weight of the free PMMA determined by GPC and b) graft density of the grafted polymer as a function of the polymerization time: solid line is the fitted data points.

The layer thickness of PMMA slightly increases with increasing polymerization time from 2.0 nm to 2.7 nm (s. Chapter 10.10.2). The maximum thickness was reached (2.7 nm) after 12 hours of polymerization time. As mentioned above, the macroradical has to diffuse to the surfaces to react with the double bond on the surfaces and get attached. Although the molecular weights of all polymers are comparable, a higher conversion of the polymerization reaction in solution does not lead to a higher layer

thickness of the polymer, because the kinetic barrier reached after complete coverage of the surface prevents the attachment of further chains at later polymerization times.

5.4.2.3 Layer thickness as a function of initiator concentration

In this series of experiments, the initiator concentration was varied and the monomer concentration ([MMA] = 2.81 mol l^{-1}), polymerization time (t = 16 hours) and temperature (T = 60 °C) were kept constant.

As shown in Figure 5-28a, the initiator concentration does not influence the layer thickness of the polymer attached to the surface (L ~ 2.5 nm). In contrast to the polymer layer thickness, the graft density of the polymer increases (Figure 5-28b) due to the reduction of the molecular weight of the polymers (s. Table 10-22).

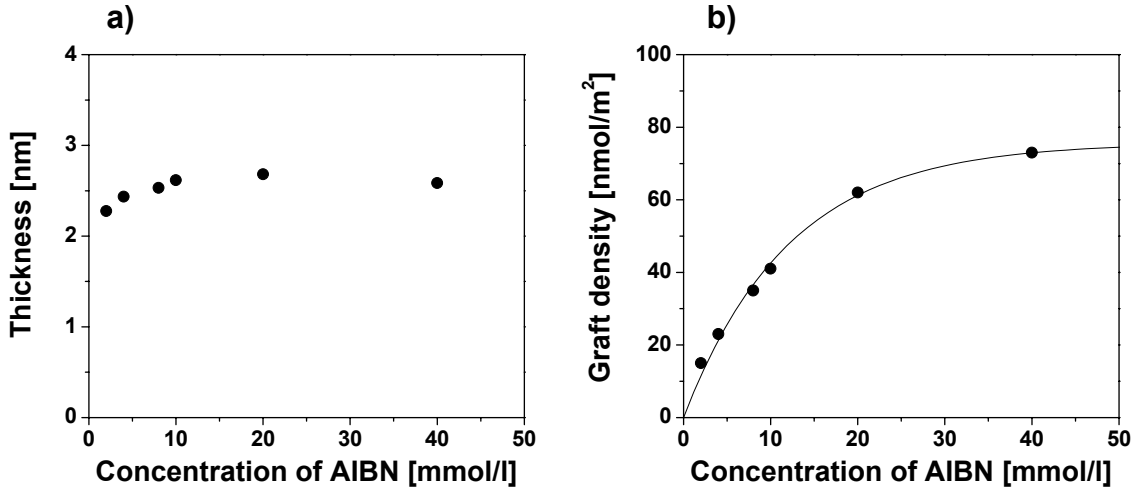

Figure 5-28: a) Polymer layer thickness and b) graft density of the polymer grafted as a function of AIBN concentration.

5.4.3 Conclusions

MPS was immobilized to TiO_2 surfaces in one-step reaction and the maximum graft density of MPS was formed to be 5 μmol m^{-2} (3 groups nm^{-2}). The layer thickness of the PMMA monolayers immobilized by the described technique exhibits value between 2 nm and 4 nm. This result is due to the fact that the available graft densities for a given set of polymerization parameters are directly related to the molecular weight of the attached chains. This observation is clearly related to the overall mechanism of the process which is based on an initial attachment of a growing chain to a surface-bound monomer. This "grafting-to" process comes to a virtual stop once the surface is covered with polymer as the already attached layer forms a kinetic barrier that hindrance the attachment of further chains. Complete coverage, however, is directly related to the molecular weight of the attached chains, i.e. lower graft densites are reached to establish this situation if longer chains are attached. Therefore, in our system the amount of grafted polymer is not strongly dependent on the reaction conditions. Even though this can be viewed as a limitation to the overall versatility of the approach it also guarantees a quite high robustness of the process as slight run-to-run variation of the polymerization parameters do not strongly influence the outcome of the reaction.

6 Stability of Unmodified and Polymer-Modified Pigments against Alkaline Solutions

6.1 Investigation of the stability against various buffer solutions

One of the key requirements for the practical use of pigments is their stability against harsh environmental conditions. In some cases, especially the stability against alkaline solutions is problematic. Many pigments are not suitable for use in amine hardening systems or in emulsion paints which are to be applied on basic substrates due to a poor stability against strong bases. Therefore, the stability of polymer-modified pigments against basic environment has been investigated and compared to that of unmodified pigments.

In order to investigate the stability of the unmodified and PMMA-modified pigments, they were suspended in various buffer solutions (1% weight percent of bare pigment, pH = 2 – 12; s. also experiment part) and heated for one hour. After the reaction, the treated pigments were filtered off, extracted with water for 24 hours and dried at 60°C in vacuum. The yield of the pigment was determined from the difference of pigment weight before and after treatment. In addition, elemental analysis and the UV absorption was used to compare the chemical composition and the color change before and after the treatment of the pigment.

Figure 6-1 shows the UV absorption of PGL1155 after treatment with various buffer solutions. In Figure 6-1, it is clearly seen that the UV absorption of the PGL1155 increases with increasing pH value of the buffer solution. This probably originates form the change of chemical constitution or physical property of pigment after treatment with buffer solution.

Table 6-1 summarizes the solubility of PGL1155 in solutions of different pH. It is evident that the solubility of the pigment increases when the pH value is increased. After treatment at pH 2.0 – 10.5, only around 14 – 24 % of the pigments are soluble under the condition described above. At pH = 11.0, the solubility of pigment increases to 49 % and the pigment completely dissolves at pH = 11.5 after 30 minutes exposure to the buffer solution. At pH = 12.0, the dissolution is already complete after 15 minutes. The results of the elemental analysis show that the chemical composition of the pigment remains more or less unchanged.

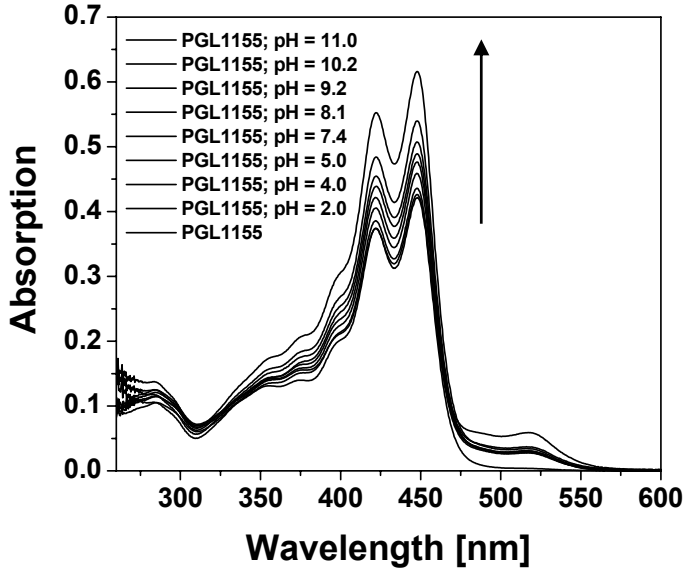

Figure 6-1: UV spectra of unmodified PGL1155 after treatment in buffer solution.

Table 6-1: Yield and elemental analysis data obtained from PGL1155 treated with buffer solutions of various pH.

	Yield [%]	**C** [%]	**H** [%]	**N** [%]
untreated	100	56.98	3.29	20.76
pH = 2.0	86	56.70	3.60	20.69
pH = 4.0	85	56.50	3.52	20.45
pH = 5.0	85	56.85	3.55	20.08
pH = 7.4	84	56.37	3.51	20.47
pH = 8.1	75	56.80	3.46	20.52
pH = 9.2	73	56.80	3.53	20.52
pH = 10.2	78	56.74	3.50	20.81
pH = 10.5	76	56.77	3.52	20.90
pH = 11.0	49	56.64	3.31	20.41
pH = 11.5	soluble after 30 minutes			
pH = 12.0	soluble after 15 minutes			

The same experiments were reported using PGL1155-PMMA hybrids. The UV absorptions obtained from PGL1155-PMMA after treatment in buffer solution are shown in Figure 6-2. Under the same conditions, the intensity of the absorption is comparable to that of untreated PGL1155-PMMA ($\delta \sim 1.32$ g PMMA per g pigment) over the entire

range of pH values. There is only a small loss of material (< 10 %) in the buffer solutions of pH value from 8.1 to 11.0 (s. Table 6-2). Even at pH 12.0, only 20 % of the pigments were lost to the buffer solution after treatment.

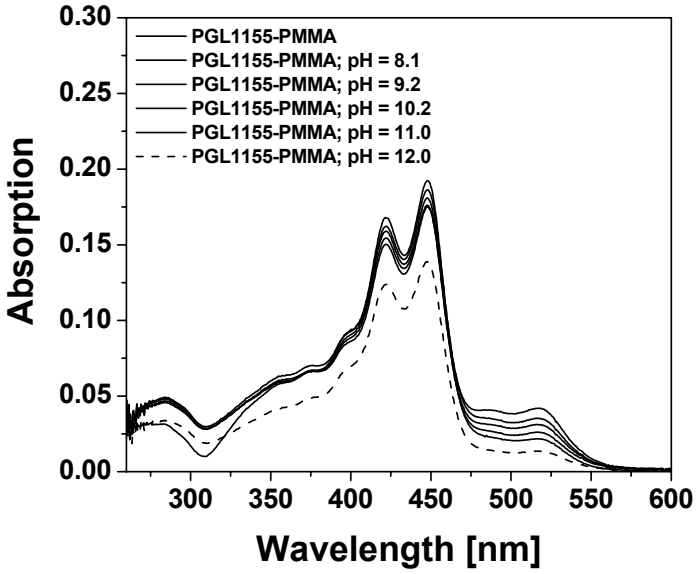

Figure 6-2: UV spectra of PMMA-modified PGL1155 (1.3 g PMMA per g pigment) after treatment in buffer solution.

Table 6-2 Yield and elemental analysis data obtained from PGL1155-PMMA treated with various buffer solutions.

			C [%]		**H** [%]		**N** [%]	
	PGL1155-PMMA*		58.85		6.11		8.93	
	Yield [%]		**C** [%]		**H** [%]		**N** [%]	
	1 hr.	2 hr.	1 hr.	2 hr.	1 hr.	2 hr.	1 hr.	2 hr.
pH = 8.1	94	97	58.39	58.00	6.10	5.94	8.80	8.94
pH = 9.2	93	95	58.28	58.08	6.23	6.12	8.95	8.83
pH = 10.2	94	93	58.35	58.12	6.21	6.15	8.77	8.70
pH = 11.0	94	91	58.41	58.22	6.21	6.32	8.87	7.83
pH = 12.0	80	–	58.88	–	6.80	–	5.49	–

* PGL1155-Azo was polymerized with 3.74 mol l^{-1} MMA at 60 °C for 16 hours: 1.3 g PMMA per g PGL1155.

6.2 Investigation of the stability of pigment with variation of the PMMA graft density

In order to further elucidate the barrier properties of the PMMA shell, a second series of experiments was performed in which PGL1155-PMMA with various graft densities of PMMA were used.

Compared to PGL1155, the PMAA-modified pigments (PGL1155-PMAA) are very stable against alkaline solutions up to pH 11.0, especially at higher graft densities of PMMA (~ 1.32 g and 0.49 g PMMA per g pigmnet) (s. Figure 6-3). At pH 12, PGL1155 is dissolved after 15 minutes. The polymer-modified pigment, however, still tolerates such conditions except for samples with very low polymer graft density ca. 0.22 g per g pigment, which are dissolved after 30 minutes.

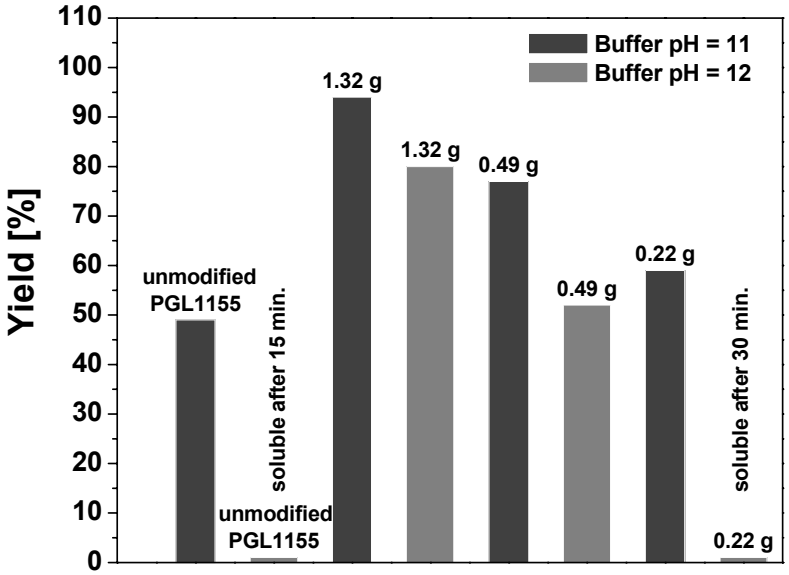

Figure 6-3: Yield of PGL1155 and PGL1155-PMMA with various graft densities of PMMA after treatment in buffer pH 11 (dark gray) and pH 12 (light gray).

6.3 Investigation of the stability of pigment with different surface- attached monolayers

In this experiment, the influence of the chemical composition of the shell surrounding the PGL1155 particles concerning the stability against the alkaline solution were also investigated under the same conditions as mentioned above.

Compared to the unmodified PGL1155, pigments with grafted PS or PHDFDA monolayers have also an improved stability against alkaline solution in the same way as described before for surface-attached PMMA monolayers if the graft density of the polymer is high enough (s. Figure 6-4). PGL1155-PS gave better results than all other polymers. This might be due to the fact that the ester groups in PMMA and PHDFDA can be hydrolyzed under basic condition yielding water swellable layers.

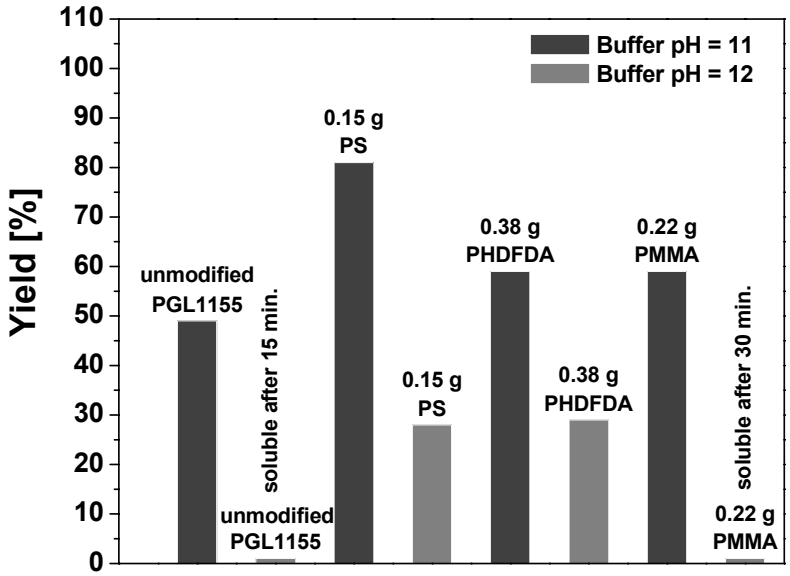

Figure 6-4: Alkaline stability of unmodified PGL1155 as well as various polymer-pigment hybrid materials in buffer solutions of pH 11 (dark gray) and pH 12 (light gray).

6.4 Discussion

As PMMA is insoluble in aqueous solution, the surface-attached PMMA forms a barrier against attack on pigment surfaces compared to non-polymer attached pigment. In addition, films with higher graft density of PMMA show higher stability against alkaline solution than those with lower ones. It might be due to fact that a thin layer is less tight than thick one. Therefore, the higher graft density can form the higher barrier prevent the attachment of the alkali ions to the pigment surfaces than that of the lower one. As a result, the alkali ions cannot access the pigment surfaces thus preventing the dissolution of the pigment.

PS and PHDFDA attached onto PGL1155 also show an improvement of the stability of the pigment against alkaline solution. It is probably due to the poor swellability of both polymers in the aqueous solution, which can prevent to the accession of the alkali ions to the pigment surfaces.

Unmodified and modified PGL1840 (PMMA-, PS- and PHDFDA-modified PGL1840) were also treated with the alkaline solution (results s. Chapter 10.10) under the same condition as mentioned for pigment PGL1155. The treatment of these pigment resulted similarly to that of non- and attached polymer onto PGL1155, i.e. higher graft density of polymer more stable than the lower one.

It can be concluded that the polymer-attached pigments show an improved stability against strong bases at a sufficiently high graft density of the attached polymers compared to non-polymer attached pigment. In other words, the organic pigment can be significantly protected by surface-attached polymer chains.

7 Experimental Section

7.1 Chemicals and solvents

α,α´-Azo-isobutyronitrile	≥ 98.0 %, Fluka
2-Aminoethyldihydrogenphosphate	≥ 99 %, Fluka
4,4´-Azo-bis-(4-cyanopentanoic acid)	≥ 98.0 %, Fluka
Acetone	≥ 99.8 %, Fluka
Aluminium oxide	for chromatography, Fluka; type 5016 A basic, 0.05 – 0.15 mm, pH = 9.5 ± 0.5 and type 507 C neutral, 0.05 – 0.15 mm, pH = 7.0 ± 0.5
Ammonia aqueous solution	28 %, Merck
Ammonium chloride	≥ 99.5 %, Fluka
Benzophenone	≥ 99.0 %, Fluka
Buffer solution pH 2.0	Citric acid / NaOH / HCl, Fluka
Buffer solution pH 4.0	Citric acid / NaOH / NaCl with addition of fungicide, Fluka
Buffer solution pH 5.0	Citric acid / NaOH, Fluka
Buffer solution pH 7.4	0.009 M $KaHPO_4$ / 0.032 M Na_2HPO_4 with addition of fungicide, Fluka
2-Chlor-4,6-diamino-1,3,5-triazine	95 %, Aldrich
Calcium hydride	≥ 97.0 %, Fluka
Chloroform	≥ 99.4 %, Fluka
Chloroform-d_3	> 99.8 %, Fluka

1,6-Diaminohexane	≥ 99.0 %, Fluka
Dichloromethane	≥ 99.9 %, Fluka; heated 24 hours over CaH_2, distilled and kept in dried molecularsiep under N_2
Dichloromethane-d_2	100 %, Fluka
Dichloromethylsilane	~ 97 %, Fluka
Dicyclohexylcarbodiimide	≥ 99.0 %, Fluka
Diethyl ether	≥ 99.5 %, Fluka
Dimethylsulfoxide	≥ 99.8 %, Fluka; for UV spectroscopy and ≥ 99.0 %, Fluka; distilled under vacuum after stirring for 16 hours with calcium hydride (CaH_2) and kept in dried molecularsiep under N_2
Dimethylsulfoxide-d_6	> 99.8 %, Aldrich
N,*N*′-Dimethylacrylamide	≥ 98.0 %, Fluka
N,*N*′-Dimethylformadehyde	99 %, Fluka; destilled under vacuum after stirring for 16 hours with CaH_2 and kept in dried molecularsiep under N_2
Ethanol	absolute for synthesis, Merck
Ethyl acetate	≥ 99.0 %, Fluka; distilled after refluxing for 6 hours over dried molecularsiep and kept in dried molecularsiep under N_2
Hexachloroplatinic acid	purum, 38 % Pt, Fluka; catalyst for hydrosilylation of olefins
Hexane Fraction	purum, Fluka
Hydrochloric acid	p.a., 37 %, Fluka
N-Hydroxysuccinimide	≥ 97.0 %, Fluka

3-Isocyanatopropyl-triethoxysilane	95.0 %, Fluka
2-Methyl-acryloyl chloride	≥ 97.0 %, Fluka
3-Methycryloylpropyl trimethoxysilane	≥ 98.0 %, Fluka
Melamine	99.0 %, Fluka
Methacrylic acid	≥ 98.0 %, Fluka
Methanol	≥ 99.0 %, Fluka
Methanol-d_4	100.0 %, Fluka
Methylmethacrylate	≥ 99.0 %, Fluka; inhibitor was removed using Al_2O_3 type 5016 A basic before distilled over CaH_2 under vacuum and kept under N_2 at – 30 °C
Molecularsiep UOP	Fluka, Type 4A, ∅ = 1.7 - 2.4 mm, pore diameter 4 Å
2,3,4,5,6-Pentafluoro-benzoyl chloride	98 %, ABCR
2-Propanol	≥ 99.0 %, Fluka
2-Propen-1-ol	> 99 %, Fluka
Paliocrom Gold L2020	BASF; 2.5 m^2 g^{-1} (N_2-BET method by supplier)
Perfluoroalkylethyl acrylate	≥ 98.0 %, Fluka; inhibitor was removed using Al_2O_3 type 5016 A basic before distilled under vacuum and kept under N_2 at – 30 °C: 1-(3,3,4,4,5,5,6,6,7,7,8,8,9,9,10,10,10-heptadecafluoro-decyloxy)prop-2-en-1-ol
Phosphorpentachloride	≥ 98.0 %, Fluka
Pigment yellow 139	66 ± 0.1 m^2 g^{-1} (N_2-BET method by supplier), BASF; Paliotol Gelb L 1840
Pigment yellow 185	44 ± 0.1 m^2 g^{-1}, (N_2-BET method by supplier), BASF; Paliotol Gelb D/L 1155;

Poly(2-ethyl-2-oxazoline)	M_w = 50 000 g mol^{-1}, Aldrich
Potassium bromide	p.a., Fluka; for IR-spectroscopy
Potassium carbonate	extra pure, Merck
Pyridine	≥ 99.8 %, Fluka
Silica gel 60	(0.063 – 0.200 mm) for chlomatography, Fluka
Sodium	> 99 %, Merck, rods (protective liquid: paraffin oil)
Sodium chloride	≥ 99.5 %, Fluka
Sodium dihydrogen phosphonate	≥ 99.0 %, Fluka
Sodium hydrogen carbonate	≥ 99.0 %, Fluka
Sodium hydroxide	≥ 98.0 %, Fluka
Sodium sulfate anhydrous	≥ 99.0 %, Fluka
di-Sodium hydrogen phosphonate	≥ 99.5 %, Fluka
tri-Sodium phosphophate	≥ 98.0 %, Fluka
Styrene	≥ 99.0 %, Fluka; inhibitor was removed using Al_2O_3 type 507 C neutral before distilled over $CuCl_2$ under vacuum and kept under N_2 at – 30 °C
Sulfuric acid	98 %, Riedel-de Haën
1,1,2-Trichlor-trifluorethane	≥ 99.5 %, Fluka
Titanium dioxide	Degussa; Titandioxid P 25, 50 ± 15 m^2 g^{-1}
Toluene	≥ 99.9 %, Fluka; dried over Na using benzophenone as indicator, destilled and kept in dired molecularsiep under N_2
Triethylamine	≥ 99 %, Fluka; destilled after refluxing for 6 hours over CaH_2 and kept und N_2

7.2 Method and characterizations

7.2.1 Differential scanning calorimeter (DSC)

DSC traces were recorded on a Seiko SII DSC 6200 with an autosampler-device DSC 6200R. The measurement was carried out in three steps: heating run from 20 °C to 100 °C, annealing for 30 s; cooling from 100 °C to 20 °C and annealing for 5 min; and finally heated from 20 °C to 190 °C. The heating rate for each step was 10 °C min^{-1}.

7.2.2 Elemental analysis

The elemental analysis was carried out at the Chemistry Laboratory of Albert-Ludwigs-Universität Freiburg. The inorganic pigments were burned with V_2O_5.

7.2.3 FTIR spectroscopy

IR spectra were recorded using an Excalibur Spectrometer BIO RAD *FTS 3000* over a frequency range from 4000 to 400 cm^{-1} with sensitivity of 1.5 and resolution of 4 cm^{-1}. KBr pellets were used as background for the measurement of solid compounds.

7.2.4 Freeze-drying procedures

5 – 20 vol.-% polymer-modified pigments were swollen in a suitable solvent (benzene for PMMA- and PS-modified pigment; water for PDMAA- and PMAA-modified pigment), frozen in liquid nitrogen and finally, the solution was evacuated in vacuum (10^{-3} mbar) until the pressure was constant.

7.2.5 Gel permeation chromatography (GPC)

The molecular weight of the formed free PS and PMMA was determined by an Agilent 1100 Series using PSS SDV columns and THF as eluent. The PSS GRAM and Suprema columns were used to determine molecular weight of the free PDMAA and PMAA using DMF and H_2O as eluent respectively. The equipment was calibrated with narrow

molecular weight distribution polymethylmethacrylate (for PMMA, and PDMAA), polystyrene (for PS) and polymethacrylic acid (for PMAA) standards.

7.2.6 Melting point determination

The melting points of all solids were determined by using a Melting Point Apparatus SMP3 BIBBY Stuart Scientific. The heating rate was 2 °C min^{-1}.

7.2.7 Nuclear magnetic resonance (NMR) spectroscopy

^{1}H- and ^{13}C-nuclear magnetic resonance (NMR) measurements were carried out on a Bruker Avance 250 MHz spectroscopy using deuterated solvents at room temperature. The substance concentration for ^{1}H-NMR was around 10 – 15 mg ml^{-1} and for ^{13}C-NMR around 100 – 150 mg ml^{-1}.

7.2.8 Titration experiment

A pH Titrator TiroLine 96 was used to determine the amount of amino groups on the TiO_2 surfaces. The pH-electrode (Blueline 12 pH) was calibrated using buffer solutions of pH 4 and 7, respectively.

7.2.9 UV-VIS spectroscopy

UV absorption measurements were carried out on a Varian UV-Visible Spectrophotometer Cary 50 Bio in a scan range from 800 to 200 nm (ave time: 0.1000 s, data interval: 0.5 nm, scan rate: 300.00 nm min^{-1}) and baseline correction.

7.2.10 X-ray photoelectron spectroscopy (XPS)

X-ray photoelectron spectroscopy (XPS) was carried out on a Perkin Elmer PHI 5600 spectrometer using Mg K_α radiation. The analyser angle was set to 45° relative to the substrate surface. The survey spectra were recorded from 0 – 1000 eV (step width: 0.4 eV, step time: 100 ms). The detail spectra were recorded using a step width of 0.05 eV and step time of 100 ms. Electron binding energies were calibrated to the C(1s)

neutral signal at 284.6 eV[159] and signals were deconvoluted using Gauss-Lorentz functions for the signals and a Shirley type function for the baseline.

7.2.11 X-ray reflectivity (XRR)

The obtained layer thickness on SiO_x substrates was determined by X-ray reflectivity measurements using a Siemens D5000 instrument. An x-ray beam with a wavelength of 0.154 nm is generated ceramic anode with a copper target at 40 kW and 20 mA.

7.3 Synthesis of 4-cyano-4-[1-cyano-3-(2,5-dioxo-pyrrolidin-1-yloxy carbonyl)-1-methyl-propylazo]-4-methyl-butyric acid 2,5-dioxo-pyrrolidin-1-yl ester (ABCC-AE)

55 mmol 4,4′-azobis(4-cyanopentanoic acid) (ABCA) and 121 mmol *N*-hydroxysuccinimide (NHS) were suspended in 200 ml $CHCl_3$ and cooled to 0 °C. Then 121 mmol dicyclohexylcarbodiimide (DCC) in 100 ml $CHCl_3$ were added drop-wise to the mixture in the presence of triehylamine (NEt_3) as a catalyst. The mixture was allowed to warm up to room temperature and continuously stirred for 24 hours. Urea was separated by filtration. About 80 % of the solvent were evaporated and the product was precipitated from cold 2-propanol. The white powder (ABCC-AE) was collected by filtration, washed with 2-propanol and dried in the vacuum; yield: 20.43 g (78 %).

DSC: 226 ± 18 kJ mol^{-1} ($T_{max.}$ ~ 123 °C)

Elemental analysis; calculation for $C_{20}H_{22}N_6O_8$ (%): C = 50.63, H = 4.67, N = 17.71

Found (%): C = 50.62, H = 5.05, N = 17.67

^{1}H-NMR (DMSO-d_6, ppm): 1.70 – 1.76 (d, 6H, C**H**$_3$); 2.48 – 2.57 (m, 2H, $COCH_2C$**H**$_2$); 2.75 – 2.96 (m, 4H, C_2**H**$_4$ of active ester and 2H, COC**H**$_2CH_2$)

^{13}C-NMR (DMSO-d_6, ppm): 22.7, 22.8, 25.8, 25.9 (**C**$_{alkyl}$); 31.7, 31.8 (CO**C**$_2H_4CO$); 71.5, 71.6 (**C**$_{tertiary}$); 118.0, 118.1 (**C**N); 167.8, 167.9, 170.2, 172.8 (**C**O)

FTIR (KBr, cm^{-1}): 2995, 2945, 2245, 1816, 1739, 1782

7.4 Synthesis of linear polythylene imine containing initiator units

7.4.1 Preparation of linear polythylene imine (LPEI) by hydrolysis of poly(2-ethyl-2-oxazoline)

1.20 mol H_2SO_4 (conc.) was slowly added to the solution of 0.30 mol poly(2-ethyl-2-oxazoline) (PEtOx; M_w 50.000 g mol^{-1}) in 200 ml deionized H_2O. The reaction mixture was refluxed for 20 hours. After the solution was cooled to 0 °C, 2.10 mol NaOH in 150 ml H_2O were slowly added. The mixture was again heated to reflux for 6 hours. The precipitated polymer (LPEI) was filtered off and washed with deionized water until the

filtrate was neutral. The polymer was dried at 60 °C in the vacuum yielding 20.00 g product (75 %).

^{1}H-NMR (CD_3OD, ppm): 2.68 (s, 4H, C**H**$_2$C**H**$_2$NH)

FTIR (KBr, cm^{-1}): 3453, 3013, 2808, 1628, 1521, 1466, 1110, 762, 618

7.4.2 Preparation of linear polythylene imine containing initiator units (LPEI-ABCC)

To the solution of 0.10 mol LPEI in 150 ml MeOH, 6 mmol ABCC-AE were slowly added and the reaction mixture was stirred in the presence of NEt_3 (20 mmol) at room temperature for 48 hours. 70 % off the solvent were evaporated and the product was precipitated in 300 ml of 0.02 M NaOH. The obtained polymer was washed with water until the pH of the filtrate was neutral. The white solid (LPEI-ABCC) was dried in the vacuum yielding 8.73 g (69 %). The polymer contained ca. 5.5 mol % initiator calculated from ^{1}H-NMR.

^{1}H-NMR (CD_3OD, ppm): 1.52 – 1.60 (m, 6H, C**H**$_3$ of initiator unit); 2.38 – 2.52 (m, 8H, C**H**$_2$ from initiator unit); 2.65 (s, 4H, C**H**$_2$ from polymer chains)

7.5 Synthesis of the melamine derivatives

7.5.1 Synthesis of 1-(4,6-diamino-[1,3,5]triazin-2-yl)-3-{3´-[tris-(2-hydroxy-ethyl)-silanyl]-propyl}-urea (Mel-Silane)

41 mmol 3-isocyanatopropyl-triethoxysilane were slowly dropped to a suspension of 40 mmol melamine in 100 ml DMSO. The mixture was heated to 60 °C for 16 hours. The solution was then frozen at 0 °C and then again warmed up to room temperature. The precipitated solid was filtered off, washed with DMSO and dried at 60 °C in the vacuum. A white powder (Mel-Silane) was obtained (8.26 g, 55 %) and a melting point of 207 – 209 °C was determined.

Elemental analysis; calculation for $C_{13}H_{27}N_7O_4Si$ (%): C = 41.81, H = 7.29, N = 26.25

Found (%): C = 42.00, H = 7.50, N = 26.58

^{1}H-NMR (DMSO-d_6, ppm): 0.5 – 0.65 (m, 2H, C**H**$_2$Si); 1.15 – 1.30 (t: J = 6.46 Hz, 9H, C**H**$_3$); 1.50 – 1.70 (m, 2H, CH$_2$C**H**$_2$CH$_2$); 3.20 – 3.35 (q: J = 6.46 Hz, 2H, NHC**H**$_2$); 3.65 – 3.85 (q: J = 6.98 Hz, 6H, OC**H**$_2$CH$_3$); 6.60 – 7.30 (d, broad: J = 73.65 Hz, 4H, N**H**$_2$ of triazine ring); 9.20 (s, 1H, N**H**CONH); 9.60 – 9.70 (t: J = 5.13 Hz, 1H, CON**H**CH$_2$)

^{13}C-NMR (DMSO-d_6, ppm): 8 (**C**H$_2$Si); 18 (OCH$_2$**C**H$_3$); 24 (CH$_2$**C**H$_2$CH$_2$); 42 (NH**C**H$_2$); 58 (O**C**H$_2$CH$_3$); 155 (NH**C**ONH); 163, 166 (**C** of triazine ring)

FTIR (KBr, cm^{-1}): 3400, 3205, 2975, 2929, 2887, 1685, 1645, 1600, 1532, 1486, 814

7.5.2 Synthesis of *N*-(6-amino-hexyl)-[1,3,5]triazine-2,4,6-triamine (Mel-C_6H_{12}-NH_2)

103 mmol 2-chlor-4,6-diamino-1,3,5-triazine were dissolved in 180 ml DMSO at 60 °C. Then 515 mmol 1,6-diaminohexane and 309 mmol potassium carbonate were added to the solution. The resulting suspension was heated to 60 °C and kept at this temperature for 18 hours. Then 800 ml H_2O were added to the suspension. A white powder (Mel-C_6H_{12}-NH_2) was separated and collected by filtration. Then, it was washed with water and dried at 60 °C in vacuum yielding 22.07 g (95 %, melting point: 158 – 165 °C.

Elemental analysis; calculation for $C_9H_{19}N_7$ (%): C = 47.98, H = 8.50, N = 43.52

Found (%): C = 47.85, H = 8.80, N = 43.80

^{1}H-NMR (DMSO-d_6, ppm): 1.09 – 1.30 (m, 8H, CH$_2$C$_4$**H**$_8$CH$_2$); 2.40 – 2.55 (m, 4H, NHC**H**$_2$ and C**H**$_2$NH$_2$); 2.96 – 3.04 (q: J = 6.63 Hz, 2H, CH$_2$N**H**$_2$); 6.02 and 6.17 (d, broad: J = 37.44 Hz, 4H, N**H**$_2$ of triazine ring); 6.28 – 6.33 (t: J = 5.66 Hz, 1H, N**H**CH$_2$)

^{13}C-NMR (DMSO-d_6, ppm): 26.5, 26.7, 29.7, 33.6, 41.9 (**C**$_{alkyl}$), 166.6, 167.2 (**C** of triazine ring)

FTIR (KBr, cm^{-1}): 3459, 3407, 3132, 2933, 2854, 1679, 1647, 1550, 1493, 1471, 815

7.5.3 Synthesis of 4-cyano-4-{1-cyano-3-[6-(4,6-diamino-[1,3,5]triazin-2-ylamino)-hexylcarbamoyl]-1-methyl-propylazo}-N-[6-(4,6-diamino [1,3,5]triazin-2-ylamino)-hexyl]-4-methyl-butyramide (Mel-ABCC)

15 mmol Mel-C_6H_{12}-NH_2 were dissolved in DMF at 80 °C in DMF. After the solution was cooled to room temperature, 7.5 mmol ABCC-AE were added. The reaction mixture was stirred for 48 hours at room temperature. The solvent was evaporated and the product (Mel-ABCC) was purified by column chromatography (first eluent; ethyl acetate:MeOH = 4:1 and second eluent; MeOH). After removal of the solvent up to 80 %, the product was precipitated from ethyl acetate yielding 3.15 g (60 %).

DSC: 231 ± 15 kJ mol^{-1} ($T_{max.}$ ~ 118 °C)

^{1}H-NMR (DMSO-*d_6*, ppm): 1.15 – 1.50 (m, 16H, $CH_2C_4\underline{\mathbf{H}}_8CH_2$); 1.60 – 1.70 (s, 6H, $C\underline{\mathbf{H}}_3$); 2.00 – 2.40 (m, 8H, $COC_2\underline{\mathbf{H}}_4C$); 3.21 – 3.08 (m, 8H, $NHC\underline{\mathbf{H}}_2$); 5.91 – 6.10 (d: J = 41.54 Hz, 8H, $N\underline{\mathbf{H}}_2$ of triazine ring); 6.33 – 6.50 (t: J = 5.67 Hz, 2H, $N\underline{\mathbf{H}}CH_2$); 7.85 – 8.05 (t: J = 5.53 Hz, 2H, CON**H**)

^{13}C-NMR (DMSO-*d_6*, ppm): 16.8, 23.4, 25.7, 29.0, 31.7, 32.1, 32.8, 36.0, 62.5 ($\underline{\mathbf{C}}_{alkyl}$); 75.0 ($\underline{\mathbf{C}}_{tertiary}$); 121 (**C**N); 169.6, 169.9 (**C** of triazine ring); 172.5, 173.1 (**C**ONH)

FTIR (KBr, cm^{-1}): 3339, 3226, 2936, 2859, 2244, 1630, 1558, 1461, 815

7.5.4 Synthesis of *N*-[6-(4,6-diamino-[1,3,5]triazin-2-ylamino)-hexyl]-2,3,4, 5,6-pentafluoro-benzamide (Mel-PFB)

4.43 mmol Mel-C_6H_{12}-NH_2 were dissolved in 25 ml DMF at 80 °C. The solution was cooled down to room temperature and NEt_3 was added to the solution. Then 4.87 mmol 2,3,4,5,6-pentafluoro-benzoyl chloride (PFB-Cl) in 5 ml CH_2Cl_2 were added drop-wise. The reaction mixture was stirred at room temperature for 16 hours. The product (Mel-PFB) was washed with CH_2Cl_2 and MeOH, and then dried in the vacuum yielding 1.15 g white solid (60 %, melting point: 130 – 134 °C).

Elemental analysis; calculation for $C_{16}H_{18}F_5N_7O$ (%): C = 45.83, H = 4.33, N = 23.38

Found (%): C = 44.57, H = 4.25, N = 23.01

^{1}H-NMR (DMSO-d_6, ppm): 1.10 – 1.60 (m, 8H, $CH_2C_4\underline{H}_8CH_2$); 3.29 – 3.08 (m, 2H, NHC$\underline{H}_2$); 3.24 -3.26 (m, 2H, C$\underline{H}_2$NHCO); 5.91 – 6.10 (d: J = 38.70 Hz, 4H, N$\underline{H}_2$ of triazine ring); 6.33 – 6.50 (t: J = 5.67 Hz, 1H, N$\underline{H}CH_2$); 8.55 – 8.65 (t, J = 5.61 Hz, 1H, CON$\underline{H}$)

^{13}C-NMR (DMSO-d_6, ppm): 26.1, 27.1, 27.2, 29.9, 30.2 ($\underline{C}_{alkyl}$); 166.3 and 167.2 ($\underline{C}$ of triazine ring); 136.1, 143.3, 144.9, 147.1 ($\underline{C}$ of aromatic); 173.7 ($\underline{C}$ONH)

FTIR (KBr, cm^{-1}): 3346, 2932, 2856, 1655, 1454, 1276, 818

7.6 Synthesis of the initiator for surface attachment

7.6.1 Synthesis of 4,4´-azobis-(4-cyanopentanoyl chloride) (ABCC)

To the suspension of 43 mmol ABCA in 100 ml CH_2Cl_2, a suspension of 384 mmol phosphorpentachloride (PCl_5) in 100 ml CH_2Cl_2 was slowly added at 0 °C. The mixture was stirred for 16 hours at room temperature. The residual insoluble PCl_5 was filtered off and 70 % of the solvent were evaporated. The precipitated PCl_5 was filtered off. The filtrate was poured into 600 ml cooled n-hexane. The product was filtered, washed with the cold n-hexane and dried in vacuum to yield 10.36 g (76 %) of ABCC.

DSC: 190 ± 8 kJ mol^{-1} ($T_{max.}$ ~ 121 °C)

^{1}H-NMR ($CDCl_3$, ppm): 1.67 and 1.73 (d, 6H, C$\underline{H}_3$); 2.47 – 3.16 (m, 8H, C$\underline{H}_2$)

^{13}C-NMR ($CDCl_3$, ppm): 23.7, 23.8 ($\underline{C}H_3$); 33.0 (C$\underline{C}H_2CH_2$); 41.7, 41.8 ($\underline{C}H_2COCl$); 71.3, 71.5 ($\underline{C}_{tertiary}$); 116.8, 116.9 ($\underline{C}$N); 172.1, 172.2 ($\underline{C}$OCl)

FTIR (KBr, cm^{-1}): 2295, 2944, 2246, 1790, 1445, 1404, 1291, 978, 787, 766, 620

7.6.2 Synthesis of symmetric dichlorosilane initiator[86]

7.6.2.1 4-(3-Allyloxycarbonyl-1-cyano-1-methyl-propylazo)-4-cyano-4-methyl-butyric acid allyl ester

To the solution of 154 mmol 2-propen-1-ol in 130 ml CH_2Cl_2, 64.3 mmol ABCC in 100 ml CH_2Cl_2 were added drop-wise in the presence of pyridine (160 mmol) at 0 °C. The reaction solution was allowed to warm up to room temperature and continuously

stirred for 16 hours. The solution was washed three times with 100 ml of 0.5 N HCl, saturated $NaHCO_3$ and water. The organic phase was dried over Na_2SO_4 and filtered off. The solvent was largely evaporated and cold MeOH was added. The obtained white solid (allyl ester) was collected, washed with cold MeOH and dried in the vacuum. 17.97 g (78 %) of the product were obtained.

DSC: 373 kJ mol^{-1} ($T_{max.}$ ~ 119 °C)

Elemental analysis; calculation for $C_{18}H_{24}N_4O_4$ (%): C = 59.99, H = 6.71, N = 15.55

Found (%): C = 60.00, H = 6.93, N = 15.67

^{1}H-NMR (CD_2Cl_2, ppm): 1.75, 1.77 (d, 6H, C**H**$_3$); 2.30 – 2.70 (m, 8H, C_2**H**$_4$); 4.63 – 4.64 (m, 4H, C**H**$_2$O); 5.26 – 5.40 (m, 4H, C**H**$_2$=CH); 5.90 – 6.03 (m, 2H, CH_2=C**H**)

^{13}C-NMR (CD_2Cl_2, ppm): 23.7, 23.9, 29.1, 29.2, 33.2 (**C**$_{alkyl}$); 65.6, 72.0 (**C**$_{tertiary}$); 117.6 (**C**N); 118.2 (**C**H_2=CH); 132.2 (CH_2=**C**H); 171.0 (**C**OO)

FTIR (KBr, cm^{-1}): 3090, 2991, 2944, 2242, 1734, 1444, 1421, 1392, 1304, 1175, 988, 941

7.6.2.2 4-{3-[4-(Chloro-dimethyl-silanyl)-butoxycarbonyl]-1-cyano-1-methyl-propylazo}-4-cyano-4-methyl-butyric acid 3-(chloro-dimethyl-silanyl)-propyl ester (ADS)

A solution of 30 mg hexachloroplatinic acid in 0.5 ml ethanol/diethyl ether (1:1, v/v) was added to 10 mmol allyl ester in 60 ml dichloromethysilane. The reaction mixture was refluxed for 6 hours. The excess of dichloromethysilane was distilled off. The product (ADS) was dried in vacuum yielding the silane in quantitative amounts.

DSC: 284 ± 10 kJ mol^{-1} ($T_{max.}$ ~ 119 °C)

^{1}H-NMR (CD_2Cl_2, ppm): 0.47 and 0.48 (d, 12H, SiC**H**$_3$); 0.86 – 0.93 (m, 4H, SiC**H**$_2$); 1.75 and 1.77 (d, 6H, C**H**$_3$); 2.44 – 2.53 (m, 12H, C**H**$_2$); 4.09 – 4.15 (t, 4H, OC**H**$_2$)

^{13}C-NMR (CD_2Cl_2, ppm): 1.6 (Si**C**H_3); 15.3 (Si**C**H_2); 22.7, 24.2, 29.6, 33.3 (**C**$_{alkyl}$); 67.1 (O**C**H_2); 72.3 (**C**$_{tertiary}$); 118.0 (**C**N); 171.7 (**C**OO)

FTIR (KBr, cm^{-1}): 2955, 2898, 2242, 1736, 1449, 1395, 1294, 1255, 1184, 1052, 841

7.7 Preparation of layer-by-layer on planar substrate through H-bonding

7.7.1 Immobilization of Mel-Silane auf planar substrate

The silicon substrate was washed with MeOH and acetone, and then dried for 30 minutes in the vacuum. 25 mmol Mel-Silane, 50 ml ethyl acetate and 2 ml NEt_3 were added. The reaction was carried out at 60 °C for 4 hours. The substrate was washed with DMSO, MeOH and acetone, respectively. The chemical composition and the layer thickness of the Mel-Silane monolayer were characterized by XP spectroscopy and x-ray reflectivity, respectively.

7.7.2 Complexation of complementary molecule on the Mel-Silane monolayer

Multilayers were deposited following a standard layer-by-layer protocol: the substrates were dipped into a solution, then washed with pure solvent and dipped into the solution of the other. This procedure was repeated until the desired number of layers was deposited. The concentration of the complementary molecules are listed in following:

- 0.50 mmol PGL1840-PFB in 20 ml dry CH_2Cl_2; 30 and 150 minutes
- 0.50 mmol Mel-PFB in 20 ml dry CH_2Cl_2; 5 – 240 minutes
- 0.50 mmol PGL1840 in 20 ml dry CH_2Cl_2; 30 minutes
- 0.15 mmol Mel-ABCC in 20 ml dry MeOH; 30 minutes
- 0.88 mmol LPEI-ABCC in 20 ml dry MeOH; 30 minutes

Each layer was determined by XPS for the chemical compositions and x-ray reflectivity for the layer thickness.

7.7.3 Generation of polymer monolayers using initiator layers bound on the surfaces via H-bonding

Initiator modified substrates (Melamine:PGL1840:Mel-ABCC and Melamine:PGL1840: LPEI-ABCC) in MMA (bulk polymerization) were degassed through 5 freeze-thaw cycles. The polymerizations were carried out at 60 °C for 4.5 hours and then the samples were washed with toluene and dried with in a stream of dry N_2. The layer thickness of polymer formed on the surfaces was determined by x-ray reflectivity. The chemical composition of the polymer grafted on the surfaces was characterized by XPS.

7.8 Surface modification of organic pigment particles

7.8.1 Immobilization of fluorinated molecules

To a suspension of 3.2 mmol pigment and 7.2 mmol NEt_3 in 50 ml dry CH_2Cl_2, 3.5 mmol PFB-Cl in 5 ml dry CH_2Cl_2 was added drop-wise at 0 °C. The reaction mixture was allowed to warm up to room temperature and stirred for 16 hours. The modified pigment particles were filtered off and washed with CH_2Cl_2, EtOH:H_2O (1:1, pH 3, adjusted by hydrochloric acid), EtOH:H_2O, and MeOH. The PFB-modified pigments were dried in the vacuum and characterized by XP spectroscopy.

7.8.2 Immobilization of initiator molecules

To a suspension of 13.2 mmol pigment and 68.2 mmol NEt_3 in 100 ml CH_2Cl_2, a solution of 6.6 mmol ABCC in 50 ml CH_2Cl_2 were added drop-wise at 0 °C. The subsequent procedures were the same as described in Chapter 7.8.1. The decomposition of azo initiator was followed by DSC measurement. The initiator graft density are summarized in Table 4-2.

7.8.3 Immobilization of monomer molecules

To a suspension of 10 mmol pigment and 36 mmol NEt_3 in 50 ml CH_2Cl_2, a solution of 11 mmol 2-methyl-acryloyl chloride in 50 ml CH_2Cl_2 was drop-wise added at 0 °C. The subsequent procedures were the same as described in Chapter 7.8.1.

7.9 Surface modification of inorganic pigment particles

7.9.1 Immobilization of initiator based on chlorosilane onto pigments

To 3 g TiO_2 (dried at 120 °C for 6 hours) in dried 50 ml Toluene, 2.56 mmol ADS in 15 ml were added drop-wise at 0 °C in the presence of NEt_3 (5 mmol). The reaction mixture was allowed to warm up to room temperature and stirred for 16 hours. The modified pigment particles were filtered off and washed with Toluene, EtOH:H_2O (1:1, pH 3, adjusted by hydrochloric acid), EtOH:H_2O, and MeOH. The ADS-modified pigment was dried in the vacuum. The chemical compositions of the initiator-modified pigments were characterized by XPS. The decomposition of azo initiator on the surfaces was followed by DSC measurement. The graft densities of the initiator are summarized in Table 5-2.

7.9.2 Immobilization of initiator based on phosphoric acids onto pigments

7.9.2.1 Amino monolayers on the pigment surfaces

The mixture of 1.00 g pigment (TiO_2 or PCG2020) and 2-aminoethyldihydrogen phosphate (AEP; 10 mmol AEP for TiO_2 and a various concentration of AEP for PCG2020) in 100 ml H_2O was refluxed at 100 °C for 16 hours. The modified pigment was filtered off and washed with water and ethanol. The product (TiO_2-AEP or PCG2020-AEP) was freeze-dried (water). The AEP monolayer was characterized by XPS. The graft density of the AEP monolayer was determined by elemental analysis using the carbon content.

7.9.2.2 Immobilization of ABCC initiator onto the amino monolayers

To a suspension of AEP-modified pigment and NEt_3 in 100 ml dry CH_2Cl_2, a ABCC solution in 25 ml dry CH_2Cl_2 was added drop-wise at 0 °C. The subsequent procedures were the same as described in Chapter 7.8.1. The characterization of the initiator-attached pigment was same as described in Chapter 7.9.1.

7.9.3 Immobilization of monomer onto pigments

5.0 g TiO_2 were dried at 120 °C for 6 hours before 10 mmol 3-Methycryloylpropyl trimethoxysilane, 120 ml dried toluene and 33 mmol NEt_3 were added. The suspension was heated up to 125 °C and kept at this temperature for 4 hours. The reaction mixture was allowed to cool down to room temperature. The subsequent procedures were the same as described in Chapter 7.9.1. The characterization of the monomer-attached pigment was same as described in Chapter 7.9.2.1.

7.10 Polymerization of vinyl monomers with initiator-modified pigments

The vinyl monomer, the initiator-modified pigment, and the good solvent for the polymer formed in the desired ratio were placed in a 100 ml schlenk tube. The mixture was degassed through 5 freeze-thaw cycles. Then the mixture was heated at 60 °C for the desired period of time. The polymer-modified pigment was separated by centrifugation and extracted with the good solvent for the polymer formed for 24 hours. The free polymer was precipitated in a poor solvent for the polymer formed and filtered off. The polymer-modified pigment and the free polymer were freeze-dried in vacuum. The polymer-modified pigments were qualitative characterized by FTIR and XPS as well as quantitative determined by UV-VIS spectroscopy and elemental analysis depending on the nature of the pigments.

7.11 Polymerization of vinyl monomer with monomer-modified pigment

The vinyl monomer, monomer-modified pigment, AIBN and the good solvent for the polymer formed in the desired ratio were placed in a 100 ml schenk tube. The subsequent procedures and the characterizations of the polymer-modified pigments were the same as described in Chapter 7.10.

7.12 Stability of unmodified and polymer-modified pigments against alkaline solutions

1 %w/w (1 gram bare pigment) of the unmodified and polymer-modified pigment were suspended in the corresponding buffer solutions (s. Table 7-1) and then heated at 100 °C for one hour. After filtration, the treated pigment was extracted with water for 24 hours and dried at 60 °C in the vacuum. The treated pigments were characterized by elemental analysis and UV-VIS spectroscopy.

Table 7-1: Buffer solutions used for the stability test.

pH	**chemicals**
2.0	Citric acid / NaOH / HCl
4.0	Citric acid / NaOH / NaCl with addition of fungicide
5.0	Citric acid / NaOH
7.4	0.009 M $KaHPO_4$ / 0.032 M Na_2HPO_4 with addition of fungicide
8.1	0.20 M Na_2HPO_4 / 0.02 M NaH_2PO_4
9.2	1.00 M NH_3 / 1.00 M NH_4Cl
10.2	10.0 M NH_3 / 1.00 M NH_4Cl
11.0	0.22 M Na_2HPO_4 / 0.02 M NaOH
12.0	0.10 M Na_2HPO_4 / 0.10 M Na_3PO_4 / 0.38 M NaOH

8 Conclusion

In this work, strategies for the surface modification of organic and inorganic pigments with polymer monolayers are described.

Two strategies, which use different types of interactions, were pursued to attach polymer molecules to the pigment surfaces. The first is based on non-covalent interactions where the attachment of the protective polymer layer was achieved through hydrogen bonding. In a second approach, the chains were covalently attached to the surfaces.

The generation of polymer layers by the built up of supramolecular assemblies based on H-bonding was investigated using first a model system with planar substrates. In these experiments, molecules were adsorbed to planar surfaces and XPS together with labeling techniques were employed to investigate the formation of the layers. It was found that the subsequent generation of multilayers based on H-bonds between complementary molecules could be used for the deposition of sufficient amounts of initiator molecules on the surfaces of organic pigments. The subsequent polymerization triggered by these surface-bound initiator moieties yielded polymer monolayers with thicknesses around 7 Å. Compared to results obtained from similar systems this appears to be a very small value. The reason for this discrepancy might originate from the poor (thermal) stability of the H-bonds through which the polymers are held on the surfaces. The chains might rip off the surface during polymerization and consequently the generation of somewhat thicker layers is not possible.

Much thicker layers are achieved if the protective polymer layers are generated from covalently attached species. Here, two approaches have been investigated. One approach uses monolayers of initiators for free radical polymerization from which the surface-anchored polymers can be grown. For the second system, polymerizable groups were deposited on the surfaces and polymers growing in solution are anchored to the surface if this group is incorporated into the polymer during chain formation.

The self-assembly of initiator or comonomer monolayers on organic pigment surfaces was achieved in one-step processes. The graft density of the initiators on the pigments was found to be 1.2 μmol m^{-2} and 0.2 μmol m^{-2}, giving an average distance between two initiator groups of 1.2 nm and 2.9 nm depending on the pigment used for modification. The monomer graft density could not be determined directly but it is assumed similar.

Two approaches were successfully used to generate initiator monolayers on inorganic pigments (TiO_2 and PCG2020): In one approach, the initiator molecules were deposited via a silane anchor whereas in a second approach a phosphate anchor was used to deposit the azo molecules in a two-step reaction sequence. The latter process yields a higher initiator density on the surfaces than the direct modification due to the fact that the reactivity of phosphates to TiO_2 is much higher than that of a monochlorosilane. The difference appears to be strong enough so that the higher graft density of the amino-functional phosphate also leads to a higher initiator graft density after the second modification as compared to the direct silanization. Initiator graft density of 0.1 µmol m^{-2} for the silane-based approach and 0.9 µmol m^{-2} for the phosphate-anchored initiators were determined, i.e. the average distance between two initiator groups was 4.1 nm for and 1.4 nm, respectively. Additionally, copolymerizable groups were immobilized on TiO_2 surfaces in one-step and the graft density of these groups was found to be 5 µmol m^{-2} (3 group nm^{-2}).

The initiator monolayers were then used for the surface-initiated polymerization of MMA onto the pigment particles. The amount of grafted polymer was determined quantitatively by UV absorption and elemental analysis depending on the chemically nature of the pigment. The amount of grafted polymer and therefore the graft density and layer thickness could be controlled by the variation of various polymerization parameters such as polymerization time and monomer concentration. Depending on the pigment, PMMA layers with thicknesses of up to 50 nm could be generated which corresponds to an average distance between to anchors of about 4 nm. Besides MMA, other monomers were also used successfully and a wide variety of polymer monolayers with different properties could be generated on the pigment surfaces.

The copolymerization of free with surface-bound monomers was also studied. The variation of typical polymerization parameters (monomer and initiator concentration as well as polymerization time) did not influence the polymer film thickness on the pigment particles. The thickness of the polymer layers was found to be rather low in all cases as compared to the values obtained via surface-initiated polymerization. Typically, layer thicknesses of 2 – 11 nm could be realized. This can be understood due to limitations in the overall mechanism of this process that is based on an initial attachment of a growing chain to a surface-bound monomer. This “grafting-to” process comes to a virtual stop once the surface is covered with polymer as the already attached layer forms a kinetic barrier that hinders the attachment of further chains. Complete coverage, however, is directly related to the molecular weight of the attached chains, i.e. conditions that lead to the attachment of high molecular weight chains will yield layers with low graft density.

In summary, this means that the amount of grafted material is largely independent on the exact set of parameters used during layer formation.

The stability of the polymer-modified pigments against bases has been investigated as a function of the pH value of various test solutions and compared to that of unmodified pigments. It was found that the coated pigments exhibit an improved stability against strong bases at a sufficiently high graft density of the attached polymers as compared to the bare pigments. It is obviously the poor swellability of the polymer monolayers in aqueous solutions, which shields the pigment surfaces from the alkaline ions. PS layers were found to be more efficient than PMMA coatings, most likely because PMMA is known to take up more water and also hydrolysis of the ester groups might cause problems in this regard.

This study shows that polymer monolayers can successfully be deposited on pigment surfaces using surface-attached initiator or monomer moieties. The properties of the pigment surfaces can be influenced and controlled by varying the process parameters applied during polymer deposition and by choosing different monomers. As an example, we have demonstrated that the stability of the pigments against basic conditions can be significantly improved.

9 Zusammenfassung

In der vorliegenden Arbeit wurden Strategien für die Modifizierung sowohl organischer als auch anorganischer Pigmente mit Polymermonolagen beschrieben.

Zwei Strategien, die sich in der Art der Wechselwirkung an den Oberflächen unterschieden, wurden verfolgt, um die Polymermoleküle an die Pigmentoberflächen anzubinden. Die erste Strategie basierte auf nichtkovalenten Wechselwirkungen. Hierbei wurden die Polymermonolagen auf den Pigmentoberflächen durch Wasserstoffbrücken verankert. Die zweite Vorgehensweise umfasste die kovalente Anbindung der Polymerschichten an die Pigmentoberfläche.

Zunächst wurden als Modelsysteme planare Substrate verwendet, um die Bildung von Polymermultilagen durch Wasserstoffbrücken zu untersuchen. Dazu wurden an der Oberfläche adsorbierte Moleküle und die Schichtbildung mittels XPS und entsprechenden Derivatisierungen untersucht. Es konnte gezeigt werden, dass die auf Wasserstoffbrücken basierende schrittweise Multilagenbildung zwischen komplementären Moleküleinheiten genutzt werden kann, um ausreichende Initiatormengen auf der Oberfläche organischer Moleküle bereitzustellen. Die nachfolgende Polymerisation, die durch diese oberflächengebundenen Initiatormoleküle gestartet werden kann, ergab Schichtdicken von etwa 7 Å. Im Vergleich zu ähnlichen Systemen scheint dieser Wert klein zu sein. Möglicherweise liegt dies an einer ungenügenden (thermischen) Stabilität der Wasserstoffbrückenbindungen, durch die das Polymer an der Oberfläche gehalten wird. Die Ketten könnten während der Polymerisation von der Oberfläche abreißen, was die Bildung dickerer Schichten verhindert.

Viel dickere Schichten konnten erreicht werden, wenn die Polymermonolagen durch kovalent gebundene Spezies erzeugt wurden. Hier sind zwei Ansätze untersucht worden. Im ersten Ansatz wurden Initiatormonolagen benutzt, so dass mittels freier radikalischen Polymerisation oberflächengebundene Polymere erzeugt werden konnten. Für das zweite System wurden copolymerisierbare Gruppen auf der Oberfläche verankert an die in Lösung gestartete Polymerketten anknüpfen können.

Die Initiator- bzw. Comonomermonolagen konnten über einen einstufigen Process erzeugt werden. Die Pfropfdichte des Initiators auf den Pigmenten war dabei 1,2 µmol m^{-2} bzw. 0,2 µmol m^{-2}, je nachdem welches Pigment für die Modifizierung verwendet wurde. Dies entspricht einem durchschnittlichen Anstand von 1,2 nm bzw.

2,9 nm zwischen zwei Initiatorgruppen. Die Monomerpfropfdichte konnte nicht direkt festgestellt werden. Es wird angenommen, dass sie ähnlich ist.

Zwei Ansätze wurden erfolgreich verwendet, um Initiatormonolagen auf anorganischen Pigmenten (TiO_2 und PCG2020) zu erzeugen: in einem Ansatz wurden Initiatormoleküle über Silananker immobilisiert, während in einem zweiten Ansatz ein Phosphatanker zur Azomolekülanbindung in einer zweistufigen Reaktion benutzt wurde. Der letztgenannte Prozess lieferte eine höhere Initiatorpfropfdichte auf den Oberflächen als die direkte Silanisierung, da die Reaktivität der Phosphate gegenüber TiO_2 viel höher als die eines Monochlorosilans ist. Der Unterschied scheint so stark zu sein, dass die höhere Pfropfdichte des aminofunktionellen Phosphates auch zu einer höheren Initiatorpfropfdichte nach der zweiten Immobilisierung im Vergleich zu einer direkten Silanisierung ist. Die Initiatorpfropfdichte beträgt 0.1 µmol m^{-2} für den Silananker und 0.9 µmol m^{-2} für den phosphatverankerten Initiator, d.h. der durchschnittliche Anstand zwischen zwei Initiatorgruppen ist 4,1 nm bzw. 1,4 nm. Zusätzlich wurden copolymerisierbare Gruppen auf den TiO_2-Oberflächen in einer einstufigen Reaktion immobilisiert. Die Pfropfdichte dieser Gruppen war 5 µmol m^{-2} (3 Gruppen nm^{-2}).

Die Initiatormonolagen wurden dann für die oberflächeninitiierte Polymerisation von MMA auf den Pigmentpartikeln verwendet. Die Menge des verankerten Polymeren an der Pigmentoberfläche wurde quantitativ durch UV-Spektroskopie und Elementaranalyse in Abhängigkeit von der chemischen Natur des Pigments bestimmt. Die Menge des verankerten Polymeren und somit auch die Pfropfdichte und die Schichtdicke konnte durch Variation der verschiedenen Polymerisationsparameter wie Polymerisationszeit und Monomerkonzentration kontrolliert werden. Je nach Pigment konnten PMMA-Schichtdicken von bis zu 50 nm erzeugt werden, was einem durchschnittlichen Abstand zwischen zwei Ankern von ungefähr 4 nm entspricht. Außer MMA wurden auch andere Monomere erfolgreich verwendet und Polymermonolagen mit stark unterschiedlichen Eigenschaften konnte auf den Pigmentoberflächen hergestellt werden.

Die Copolymerisation freier und oberflächengebundener Monomere wurde ebenfalls untersucht. Die Variation typischer Polymerisationsparameter (Monomer- und Initiatorkonzentration sowie Polymerisationszeit) hatte keinen Einfluss auf die Polymerschichtdicke auf den Pigmentpartikeln. Die Schichtdicke der Polymeren war in allen Fällen niedriger im Vergleich zu den Werten, die durch oberflächeninitiierte Polymerisation erhalten wurden: typische Schichtdicken von 2 – 11 nm wurden erhalten. Dies könnte die direkte Folge davon sein, dass bei dieser Methode wachsende Polymerketten an oberflächengebundene Monomere anbinden müssen. Dieser „grafting-

to“ Prozess wird immer unwahrscheinlicher, je stärker die Oberfläche mit Polymeren bedeckt ist, weil die bereits angebundene Schicht eine kinetische Barriere darstellt, die das Anbinden weiterer Ketten verhindert. Eine vollständige Bedeckung der Oberfläche ist aber neben der Pfropfdichte auch von der Molmasse der angebundenen Ketten abhängig, d.h. Bedingungen, die zur Bildung höhermolekularer Ketten führen, ergeben Schichten mit niedriger Pfropfdichte. Zusammenfassend bedeutet dies, dass die Menge des angebundenen Materials weitgehend unabhängig von den Polymerisationsparametern ist.

Die Basenstabilität polymermodifizierter Pigmente wurde in Abhängigkeit des pH-Werts verschiedener Testlösungen untersucht und mit der Basenstabilität unmodifizierter Pigmente verglichen. Es wurde gefunden, dass beschichtete Pigmente mit einer ausreichend hohen Pfropfdichte der angebundenen Polymere eine verbesserte Basenstabilität im Vergleich zu den unbeschichteten Pigmenten aufwiesen. Offensichtlich schirmen die in wässrigen Lösungen schlecht quellbaren Polymermonolagen die Pigmentoberflächen gegen die alkalischen Ionen ab. Die PS-Schichten waren dabei effizienter als PMMA-Schichten, weil PMMA bekannt dafür ist, dass es mehr Wasser aufnehmen kann. Auch die Hydrolyse der Estergruppen im Polymeren könnte Probleme in dieser Hinsicht verursachen.

Diese Arbeit zeigt, dass Polymermonolagen auf Pigmentoberflächen mit oberflächengebundenen Initiator- oder Monomereinheiten erfolgreich erzeugt werden können. Die Eigenschaften der Pigmentoberflächen können beeinflusst und kontrolliert werden, indem man die Prozessparameter während der Polymerisation verändert und indem man unterschiedliche Monomere wählt. Durch solche Modifizierungen kann beispielsweise die Pigmentstabilität gegenüber Basen erheblich verbessert werden.

10 Appendix

10.1 XP spectra of unmodified PGL1840 and PFB-modified PGL1840

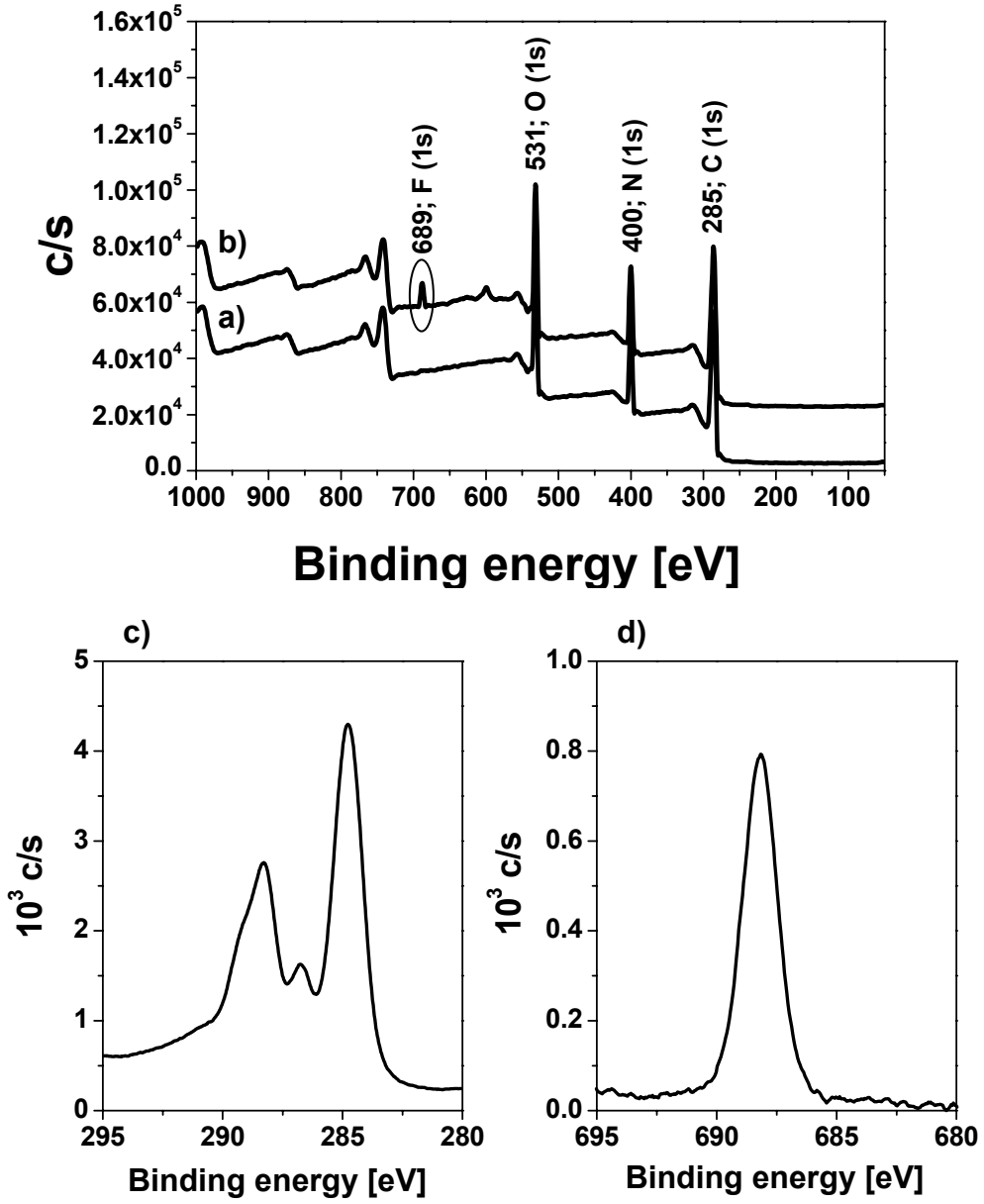

Figure 10-1: XP survey spectra of a) unmodified PGL1840 and b) PFB-modified PGL1840 generated through the reaction of imino groups on the pigment surfaces and pentafluorobenzoyl chloride (PFB-Cl); detail spectra of c) C(1s) and d) F(1s) from PGL1840-PFB.

Table 10-1: Atomic sensitivities and intensities of C(1s), N(1s), O(1s) and F(1s) from PFB-modified PGL1840.

atom	sensitivity	integrated intensity	integrated intensity / sensitivity
C	0.314	12660	40318
N	0.499	5634	11291
O	0.733	9854	13443
F	1.000	1618	1618

10.2 DSC measurements of the Pigment-Azo before and after polymerization at room temperature

Table 10-2: Graft densities of the azo initiator on the pigment particles as determined by DSC as well as the average distance between two azo groups.

Pigment-Azo		I_{dec}* [J g^{-1}]	δ_{Azo} [µmol g^{-1}]	Γ_{Azo} [µmol m^{-2}]	average distance between azo groups *d* [nm]
PGL1155-Azo	before[1]	9.29 ± 0.47	51	1.2	1.2
	after[2]	7.43 ± 0.53	41	0.9	1.4
PGL1840-Azo	before[1]	2.72 ± 0.26	11	0.2	2.9
	after[2]	2.29 ± 0.03	8	0.1	4.1

* average of 3 measurements.
1 before polymerization.
2 after polymerization at roomtemparature ([MMA] = 4.67 mol l^{-1}, t = 16 hours).

10.3 Calibration curve via integration of the UV absorption band of various unmodified PGL1840 concentrations

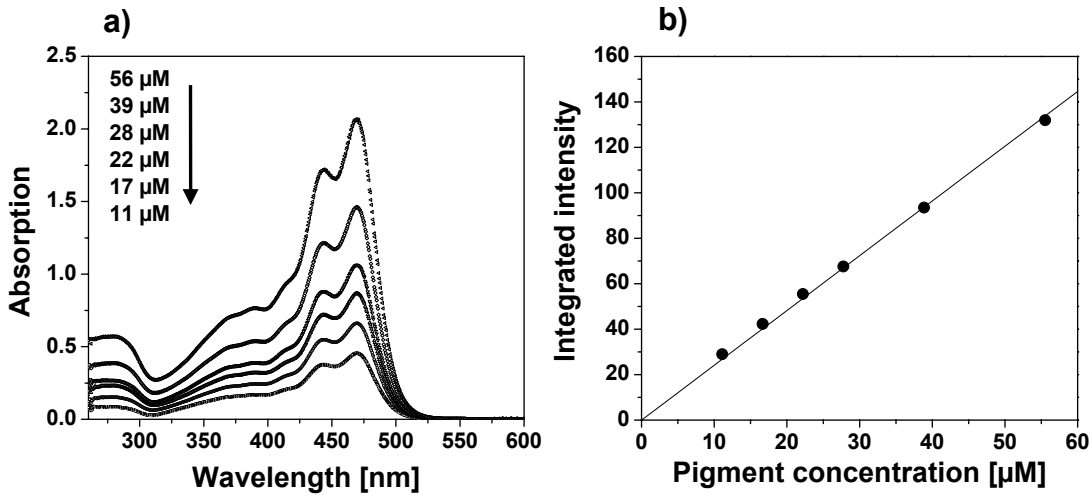

Figure 10-2: a) UV spectra of unmodified PGL1840 with various pigment concentration; b) calibration curve via integration of the UV absorption between 400 nm and 500 nm as a function of the pigment concentration.

10.4 "Grafting-from" polymerization on PGL1840 surfaces using self-assembled azo-initiator monolayers (PGL1840-Azo)

10.4.1 Layer thickness as a function of monomer concentration

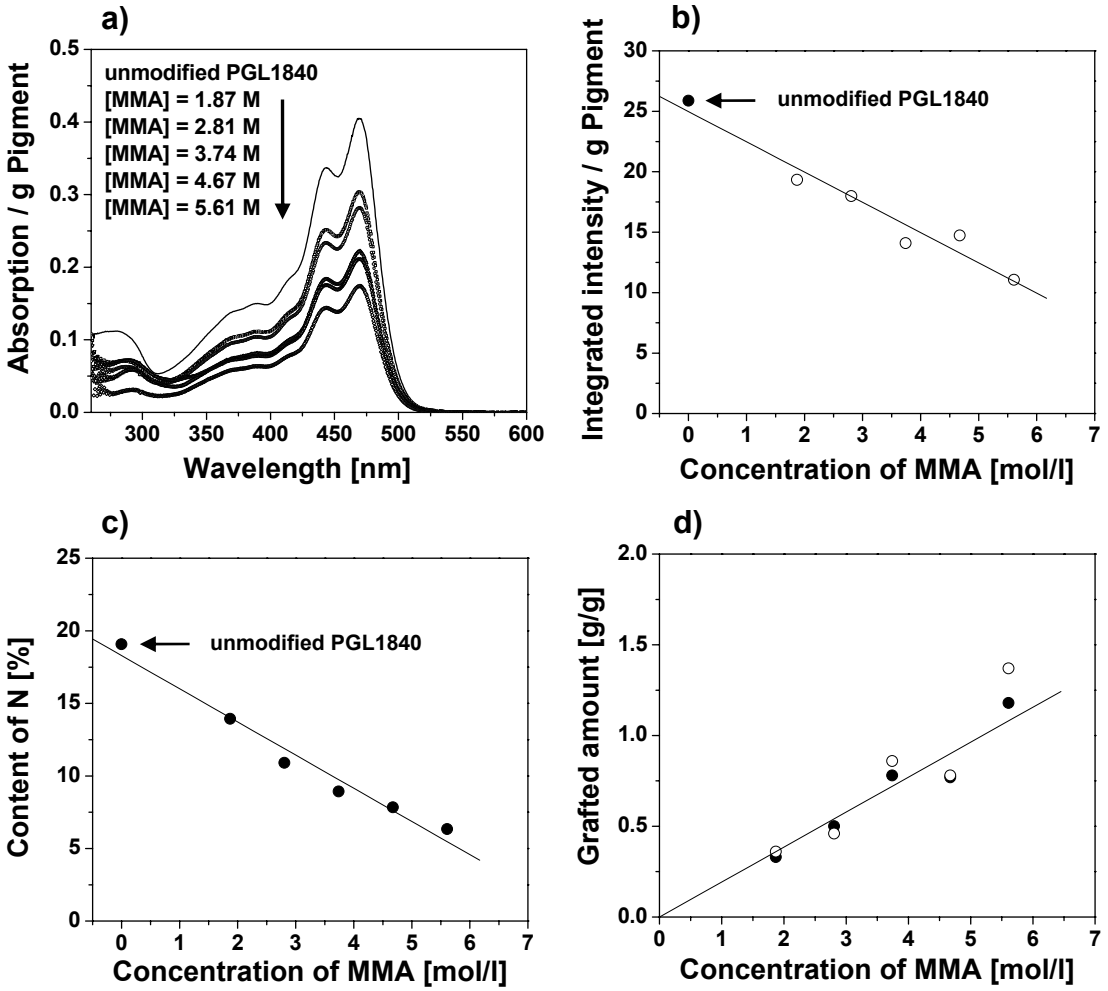

Figure 10-3: a) UV absorption of PMMA-grafted PGL1840 in comparison to unmodified PGL1840 and b) integrated intensity of the absorption signal between 400 nm and 500 nm (per gram pigment) as a function of the MMA concentration used for the preparation of the materials; c) nitrogen content of PMMA-modified PGL1840 and d) polymer grafted amount as a function of the MMA concentration calculated from c) [●] for compared the results obtained from UV absorption [○] are shown: (T = 60 °C and t = 16 hours).

Table 10-3: Graft densities and layer thickness of polymer-modified PGL1840 calculated from UV spectra and elemental analysis as well as number-average molecular weight of free PMMA as determined by GPC and polydispersity (D).

MMA[1] [mol l^{-1}]	δ [g m^{-2}]		L [nm]		M_w [10^6 g mol^{-1}]	D	Γ [nmol m^{-2}]	
	UV[2]	% N[3]	UV[2]	% N[3]			UV[2]	% N[3]
1.87	0.005	0.005	5	4	0.98	2.5	12	11
2.81	0.007	0.008	6	6	1.04	2.3	13	14
3.74	0.013	0.012	11	10	1.22	2.1	20	18
4.67	0.012	0.012	10	10	1.15	1.8	16	16
5.61	0.021	0.018	17	15	1.32	1.7	23	19

1 polymerization was carried out at T 60 °C for 16 hours.
2 calculated using the data from UV absorption.
3 calculated using the nitrogen content measured by elemental analysis.

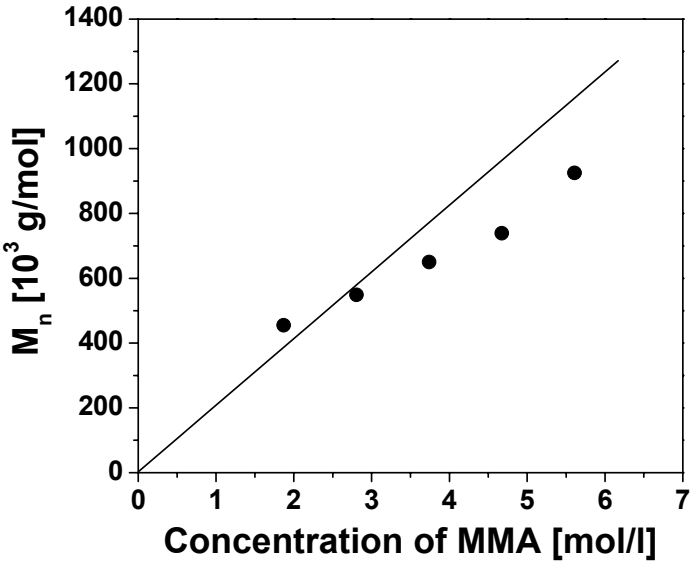

Figure 10-4: Number-average molecular weight of free PMMA as determined by GPC [●] in comparison to those calculated from Equation 4-10 (solid line) as a function of the MMA concentration.

10.4.2 Graft density as a function of polymerization time

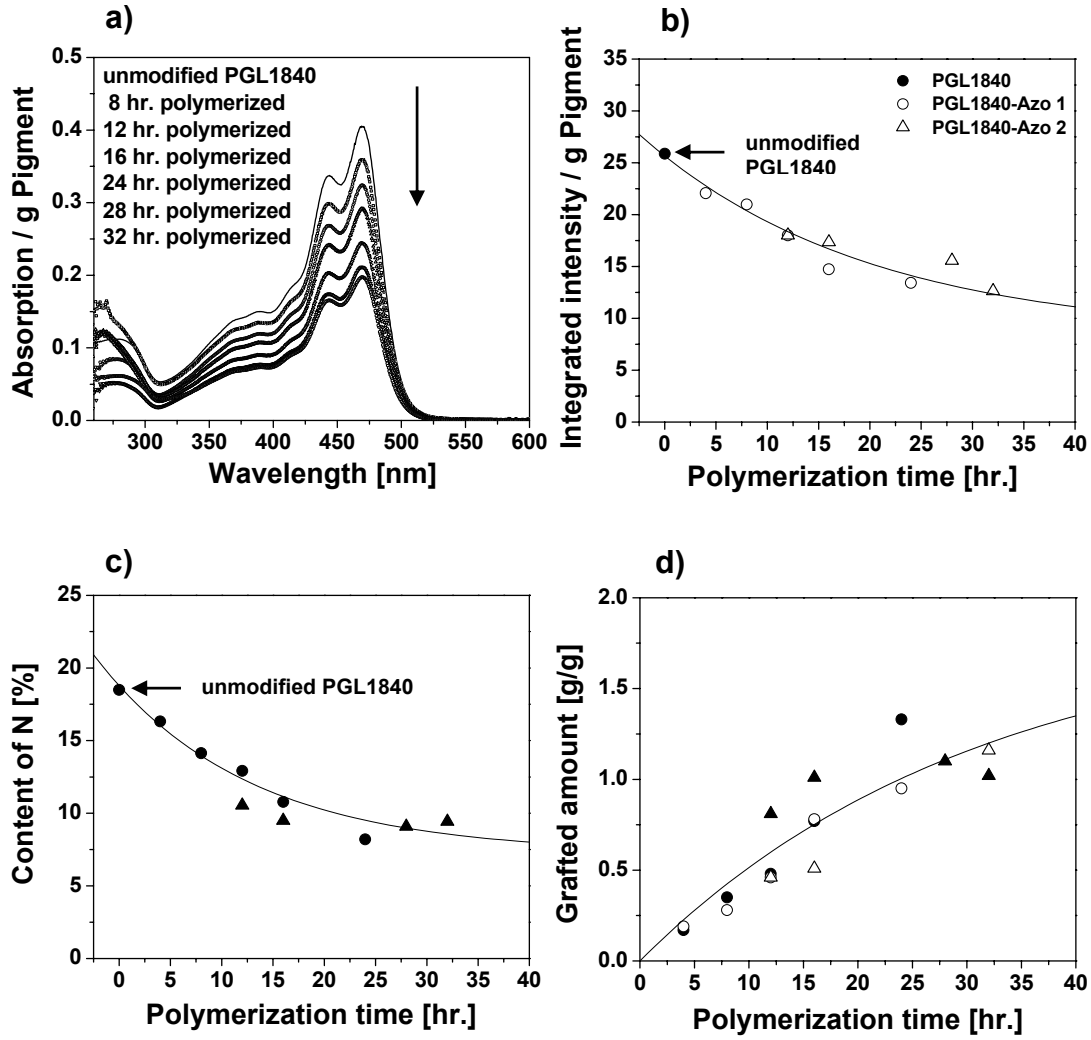

Figure 10-5: a) UV absorption spectra obtained from PMMA-grafted PGL1840 in comparison to unmodified PGL1840; b) integral intensity of the UV band as a function of polymerization time: PGL1840-Azo 1 [○] and PGL1840-Azo 2 [△] indicate independent series of experiments; c) nitrogen content and d) grafted amount calculated from nitrogen content (solid symbol; ● and ▲) in comparison to calculated from UV absorption (open symbol; ○ and △) as a function of polymerization time: ([MMA] = 4.67 mol l^{-1}, T = 60 °C).

Table 10-4: Graft densities and layer thickness of PMMA-modified PGL1840 calculated from UV spectra and elemental analysis as well as number-average molecular weight of free PMMA as determined by GPC and polydispersity (D).

t[1] [hours]	δ [g m^{-2}]		L [nm]		M_n [g mol^{-1}]	D	Γ [nmol m^{-2}]	
	UV[2]	% N[3]	UV	%N			UV	% N
PGL1840-Azo 1								
4	0.003	0.003	2	2	737000	1.6	4	3
8	0.004	0.005	3	4	736000	1.6	6	7
12	0.007	0.007	6	6	729000	1.5	10	10
16	0.012	0.012	10	10	739000	1.6	16	16
24	0.014	0.020	12	17	751000	1.6	19	27
PGL1840-Azo 2								
12	0.007	0.012	6	10	743000	1.6	9	17
16	0.008	0.015	6	13	741000	1.6	10	21
24	–	0.017	–	14	746000	1.7	–	22
28	0.010	0.015	9	13	737000	1.7	14	21
32	0.018	0.031	15	26	737000	1.7	24	42

1 polymerization was carried out at T 60 °C for 16 hours.
2 calculated using the data from UV absorption.
3 calculated using the nitrogen content measured by elemental analysis.

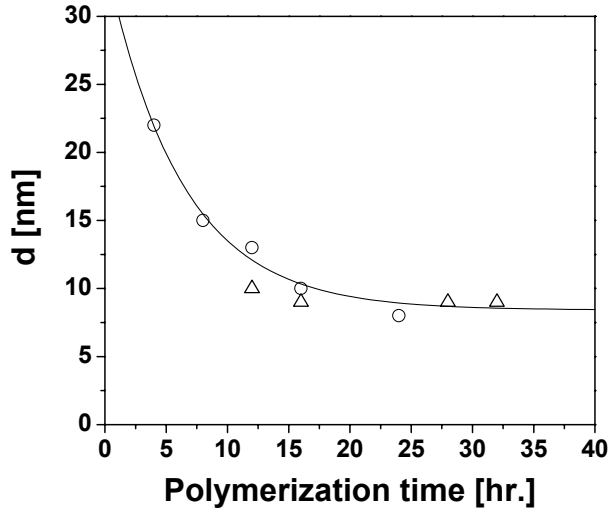

Figure 10-6: Average distance between two grafted polymer chains on the pigment PGL1840 as a function of polymerization time: ○ and △ indicate independent series of experiments.

10.4.3 Polymerization with different monomers using PGL1840-Azo

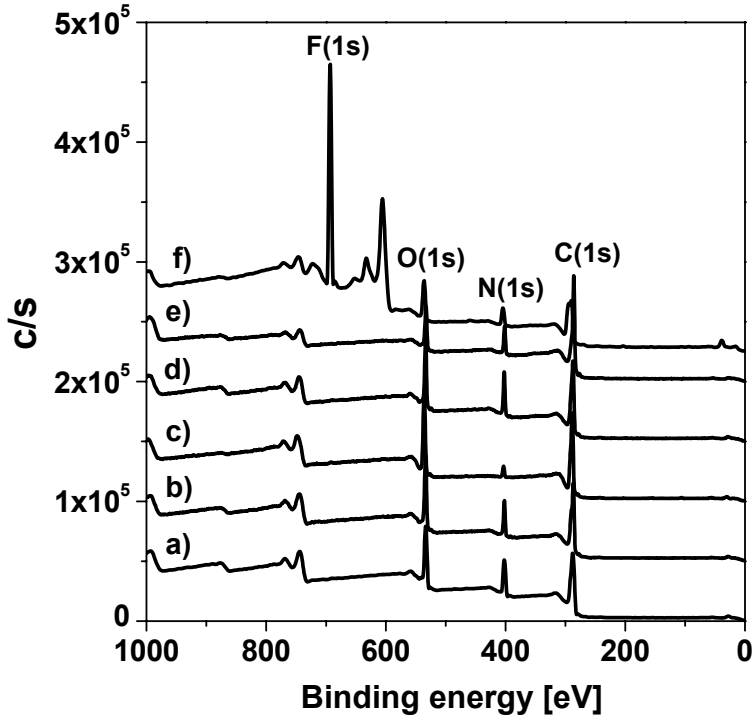

Figure 10-7: XP spectra of a) unmodified PGL1840, b) PGL1840-PMAA [L ~ 6 nm], c) -PMMA [L ~ 10 nm], d) -PDMAA [L ~ 2 nm], e) -PS [L ~ 2 nm] and f) -PHDFDA [L ~ 5 nm]: (polymerization condition s. Table 4-3).

Table 10-5: Binding energies (BE; eV) of C(1s) and contributions from structural features of the polymer-modified PGL1840 to the overall C(1s) intensity.

assignment	PGL1840 eV; (%)	PMAA eV; (%)	PMMA eV; (%)	PDMAA eV; (%)	PS eV; (%)	PHDFDA eV; (%)
C-C, C-H	284.6; (52)	284.6; (57)	284.4; (52)	284.6; (52)	284.6; (72)	284.5; (33)
C-O	286.6; (10)	286.4; (10)	285.7; (20)	286.3; (19)	286.5; (9)	286.4; (14)
C-N	288.0; (13)	287.9; (13)	287.0; (13)	287.8; (12)	288.2; (7)	287.9; (9)
CONH; COO	288.9; (18)	288.9; (15)	288.5; (13)	288.7; (14)	289.2; (8)	288.9; (11)
$\pi \rightarrow \pi^*$	290.9; (7)	290.7; (5)	289.3; (3)	290.9; (3)	291.3; (4)	290.5; (4)
CF_2	–	–	–	–	–	291.4; (25)
CF_3	–	–	–	–	–	293.5; (4)

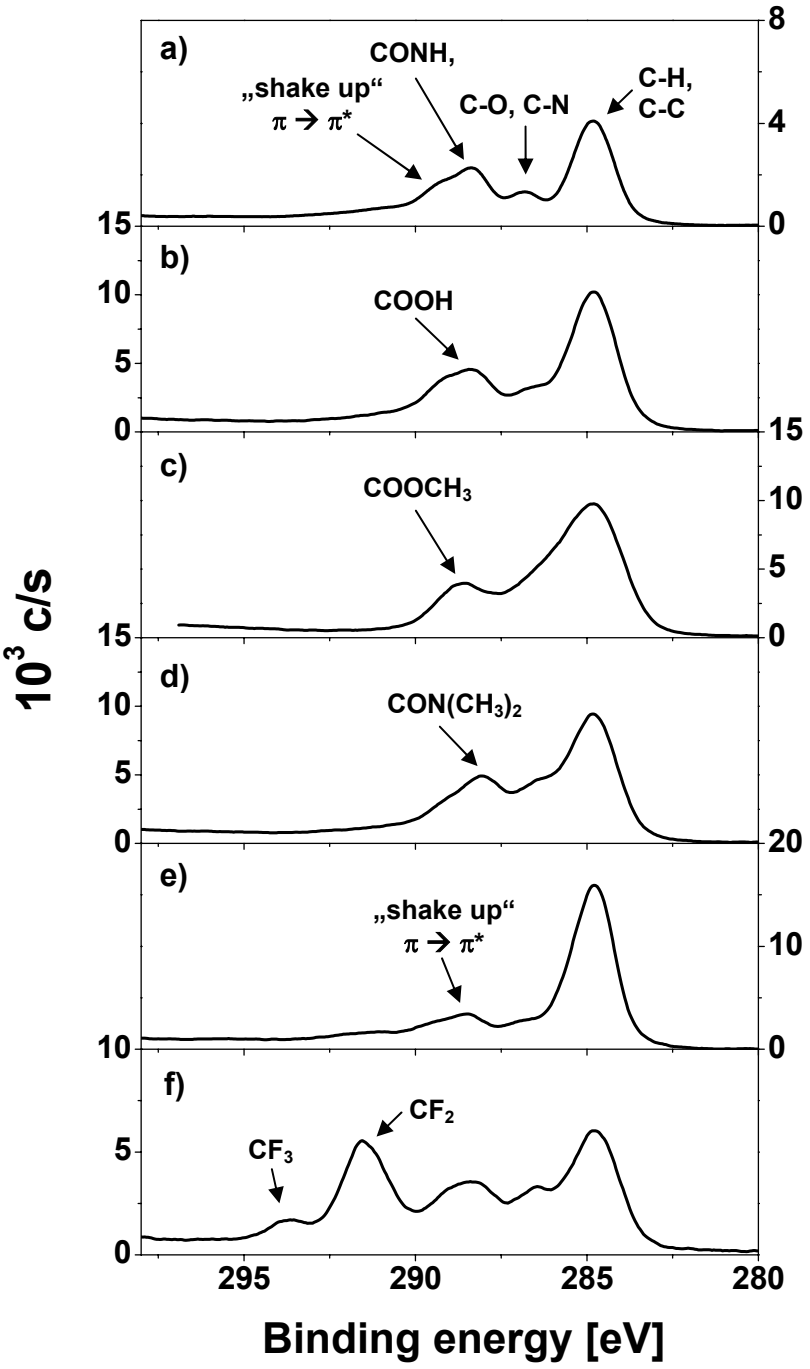

Figure 10-8: Detail scan of the C(1s) signals of polymer-modified pigment compared to the unmodified pigment: a) unmodified PGL1840, b) PGL1840-PMAA, c) -PMMA, d) -PDMAA, e) -PS and f) –PHDFDA.

10.5 Fitted curves of C(1s) detail spectra of various polymer-attached PGL1840

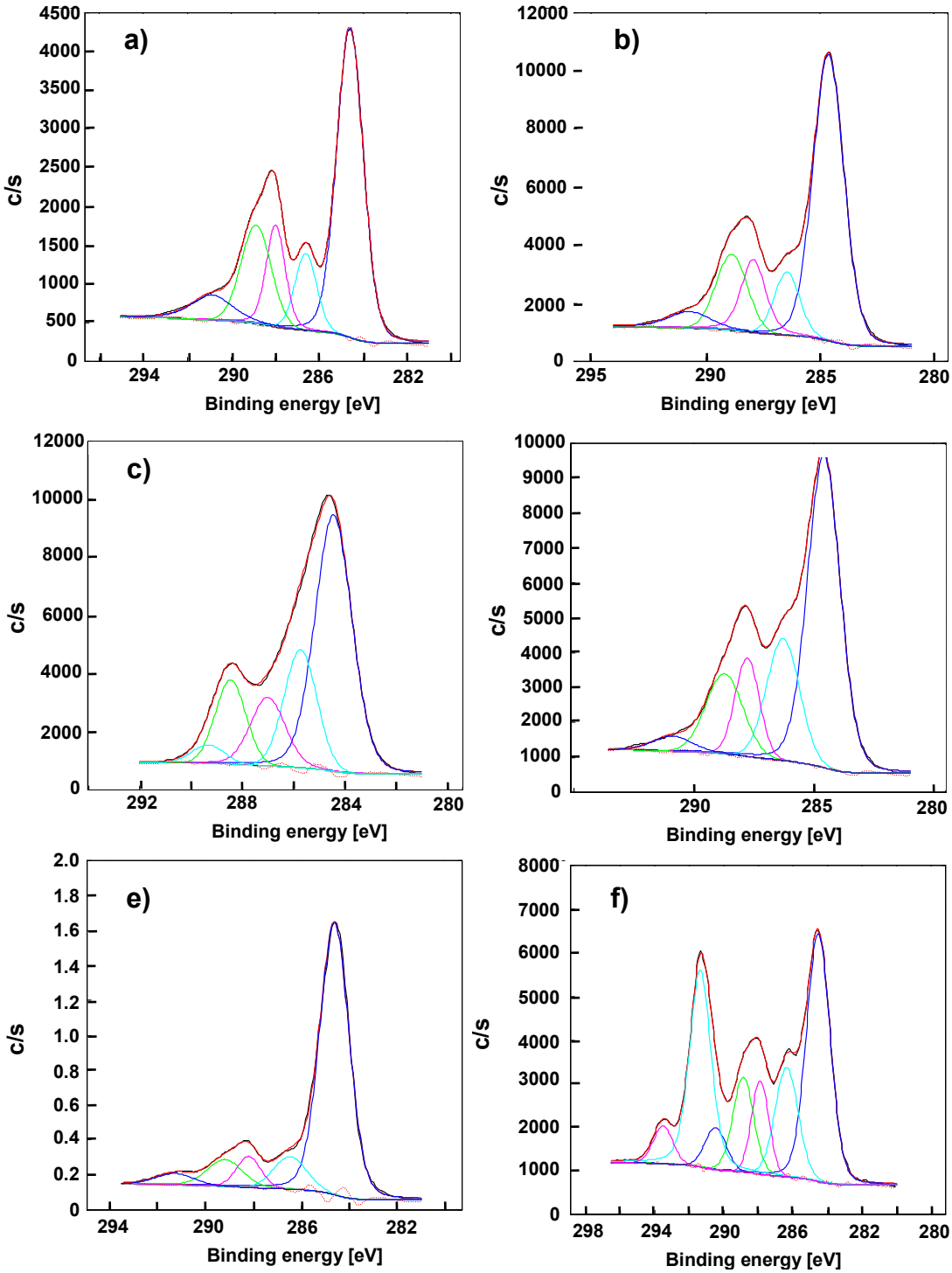

Figure 10-9: C(1s) detail spectra of a) unmodified PGL1840, b) PGL1840-PMAA, c) -PMAA, d) -PDMAA, e) -PS and f) -PHDFDA.

10.6 Fitted curves of C(1s) detail spectra of various polymer-attached PGL1155

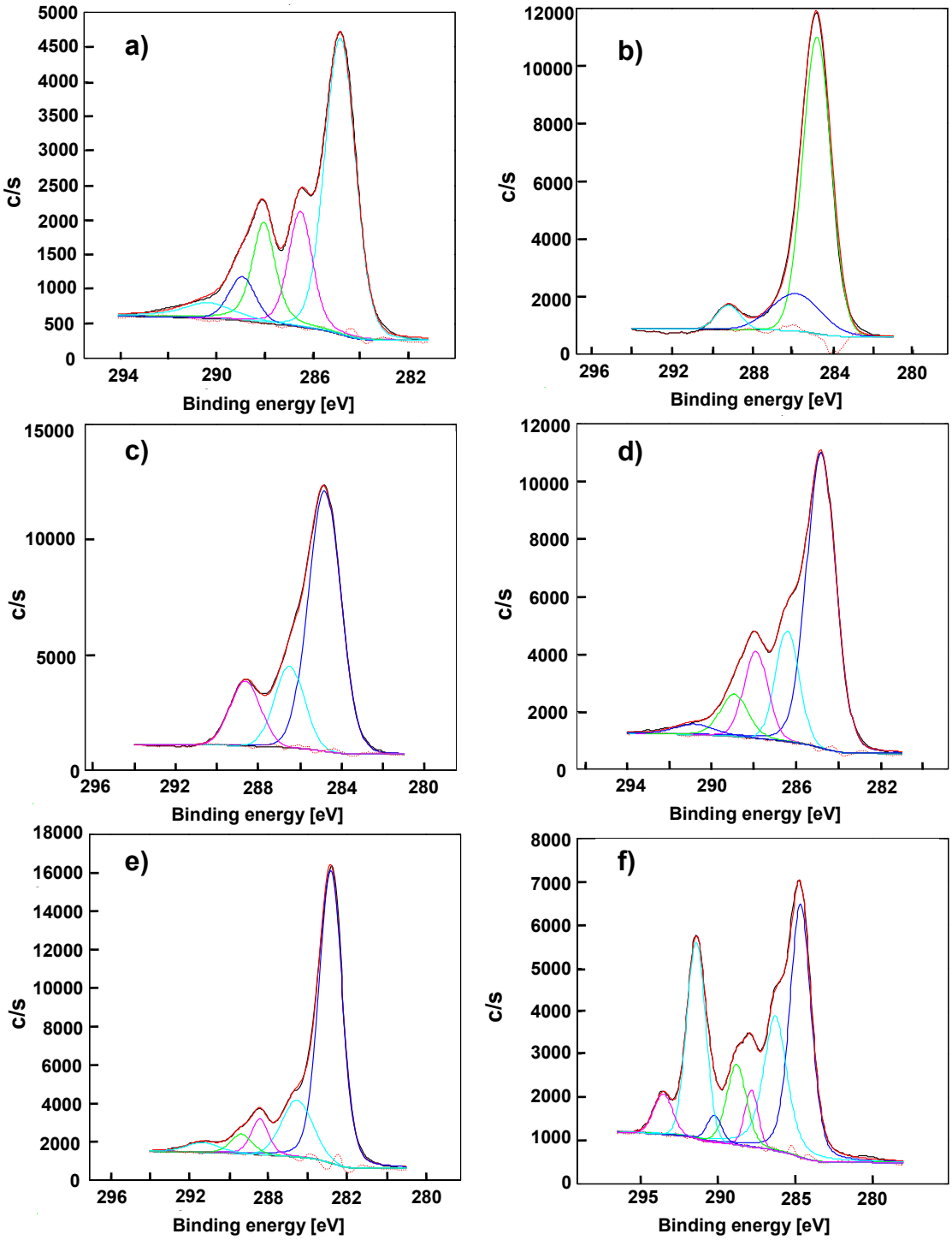

Figure 10-10: C(1s) detail spectra of a) unmodified PGL1155, b) PGL1155-PMAA, c) -PMAA, d) -PDMAA, e) -PS and f) -PHDFDA.

Table 10-6: Layer thickness L of the different polymer-attached PGL1840 surfaces.

monomer	concentration [mol l^{-1}]	*L** [nm]
MMA	1.87	4.1
	2.81	6.3
	3.74	9.9
	4.67	9.7
	5.61	14.9
MAA	3.54	2.3
	4.72	6.1
DMAA	3.88	1.0**
styrene	3.49	1.0
	4.36	1.5
	5.24	1.5
	8.73	1.3
HDFDA	0.90	4.9

* calculated from nitrogen content measured by elemental analysis using Equation 4-6 and Equation 4-7, respectively.
** determined from the integral intensity of UV absorption and subsequently using Equation 4-7.

Table 10-7: Yield of non-attached polymer obtained from the polymerization of vinyl monomers using unmodified PGL1840 and PGL1840-Azo as well as nitrogen contents of composite material according to elemental analysis.

	PGL1840		PGL1840-Azo	
	N [%]	*y*** [%]	N [%]	*y* ** [%]
untreated pigment	18.50	–	18.83 ± 0.22***	–
[MMA]* = 4.67 mol l^{-1}	17.32	3.8	10.78	26.2
[MAA]* = 3.54 mol l^{-1}	16.83	73.7	16.33	96.7
[DMAA]* = 3.88 mol l^{-1}	18.50	61.6	18.80	95.5
[styrene]* = 8.73 mol l^{-1}	20.05	2.0	16.98	3.4
[HDFDA]* = 0.90 mol l^{-1}	19.62	0.0	14.99	39.5

* pigments were polymerized with the corresponding monomer solution: MMA and styrene in toluene, MAA in water, DMAA in $CHCl_3$ amd HDFDA in freon.
** yield of non-attached polymer obtained.
*** average of 6 measurements.

Table 10-8: Determination of PGL1840 pigment content in free polymer using UV absorption.

polymer	concentration of monomer [mol l^{-1}]	pigment in free polymer [%]	
		PGL1840*	PGL1840-Azo*
PMMA	1.87	−	0.1
	2.81	−	0.2
	3.74	−	0.5
	4.67	0.0	0.2
	5.61	−	1.0
PMAA	3.54	34.6	37.0
	4.72	−	75.0
PDMAA	3.88	5.6	11.5

* corresponding monomer was polymerized with PGL1840 (non-attached initiator) or PGL1840-Azo (initiator-attached pigment): T = 60 °C and t = 16 hours.

10.7 Grafting of polymer on PGL1840 surfaces through copolymerization of surface-attached monomer

10.7.1 Layer thickness as a function of monomer concentration

Table 10-9: Graft densities and layer thickness of PMMA-modified PGL1840 calculated from nitrogen content measured by elemental analysis as well as number-average molecular weight of free polymer as determined by GPC and polydispersity (D).

MMA [mol l^{-1}]	N [%]	δ [g m^{-2}]	L [nm]	M_n [g mol^{-1}]	D	Γ [nmol m^{-2}]
1.87	16.41	0.002	2	51100	1.7	48
2.81	16.04	0.003	2	68500	1.7	42
3.74	15.83	0.003	3	95100	1.8	33
4.67	15.25	0.004	3	171000	1.9	22
5.61	15.46	0.004	3	268000	2.2	13

[AIBN] = 10 mmol l^{-1}, T = 60 °C and t = 16 hours.

10.7.2 Influence of the polymerization time

Table 10-10: Graft densities and layer thickness of PMMA-modified PGL1840 calculated from nitrogen content measured by elemental analysis as well as number-average molecular weight of free polymer as determined by GPC and polydispersity (D).

t [hours]	N [%]	δ [g m^{-2}]	L [nm]	M_n [g mol^{-1}]	D	Γ [nmol m^{-2}]
4	17.26	0.002	1	124000	2.1	13
8	16.56	0.002	2	109000	1.8	21
12	16.36	0.003	2	109000	1.8	23
16	16.26	0.003	2	104000	1.7	25
25	16.33	0.003	2	96800	1.8	26
32	16.04	0.003	2	93300	1.9	31

[MMA] = 3.74 mol l^{-1}, [AIBN] = 10 mmol l^{-1}, T = 60 °C.

10.7.3 Influence of the initiator concentration

Table 10-11: Graft densities and layer thickness of PMMA-modified PGL1840 calculated from nitrogen content measured by elemental analysis as well as number-average molecular weight of free polymer as determined by GPC and polydispersity (D).

AIBN [mol l^{-1}]	N [%]	δ [g m^{-2}]	L [nm]	M_n [g mol^{-1}]	D	Γ [nmol m^{-2}]
2	3.36	0.003	2	273000	2.0	10
6	3.29	0.002	2	124000	1.8	20
8	3.48	0.003	3	127000	1.8	25
10	3.47	0.003	3	104000	1.7	30
15	3.46	0.003	3	80800	1.7	38
20	3.37	0.003	2	72500	1.7	38

[MMA] = 3.74 mol l^{-1}, T = 60 °C, t = 16 hours.

10.7.4 Polymerization with perfluorinated monomer (HDFDA)

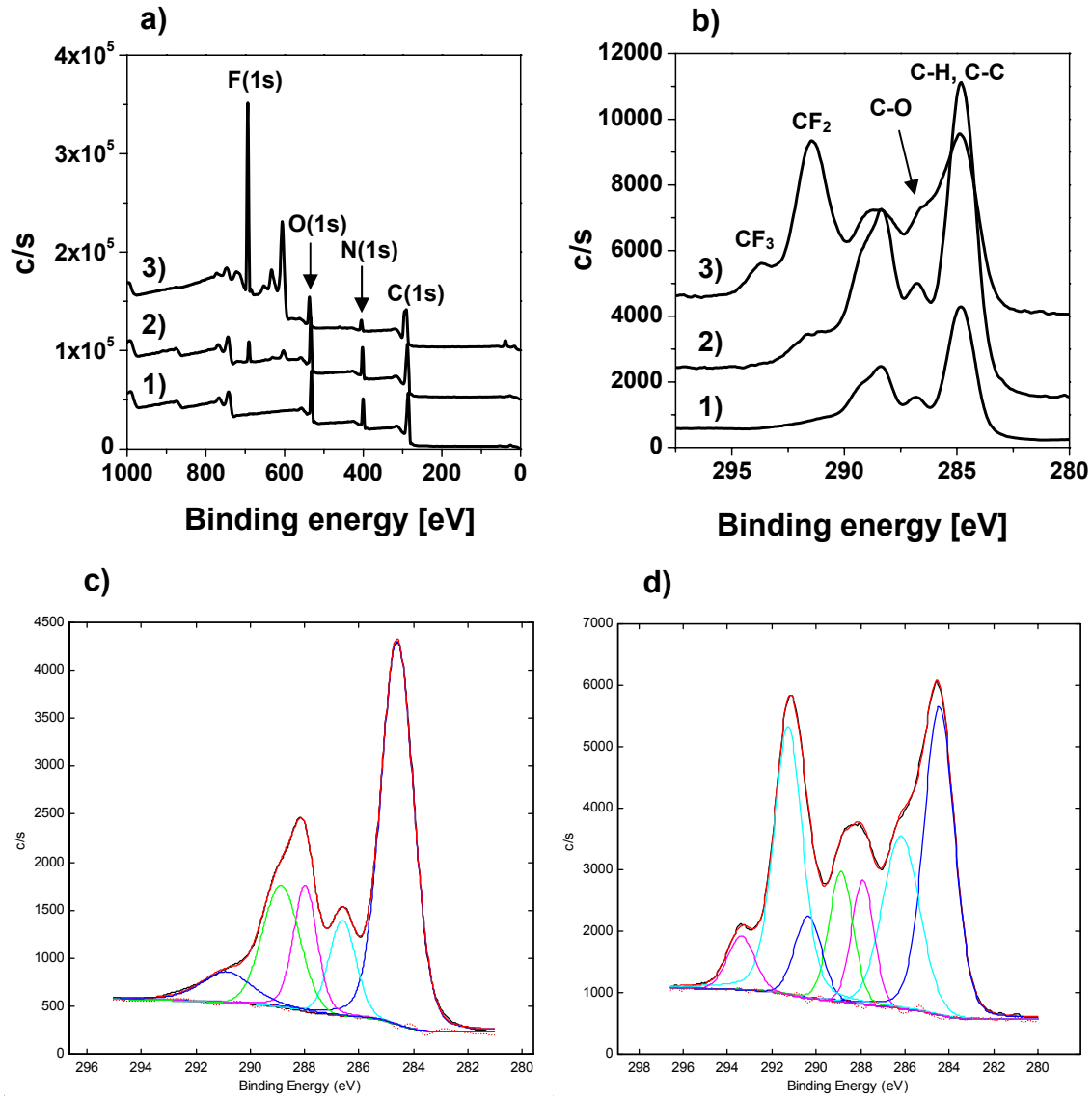

Figure 10-11: a) XP survey spectra and b) C(1s) detail spectra of unmodified PGL1840 (1), PGL1840 without surface-attached monomer (2) and PGL1840-MA copolymerized with HDFDA in the presence of AIBN (3); c) evaluation of C(1s) signals of PGL1840 (b2) and d) that of PGL1840-HDFDA (b3) using Gauss-Lorentz functions for the signals and a Shirley type function for the baseline.

Table 10-12: Components of the C(1s) signals of surface-modified pigments from Figure 10-11b and their assignments to functionalities within the materials.

PGL1840 **BE (eV); (%) ; assignments**	**PGL1840*** **BE (eV); (%) ; assignments**	**PGL1840-PHDFDA*** **BE (eV); (%) ; assignments**
284.6; (52); C-C, C-H	284.6; (50); C-C, C-H	284.5; (33); C-C, C-H
286.6; (10); C-O	286.6; (11); C-O	286.4; (14); C-O
288.0; (13); C-N	288.0; (14); C-N	287.9; (9); C-N
288.9; (18); CONH	288.9; (16); CONH	288.9; (11); CONH, COO
290.9; (7); $\pi \rightarrow \pi^*$	290.6; (5); $\pi \rightarrow \pi^*$	290.5; (4); $\pi \rightarrow \pi^*$
	291.6; (4); CF_2	291.4; (25); CF_2
		293.5; (4); CF_3

* PGL1840 (non-attached monomer) or PGL1840-PHDFDA (MA-attached PGL1840) was copolymerized with HDFDA (0.90 mol l^{-1}) in presence of AIBN (10 mmol l^{-1}) at 60 °C for one hour.

10.8 "Grafting-from" polymerization on inorganic pigment surfaces via self-assembled azo-initiator monolayers (SAIMs)

10.8.1 Graft density as a function of monomer concentration

10.8.1.1 PCG2020-ABCC as surface-initiated polymerization

Table 10-13: Carbon contents, graft densities and layer thickness of PMMA-attached PCG2020 calculated from carbon content measured by elemental analysis as well as number-average molecular weight of free polymer as detemined by GPC and polydipersity (D).

MMA [mol l^{-1}]	C [%]	δ [mg m^{-2}]	L [nm]	M_n [g mol^{-1}]	M_w [g mol^{-1}]	D	Γ [nmol m^{-2}]
0.935	2.23	15	13	133000	314000	2.4	112
1.870	2.28	15	13	235000	607000	2.6	65
2.805	3.81	25	21	379000	1070000	2.8	67
3.740	3.69	25	21	494000	1360000	2.8	50
4.674	5.44	36	30	617000	1700000	2.7	59

T = 60 °C and t = 16 hours

10.8.1.2 TiO_2-ABCC as surface-initiated polymerization

Table 10-14: Carbon contents, graft densities and layer thickness of PMMA-attached PCG2020 calculated from carbon content measured by elemental analysis as well as number-average molecular weight of free polymer as detemined by GPC and polydipersity (D).

MMA [mol l^{-1}]	C [%]	δ [mg m^{-2}]	L [nm]	M_n [g mol^{-1}]	M_w [g mol^{-1}]	D	Γ [nmol m^{-2}]
0.935	8.78	3	2	145000	421000	2.9	20
1.870	15.29	5	4	276000	820000	3.0	18
2.805	21.65	7	6	414000	1160000	2.8	17
3.740	29.61	10	8	649000	1850000	2.9	15
4.674	36.81	12	10	893000	2400000	2.7	14

T = 60 °C and t = 16 hours.

10.8.1.3 TiO_2-ADS as surface-initiated polymerization

Table 10-15: Carbon contents, graft densities and layer thickness of PMMA-attached PCG2020 calculated from carbon content measured by elemental analysis as well as number-average molecular weight of free polymer as detemined by GPC and polydipersity (D).

MMA [mol l^{-1}]	C [%]	δ [mg m^{-2}]	L [nm]	M_n [g mol^{-1}]	M_w [g mol^{-1}]	D	Γ [nmol m^{-2}]
0.935	3.90	1.3	1.1	129000	401000	3.1	10
1.870	4.42	1.5	1.2	223000	768000	3.5	7
2.805	5.40	1.8	1.5	330000	955000	2.9	5
3.740	7.34	2.4	2.0	557000	1630000	2.9	4
4.674	8.55	2.9	2.4	654000	1600000	2.4	4

T = 60 °C and t = 16 hours.

10.8.2 Graft density as a function of polymerization time

10.8.2.1 TiO_2-ABCC as surface-initiated polymerization

Table 10-16: Carbon contents, graft densities and layer thickness of PMMA-attached PCG2020 calculated from carbon content measured by elemental analysis as well as number-average molecular weight of free polymer as detemined by GPC and polydipersity (D).

t [hours]	C [%]	δ [mg m^{-2}]	L [nm]	M_n [g mol^{-1}]	M_w [g mol^{-1}]	D	Γ [nmol m^{-2}]
4	11.27	4	3	377000	1170000	3.1	10
8	14.05	5	4	480000	1180000	2.5	10
12	19.31	6	5	504000	1130000	2.2	13
16	21.65	7	6	414000	1160000	2.8	17
24	24.33	8	7	537000	1250000	2.3	15
32	29.92	10	8	542000	1140000	2.1	18

[MMA] = 2.81 mol l^{-1}, T = 60 °C and t = 16 hours.

10.8.2.2 TiO_2-ADS as surface-initiated polymerization

Table 10-17: Carbon contents, graft densities and layer thickness of PMMA-attached PCG2020 calculated from carbon content measured by elemental analysis as well as number-average molecular weight of free polymer as detemined by GPC and polydipersity (D).

t [hours]	C [%]	δ [mg m^{-2}]	L [nm]	M_n [g mol^{-1}]	M_w [g mol^{-1}]	D	Γ [nmol m^{-2}]
4	3.93	1.3	1.1	672000	1570000	2.3	1.9
8	5.25	1.8	1.5	830000	1650000	2.0	2.1
12	5.43	1.8	1.5	655000	1440000	2.2	2.8
16	7.34	2.4	2.0	557000	1630000	2.9	4.4
20	9.16	3.1	2.5	752000	1590000	2.1	4.1
24	8.14	2.7	2.3	826000	1720000	2.1	3.3
32	10.74	3.6	3.0	836000	1790000	2.1	4.3

[MMA] = 3.74 mol l^{-1}, T = 60 °C and t = 16 hours.

10.9 Grafting of polymers via copolymerization of surface-attached monomer monolayers on inorganic pigment surfaces

10.9.1 Graft density as a function of monomer concentration

Table 10-18: Carbon contents, graft densities and layer thickness of PMMA-attached PCG2020 calculated from carbon content measured by elemental analysis as well as number-average molecular weight of free polymer as detemined by GPC and polydipersity (D).

MMA [mol l^{-1}]	C [%]	δ [mg m^{-2}]	L [nm]	M_n [g mol^{-1}]	M_w [g mol^{-1}]	D	Γ [nmol m^{-2}]
0.935	6.08	2.0	1.7	25600	34800	1.4	79
1.870	7.58	2.5	2.1	37200	58200	1.6	68
2.805	9.65	3.2	2.7	52100	84200	1.6	62
3.740	12.05	4.0	3.3	70500	117000	1.7	57
4.674	15.77	5.3	4.4	102000	169000	1.7	52

[AIBN] = 20 mmol l^{-1}, T = 60 °C and t = 16 hours.

10.9.2 Graft density as a function of polymerization time

Table 10-19: Carbon contents, graft densities and layer thickness of PMMA-attached PCG2020 calculated from carbon content measured by elemental analysis as well as number-average molecular weight of free polymer as detemined by GPC and polydipersity (D).

t [hour]	C [%]	δ [mg m^{-2}]	L [nm]	M_n [g mol^{-1}]	M_w [g mol^{-1}]	D	Γ [nmol m^{-2}]
4	7.13	2.4	2.0	69300	140000	2.0	34
8	7.71	2.6	2.1	59200	101000	1.7	43
12	8.61	2.9	2.4	48800	83100	1.7	59
16	9.65	3.2	2.7	52100	84200	1.6	62
20	9.34	3.1	2.6	48500	84900	1.7	64
24	9.55	3.2	2.7	48700	86400	1.8	65
32	9.65	3.2	2.7	44600	78000	1.8	72

[MMA] = 2.81 mol l^{-1}, [AIBN] = 20 mmol l^{-1} and T = 60 °C.

10.9.3 Layer thickness as a function of initiator concentration

Table 10-20: Carbon contents, graft densities and layer thickness of PMMA-attached PCG2020 calculated from carbon content measured by elemental analysis as well as number-average molecular weight of free polymer as detemined by GPC and polydipersity (D).

AIBN [mmol l^{-1}]	C [%]	δ [mg m^{-2}]	L [nm]	M_n [g mol^{-1}]	M_w [g mol^{-1}]	D	Γ [nmol m^{-2}]
2	8.19	2.7	2.3	182000	348000	1.9	15
4	8.76	2.9	2.4	125000	348000	1.8	23
8	9.11	3.0	2.5	86100	149000	1.7	35
10	9.42	3.1	2.6	75900	131000	1.7	41
20	9.65	3.2	2.7	52100	84200	1.6	62
40	9.30	3.1	2.6	42400	70300	1.7	73

[MMA] = 2.81 mol l^{-1}, T = 60 °C and t = 16 hours.

10.10 Stability of unmodified and polymer-modified PGL1840 pigments against alkaline solutions

10.10.1 Investigation of the stability against various buffer solutions

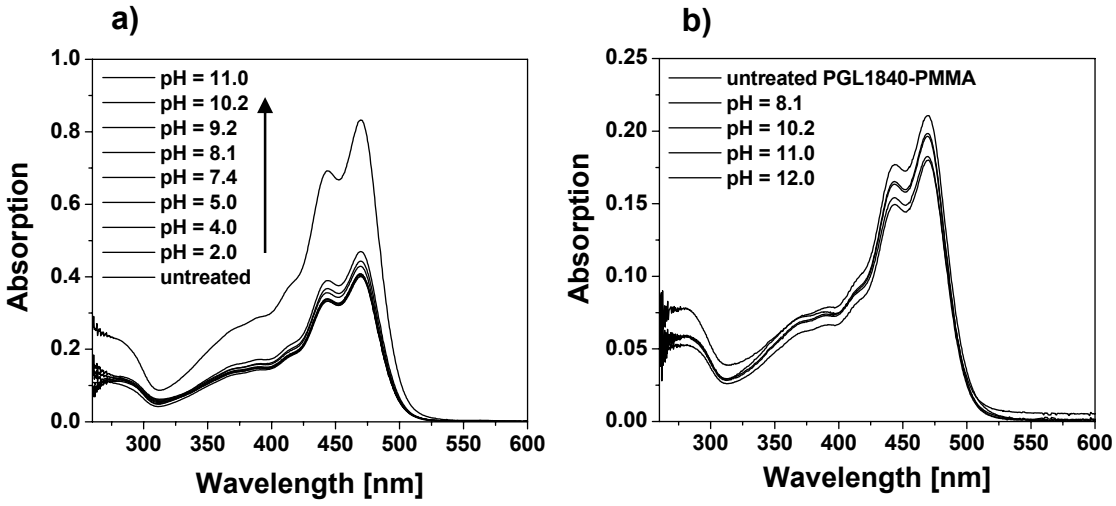

Figure 10-12: UV spectra of a) unmodified PGL1840 and b) PMMA-modified PGL1840 (1.0 g PMMA / g pigment) after treatment in buffer solution.

Table 10-21: Yield and elemental analysis data obtained from PGL1840 treated with buffer solutions of various pH.

	Yield [%]	**C** [%]	**H** [%]	**N** [%]
untreated	100	52.32	2.47	19.07
pH = 2.0	96	51.17	2.79	19.39
pH = 4.0	92	51.24	2.77	19.87
pH = 5.0	83	51.20	2.78	19.59
pH = 7.4	80	51.12	2.78	19.23
pH = 8.1	64	51.41	2.32	18.86
pH = 9.2	66	51.23	2.83	18.52
pH = 10.2	71	51.46	2.54	18.63
pH = 10.5	27	–	–	–
pH = 11.0	35	51.34	2.74	18.69
pH = 12.0	soluble after 15 minutes			

Table 10-22: Yield and elemental analysis data obtained from PGL1840-PMMA treated with various buffer solutions.

	Yield [%]	**C** [%]	**H** [%]	**N** [%]
PGL1840-PMMA*	100	57.36	5.61	9.43
pH = 8.1	95	55.30	5.48	9.20
pH = 10.2	91	55.62	5.64	8.97
pH = 11.0	90	55.55	5.61	8.61
pH = 12.0	90	55.68	5.59	8.47

* PGL1840-Azo was polymerized with 4.67 mol l^{-1} MMA at 60 °C for16 hours: 1.0 g PMMA per g PGL1840.

10.10.2 Investigation of the stability with variation of the PMMA graft density and with different surface-attached polymer monolayers

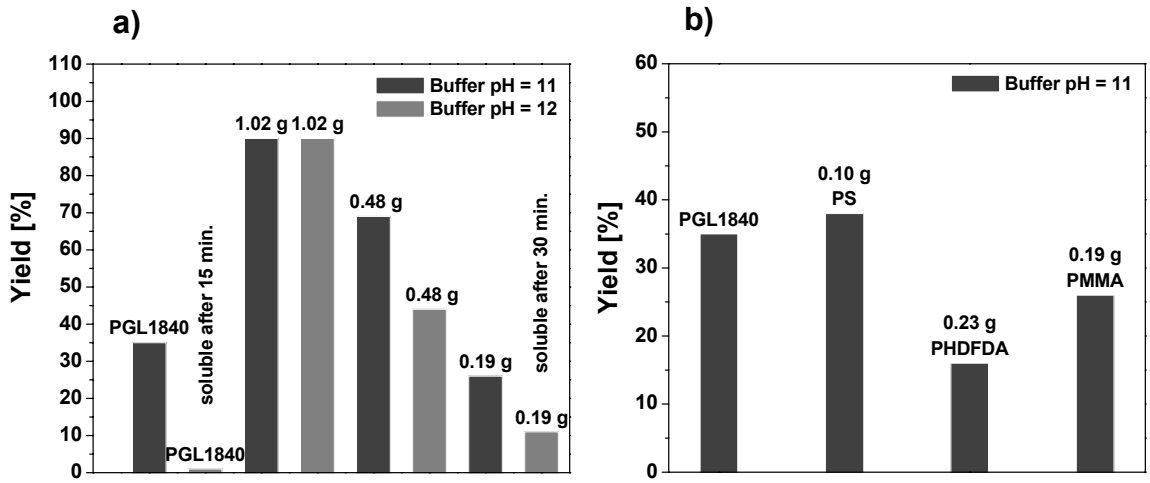

Figure 10-13: a) Yield of PGL1840 and PGL1840-PMMA with various graft densities of PMMA; b) alkaline stability of unmodified pigment and various polymer-pigment hybrid materials after treatment in buffer pH 11 (dark gray) and pH 12 (light gray).

11 Literature

(1) Christie, R. M. *Colour Chemistry*; The Royal Society of Chemistry, 2001.

(2) Zollinger, H. *Color Chemistry: syntheses, properties and applications of organic dyes and pigments*; Weinheim; NewYork: VCH, 1987.

(3) Buxbaum, G. *Industrial Inorganic Pigments*; 2. ed.; Wiley-VCH: New York, 1998.

(4) Herbst, W.; Hunger, K. *Industrial Organic Pigments: Production, Properties, Application*; 2. ed.; VCH Verlagsgesellschaft mbH: Weinheim, 1997.

(5) Jaffe, E. E.; Hammel, N.; Kanouni, M.; Misogianes, M.; Hilfiker, F. R. In *Paint&Coating Industry*, 2003.

(6) Jaffe, E. E.; Campbell, C. D.; Hendi, S. B.; Babler, F. *Journal of Coatings Technology* **1994**, *66*, 47.

(7) Hollemann, A. F.; Wiberg, E. *Lehrbuch der Anorganischen Chemie*; 34 ed.; Walter de Gruyter: Berlin, Germany, 1995.

(8) Adams, R. *Environment Matters (GB)* **1990**.

(9) Clarke, G. *Ind. Min. (London)* **1988**, *251*, 17.

(10) Williams, D. *Eur. Chem. News* **1996**, *17-23 June*, 36.

(11) Rohe, D. *Chemische Industrie* **1996**, *10*, 16.

(12) Amati, D.; Kovats, E. S. *Langmuir* **1988**, *4*, 329.

(13) Gamble, L.; Jung, L. S.; Campbell, C. T. *Langmuir* **1995**, *11*, 4505.

(14) Gamble, L.; Henderson, M. A.; Campbell, C. T. *Journal of Physical Chemistry B* **1998**, *102*, 4536.

(15) Fadeev, A. Y.; Helmy, R.; Marcinko, S. *Langmuir* **2002**, *18*, 7521.

(16) Marcinko, S.; Helmy, R.; Fadeev, A. Y. *Langmuir* **2003**, *19*, 2752.

(17) Moses, P. R.; Wier, L. M.; Lennox, J. C.; Finklea, H. O.; Lenhard, J. R.; Murray, R. W. *Analytical Chemistry* **1978**, *50*, 576.

(18) Finklea, H. O.; Murray, R. W. *Journal of Physical Chemistry* **1979**, *83*, 353.

(19) Mahon, M.; Wulser, K. W.; Langell, M. A. *Langmuir* **1991**, *7*, 486.

(20) Tsubokawa, N.; Kogure, A. *Journal of Polymer Science Part a-Polymer Chemistry* **1991**, *29*, 697.

(21) Xiao, S. J.; Textor, M.; Spencer, N. D.; Sigrist, H. *Langmuir* **1998**, *14*, 5507.

(22) Fadeev, A. Y.; McCarthy, T. J. *Journal of the American Chemical Society* **1999**, *121*, 12184.

(23) Shafi, K.; Ulman, A.; Yan, X. Z.; Yang, N. L.; Himmelhaus, M.; Grunze, M. *Langmuir* **2001**, *17*, 1726.

(24) Guerrero, G.; Mutin, P. H.; Vioux, A. *Chemistry of Materials* **2001**, *13*, 4367.

(25) Gao, W.; Dickinson, L.; Grozinger, C.; Morin, F. G.; Reven, L. *Langmuir* **1996**, *12*, 6429.

(26) Helmy, R.; Fadeev, A. Y. *Langmuir* **2002**, *18*, 8924.

(27) Randon, J.; Paterson, R. *Journal of Membrane Science* **1997**, *134*, 219.

(28) Duval, R.; Yvin, J. C. In *French Patent 2 773 172*, 1997.

(29) Alberti, G.; Casciola, M.; Costantino, U.; Vivani, R. *Advanced Materials* **1996**, *8*, 291.

(30) Clearfield, A. *Progress in Inorganic Chemistry* **1998**, *47*, 371.

(31) *The Colour Index*; 3 rd ed.; Society of Dyers and Colourist: Bradford, England, 1988.

(32) Smith, H. M. *High Performance Pigments*; Wiley-VCH Verlag-GmbH: Weinheim, Germany, 2002.

(33) *DIN 53 206 Teil 1: Teilchengrößenanalyse, grundbegriffe*.

(34) Li, Q.; Feke, D. L.; ManasZloczower, I. *Rubber Chemistry and Technology* **1995**, *68*, 836.

(35) Kämpf, G. *Farbe+Lack* **1965**, *71*, 353.

(36) Cowley, A. C. D.; Gallon, M. R. *Journal of the Oil & Colour Chemists Association* **1988**, *71*, 310.

(37) Cowley, A. C. D.; Slater, R. *Plastics Engineering* **1989**, *45*, 41.

(38) Andrew, D.; Joins, R.; Leary, B.; Boger, D. V. *Journal of Colloid and Interface Science* **1991**, *147*, 479.

(39) Siffert, B.; Li, J. F. *Colloids and Surfaces* **1992**, *62*, 307.

(40) Weiss, A.; Dingenouts, N.; Ballauff, M.; Senff, H.; Richtering, W. *Langmuir* **1998**, *14*, 5083.

(41) Schaller, C.; Schauer, T.; Dirnberger, K.; Eisenbach, C. D. *Progress in Organic Coatings* **1999**, *35*, 63.

(42) Schaller, C.; Schauer, T.; Dirnberger, K.; Eisenbach, C. D. *European Physical Journal E* **2001**, *6*, 365.

(43) Lin, Y.; Smith, T. W.; Alexandridis, P. *Langmuir* **2002**, *18*, 6147.

(44) Zhang, T. Y.; Zhou, C. L. *Dyes and Pigments* **1997**, *35*, 123.

(45) Joppien, G. R.; Hamann, K. *Journal of the Oil & Colour Chemists Association* **1977**, *60*, 412.

(46) Dietz, E.; Hamann, K. *Angewandte Makromolekulare Chemie* **1976**, *51*, 53.

(47) Laible, R.; Hamann, K. *Advances in Colloid and Interface Science* **1980**, *13*, 65.

(48) Tsubokawa, N.; Kuroda, A.; Sone, Y. *Journal of Polymer Science, Part A: Polymer Chemistry* **1989**, *27*, 1701.

(49) Boven, G.; Oosterling, M.; Challa, G.; Schouten, A. J. *Polymer* **1990**, *31*, 2377.

(50) Tsubokawa, N.; Hosoya, M.; Yanadori, K.; Sone, Y. *Journal of Macromolecular Science, Chemistry* **1990**, *A27*, 445.

(51) Browne, T.; Chaimberg, M.; Cohen, Y. *Journal of Applied Polymer Science* **1992**, *44*, 671.

(52) Prucker, O.; Rühe, J. *Langmuir* **1998**, *14*, 6893.

(53) Prucker, O.; Rühe, J. *Macromolecules* **1998**, *31*, 592.

(54) Prucker, O.; Rühe, J. *Macromolecules* **1998**, *31*, 602.

(55) Tsubokawa, N.; Kobayashi, M.; Ogasawara, T. *Progress in Organic Coatings* **1999**, *36*, 39.

(56) Tsubokawa, N.; Kobayashi, M.; Ogasawara, T. *Journal of Dispersion Science and Technology* **1999**, *20*, 1467.

(57) Bialk, M.; Prucker, O.; Rühe, J. *Colloids and Surfaces a-Physicochemical and Engineering Aspects* **2002**, *198*, 543.

(58) Lelu, S.; Novat, C.; Graillat, C.; Guyot, A.; Bourgeat-Lami, E. *Polymer International* **2003**, *52*, 542.

(59) Tsubokawa, N.; Kobayashi, K.; Sone, Y. *Polymer Journal (Tokyo, Japan)* **1987**, *19*, 1147.

(60) Shirai, Y.; Kawatsura, K.; Tsubokawa, N. *Progress in Organic Coatings* **1999**, *36*, 217.

(61) Shirai, Y.; Tsubokawa, N. *Reactive & Functional Polymers* **1997**, *32*, 153.

(62) Krenkler, K. P.; Laible, R.; Hamann, K. *Angewandte Makromolekulare Chemie* **1976**, *53*, 101.

(63) Horn, J.; Hoene, R.; Hamann, K. *Macromolecular Chemistry Supply* **1975**, *35*, 329.

(64) Papirer, E.; Nguyen, V. T.; Donnet, J.-B. *Journal of Polymer Science* **1979**, *17*, 1015.

(65) Bridger, K.; Fairhurst, D.; Vincent, B. *Journal of Colloid and Interface Science* **1979**, *68*, 190.

(66) Bridger, K.; Vincent, B. *European Polymer Journal* **1980**, *16*, 1017.

(67) Hashimoto, K.; Fujisawa, T.; Kobayashi, M.; Yosomiya, R. *Journal of Applied Polymer Science* **1982**, *27*, 4529.

(68) Benouada, H.; Hommel, H.; Legrand, A. P.; Balard, H.; Papirer, E. *Journal of Colloid and Interface Science* **1988**, *122*, 441.

(69) Dmitrenko, A. V.; Shadrina, N. E.; Ivanchev, S. S.; Ulinskaya, N. N.; Volkov, A. M. *Journal of Chromatography* **1990**, *520*, 21.

(70) Yoshikawa, S.; Iida, T.; Tsubokawa, N. *Progress in Organic Coatings* **1997**, *31*, 127.

(71) Zajac, R.; Chakrabarti, A. *Physical Review E* **1995**, *52*, 6536.

(72) Kopf, A.; Baschnagel, J.; Wittmer, J.; Binder, K. *Macromolecules* **1996**, *29*, 1433.

(73) Vidal, A.; Guyot, A.; Kennedy, J. P. *Polymer Bulletin* **1980**, *2*, 315.

(74) Vidal, A.; Guyot, A.; Kennedy, J. P. *Polymer Bulletin* **1982**, *6*, 401.

(75) Herrmann, W. A.; Stumpf, A. W.; Priermeier, T.; Bogdanovic, S.; Dufaud, V.; Basset, J. M. *Angewandte Chemie-International Edition in English* **1996**, *35*, 2803.

(76) Jordan, R.; Ulman, A. *Journal of the American Chemical Society* **1998**, *120*, 243.

(77) Jordan, R.; Ulman, A.; Kang, J. F.; Rafailovich, M. H.; Sokolov, J. *Journal of the American Chemical Society* **1999**, *121*, 1016.

(78) Ingall, M. D. K.; Honeyman, C. H.; Mercure, J. V.; Bianconi, P. A.; Kunz, R. R. *Journal of the American Chemical Society* **1999**, *121*, 3607.

(79) Zhao, B.; Brittain, W. J. *Macromolecules* **2000**, *33*, 342.

(80) Tsubokawa, N.; Yamada, A.; Sone, Y. *Polymer Bulletin* **1983**, *10*, 63.

(81) Tsubokawa, N. *Journal of Polymer Science Part C-Polymer Letters* **1983**, *21*, 705.

(82) Tsubokawa, N.; Handa, S. *Journal of Macromolecular Science-Pure and Applied Chemistry* **1993**, *A30*, 277.

(83) Tsubokawa, N.; Satoh, M. *Journal of Applied Polymer Science* **1997**, *65*, 2165.

(84) Tsubokawa, N.; Fujiki, K.; Sone, Y. *Polymer Journal* **1988**, *20*, 213.

(85) Fujiki, K.; Tsubokawa, N.; Sone, Y. *Polymer Journal* **1990**, *22*, 661.

(86) Prucker, O., Bayreuth, 1995.

(87) Hashimoto, K.; Fujisawa, T.; Kobayashi, M.; Yosomiya, R. *Journal of Macromolecular Science-Chemistry* **1982**, *A18*, 173.

(88) Trachenko, V. I.; Zil'berman, Y. N.; Shatskaya, T. F.; Pomerantseva, E. G. *Polymer Science USSR* **1986**, *28*, 646.

(89) Caruso, F. *Advanced Materials* **2001**, *13*, 11.

(90) Bourgeat-Lami, E. *In Dendrimers, Assemblies and Nanocomposites,*; Guyot A and Arshady R MML Series ed.; Citus Books: London, 2002.

(91) Bourgeat-Lami, E. *Journal of Nanoscience and Nanotechnology* **2002**, *2*, 1.

(92) Templetonknight, R. *Chemistry & Industry* **1990**, 512.

(93) Templetonknight, R. L. *Journal of the Oil & Colour Chemists Association* **1990**, *73*, 459.

(94) Caris, C. H. M.; Vanelven, L. P. M.; Vanherk, A. M.; German, A. L. *British Polymer Journal* **1989**, *21*, 133.

(95) Janssen, R. Q. F.; Vanherk, A. M.; German, A. L. *Jocca-Surface Coatings International* **1993**, *76*, 455.

(96) Bourgeat-Lami, E.; Lang, J. *Journal of Colloid and Interface Science* **1998**, *197*, 293.

(97) Bourgeat-Lami, E.; Lang, J. *Journal of Colloid and Interface Science* **1999**, *210*, 281.

(98) Corcos, F.; Bourgeat-Lami, E.; Novat, C.; Lang, J. *Colloid and Polymer Science* **1999**, *277*, 1142.

(99) Sondi, I.; Fedynyshyn, T. H.; Sinta, R.; Matijevic, E. *Langmuir* **2000**, *16*, 9031.

(100) Bell, T. W.; Hou, Z. *Angewandte Chemie-International Edition in English* **1997**, *36*, 1536.

(101) Chang, S. K.; Vanengen, D.; Fan, E.; Hamilton, A. D. *Journal of the American Chemical Society* **1991**, *113*, 7640.

(102) Rebek, J. *Chemical Society Reviews* **1996**, *25*, 255.

(103) Bong, D. T.; Clark, T. D.; Granja, J. R.; Ghadiri, M. R. *Angewandte Chemie-International Edition* **2001**, *40*, 988.

(104) Kimizuka, N.; Kawasaki, T.; Hirata, K.; Kunitake, T. *Journal of the American Chemical Society* **1998**, *120*, 4094.

(105) Sherrington, D. C.; Taskinen, K. A. *Chemical Society Reviews* **2001**, *30*, 83.

(106) Zerkowski, J. A.; Mathias, J. P.; Whitesides, G. M. *Journal of the American Chemical Society* **1994**, *116*, 4305.

(107) Zerkowski, J. A.; Whitesides, G. M. *Journal of the American Chemical Society* **1994**, *116*, 4298.

(108) Paleos, C. M.; Tsiourvas, D. *Advanced Materials* **1997**, *9*, 695.

(109) Lehn, J. M. *Pure and Applied Chemistry* **1994**, *66*, 1961.

(110) Sijbesma, R. P.; Beijer, F. H.; Brunsveld, L.; Folmer, B. J. B.; Hirschberg, J.; Lange, R. F. M.; Lowe, J. K. L.; Meijer, E. W. *Science* **1997**, *278*, 1601.

(111) Huo, Q.; Russell, K. C.; Leblanc, R. M. *Langmuir* **1998**, *14*, 2174.

(112) Marchi-Artzner, V.; Artzner, F.; Karthaus, O.; Shimomura, M.; Ariga, K.; Kunitake, T.; Lehn, J. M. *Langmuir* **1998**, *14*, 5164.

(113) Kawasaki, T.; Tokuhiro, M.; Kimizuka, N.; Kunitake, T. *Journal of the American Chemical Society* **2001**, *123*, 6792.

(114) Lange, R. F. M.; Meijer, E. W. *Macromolecules* **1995**, *28*, 782.

(115) Zerkowski, J. A.; Seto, C. T.; Wierda, D. A.; Whitesides, G. M. *Journal of the American Chemical Society* **1992**, *112*, 9025.

(116) Simanek, E. E.; Isaacs, L.; Li, X. H.; Wang, C. C. C.; Whitesides, G. M. *Journal of Organic Chemistry* **1997**, *62*, 8994.

(117) Simanek, E. E.; Wazeer, M. I. M.; Mathias, J. P.; Whitesides, G. M. *Journal of Organic Chemistry* **1994**, *59*, 4904.

(118) Seto, C. T.; Whitesides, G. M. *Journal of the American Chemical Society* **1990**, *112*, 6409.

(119) Kotera, M.; Lehn, J. M.; Vigneron, J. P. *Journal of the Chemical Society-Chemical Communications* **1994**, 197.

(120) Marsh, A.; Nolen, E. G.; Gardinier, K. M.; Lehn, J. M. *Tetrahedron Letters* **1994**, *35*, 397.

(121) Lehn, J. M.; Mascal, M.; Decian, A.; Fischer, J. *Journal of the Chemical Society-Chemical Communications* **1990**, 479.

(122) Kurzer, F.; Douraghi.K *Chemical Reviews* **1967**, *67*, 107.

(123) Detar, D. F.; Silverst.R *Journal of the American Chemical Society* **1966**, *88*, 1013.

(124) Detar, D. F.; Silverst.R; Rogers, F. F. *Journal of the American Chemical Society* **1966**, *88*, 1024.

(125) Hesse, M.; Meier, H.; Zeeh, B. *Spektroskopische Methoden in der organischen Chemie*; 5. ed.; Thieme Verlag: Stuttgart, 1995.

(126) Masson, J. C. In *Polymer Handbooks*; 3rd ed.; Immergut, E. H., Ed.; John Wiley & Sons: New York, 1989.

(127) Cline, G. W.; Hanna, S. B. *Journal of Organic Chemistry* **1988**, *53*, 3583.

(128) Wagner, P.; Hegner, M.; Kernen, P.; Zaugg, F.; Semenza, G. *Biophysical Journal* **1996**, *70*, 2052.

(129) Beamson, G.; Briggs, D. *High Resolution XPS of Organic Polymers (The Scienta ESCA300 Database)*; John Wiley and Sons: New York, 1992.

(130) Muilenberg, G. E. *Phi Handbook of X-ray Photoelectron Spectroscopy*; Perkin-Elmer Corporation: Eden Prarie, 1979.

(131) Stöhr, T.; Rühe, J. *Macromolecules* **2000**, *33*, 4501.

(132) Korn, M.; Killmann, E. *Journal of Colloid and Interface Science* **1980**, *76*, 19.

(133) Felter, R. E. *Journal of Polymer Science Part C-Polymer Letters* **1974**, *12*, 147.
(134) Wunderlich, W. In *Polymer Handbooks*; 3rd ed.; Immergut, E. H., Ed.; John Wiley & Sons: New York, 1989.
(135) Odian, G. *Principles of polymerization*; 3. rd ed.; John Wiley & Sons, Inc., 1991.
(136) Schimmel, M., Johannes Gutenberg-Universität Mainz, 1998.
(137) Cowie, J. M. G. *Chemie und Physik der synthetischen Polymeren*, 1997.
(138) Mayo, F. R. *Journal of the American Chemical Society* **1943**, *65*, 2324.
(139) Jackson, C.; Chen, Y.-J.; Mays, J. W. *Journal of Applied Polymer Science* **1996**, *61*, 865.
(140) Metzner, B., Bayreuth, 1995.
(141) Clark, D. T.; Dilks, A. *Journal of Polymer Science Part a-Polymer Chemistry* **1977**, *15*, 15.
(142) Castner, D. G.; Lewis, K. B.; Fischer, D. A.; Ratner, B. D.; Gland, J. L. *Langmuir* **1993**, *9*, 537.
(143) Author, A. In *Handbook of Composites*; Lubin G. ed.; Van Nostrand Reinhold: New York, 1982.
(144) Chaimberg, M.; Cohen, Y. *AIChE Journal* **1994**, *40*, 294.
(145) Zhang, H.; Rühe, J. *Macromolecules* **2003**, *36*, 6593.
(146) Kataby, G.; Prozorov, T.; Koltypin, Y.; Cohen, H.; Sukenik, C. N.; Ulman, A.; Gedanken, A. *Langmuir* **1997**, *13*, 6151.
(147) Jang, J.; Kim, E. K. *Journal of Applied Polymer Science* **1999**, *71*, 585.
(148) Vanooij, W. J.; Sabata, A. *Scandinavian Journal of Metallurgy* **1992**, *21*, 32.
(149) Quinton, J.; Thomsen, L.; Dastoor, P. *Surface and Interface Analysis* **1997**, *25*, 931.
(150) Quinton, J. S.; Dastoor, P. C. *Surface and Interface Analysis* **1999**, *28*, 12.
(151) Quinton, J. S.; Dastoor, P. C. *Surface and Interface Analysis* **2000**, *30*, 21.
(152) Yee, C.; Kataby, G.; Ulman, A.; Prozorov, T.; White, H.; King, A.; Rafailovich, M.; Sokolov, J.; Gedanken, A. *Langmuir* **1999**, *15*, 7111.
(153) Horner, M. R.; Boerio, F. J.; Clearfield, H. M. *Silanes and Other Coupling Agents*; Mittal KL ed.: Netherlands, 1992.
(154) Bain, C. D.; Troughtoyt, E. B.; Tao, Y.-T.; Evall, J.; Whitesides, G. M.; Nuzzoj, R. G. *Journal of American Chemistry Social* **1989**, *111*, 321.
(155) Wasserman, S. R.; Whitesides, G. M.; Tidswell, I. M.; Ocko, B. M.; Pershan, P. S.; Axe, J. D. *Journal of American Chemistry Social* **1989**, *111*, 5852.
(156) Ishida, H.; Chiang, C. H.; Koenig, J. L. *Polymer* **1982**, *23*, 251.
(157) Naviroj, S.; Koenig, J. L.; Ishida, H. *Journal of Macromolecular Science-Physics* **1983**, *B22*, 291.
(158) Zaper, A. M.; Koenig, J. L. *Polymer Composites* **1985**, *6*, 156.
(159) Briggs, D. *Surface analysis of polymer by XPS and static SIMS*; Cambridge University Press: Cambridge, 1998.

Danksagung

Die vorliegende Arbeit wurde am Institut für Mikrosystemtechnik der Albert-Ludwigs-Universität Freiburg, Fakutät für Angewandte Wissenschaften, im März 2000 begonnen und im Juli 2004 abgeschlossen.

Herrn Prof. Dr. J. Rühe danke ich für die Überlassung des Themas, die Bereitstellung des Arbeitsplatzes sowie für sein stetes Interesse an der Arbeit und seine hilfreichen Anregungen.

Herrn Dr. Oswald Prucker, Herrn Dr. Hironobu Murata und Herrn Dr. Haining Zhang sei gedankt für die Bereitschaft zur Diskussion meiner Arbeit.

Mein Dank gilt auch Herrn Dr. Martin Könemann von der BASF AG für die Einführung in das „Know-How“ von Pigmenten und für die anregenden Diskussionen über Pigmente.

Herrn Dr. Haining Zhang und Herrn Daniel Freidank danke ich für die Einführung in die Röntgenreflektometrie.

Bei Dr. Oswald Prucker, Dr. J.D. Jeyaprakash S. Samuel, Dr. Cong-Duan Vo und Ulrike Mock bedanke ich mich für die sorgfältige Durchsicht meiner Arbeit.

Daniela Mössner danke ich für die Durchführung zahlreicher Synthesen und für die Durchführung der XPS-Messungen, Natalie Schatz für die Durchführung der GPC-Messungen und Dorothea Boy für die Aufnahme der IR- und UV-Spektren.

Ich bedanke mich bei allen Mitarbeitern der Elementaranalyseabteilung der Albert-Ludwigs-Universität Freiburg für die durchgeführten Messungen.

Für Hilfe in Sachen Bürokratie bedanke ich mich Frau Waltraud Hanser und Frau Petra Hettich.

Dorothea B., Daniela M., Franziska D., Petra B., Natalie S., Sidar D., Ulrike M., Bernd B., Bon-Jung C., Daniel F., Daniel M., Haining Z., Hironobu M, Jörg P., Martin S., Rupert K. und Thorsten N. danke ich ganz herzlich für viele Erlebnisse, die ich mit Euch genießen durfte.

Für die Verbesserung meiner deutschen Sp**R**ache danke ich besonders Ul**L**ike, Daniel F**L**eidank, **L**upe**L**t Kon**L**adi und Jö**L**g.

Mein Dank gilt auch allen Mitgliedern des Arbeitskreises für die große Hilfsbereitschaft, stete Unterstützung und das angenehme Arbeitsklima.

Danken möchte ich auch der thailändischen Regierung sowie der BASF AG für die finanzielle Unterstützung meines Studiums in Deutschland.

Besonderer Dank gilt meiner Mutter und meiner Schwester, Frau Sudthanom Homdok und ihrer Familie, Frau Petra Hettich und meinen Ersatzeltern „Hilde & Albert Wiloth“ für ihre seelische Unterstützung während meines Studiums in Deutschland.

Meine Doktorarbeit widme ich meinem Vater und meinem Bruder.